Improved early *in vitro* prediction of drug induced liver injury in man: Assessment of novel 3D hepatic models

Zur Erlangung des akademischen Grades eines

DOKTORS DER NATURWISSENSCHAFTEN

(Dr. rer. nat.)

Fachbereich Chemie

Technische Universität Kaiserslautern

genehmigte

DISSERTATION

von

Esther Johann, M.Sc.

aus

Merzig

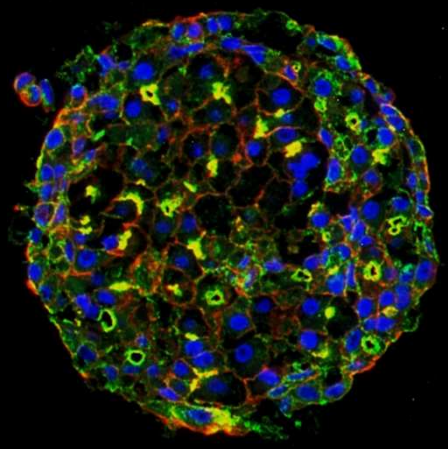

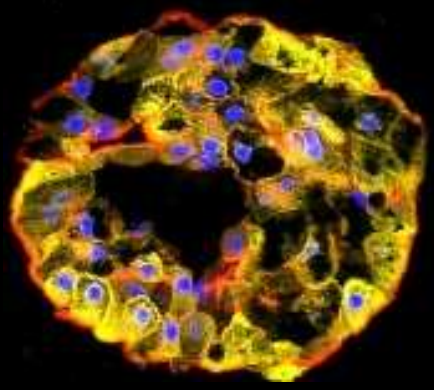

Genehmigte Version

Vorsitzender der Promotionskommission: Prof. Dr. Christoph van Wüllen

Erster Berichterstatter: Prof. Dr. Dr. Dieter Schrenk

Zweiter Berichterstatter: Dr. Stefan Otto Müller, ERT

Tag der mündlichen Prüfung: 13. August 2018

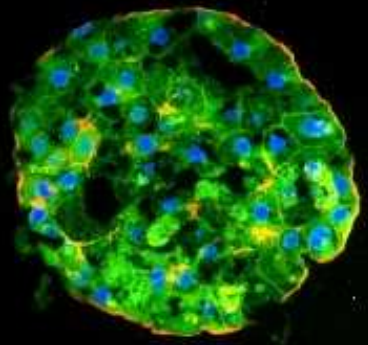

D386

Für Mama

Declaration of Originality

I hereby declare that the present thesis represents my own work, it was performed without outside help and no other sources of information have been used than those indicated. All informations that were gathered from released or unreleased sources were marked definetly as such.

Date _____ Signature _____

Acknowledgements

First, I would like to thank Dr. Brigitte Simon-Hettich and Dr. Philip Hewitt for giving me the opportunity to prepare my doctoral thesis on this very interesting project in the early non-clinical safety department at Merck KGaA, Darmstadt.

Special thanks go to Dr. Philip Hewitt and Dr. Stefan O. Müller for supporting my work and giving useful suggestions and help whenever I needed it during the whole time I worked on my thesis.

Many thanks also go to Prof. Dr. Dr. Dieter Schrenk for offering the possibility to prepare my thesis externally at Merck KGaA and additionally for the excellent teaching I may have received within the study course.

I´d like to thank all members of the MIP-DILI project team for the fruitful project meetings and the mutual support.

For the great support in the lab and all the invaluable technical hints I'd like to thank Margret Kling and Yvonne Walter, you always had good ideas. Furthermore, many thanks to Claudia Klement, Johanna Sebbel and Bettina von Eiff for the great support in the Lab. Additionally, many thanks go to the department of pathology, thanks to Angelika Schäfer-Schwebel, Ellen Wagner and Bernd Pohl for the great support and practical advice. Many thanks go to Dr. Anja Knippel for the great support on the evaluation of all those spheroid microdissections.

I'd also like to thank Tobias C. Fuchs, Germaine L. Truisi and Yasmin Dietz for supporting me whenever a question came up and for always having useful and clever ideas.

Special thanks go to all eNCS colleagues. Thank you for making me feel comfortable, making me smile and smiling back.

Additionally, I want to thank my family and all my friends for keeping me up and believing in me. In particular, I want to thank my parents: Danke Mama und Papa, dass ihr mir mein Studium ermöglicht habt und immer an mich geglaubt habt. Danke für eure Geduld mit mir! Mama, ich hoffe Du bist stolz auf mich, auch wenn Du die Fertigstellung meiner Arbeit leider nicht mehr miterleben konntest; ich vermisse Dich jeden Tag!

Special thanks also got to my brother Sven, my sister (in law) Shermineh as well as my niece Helena, you always kept me up when things were tough.

Last, but not less important, I'd like to thank Dr. Thomas Broschard and Dr. Gregor Tuschl for giving me the opportunity to gain knowledge in the setting of exposure levels for leachables & extractables, chemicals as well as for active pharmaceutical ingredients.

Abstract

Increasing costs due to the rising attrition of drug candidates in late developmental phases alongside post-marketing withdrawal of drugs challenge the pharmaceutical industry to further improve their current preclinical safety assessment strategies. One of the most common reasons for the termination of drug candidates is drug induced hepatotoxicity, which more often than not remains undetected in early developmental stages, thus emphasizing the necessity for improved and more predictive preclinical test systems. One reason for the very limited value of currently applied *in vitro* test systems for the detection of potential hepatotoxic liabilities is the lack of organotypic and tissue-specific physiology of hepatocytes cultured in ordinary monolayer culture formats.

The thesis at hand primarily deals with the evaluation of both two- and three-dimensional cell culture approaches with respect to their relative ability to predict the hepatotoxic potential of drug candidates in early developmental phases. First, different hepatic cell models, which are routinely used in pharmaceutical industry (primary human hepatocytes as well as the three cell lines HepG2, HepaRG and Upcyte hepatocytes), were investigated in conventional 2D monolayer culture with respect to their ability to detect hepatotoxic effects in simple cytotoxicity studies. Moreover, it could be shown that the global protein expression levels of all cell lines substantially differ from that of primary human hepatocytes, with the least pronounced difference in HepaRG cells.

The introduction of a third dimension through the cultivation of spheroids enables hepatocytes to recapitulate their typical native polarity and furthermore dramatically increases the contact surface of adjacent cells. These differences in cellular architecture have a positive influence on hepatocyte longevity and the expression of drug metabolizing enzymes and transporters, which could be proven via immunofluorescent (IF) staining for at least 14 days in PHH and at least 28 days in HepaRG spheroids, respectively. Additionally, the IF staining of three different phase III transporters (MDR1, MRP2 and BSEP) indicated a bile canalicular network in spheroids of both cell models. A dose-dependent inducibility of important cytochrome P450 isoenzymes in HepaRG spheroids could be shown on the protein level via IF for at least 14 days. CYP inducibility of HepaRG cells cultured in 2D and 3D was compared on the mRNA level for up to 14 days and inducibility was generally lower in 3D compared to 2D under the conditions of this study. In a comparative cytotoxicity study, both PHH and HepaRG spheroids as well as HepaRG monolayers have been treated with five hepatotoxic drugs for up to 14 days and viability was measured at three time points (days 3, 7 and 14). A clear time- and dose-dependent onset of the drug-induced hepatotoxic effects was observable in all conditions tested, indicated by a shift of the respective EC_{50} value towards lower doses by increasing exposure. The observed effects were most

pronounced in PHH spheroids, thus indicating those as the most sensitive cell model in this study. Moreover, HepaRG cells were more sensitive in spheroid culture compared to monolayers, which suggests a potential application of spheroids as long-term test system for the detection of hepatotoxicities with slow onset. Finally, the basal protein expression levels of three antigens (CYP1A2, CYP3A4 and NAT 1/2) were analyzed via Western Blotting in HepaRG cells cultured in three different cell culture formats (2D, 3D and QV) in order to estimate the impact of the cell culture conditions on protein expression levels. In the QV system enables a pump-driven flow of cell culture media, which introduces both mechanical stimuli through shear and molecular stimuli through dynamic circulation to the monolayer. Those stimuli resulted in a clearly positive effect on the expression levels of the selected antigens by an increased expression level in comparison to both 2D and 3D. In contrast, HepaRG spheroids showed time-dependent differences with the overall highest levels at day 7.

The studies presented in this thesis delivered valuable information on the increased physiological relevance in dependence on the cell culture format: three-dimensionality as well as the circulation of media lead to a more differentiated phenotype in hepatic cell models. Those cell culture formats are applicable in preclinical drug development in order to obtain more relevant information at early developmental stages and thus help to create a more efficient drug development process. Nonetheless, further studies are necessary to thoroughly characterize, validate and standardize such novel cell culture approaches prior to their routine application in industry.

Zusammenfassung

Steigende Kosten aufgrund der zunehmenden Terminierung von Wirkstoffkandidaten in späten Entwicklungsphasen sowie der Marktrücknahme von Arzneimitteln stellen die pharmazeutische Industrie vor die Herausforderung, ihre üblichen standardisierten Sicherheitsprüfungen weiterzuentwickeln. Dabei stellt Arzneimittel-induzierte Hepatotoxizität einen der Hauptgründe für das Scheitern neuer Wirkstoffkandidaten dar, weswegen die Notwendigkeit zur Entwicklung prädiktiver Modelle unumgänglich ist. Ein Grund für die sehr limitierte Aussagekraft der herkömmlichen *in vitro* Testsysteme zur Erfassung potentieller Hepatotoxizität besteht darin, dass die organ- und gewebespezifischen Eigenschaften in gewöhnlichen Zellkulturformaten nahezu gänzlich verloren gehen.

Die vorliegende Arbeit beschäftigt sich mit der Bewertung zwei- und dreidimensionaler Zellkulturmodelle mit Bezug auf deren jeweilige Aussagekraft auf potentielle hepatotoxische Effekte von Wirkstoffen im Rahmen der frühen Arzneimittelentwicklung hinweisen zu können. Dabei wurden zunächst verschiedene hepatische Zellmodelle (Primäre humane Hepatozyten (PHH) sowie die drei Zelllinien HepG2, HepaRG und Upcyte Hepatozyten) in der üblichen, zweidimensionalen Zellrasen-Konfiguration auf ihre Fähigkeit untersucht, in einfachen Zytotoxizitätsstudien hepatotoxische Effekte zu detektieren. Darüber hinaus zeigten Proteomanalysen der vier Zellmodelle, dass die Proteinexpression der Zelllinien erheblich vom Expressionsmuster primärer Hepatozyten abweicht, wobei der geringste Unterschied in HepaRG Zellen zu sehen war.

Die Einführung einer dritten Dimension durch die Kultivierung von Späroiden ermöglicht den Hepatozyten die Ausbildung einer zelltypischen Polarität sowie eine enorme Vergrößerung der Interaktionsfläche zwischen benachbarten Zellen. Diese Veränderungen der zellulären Architektur haben einen positiven Einfluss auf die Langlebigkeit der Zellen mit einer stabilen Expression wichtiger fremdstoffmetabolisierender Enzyme und Transporter, was mittels Immunfluoreszenzfärbungen über einen Zeitraum von mindestens 14 Tagen in PHH Sphäroiden und 28 Tagen in HepaRG Sphäroiden gezeigt werden konnte. Des Weiteren deuteten die Färbungen dreier Phase III Transporter (MDR1, MRP2 und BSEP) auf ein kanalikuläres Netzwerk in den Sphäroiden beider Zellmodelle hin. Eine dosisabhängige Induzierbarkeit wichtiger Cytochrom P450 Isoenzyme konnte zudem in HepaRG Sphäroiden auf Proteinebene mittels IF gezeigt werden, die jedoch auf mRNA Ebene im Vergleich zur Zellrasenkultivierung überwiegend geringer ausfiel. In einer vergleichenden Zytotoxizitätsstudie wurden HepaRG und PHH Sphäroide sowie HepaRG Zellrasen für maximal 14 Tage mit fünf hepatotoxischen Arzneimitteln behandelt und die Viabilität wurde and drei Zeitpunkten bestimmt (3, 7 und 14 Tage). Eine deutliche Zeitabhängigkeit der zytotoxischen Effekte konnte in allen getesteten Bedingungen dahingehend beobachtet

werden, dass der EC_{50} Wert mit längerer Behandlungsdauer deutlich sank. Die beobachteten Effekte waren am deutlichsten in PHH Sphäroidkultur, die somit das sensitivste Zellkultursystem darstellte. Des Weiteren zeigten sich HepaRG Zellen in Sphäroidkultur sensitiver als in Zellrasenkultur, was wertvolle Hinweise auf die potentielle Anwendung von Sphäroiden als Langzeitkultur-Modell lieferte. Letztlich wurde die Proteinexpression dreier Antigene (CYP1A2, CYP3A4 und NAT 1/2) mittels der Western Blot Methode durchgeführt, um die basale Expression Dieser in drei verschieden Zellkulturformaten (2D, 3D und QV) in HepaRG Zellen über einen Zeitraum von 14 Tagen zu vergleichen. Das QV Zellkulturformat ermöglicht einen pumpenbetriebenen Fluss des Zellkulturmediums, welcher dem Zellrasen mechanische Stimuli durch Scherkräfte sowie molekulare Stimuli durch die dynamische Zirkulation zuführt. Diese Stimuli zeigten einen deutlich positiven Effekt auf die Expression der untersuchten Antigene; zu jedem Zeitpunkt (Tag 3, Tag 7 und Tag 14) zeigten HepaRG Zellen im QV Format eine deutlich erhöhte Expression im Vergleich zur Kultivierung in 2D und 3D. Die Expression in HepaRG Sphäroiden zeigte zeitliche Schwankungen mit der generell höchsten Expression an Tag 7.

Die in dieser Arbeit durchgeführten Studien liefern wertvolle Hinweise auf die erhöhte physiologische Relevanz in Abhängigkeit des Zellkulturformats: Dreidimensionalität sowie die Zirkulation des Zellkulturmediums führen zu einem physiologisch relevanteren Phänotyp der hepatischen Zellmodelle. Diese Zellkulturformate können in der präklinischen Arzneimittelentwicklung eingesetzt werden, um zu früheren Zeitpunkten humanrelevantere Informationen zu erhalten und somit den Entwicklungsprozess effizienter gestalten. Weitere Studien sind jedoch nötig, um ein neues Zellkulturformat umfangreich zu charakterisieren, zu validieren und zu standardisieren, damit Dieses Anwendung in der industriellen Routine finden kann.

Content

List of Abbreviations

%	percent
3R	Reduction, Refinement, Replacement
ABC	ATP binding cassette
ABCB	ATP-binding cassette subfamily B
ABCC	ATP-binding cassette subfamily C
ADME	Absorption, distribution, metabolism, excretion
ADP	Adenosine diphosphate
ADR	Adverse drug reactions
AhR	Aryl-hydrocarbon receptor
ALT	Alanine transferase
AMI	Amiodaron
APAP	Acetaminophen
APC	Antigen presenting cell
AT	Aminotransferase
ATP	Adenosine triphosphate
AUC	Area under the curve
BOS	Bosentane
BSA	Bovine serum albumin
BSEP	Bile salt export pump
BUS	Buspirone
℃	Degrees celsius
CAR	Constitutive androstane receptor
Ck19	Cytokeratin 19
CLF	Cholyl-lysyl fluorescein
C_{max}	Peak plasma concentration
CO_2	Carbon dioxide
COX	Cyclooxygenase
CPZ	Chlorpromazine
CYP	Cytochrome P-450 monooxygenase
d	Day
Da	Dalton
DCF	Diclofenac
DEPC	Diethylpyrocarbonate
DDI	Drug-drug interaction
DILI	Drug-induced liver injury
DME	Drug metabolizing enzyme
DMET	Drug metabolizing enzymes and transporter
DMEM	Dulbecco´s modified eagle medium
DMPK	Drug metabolism and pharmacokinetics
DMSO	Dimethyl sulphoxide
DNA	Desoxyriboneucleic acid
DPBS	Dilbeccos phosphate buffered saline
e.g.	*Exempli gratia* (for example)
EC_{50}	Effective concentration 50%
ECAR	Extracellular acidification rate

ECCAC	European Collection of Authenticated Cell Cultures
ECM	Extracellular matrix
EDTA	Ethylenediaminetetraacetic acid
EFPIA	European Federation of Pharmaceutical Industries and Associations
EH	Epoxide hydrolase
EIF	Eukaryotic initiation factor
EMA	European medicines agency
ER	Endoplasmic reticulum
EtOH	Ethanol
EU	European Union
EURL	European union reference laboratory
FACS	fluorescence-activated cell sorting
FBS	Fetal bovine serum
FDA	Food and drug administration
FLU	Flumazenil
FMO	Flavine-dependent monooxygenase
g	Gram
g	Gravity acceleration
Glu	Glucose
GLU-GAL	Glucose-galactose assay
GSH	Glutathion
GST	Glutathion S-transferase
h	Hour
H&E	Hematoxilin and eosin
HCl	Hydrochloric acid
HCA/HCS	High content analysis/ High content screening
hENT1	Human equilibrative nucleoside transporter 1
hESC	Human embryonic stem cell
HLA	Human leukocyte antigen
HPC	Hepatic progenitor cells
HSC	Hepatic stellate cell
i.e.	*Id est* (that is)
ICH	International conference of harmonisation
iDILI	Idiosyncratic Drug-induced liver injury
IF	Immunofluorescence
IMI	Innovative medicines initiative
iPSC	Induced pluripotent stem cell
iTRAQ	Isobaric tags for relative and absolute quantitation
ITS	Insulin transferrin selenium
k	Kilo
K_{OW}	Partition coefficient octanol/water
Keap1	Kelch-like ECH-associated protein 1
L	Liter
LCMS/MS	Liquid chromatography coupled mass spectrometry
LDH	Lactate dehydrogenase
LPS	lipopolysaccharide
LSEC	Liver sinusoidal endothelial cells
LTKB	Liver toxicity knowledge base
µ	Micro

m	Milli
M	Mol
mA	Milliampere
MAO	Monoamineoxidase
Mdr	Multidrug resistance protein
MET	Metformin
MFI	Mean fluorescence intensity
min	Minute
mio	Million
MIP-DILI	Mechanism-based integrated systems for the prediction of drug-induced liver injury
MMP	Mitochondrial membrane potential
MPS	Microphysiological system(s)
mRNA	Messenger RNA
MRP	Multidrug resistance-associated protein
mtDNA	Mitochondrial DNA
mTOR	mechanistic Target of Rapamycin
n	nano
NAFLD	Non-alcoholic fatty liver disease
NAT 1/2	N-acetyltransferase 1/2
NAPQI	N-Acetyl-p-benzoquinone imine
NCBI	National center for biotechnology information
NCE	New cemical entity
NEF	Nefazodone
NGS	Next generation sequencing
NOAEL	No observed adverse effect level
Nrf2	Nuclear factor [erythroid-derived 2]-like 2 protein
O_2	Oxygen
OATP	Organic anion transport protein
OCR	Oxygen consumption rate
OCT	Organic cation transporter
OD	Optical density
OECD	Organisation for economic Co-operation and development
OMEP	Omeprazol
P70S6K	Ribosomal protein S6 kinase beta1
PAS	Periodic acid Schiff reaction
PB	Phenobarbital
PER	Perhexiline
PBS	Phosphate buffered saline
P-gp	P-glycoprotein
pH	Negative of the base 10 logarithm of the activity of the hydrogen ion
PHH	Primary human hepatocytes
p-i	Pharmacological Interaction of Drugs with Immune Receptors
PPAR	Peroxisome proliferator-activated receptor
PRX	Peroxiredoxin
PXR	Pregnane-X-receptor
QV	Quasi-vivo
REACH	Registration, Evaluation, Authorisation and Restriction of Chemicals
RFU	Relative fluorescent units

RIF	Rifampicine
RNA	Ribonucleic acid
ROS	Reactive oxygen species
rpm	Rotations per minute
RT	Room temperature
s	Second
SAPE	R-Phycoerythrin
SAR	Structure activity relationship
SDS-PAGE	Sodium dodecylsulfate polyacrylamide gel electrophoresis
SMEs	Small and medium sized enterprises
SOD	Superoxide dismutase
SOP	Standard operating procedure
SULT	Sulfotransferase
TCA	Tricarboxylic acid
TPMT	Thiopurin-S-Methyltransferase
tRNA	Transfer RNA
TRO	Troglitazone
TS	Test site
UDP	Ubiquitine diphosphate
UGT	UDP-Glucoronosyl transferase
ULAP	Ultra-low attachment plate
V	Volts
XIM	Ximelagatran

1 Introduction

1.1 Toxicology

The interdisciplinary scientific field of toxicology, named from the Greek *toxicon* = poison and *logos* = science, concerns adverse effects of chemical, biological or physical agents on living organisms.

Paracelsus (Philippus Theophrastus Aureolus Bombastus von Hohenheim, 1493 – 1541), a physician who introduced chemicals to medicine (Borzelleca, 2000), defined a statement on poisonous effects of things, which today is still a fundamental toxicological concept:

„All things are poison and nothing is without poison, only the dose permits something not to be poisonous "

Paracelsus stated that the dose makes the poison, which is today defined as the dose-response relationship. Over time, toxicology emerged from basic observational practice of potential adverse outcomes after contact of organisms with agents towards a highly sophisticated field in science, which becomes more and more evident since the exposure to agents, especially in the context of industrialization, grows steadily. The progress of scientific methods alongside advanced knowledge in all scientific fields has enabled a revelation in our understanding of underlying mechanisms that may lead to adverse outcomes (Milles, 1999).

Today, toxicology is essential in many industries, e.g. pharmaceutical, food, cosmetic, environmental and forensic toxicology; and it is always focused on the adverse effect an agent may cause to people, animals and environment. The focus is driven by the definition of an agent's dose that is "safe" and toxicity studies are required before bringing a product on the market. In the pharmaceutical industry, those assessments are often conducted using a battery of *in vitro* and *in vivo* experiments, being required by law before any exposure to humans.

For pharmaceutical development, animal experiments are required by law and are used to help understand potential adverse outcomes of a drug candidate. However, they are limited predictors of what happens in humans, since the non-clinical species used in drug development have many known differences to humans (e.g. different substrate specificities of enzymes or different anatomic features like absence of gall bladder in rats).

In 1959, the scientists William Russell and Rex Burch published ‚The Principles of Humane Experimental Technique' which proposed the concept of *3Rs* – which aims to *Reduce, Refine* and *Replace* animal experiments whenever possible. This will only be possible

through conscious planning and maximization of information that can be generated as well as development and consideration of alternative test strategies, which are able to cover endpoints without the necessity of animal models. The use of animal models can be reduced by covering the maximum feasible number of endpoints in a single experiment. Secondly, continuous progress has been made in gathering a maximum of information via *in vitro* and *in silico* methods prior to animal testing since more information means refined planning of animal studies and reduced suffering to those animals within a study. Finally, replacement evolves from the progress of alternative methods, such as novel *in vitro* and *in silico* models, which optimally are able to cover endpoints reliably without the use of *in vivo* studies.

The 3R principle is widely accepted as an ethical code in chemical, pharmaceutical and cosmetics industries as they permanently strive to develop and validate novel alternatives for the accurate prediction of potential adverse outcomes in humans, animals and the environment.

Those progresses are actively supported by the European Union and the European Union Reference Laboratory for alternatives to animal testing (EURL ECVAM), funded in 1991 by the Joint Research Centre (Institute for Health and Consumer Protection), which aims to assist and promote the development and promotion of alternative test methods and further coordinates the evaluation of those at the European level.

1.1.1 Toxicology in drug development

Drug discovery and development describes the process a new molecular (chemical or biological) entity must pass through before eventually being marketed. This process is time and cost intensive and takes on average 10 – 15 years from discovery to the market and the estimated costs for research and development are about 1.2 billion US dollars per drug (EFPIA, 2014). Drug discovery and development is a tiered process by which the number of drug candidates decreases with every tier, as unfavorable candidates are sorted out (figure 1.1).

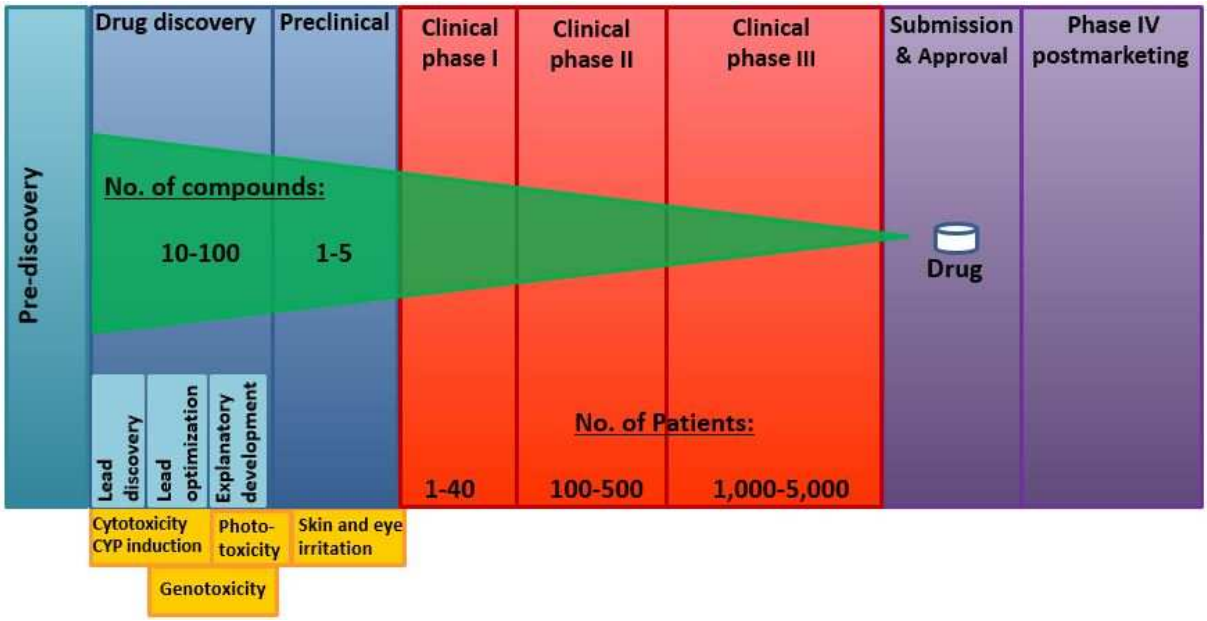

Figure 1.1: Drug discovery and development process from discovery to marketing. The discovery phase can be further divided into lead discovery (LD), lead optimization (LO) and exploratory development (ED), in which supportive *in vitro* test batteries are implied, but may vary across companies (adapted from PhRMA 2015, modified).

This process starts within basic research, in which a solid knowledge base is built to understand the molecular mechanisms underlying a certain disease and thus enabling the elucidation of potential biological targets (usually a protein or a gene, referred to as "pre-discovery in figure 1.1) that are manipulatable by a potential new drug candidate. Thereby, the targets need to be validated and their distinct involvement in the disease must be proven and subsequently, test molecules must be tested for their ability to interact with the target depending on how it needs to be altered in order to ameliorate or eliminate the outcome of the disease.

A common way to select compounds in those early stages is the screening of large compound libraries for their potential ability to interact with the drug target of interest. This process is known as Hit Discovery and often results in lists of more than 1,000 compounds. In order to narrow the number of hits, *in silico* methods are used, which sort out unfavorable compounds by physicochemical properties given by a compound's structure (SAR = structure activity relationship). Subsequently, the compounds are ranked according to their potency for target activity and the effective concentration should be relevant to achievable plasma concentrations. Early tests of drug efficacy (*in vivo*) as well as absorption, distribution, metabolism, excretion (ADME, *in vitro* and *in vivo*) and toxicity (*in vitro*) are conducted to identify the most valuable lead compounds and eventually the preclinical candidates (1- 5 candidates) for regulatory preclinical testing.

During the preclinical phase, the compounds must pass a battery of tests including efficacy, formulation analysis/optimization, drug metabolism and pharmacokinetics (DMPK) toxicity

and safety pharmacology (*in vitro* and *in vivo*). This battery ensures that a drug candidate is appropriate for entering clinical trials.

In phase I clinical trials, the drug candidate is either tested in healthy volunteers or patients (first in human), depending on the severity of the targeted disease – e.g. therapeutics that are developed for the life-prolongation of severe, life-threatening diseases such as late stage cancer medication are tested in patients as the severity of expected side effects is accepted for the patient population but not for healthy volunteers, whereas drug candidates for the therapy of non-life-threatening diseases, for which no severe side effects are expected, are tested in volunteers. The major aims of phase one clinicals trials are to address the tolerability, side effects and pharmacokinetics. If phase I is passed by a candidate, it enters phase II clinical trial, in which it is administered to a small group of patients (100 – 500) depending on the intended indication. Phase II studies are considered as proof of concept trials, in which the therapeutic efficacy of the candidate is confirmed. Following phase II, a larger group of patients are exposed during phase III in order to assess the candidate's safety, dose-response relationship and risk-benefit analyses. After the successful completion of all phases and approval of the marketing application by the regulatory authorities, the new drug is launched onto the market, where it enters phase IV (post-marketing phase or pharmacovigilance) in which adverse effects of either very low incidence or in specific subpopulations may be monitored.

1.1.2 Strategies of early safety assessment

During pre-clinical drug development, a potential drug candidate is assessed in terms of safety via a battery of *in vitro* and *in vivo* tests to deliver a comprehensive toxicological profile. Already during lead discovery, *in silico* toxicology is used to enable toxicity prediction(s) (Simon-Hettich et *al.*, 2006) based on the chemical structure, which helps to prioritize compounds and/or optimize high throughput hit. Subsequently, *in vitro* and *in vivo* toxicity studies are conducted in order to support candidate selection. These later stage studies are performed in accordance with the recommendations of regulatory authorities (e.g. U.S. Food and Drug Administration (FDA)), which are responsible for the approval of clinical trials and marketing authorization of new drugs. Many guidelines exist that describe the safety testing strategies required during development, with two major sources: The International Conference on Harmonization of Technical Requirements for Registration of Pharmaceuticals for Human Use (ICH) and the Organization for Economic Co-operation and Development (OECD). Guidelines exist that cover all safety aspects, e.g. carcinogenicity, genotoxicity, safety pharmacology etc. All studies that are required for approval are performed according to accepted guidelines under Good Laboratory Practice and/or other company-specific quality management procedures in order to guarantee a study´s quality.

Overall, toxicology in the pharmaceutical industry aims to a) characterize a drug's safety profile, b) assess the risk associated with drug intake and c) comply with regulatory requirements.

However, attrition of drug candidates cannot be fully eliminated, either due to poor efficacy or safety issues, which account for a high percentage of failures in later stages of drug development (Arrowsmith, 2011a/b, Kola and Landis, 2004, Kenna et *al.*, 2018). This puts pressure on the pharmaceutical industry to improve their strategies of early non-clinical safety assessment, including the development of advanced *in vitro* approaches with higher physiological relevance.

1.2 Drug-induced liver injury

1.2.1 Morphology and physiology of the liver

The liver is the largest gland in the human organism and manages a variety of different functions. In addition to the utilization of nutritional components and the generation of essential proteins, it produces bile in order to emulsify nutritional lipids for a more efficient gastrointestinal absorption. It is localized in the right upper abdomen below the diaphragm and it can be defined macroscopically into four lobes. The blood supply is supplied by two different vessels: the hepatic artery transports blood with high oxygen content from the lungs to the liver whereas the portal vein supplies nutritional components absorbed by the intestines.

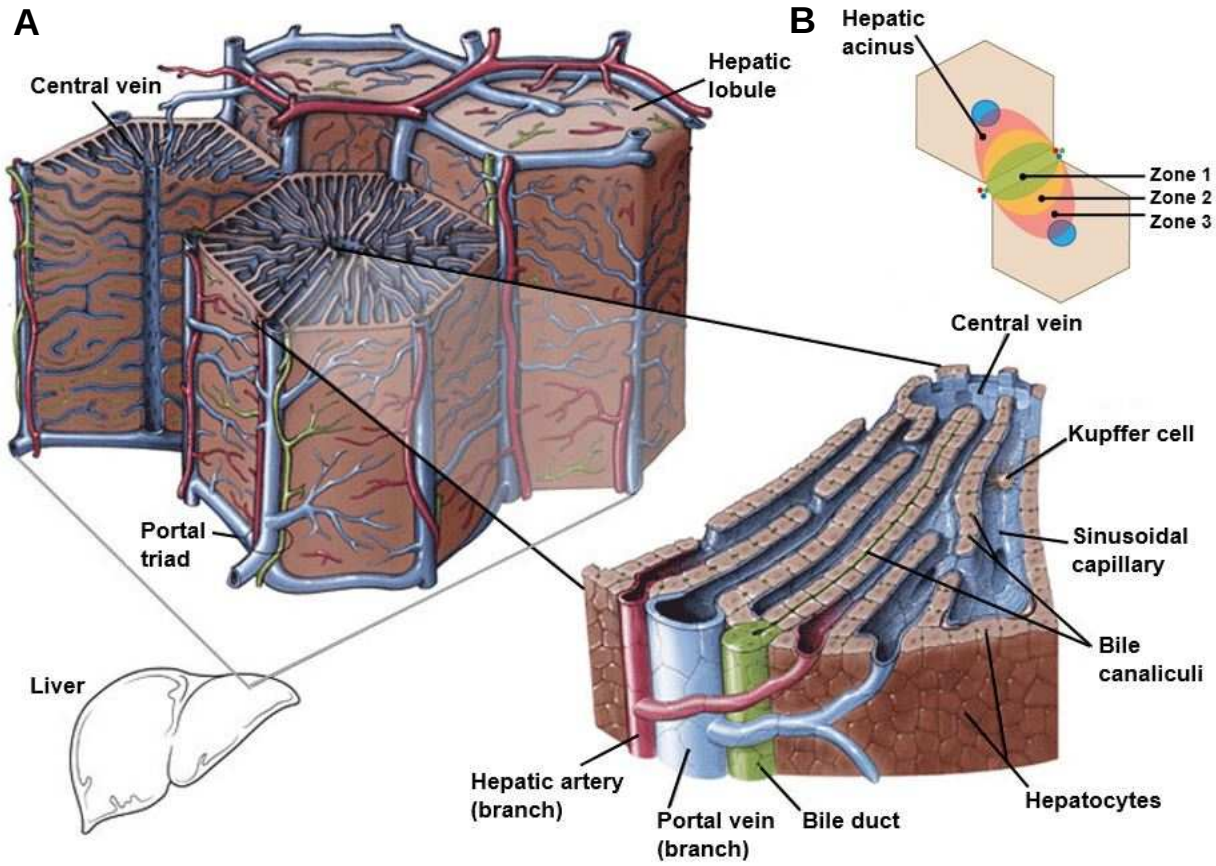

Figure 1.2: Schematic overview of hepatic microarchitecture. A: Hepatocytes are arranged in radial chords from central veins to portal triads, separated from one another by sinusoidal capillaries. Biliary system between hepatocytes is separated from capillary system by various junctions. B: schematic description of lobules (hexagonal) as structural unit and acini (oval) as functional unit showing hepatic zonation (Figure taken from Hitachi Medical Systems America Inc., modified).

Microscopically, two different unique units exist, of which the lobule represents the structural unit and the acinus represents the functional unit. The lobule consists of the central vein at the center of the structural unit and portal triads build the border to the next lobules and hepatocytes radiate in cords from the central vein to the perimeter of the lobule (figure 1.2).

In contrast, the functional unit is based on the microcirulation and is limited peripherally by the central veins. Within the acinus, the molecular environment changes from the centre to the periphery, including various physiological gradients, resulting in three distinct zones in which hepatocytes are metabolically adapted (table 1.1) (Probst and Jungermann 1983, Reid et *al.*, 1992, Turner et *al.*, 2011).

Table 1.1: Microenvironment differences and main hepatocyte functions in zones 1, 2 and 3

Zone	Microenvironment	Primary function
1- periportal	O_2↑, CO_2↓, P-450↓	Oxidative metabolism, Gluconeogenesis, Ureagenesis
2- midlobular	Mixture of zones 1 and 3	Mixture of zones 1 and 3
3- pericentral	O_2↓, CO_2↑, P-450↑	Glycolysis, Liponeogenesis, Xenobiotic metabolism

These zonal differences consequently result in different gene expression patterns and also susceptibilities to injury may vary (Black et *al.*, 1984). For example, xenobiotics such as Acetaminophen, which are metabolized to reactive species by CYP enzymes, often produce zone 3 hepatotoxicity due to the higher P-450 expression that subsequently leads to enhanced generation of reactive species (Zimmerman, 1999).

1.2.1.1 *Microstructure and cell types*

Hepatocytes are arranged in cords, which are commonly one hepatocyte thick and separated from one another by sinusoids, the hepatic capillaries. The exchange of substances takes place through the generously fenestrated endothelium of the sinusoids, whereby molecules up to 250kDa can easily pass into the interstitial space, called space of Disse (figure 1.3).
About 70% of the hepatocyte surface is exposed to the space of Disse and exchange takes place in both ways, via both active and passive transport mechanisms (figure 1.3).

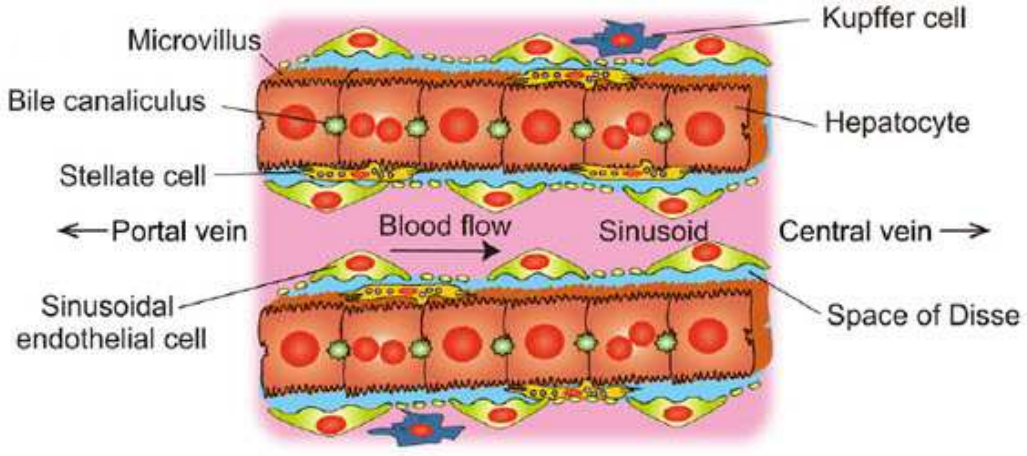

Figure 1.3: Schematic overview of sinusoidal architecture including the major cell types. Endothelial cells are generously fenestrated and line the space of Disse. Bile canaliculi are junctionally separated from the sinusoidal domain. (Figure taken from Yamada and Utoh et *al.*, 2012)

Table 1.2: Overview of metabolic functions performed in the liver. Hepatocytes account for a variety of metabolic turnover tasks

Carbohydrate metabolism	• Providing constant blood glucose
	• Gluconeosynthesis-glucogenolysis-gluconeogenesis-glycolysis
	• Recycling of fructose and galactose
Protein metabolism	• Synthesis of liver-specific plasma proteins
	• Modification and degradation of amino acids and proteins
	• Urea synthesis
Lipid metabolism	• *De novo* synthesis of fatty acids from glucose
	• Synthesis of triglycerides and lipoproteins
	• Synthesis and ester interchange of cholesterol
	• Synthesis of bile acids
	• Degradation of lipids and fatty acids
Biliary excretion	• Bile production
	• Heme synthesis
	• Glucuronidation of bilirubin

Hepatocytes (parenchymal) account for 80% of total liver mass and the majority of the liver´s physiological functions, including xenobiotic transformation and elimination of metabolites (Rhodes et *al.*, 2011). Hepatocytes are of cuboidal shape and are generally rich in mitochondria, both smooth and rough endoplasmic reticulum as well as lysosomes as a result of the broad spectrum of metabolic tasks, which are briefly listed in table 2. Based on the zonal microenvironment, hepatocytes are very heterogeneous in both functional and morphological aspects (Traber et *al.*, 1988, Gebhardt et *al.*, 1992, Lindros et *al*., 1997). Under normal conditions, parenchymal cell size increases from zone 1 to 3 in addition to distinct zonal variation of cellular components, including endoplasmic reticulum, mitochondria and glycogen storage as a consequence of the higher metabolic capacity (Michaels et *al.*, 1984, Ferri et *al.*, 2005).

Given the unique microenvironment, hepatocytes are highly polarized cells with two distinct domains, separated from one another by junctional complexes (figure 1.3). These membrane domains exhibit structural, functional and thus compositional differences and are essential for the overall metabolic function (van Montfoord et *al.*, 2003).

Under physiologic conditions, hepatocytes are responsible for the efficient transport of endogenous and exogenous substrates from blood into bile (Klaassen and Watkins, 1990). Bile production is primarily concerned with the delivery of components to the gastrointestinal system that are essential for fat absorption (Rhodes et *al.*, 2007); but bile also contains metabolites from endo- and exogenous transformation processes that need to be excreted. This requires a coordinated transport machinery for both biliary and sinusoidal domain and perturbation of these can lead to intrahepatic cholestasis (Hubbard et *al.*, 1985, Simons and Fuller, 1985, Klaassen and Aleksunes, 2010).

Although hepatocytes account for the majority of liver mass, various other hepatic cell types exist, which are much lower in percentage but are physiologically essential.

Liver sinusoidal endothelial cells (LSEC) line the walls of hepatic sinusoids and are flattened and elongated cells with fenestrations of 50-200nm. They allow free diffusion of many substances resulting in enhanced hepatocyte exposure to soluble components (Braet and Wisse, 2002, Cogger et al., 2010, DeLeve et al., 2007a). LSEC play an important role as they serve as a 'selective sieve' for substances passing from blood to hepatocytes and vice versa; they act as a 'scavenger system' by clearing the blood of macromolecular waste products (DeLeve et al., 2007a) and contribute to hepatic immunity (DeLeve et al., 2004; Perri and Shah, 2005).

LSEC are also capable for biotransformation and thus are a potential target for some types of chemical-induced toxicities (Deaciuc et al., 2001, Xie et al., 2010). Although metabolic capacity is below one tenth of that of hepatocytes, their role in clearance has been underestimated (Schrenk et al., 1991, Sacerdoti et al., 2003, Wu et al., 2008).

Hepatic stellate cells (HSC), also known as Ito-cells, reside in the space of Disse and show extensive dendrite-like structures actually "embracing" the sinusoids enabling intensive intercellular communication through soluble mediators (Asahina et *al.*, 2009, Friedmann et *al.*, 2008). HSC also store vitamin A, control turnover and production of extracellular matrix components such as collagens, elastin and proteoglycans (Wang et *al.*, 2010, Parola and Pinzani, 2009). During liver injury, HSC are activated and produce both cytokines and growth factors, which can contribute to both the inflammatory response and regeneration (Ramadori et *al.*, 2008, Parola and Pinzani, 2009).

Kupffer cells (KC) are resident hepatic macrophages with a pronounced endocytotic capacity (Jaeschke et *al*., 2007; Roberts et *al.*, 2006). They play a crucial role in immune surveillance by being able to control immune responses to infections via antigen presentation and impacting the activation and proliferation of T-cells (Kolios et *al*., 2006). During liver injury, KC have been found to stimulate liver regeneration and are also able to modulate hepatocyte metabolism by downregulation of xenobiotic metabolism (Sunman et *al.*, 2004, Higuchi et *al.*, 2007, Morgan et *al.*, 2009).

Cholangiocytes are biliary epithelial cells lining the bile ducts and account for ~5% of the hepatic cell population. They are heterogenous in morphology, expression and secretion patterns, as well as in the response to hormones, cytokines, bile acids and toxins (Marzioni et *al.*, 2002, Glaser et *al.*, 2006). Functionally, cholangiocytes have an important impact on regulating hepatic immune responses through cytokine secretion and are also capable of direct interaction with immune cells through expression of adhesion molecules (Fava et *al.*, 2005, Glaser et *al.*, 2009). Cholangiocytes are actively involved in various absorption and secretion processes and bile secretion is initiated by the release of bicarbonate that

generates bile salt independent flow (Tietz and LaRusso, 2006, Xia et *al.*, 2006). In diseased states, the role of these cells has been underestimated regarding the large number of injuries for which cholangiocytes are the primary target (Glaser et *al.*, 2009, Strazzabosco and Fabris, 2008).

Hepatic progenitor cells (HPC) are bipotential stem cells that are responsible for the enormous hepatic regenerative capacity and reside in the most peripheral hepatic branches, called canals of Hering (Gaudio et *al.*, 2009, Turner et *al.*, 2011). Under normal conditions HPC remain quiescent and serve as a reserve compartment, which is only activated when continuous damage and/ or severe cell loss occurs by expanding and maturation to either hepatocytes or cholangiocytes (Vig et *al.*, 2006, Santoni-Rugiu et *al.*, 2005, Libbrecht et *al.*, 2001, Bird et *al.*, 2008).

Both the biotransformation of xenobiotics and the high exposure level of the liver to orally administered foreign substances makes the liver one of the major organs of toxicological interest.

1.2.2 Xenobiotic metabolism

A critical task of the liver is to enzymatically transform toxic or potentially toxic compounds into harmless and excretable molecules. While hydrophilic and volatile substances are more likely to get rapidly eliminated via bile/ urine and exhalation, respectively, the elimination of lipophilic substances requires them to undergo transformation into more hydrophilic derivates, which can then be excreted. This transformation process is covered by a large variety of xenobiotic metabolizing enzymes and is as an evolutionary necessity to cover the large number of foreign chemical structures that can enter the human body. The effective and fast elimination of molecules depends on the following:

- Metabolites should be sufficiently water soluble
- Metabolites should not have biological activity that could cause toxic effects
- The substrate specificity of the enzyme system should be sufficiently broad in order to enable metabolism of all xenobiotics

It is almost impossible to fulfil all of these attributes since increased hydrophilic properties could generate metabolites being more reactive than their parent compounds, which is called toxification.

The metabolism of xenobiotics and the better understanding of its mechanisms is an essential part of drug development. A clear understanding of the pharmacokinetics of drugs can help in the understanding of unexpected toxicological effects or reveal differences between species and individuals.

Biotransformation occurs generally in three different phases, each of them composed of a specialized enzymatic or transport machinery. Phase one is a functionalizing step in which enzymes catalyze the insertion of a functional group into the substrate in order to facilitate the reactions taking place in phase two (members of the Cytochrome-P450 (CYP) family). One feature of CYP enzymes is their overlapping substrate specificity whereby a low turnover is implied and a total of over hundred different enzymes are involved in xenobiotic metabolism whereof a majority is manipulatable by substrates (Sipes and Gandolfi, 1991, Klaassen and Rozman, 1991). The division into subfamilies occurs by sequence affinity of the isoenzymes. CYPs are membrane bound enzymes, localised in the smooth endoplasmic reticulum and are associated with CYP-reductase when activated. The following table gives an overview of the enzymes involved in drug metabolism in phases I and II.

Table 1.3: Most important enzymes for functionalization (Phase I) and conjugation (phase II) reactions in drug metabolism.

Phase I	Phase II
Cytochrome P450 monooxygenases (CYP)	Glutathione-S-transferases (GST)
Monoamineoxidases (MAO)	UDP-glucuronosyl-transferases (UGT)
Cyclooxygenases (COX)	Sulfotransferases (SULT)
Flavin-dependent monooxygenases (FMO)	Acetyltransferases (AT)
Hydrolases	
Reductases	

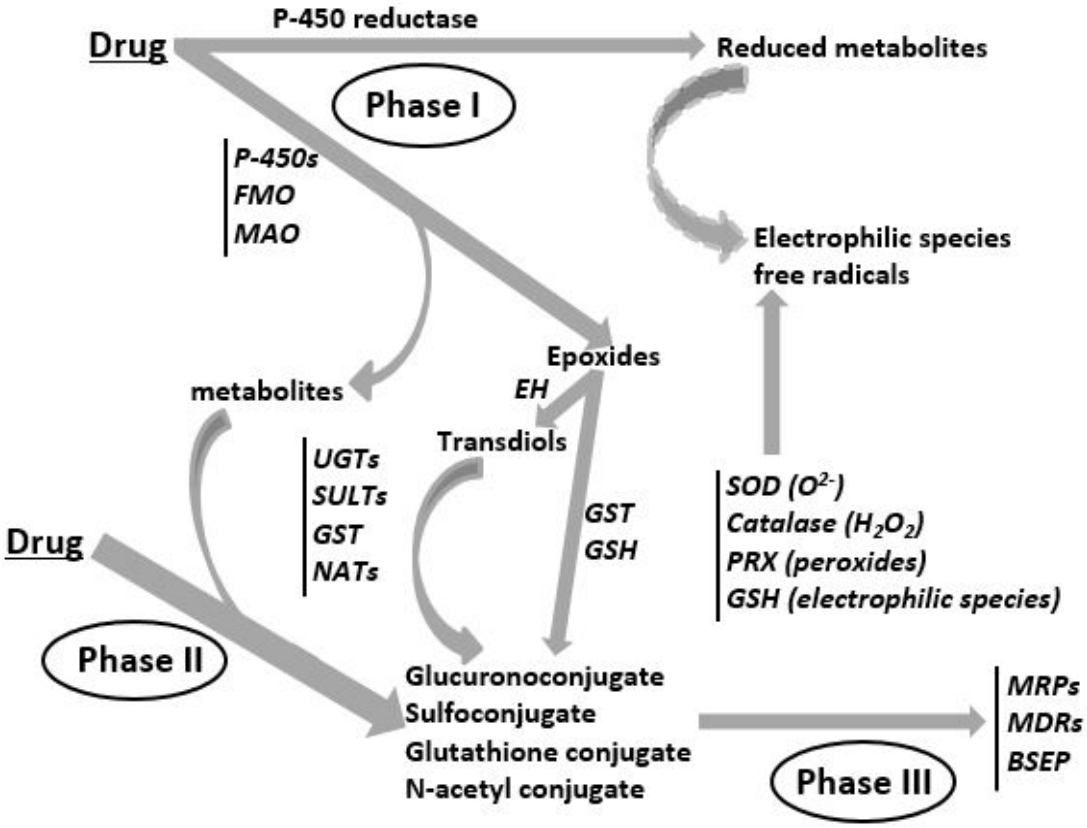

Figure 1.4: Overview of metabolic possibilities a drug can undergo. Depending on the physicochemical properties of the mother compound, metabolism via phase I or direct conjugation through phase II is possible as well as the generation of reactive metabolites, which can be deactivated in several ways. P-450 = Cytochrome P-450; FMO = Flavin-dependent monooxygenase; MAO = Monoamineoxidase; EH = Epoxidhydrolase; UGT = UDP-glucuronosyltransferase; SULT = Sulfotransferase; GST = Glutathione-S-transferase; NAT = N-acetylatransferase, GSH = Glutathion; SOD = Superoxide-dismutase; PRX = Peroxiredoxin; MRP = Multidrug resistance related protein; MDR = Multidrug resistance protein; BSEP = Bile salt export pump.

Most oral xenobiotics, among them potential toxins, are absorbed by the intestines and absorbed into the blood from where they enter the liver via the portal vein. In general, the metabolism of a lipophilic substance starts with functionalization by phase I enzymes, which either transfer oxygen or remove electrons from the molecule. Enzymes of phase I are mainly oxidoreductases and hydrolases or dehydrogenases, which either remove or insert hydrogen into their substrate. Generally, CYPs transfer single oxygen atoms from molecular oxygen to their substrates (Sipes and Gandolfi, 1991; Ziegler, 1988; Armstrong, 1987).

Most important for drug metabolism are the CYP families 1 to 3 (Ingelmann-Sundberg, 2001 and 2003). The CYP1 isoenzymes transform planar lipophilic substances and their expression is inducible via the AhR (arylhydrocarbon receptor). The CYP2 isoenzymes are numerous and many are involved in drug metabolism (e.g. CYPs 2B6, 2D6 and 2C9), whereas CYP3 isoenzymes represent 30% of hepatic CYP and have a broad and diverse spectrum of substrates (Ingelmann-Sundberg, 2001 and 2003; Sipes and Gandolfi, 1991). CYP3A4 accounts for the metabolism of approximately 50% of the marketed drugs, thus

playing an important role in the hepatotoxicity assessment applications in early drug development (Ingelmann-Sundberg 2001 and 2003).

Following phase I transformation, three different fates can occur. First, a direct excretion of the product is possible or second, the intermediate enters phase II. The third option occurs in cases where phase I metabolism generates reactive species with either electrophilic or nucleophilic properties. These reactive intermediates can bind to endogenous macromolecules such as proteins, DNA or lipids and thus may have an important impact on cell function and viability (Goldstein and Faletto, 1993; Guengerich and Liebler, 1985).

Phase II metabolism has the aim to add hydrophilic groups to the products of phase I by conjugation with a hydrophilic endogenous molecule, such as glutathione or glucuronic acid in order to facilitate effective elimination (figure 1.4). The fact that phase II reactions require both energy and valuable molecules emphasizes the importance of this step. The conjugation with endogenous agents facilitates an effective excretion by increasing water solubility. One of the most important phase II reactions is conjugation to glutathione, a detoxification reaction that not only enhances hydrophilic properties but also acts as a scavenger for electrophilic metabolites that would otherwise react with cellular macromolecules (Goldstein and Faletto, 1993; Guengerich and Liebler, 1985). In summary, phase II enzymes conjugate drug metabolites with body-own molecules in order to facilitate excretion via transporters in phase III.

Phase III metabolism is concerned with an effective excretion of drug metabolites and can take place via kidney (urine) or liver (bile), depending on the metabolite's physicochemical properties. If sufficiently water soluble, metabolites diffuse into blood and are filtrated in the kidney, whereas hepatobiliary excretion occurs by active transport from the hepatocyte into the bile canaliculus. The transporters are members of the ABC-binding cassette transporter family, called multidrug resistance proteins (MRPs) and multidrug resistance-associated proteins (MDRs).

1.3 Hepatotoxicity in drug development

Besides drug-mediated cardiotoxicity, drug-induced liver injury (DILI) has emerged as a frequent cause of drug withdrawal in late developmental stages or even post marketing (Kenna et *al.*, 2018). This points to serious limitations in the current preclinical *in vitro* and *in vivo* testing strategies. There is a broad spectrum of DILI manifestations, ranging from a variety of metabolic diseases and jaundice to acute liver failure due to massive hepatocyte necrosis. The reason for this is given by the unique role of the liver as the central organ for both nutrient and xenobiotic metabolism, which gives evidence that the liver is often the primary target organ for chemical insult.

Generally, DILI can be separated into two fundamental classes:

1. Dose-dependent hepatotoxicity, which is defined by adverse effects due to drug intake beyond pharmacological doses, appears in a dose-dependent fashion and is typically reproducible in various commonly used animal models such as rat or dog.
2. Human-specific adverse drug reactions, which cannot be easily predicted in animal models. These idiosyncratic reactions can occur at therapeutic exposure levels and are usually very rare, ranging from 1 in 10,000 to 1 in 100,000 patients treated.

For the latter several reasons exist explaining the inability to fully cover those events during preclinical and even clinical phases:

- Human specificity cannot be fully modelled in the commonly used animal models due to substantial inter-species differences in physiology and drug metabolism.
- Human *in vitro* models lack physiological integration and are mostly composed of single cell types, which do not mimic the *in vivo* microenvironment. This is emphasized by the fact that in a variety of adverse effects both homogenous and heterogenous cross-talk is required for a toxic insult to emerge to overt hepatotoxicity.
- Idiosyncratic reactions have generally low incidences and the relatively small number of participants in clinical phases I and II make the detection very unlikely.
- Preclinical test strategies are not capable of covering risk factors that may contribute to DILI development in individuals. These factors include genetic (e.g. CYP polymorphisms), as well as lifestyle aspects and predisposition (e.g. nutritional state, co-morbidity and co-administered drugs or alcohol intake).

There is an urgent need for more predictive test systems to elucidate potential risks in man or in susceptible subpopulations. Regarding the many facets of DILI in man, it is important for innovative applications to focus on the underlying mechanisms and to not only predict hepatotoxicity so that the pattern and severity of the outcome can be better understood. In the following, the five main mechanisms of hepatotoxicity are briefly described.

1.3.1 Reactive metabolites

Although the human detoxification system is exceedingly efficient in the elimination of large numbers of different chemical structures due to overlapping substrate specificities, it is feasible that a compound can be metabolized into a more reactive derivate. Reactive metabolites are mostly electrophilic and may react with a variety of subcellular structures, such as proteins, membranes or nucleic acids and thus inactivate or destroy them. The most prominent example for this is acetaminophen, also known as (Paracetamol), which leads to metabolite-mediated severe acute liver failure when taken at very high doses. Acetaminophen is metabolized to N-acetyl-p-benzo-quinoneimine (NAPQI) by CYP2E1,

which is strongly electrophilic and normally quenched by conjugation to glutathione (GSH). In the case of acetaminophen overdose, the intracellular scavenger GSH depletes and NAPQI then covalently binds to cellular proteins, leading to multiple scenarios, e.g. oxidative stress or mitochondrial dysfunction (Mitchell et *al.*, 1973; Donnelly et *al.*, 1994; Meyers et *al*., 1988).

1.3.2 Inhibition of bile salt transporters

Bile formation is an essential hepatic function for both an efficient digestion of nutrients as well as for the elimination of metabolites with less hydrophilic properties. The perturbation of bile secretion can lead to retention of bile within the liver and subsequently to an impaired gastrointestinal performance and also hepatocyte apoptosis and/or necrosis due to bile salt intoxication (Patel et *al.*, 1998). Although cholestatic pathogenesis is multifactorial, hydrophobic bile acids are especially cytotoxic and the failure to secrete them results in liver injury, cirrhosis and death from liver failure (Rodrigues et *al.*, 1998; Strautnieks et *al.*, 1998). Bile acids are actively secreted by the bile salt export pump (BSEP), which displays a hepatic target for drugs or their respective metabolites via blocking or covalent binding and thus impairing or inhibiting BSEP performance. This subsequently leads to a toxic intrahepatocellular retainment of bile salts, which can manifest as cholestasis.

1.3.3 Mitochondrial dysfunction

Since the liver is a versatile organ, which requires high energy levels, hepatocytes are densely packed with mitochondria in order to sufficiently supply ATP. However, mitochondria also fulfil a variety of functions to maintain cellular homeostasis, including fatty acid oxidation, steroid- and heme synthesis, thermogenesis and apoptosis signalling. Furthermore, mitochondria contain their own set of organelle-specific genes, called mitochondrial DNA (mtDNA). Due to this complex panel of different functions, mitochondria are a common target of drugs, which can cause disturbed function. Regarding only the mitochondrial respiratory chain, which contains five different complexes in order to produce ATP through electron transport, it becomes very clear that mitochondria has many possible action points where drugs can have an impact on the function of mitochondria.

Another mechanism is related to the onset of mitochondrial permeability transition (MPT), caused by opening of permeability transition pores in the inner mitochondrial membrane. Permeability transition pore opening subsequently causes mitochondrial depolarization, as well as swelling and can lead to both, apoptosis and necrosis (Lemasters et *al.*, 1998; Pessayre et *al.*, 1999; Berson et *al.*, 2001). Mitochondrial swelling often causes ruptures in the outer membrane and thus precedes the release of cytochrome c, which can initiate apoptosis via activation of cytosolic caspases (Haouzi et *al.*, 2000; Hatano et *al.*, 2000).

Generally, microvesicular steatosis is the histological hallmark of severe metabolic perturbations due to mitochondrial dysfunction, leading to energy shortage and decreased delivery of energy substrates, which can also lead to impairments of other organs, e.g. hepatic and renal failure or pancreatitis (Fromenty and Pessayre, 1995).

1.3.4 Lysosomal dysfunction

Lysosomes are important intracellular vesicles that are responsible for the degradation of the major groups of macromolecules, which are taken up by endocytosis, by various hydrolytic enzymes. This enzymatic machinery only works in the acidic lysosomal microenvironment, which prevents uncontrolled cytosolic (pH neutral) digestion in the case of lysosome rupture. Perturbation of these catabolic centres by drugs can result in e.g. phospholipidosis, which is characterized by the formation of lamellar bodies (Robinson et *al.*, 1985; Anderson and Borlak, 2006). Lamellar bodies can be described as cytosolic inclusions consisting of concentric structures of non-degraded phospholipids and are commonly induced by cationic amphiphilic drugs like amiodarone (Kodavanti and Mehendale, 1990; Halliwell et *al*., 1997). These drugs bind to phospholipids, which then become undegradable and can lead to immune reactions after uptake by marcophages (Halliwell et *al.*, 1997). Drugs can also inhibit phospholipases, which also results in lamellar bodies (Reasor and Kacew, 2001).

1.3.5 Immune-mediated liver injury

Drug hypersensitivity reactions are of idiosyncratic nature and they remain challenging to detect before a new drug enters the market. Regarding the uniqueness of every individual's immune composition, drugs can induce hypersensitivity reactions in single patients and the outcome is broad, ranging from anaphylactic effects restricted to cutaneous reactions to severe effects on the respiratory or cardiovascular system (Moebs and Pfuetzner, 2017).
Generally, two concepts exist that describe how a certain drug can elicit immune effects within the liver, namely the hapten concept and the p-i concept.

- The hapten concept postulates that drugs with a molecular weight below 1,000 Da are too small to initiate an immune response per se, so that those compounds can covalently bind to proteins or peptides and thus a so called neoantigen is formed, which can cause response of both the innate and the specific immune system (Naisbitt et *al.*, 2000; Pichler, 2002; Padovan et *al.*, 1997).
- In contrast, the "p-i" concept stands for "direct pharmacological interaction of drugs with immune receptors" and states that small molecules can specifically and reversibly bind to some highly variable antigen specific receptors and may cause

inflammatory reactions of different types (Pichler, 2002 and 2008; Naisbitt et *al.*, 2003).

1.4 EU Project MIP-DILI

The work carried out for this thesis was part of the IMI (Innovative Medicines Initiative) EU funded project MIP-DILI ('**M**echanism-based **I**ntegrated systems for the **P**rediction of **D**rug-**I**nduced **L**iver **I**njury'). The IMI's overarching aim is the improvement of patient health by speeding up the development process and also patient access to innovative medicines, especially in therapeutic areas with an unmet need.

The major focus of MIP-DILI was the improvement and further development of preclinical testing strategies for the prediction of drug-induced liver injury in man. MIP-DILI is a collaboration between industrial EFPIA (European Federation of Pharmaceutical Industries and Associations), SME's (small and medium-sized enterprises) and academic partners.

Drug-induced liver injury has emerged as the most common cause of liver failure and post-marketing withdrawal of drugs in western countries (Kenna et *al.*, 2018). Thus, predicting DILI in early drug developmental stages remains challenging and the project consortium attempted to address this issue focusing on the five main mechanisms leading to DILI (see 1.2.3).

The project aims to first deepen the understanding of the underlying scientific background of DILI and use this knowledge to both evaluate current standard approaches as well as to develop improved test methods (figure 1.5). This also implies that the inter-individual differences among patients are considered and implemented in emerging test systems for the better elucidation of differences in susceptibility towards chemical insults.

The information generated will also add massive value on the development of mathematical modelling approaches for an improved predictivity by *in silico* tools.

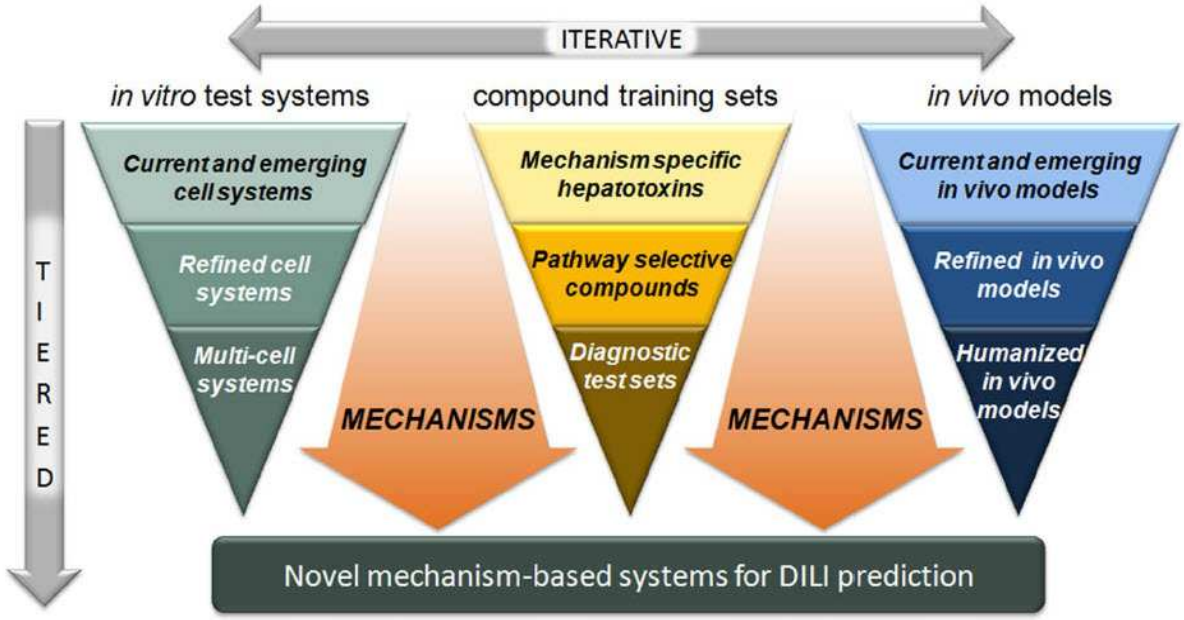

Figure 1.5: Schematic overview of the MIP-DILI project strategy. The approach concerns three aspects, *in vitro* and *in vivo* systems as well as mechanism addressing compound sets. The currently used test systems are assessed at first and subsequently refined and further developed towards enhanced human relevance. (figure taken from the MIP-DILI project consortium, 2012)

MIP-DILI aims to identify and validate an improved panel of *in vitro* best practice assays for predicting DILI in the human population. This will be achieved by an iterative tiered approach with respect to test compounds and test systems with the background that DILI manifests as a broad spectrum of biological processes that range from effects on single pathways in single cells to complex multi-cellular processes. By integration of bioanalysis, modelling and systems biology at every tier, both current and emerging *in vitro* and *in vivo* test systems will be reflected with respect to:

- Human hepatic physiology
- Adaptive hepatic response
- Changes in liver cell populations following drug exposure
- Complex multi-cellular and time-dependent events in the liver associated with DILI

This strategy is underpinned by the selection of appropriate reference compounds, including model hepatotoxicants, that selectively target specific pathways, drugs that address specific forms of DILI as well as drugs that cause DILI in man but not in preclinical test systems. Negative controls are also included, of which several have structural similarity to hepatotoxicants but are not associated with DILI. Based on these aspects, a training compound set was defined, which is described in table 1.4.

Table 1.4: MIP-DILI training compound set. Drugs that have been associated with at least one DILI mechanism as well as DILI negative compounds.

Compound	Therapeutic function	Postulated mechanisms	References
Acetaminophen	Analgesic	Reactive metabolite	Court et al., 2001; Laine et al., 2009
Amiodarone	Antiarrythmic	Mitochondrial/lysosomal dysfunction	Elsherbiny et al., 2008; Shayeganpour et al., 2006; Ohyama et al., 2000; Zahno et al., 2011; Hosomi et al., 2011
Bosentane	Antihypertensic	BSEP inhibition	Weber et al., 1999; Dingemanse et al., 2004
Buspirone	Anxiolytic	Negative	Zhu et al., 2005
Diclofenac	Analgesic	Mitochondrial dysfunction/reactive metabolite/BSEP inhibition	Kumar et al., 2002; Darnell et al, 2012; Kumar et al., 2002; Naisbitt et al., 2007; Shen et al., 1999; Kishida et al., 2012
Entacapone	Parkinson's disease	Negative	Lautala et al., 2000
Fialuridine	Hepatitis B therapy	Mitochondrial dysfunction	Govindarajan et al., 2008; Lai et al., 2004
Metformin	Antidiabetic	Negative	Tzvetkov et al., 2009
Nefazodone	Antidepressant	Reactive metabolite/ BSEP inhibition	Von Moltke et al., 1999; Kalgutkar et al., 2005; Hosomi et al., 2011
Perhexiline	Antianginal	Lysosomal dysfunction/ BSEP inhibition	Davies et al., 2005
Pioglitazone	Antidiabetic	Negative	Jaakola et al., 2006; Banghman et al., 2005; Alvarez-Sanchez et al., 2006
Tolcapone	Parkinson's disease	Reactive metabolite/ BSEP inhibition	Lautala et al., 2000; Smith et al., 2003
Troglitazone	Antidiabetic	Mitochondrial/ lysosomal dysfunction/ reactive metabolite/ BSEP inhibition	Saha et al., 2010; Yamamoto et al., 2002; Yoshikawa et al., 2009; Hosomi et al., 2011; Vignati et al., 2005
Ximelagatran	Anticoagulant	Immune-mediated	Clement et al., 2003; Darnell et al., 2010

The work described in this thesis is part of the *in vitro* work package, which focuses on the assessment of:

- How the current, routinely used *in vitro* test systems physiologically compare to each other as well as to human liver

- How emerging in vitro approaches add value to the current status
- How these novel approaches can be applied to routine preclinical safety assessment, as well as to what purpose they may contribute

1.5 Hepatic cell systems

1.5.1 Primary human hepatocytes

Primary human hepatocytes (PHH) are considered to be the gold standard for the majority hepatic *in vitro* applications, due to their high physiological relevance. Because of their origin, PHH retain much of their *in vivo* functionality and provide valuable results in pharmacological and toxicological *in vitro* research (Godoy et *al.*, 2013; Gerets et *al.*, 2012). Additionally, the fact that each PHH preparation is obtained from a different donor offers the possibility to investigate a limited range of genetic polymorphisms. However, donor-variability is also a challenge since inter-individual differences, as well as alterations due to isolation procedure cause variations in experimental results, thus hampering the standardization of PHH *in vitro* models (Rogue et *al.*, 2012). However, PHH also suffer from other limitations since it is known that the cells quickly lose their metabolic capacity when cultured as conventional 2D monolayers, so that physiologically relevant hepatotoxicity testing is only possible in short-term applications (Godoy et *al.*, 2013; Gerets et *al.*, 2012). The fact that many drugs as well as most drug-induced toxicities are characterized by chronic intake emphasizes the need for a culture system that allows prolonged repeat dose testing. Advanced culturing methods, like the collagen sandwich culture approach, allow PHHs to maintain their physiological functions for up to two weeks (Tuschl and Müller, 2005). In this format, cells keep their native shape thus essential polarity, however, this format is only applicable in larger culture dimensions and requires high cell numbers so that upscaling towards higher throughput screening remains difficult. PHH from one donor are limited in number, so that on the one hand large-scale use is often limited and on the other hand every batch needs to be validated. The consequence for the pharmaceutical industry is that PHH are, despite their high metabolic capacity, not easily applicable at high throughput screening or subchronic to chronic risk assessment and are relatively expensive especially for very early stages of drug development.

1.5.2 HepG2 cells

HepG2 cells are a hepatic cell line obtained from a human hepatoma and is widely used in *in vitr*o culture models, mainly due to their unlimited availability. They are a highly proliferative cell line with an average doubling time of approximately 33 hours and display a variety of physiological functions, such as albumin and Urea synthesis and glycogen storage. Although

HepG2 cells are often the first choice in early screening assays due to easy handling and low cost, they lack physiological relevance in terms of hepatic drug metabolism (Sison-Young and Mitsa et *al.*, 2015). It is well known that tumour derived cells undergo reprogramming, leading to uncontrolled growth and thus often dedifferentiate. In addition, artificial environment of plastic dishes and high-sugar culture media, results in very low drug metabolising activities. However, HepG2 cells are still a useful tool for early screenings or cytotoxicity assessment due to the stable phenotype as well as the resulting reproducibility (Gerets et *al.*, 2012). Their lack of metabolic capacity makes this cell line unattractive to more in-depth investigations of DILI prediction and mechanism analysis.

1.5.3 HepaRG®

HepaRG is a cell line derived from human hepatoma progenitor cells, which can differentiate in the presence of DMSO (Dimethylsulfoxide) into two different lineages namely hepatocytes and cholangiocytes. The differentiated cells are equally composed of both cell types, hepatocyte-like cells and cholangiocyte-like cells, which are microscopically distinguishable due to their shape and appearance (Aninat et *al.*, 2006; Gunguen-Guillouzo et *al*., 2004). Fully differentiated, HepaRG cells have several advantages in comparison to other cell lines, such as HepG2. The cells show a high degree of differentiation and stably maintain various hepatic functions of toxicologic interest, including CYP-dependent metabolism, CYP inducibility and expression of phase III transporters. Alongside with those enhanced functions related to xenobiotic metabolism, HepaRG already display a well-defined co-culture and thus heterogenous communication as well as the cell line related benefits of good reproducibility and easy handling. Overall, HepaRG cells are a promising *in vitro* model that, under properly defined culture conditions, can serve as an attractive surrogate model for primary human hepatocytes.

1.5.4 Upcyte® hepatocytes

Upcyte hepatocytes are a relatively new cell model developed by viral transduction of primary human hepatocytes with genes that upregulate proliferation (Braspenning et *al.*, 2010). The basal expression levels of drug metabolising enzymes (Phase I and II) have been reported comparable to 5-day cultures of primary human hepatocytes and that CYP inducibility of important CYPs is reported (Burkard et al., 2012). These features should mean that these cells have the advantages of PHH regarding metabolism and the limitless availability of cell lines, therefore displaying an attractive tool for early stages of drug development. Within the MIP-DILI project upcyte hepatocytes were only included in the initial cytotoxicity assessment of cell models. After the proteomic analysis revealed that upcyte

hepatocytes express drug metabolising enzymes at much lower levels, comparable to that of HepG2, they were dropped from further studies (Sison-Young and Mitsa et *al.*, 2015).

1.6 Personal contributions

This thesis was embedded in the EU-funded project MIP-DILI, which represents a collaboration of both industrial and academic partners with diverse scientific expertise. All generated data in this multidisciplinary team belongs to the MIP-DILI consortium. With the consent of the consortium, internal and external generated data of the cell models and the training compounds was used for this thesis. An overview of my personal contributions is given in the following paragraphs.

Comprehensive multi-site cytotoxicity assessment

Training compound selection was performed by AstraZeneca, based on literature search with focus on well studied compounds that cover the main DILI mechanisms.

I performed cytotoxicity experiments for the 13 training compounds in HepG2, HepaRG and Upcyte cells including two time points (24h and 72h) and two endpoints (ATP and Resazurin). Furthermore, I was mainly involved in the data collection from all participants as well as in the statistical analysis and the preparation of the publication manuscript. Interpretation of results and literature search was performed by Rowena Sison-Young (University of Liverpool), Volker Lauschke (Karolinska Institutet Stockholm) and myself.

Proteomic comparison of cell models

Cell culture and protein sample processing for HepG2, HepaRG and Upcyte cells was performed by myself. Protein samples were shipped to one partner (University of Liverpool), where further processing, analysis and statistical analysis was performed. Interpretation of results was performed by the University of Liverpool and discussed by all participating partners.

Spheroid cell culture

I performed the complete cell culture work (seeding, medium change and dosing for up to 28 days) as well as sample processing (viability measurement, preparation of paraffin-embedded and cryo microdissections, H&E staining and immunofluorescent staining, imaging and image analysis) on my own responsibility. I was responsible for image generation, analysis and biological interpretation of results. Results obtained in H&E stained microdissections were evaluated and discussed by Dr. Anja Knippel and myself. Statistical analysis, interpretation including literature search and discussion of the results were performed by myself.

Sample preparation (cell culture and lysis) and processing (hybridization, labelling and amplification) for the CYP induction study via branched DNA in HepaRG cells cultured in 2D and 3D were performed by myself. Yvonne Walter performed the measurement itself as well

as the primary raw data analysis; figure generation, data interpretation, literature search and discussion were performed by myself.

Comparison of cell culture formats

I performed the complete cell culture for each format as well as the protein isolation and further processing (protein quantification, SDS-PAGE Gel electrophoresis and western blotting). Moreover, literature seach, biological interpretation and discussion of the results was performed on my own responsibility.

2 Materials and Methods

2.1 Materials

2.1.1 Consumables

Name	Manufacturer, Corporate headquarters
15mL tubes, BD Falcon™	Becton Dickinson GmbH, Heidelberg, Germany
50mL tubes, BD Falcon™	Becton Dickinson GmbH, Heidelberg, Germany
24-well cell culture plates, clear BD Falcon	Becton Dickinson GmbH, Heidelberg, Germany
96-well cell culture plates, clear BD Falcon	Becton Dickinson GmbH, Heidelberg, Germany
96-well cell culture plates, black/clear BD Falcon	Becton Dickinson GmbH, Heidelberg, Germany
96-well cell culture plates, white/clear BD Falcon	Becton Dickinson GmbH, Heidelberg, Germany
96-well ultra-low attachment plates, round bottom	Corning Inc., Corning (NY), USA
96-well ultra-low attachment plates, round bottom, Nunclon sphera	Thermo Fisher Scientific, Waltham (MA), USA
Adhesive PCR foil seals, ABgene®	Thermo Fisher Scientific, Waltham (MA), USA
ART 10 REACH, disposable tips	Molecular BioProducts, San Diego (CA), USA
ART 20, disposable tips	Molecular BioProducts, San Diego (CA), USA
ART 100, disposable tips	Molecular BioProducts, San Diego (CA), USA
ART 200, disposable tips	Molecular BioProducts, San Diego (CA), USA
ART 1000E, disposable tips	Molecular BioProducts, San Diego (CA), USA
ART 1000G, disposable tips	Molecular BioProducts, San Diego (CA), USA
Bis-Tris gels for SDS-Page, 4-12%	Thermo Fisher Scientific, Waltham (MA), USA
Bottle Top Filters	Nalgene, Rochester (NY), USA
Cell counting chamber (Fuchs-Rosenthal)	LO-Laboroptik, Lancing, UK
CellStar cell culture flasks, 75cm^2	Greiner bioOne GmbH, Frickenhausen, Germany
CellStar cell culture flasks, 175cm^2	Greiner bioOne GmbH, Frickenhausen, Germany
Cell scrapers	Iwaki® cell biology, Asahi Techno Glass Corporation, Chiba, Japan

Coverslips, precoated	Roche Diagnostics GmbH, Mannheim, Germany
Coverslips, round	VWR International GmbH, Darmstadt, Germany
Cryomolds biopsy	Sakura Finetek Japan Co., Ltd., Tokyo, Japan
ECL Hyperfilm	GE Healthcare UK Ltd., Buckinghamshire, UK
Glass vials, brown, 1.5mL	VWR International GmbH, Darmstadt, Germany
HistBond +S adhesion glass slides	Marienfeld
iBlot, dry blot stacks mini	Thermo Fisher Scientific, Waltham (MA), USA
Parafilm, M	Bemis® Company Inc., Neenah (WI), USA
PCR tubes	Thermo Fisher Scientific, Waltham (MA), USA
Pipette tips 0.5 – 10µL	Brand GmbH&Co. KG, Wertheim, Germany
Pipette tips, 2 – 200µL	Brand GmbH&Co. KG, Wertheim, Germany
Pipette tips, 5 – 300µL	Brand GmbH&Co. KG, Wertheim, Germany
Pipette tips, 50 – 1000µL	Brand GmbH&Co. KG, Wertheim, Germany
Pipette tips, 12,5 µL, sterile, filter	Integra Biosciences AG, Zizers, Switzerland
Pipette tips, 125µL, sterile, filter	Integra Biosciences AG, Zizers, Switzerland
Pipette tips, 300µL, sterile, filter	Integra Biosciences AG, Zizers, Switzerland
Pipette tips, 1,250µL, sterile, filter	Integra Biosciences AG, Zizers, Switzerland
QV 900 6-well plates	Kirkstall Ltd, Rotherham, UK
QV 900 tubing 16”	Kirkstall Ltd, Rotherham, UK
QV 900 tubing 32”	Kirkstall Ltd, Rotherham, UK
QV 900 luerlocks female 16”	Kirkstall Ltd, Rotherham, UK
QV 900 luerlocks female 32”	Kirkstall Ltd, Rotherham, UK
QV 900 luerlocks male 16”	Kirkstall Ltd, Rotherham, UK
QV 900 luerlocks male 32”	Kirkstall Ltd, Rotherham, UK
QV 900 reservoir bottles, 25mL	Kirkstall Ltd, Rotherham, UK
QV 900 sterile filter, 0.2µm	Kirkstall Ltd, Rotherham, UK
Safe lock tubes, 1.5mL	Eppendorf KG, Hamburg, Germany
Safe lock tubes, 2mL	Eppendorf KG, Hamburg, Germany
Safe lock tubes, 5mL	Eppendorf KG, Hamburg, Germany
Serological pipettes, 1mL	Corning Inc., Corning (NY), USA
Serological pipettes, 5mL	Corning Inc., Corning (NY), USA
Serological pipettes, 10mL	Corning Inc., Corning (NY), USA
Serological pipettes, 25mL	Corning Inc., Corning (NY), USA
Serological pipettes, 50mL	Corning Inc., Corning (NY), USA
Superfrost glass slides	Thermo Fisher Scientific, Waltham (MA), USA
Superfrost plus adhesion glass slides	Thermo Fisher Scientific, Waltham (MA), USA

2.1.2 Chemicals and Reagents

Name	Manufacturer, Corporate headquarters
2-propanol	Merck KGaA, Darmstadt, Germany
Acetic acid, 96%	Merck KGaA, Darmstadt, Germany
Accutase cell dissociation reagent	Thermo Fisher Scientific, Waltham (MA), USA
Adefodur developer	Adefo Chemie GmbH, Dietzenbach, Germany
Adefodur fixer	Adefo Chemie GmbH, Dietzenbach, Germany
Antioxidant	Thermo Fisher Scientific, Waltham (MA), USA
Bradford reagent	BioRad Laboratories Inc., Hercules (CA), USA
BSA standard, 2mg/mL	Sigma-Aldrich (part of Merck KGaA), Munich, Germany
Collagen, from rat tail	Roche Diagnostics GmbH, Mannheim, Germany
Cytobuster protein extraction reagent, Calbiochem®	Merck KGaA, Darmstadt, Germany
DEPC treated water, Ambion®	Thermo Fisher Scientific, Waltham (MA), USA
Dexamethasone	Sigma-Aldrich (part of Merck KGaA), Munich, Germany
D-Glucose	Sigma-Aldrich (part of Merck KGaA), Munich, Germany
D-Galactose	Sigma-Aldrich (part of Merck KGaA), Munich, Germany
DMEM	Thermo Fisher Scientific, Waltham (MA), USA
DMEM/F-12	Thermo Fisher Scientific, Waltham (MA), USA
DMSO	Sigma-Aldrich (part of Merck KGaA), Munich, Germany
DPBS -/-	Thermo Fisher Scientific, Waltham (MA), USA
DPBS +/+	Thermo Fisher Scientific, Waltham (MA), USA
ECL Western Blot detection kit	GE Healthcare UK Ltd., Buckinghamshire, UK
Ethanol, 96%	Sigma-Aldrich (part of Merck KGaA), Munich, Germany
Epidermal growth factor	Thermo Fisher Scientific, Waltham (MA), USA
FBS, Fetal bovine serum	Thermo Fisher Scientific, Waltham (MA), USA
Formalin solution 4%	Merck KGaA, Darmstadt, Germany
Gentamicin	Thermo Fisher Scientific, Waltham (MA), USA
HCl, 1N	Sigma-Aldrich (part of Merck KGaA), Munich, Germany
HepaRG induction supplement	Thermo Fisher Scientific, Waltham (MA), USA
HepaRG metabolism supplement	Thermo Fisher Scientific, Waltham (MA), USA

HepaRG thaw, plate & general-purpose supplement	Thermo Fisher Scientific, Waltham (MA), USA
HepaRG tox supplement	Thermo Fisher Scientific, Waltham (MA), USA
Hepatocyte growth factor	Thermo Fisher Scientific, Waltham (MA), USA
Hoechst 33342	Thermo Fisher Scientific, Waltham (MA), USA
Insulin-transferrin-selenium	Thermo Fisher Scientific, Waltham (MA), USA
L –glutamine	Thermo Fisher Scientific, Waltham (MA), USA
Lysis Mixture	Affymetrix®, Santa Clara (CA), USA
Matrigel	Corning Inc., Corning (NY), USA
Matrigel high concentration	Corning Inc., Corning (NY), USA
Methanol	Sigma-Aldrich (part of Merck KGaA), Munich, Germany
Normal goat serum	Sigma-Aldrich (part of Merck KGaA), Munich, Germany
O.C.T. compound	VWR International GmbH, Darmstadt, Germany
Penicillin/ Streptomycin	Thermo Fisher Scientific, Waltham (MA), USA
Phosphatase inhibitor cocktail set II, Calbiochem®	Merck KGaA, Darmstadt, Germany
Protease inhibitor cocktail set III, Calbiochem®	Merck KGaA, Darmstadt, Germany
Proteinase K	Affymetrix®, Santa Clara (CA), USA
Protein ladder, prestained	Thermo Fisher Scientific, Waltham (MA), USA
Pura matrix	Corning Inc., Corning (NY), USA
Resazurin sodium salt	Sigma-Aldrich (part of Merck KGaA), Munich, Germany
RNAse away	Molecular BioProducts, San Diego (CA), USA
Rhodamine - Phalloidine	Thermo Fisher Scientific, Waltham (MA), USA
Triton x-100	Sigma-Aldrich (part of Merck KGaA), Munich, Germany
Trypan blue solution	Sigma-Aldrich (part of Merck KGaA), Munich, Germany
Trypsin EDTA	Thermo Fisher Scientific, Waltham (MA), USA
Tween-20	Sigma-Aldrich (part of Merck KGaA), Munich, Germany
Williams medium E, no glutamine	Thermo Fisher Scientific, Waltham (MA), USA
Williams medium E, no sodium bicarbonate, powder	Sigma-Aldrich (part of Merck KGaA), Munich, Germany
Xylene	Merck KGaA, Darmstadt, Germany

2.1.3 Test compounds

Name	Manufacturer, Corporate headquarters
Acetaminophen	Sigma-Aldrich (part of Merck KGaA),

	Munich, Germany
Amiodarone	Sigma-Aldrich (part of Merck KGaA), Munich, Germany
Bosentane	Sigma-Aldrich (part of Merck KGaA), Munich, Germany
Buspirone	Sigma-Aldrich (part of Merck KGaA), Munich, Germany
Chlorpromazine	Sigma-Aldrich (part of Merck KGaA), Munich, Germany
Diclofenac	Sigma-Aldrich (part of Merck KGaA), Munich, Germany
Entacapone	Sigma-Aldrich (part of Merck KGaA), Munich, Germany
Metformin	Sigma-Aldrich (part of Merck KGaA), Munich, Germany
Nefazodone	Sigma-Aldrich (part of Merck KGaA), Munich, Germany
Perhexiline	Sigma-Aldrich (part of Merck KGaA), Munich, Germany
Pioglitazone	Sigma-Aldrich (part of Merck KGaA), Munich, Germany
Tolcapone	Sigma-Aldrich (part of Merck KGaA), Munich, Germany
Troglitazone	Sigma-Aldrich (part of Merck KGaA), Munich, Germany
Ximelagatran	AstraZeneca, Cambridge, UK

2.1.4 Cells

Name	Manufacturer, Corporate headquarters
HepG2, cryopreserved	European collection of cell lines, Salisbury, England
HepaRG, cryopreserved	Thermo Fisher Scientific, Waltham (MA), USA
Upcyte hepatocytes, cryopreserved	Medicyte GmbH, Heidelberg, Germany
Primary human hepatocytes, cryopreserved	Thermo Fisher Scientific, Waltham (MA), USA
Primary human hepatocytes, cryopreserved	KaLy cell, Plobsheim, France

2.1.5 Kits

Name	Manufacturer, Corporate headquarters
CellTiter-Glo®	Promega, Fitchburg, USA
ECL Western Blot Detection kit	GE Healthcare UK Ltd., Buckinghamshire, UK
HyStem® cell culture scaffold kit	Sigma-Aldrich (part of Merck KGaA), Munich, Germany

QuantiGene human 10-plex kit	Affymetrix®, Santa Clara (CA), USA
QuantiGene human single plex kit miRNA-122	Affymetrix®, Santa Clara (CA), USA

2.1.6 Antibodies

Antigene, host	Manufacturer, Corporate headquarters
Albumin, mouse monoclonal	SantaCruz biotechnologies
AlexaFluor 488 goat anti-mouse	Thermo Fisher Scientific, Waltham (MA), USA
AlexaFluor 488 goat anti-rabbit	Thermo Fisher Scientific, Waltham (MA), USA
CYP 1A2, mouse monoclonal	SantaCruz biotechnologies, Santa Cruz (CA), USA
CYP 2B6, mouse monoclonal	SantaCruz biotechnologies, Santa Cruz (CA), USA
CYP 2C9, rabbit polyclonal	SantaCruz biotechnologies, Santa Cruz (CA), USA
CYP 2D6, rabbit polyclonal	SantaCruz biotechnologies, Santa Cruz (CA), USA
CYP 3A4, mouse monoclonal	SantaCruz biotechnologies, Santa Cruz (CA), USA
BSEP, mouse monoclonal	SantaCruz biotechnologies, Santa Cruz (CA), USA
GPx-4, mouse monoclonal	SantaCruz biotechnologies, Santa Cruz (CA), USA
Lamp-1, mouse monoclonal	SantaCruz biotechnologies, Santa Cruz (CA), USA
NAT 1/2, mouse monoclonal	SantaCruz biotechnologies, Santa Cruz (CA), USA
SULT-1, mouse monoclonal	SantaCruz biotechnologies, Santa Cruz (CA), USA

2.1.7 Equipment

Name	Manufacturer, Corporate headquarters
Centrifuge 5415R	Eppendorf, Hamburg, Germany
Centrifuge, Megafuge 1.0R, Heraeus®	Thermo Fisher Scientific, Waltham (MA), USA
Centrifuge, Multifuge 3 S-R, Heraeus®	Thermo Fisher Scientific, Waltham (MA), USA
Cryostat	Leica Camera AG, Wetzlar, Germany
Embedding station	Leica Camera AG, Wetzlar, Germany
Eppendorf pipettes (10µL, 100µL, 200µL, 300µL, 1000µL)	Eppendorf, Hamburg, Germany
Film processor	GE Healthcare UK Ltd., Buckinghamshire, UK

Fume hood	Thermo Fisher Scientific, Waltham (MA), USA
iBlot® dry blotting system	Thermo Fisher Scientific, Waltham (MA), USA
Incubator, Heraeus® HeraCell®	Thermo Fisher Scientific, Waltham (MA), USA
Integra viaflo electronic pipettes	Integra Biosciences AG, Zizers, Switzerland
Luminex	Luminex corporation, Austin (TX), USA
Lumistar luminometer	BMG labtech, Ortenberg, Germany
Microtome	Leica Camera AG, Wetzlar, Germany
Microscope IX10	OlympusDeutschland GmbH, Hamburg, Germany
Microscope camera	OlympusDeutschland GmbH, Hamburg, Germany
Pipet boy	VWR International GmbH, Darmstadt, Germany
Power pack	BIORAD Medical Diagnostics GmbH, Dreieich, Germany
SDS Page gel chamber	Thermo Fisher Scientific, Waltham (MA), USA
Shaker Titramax 101	Heidolph Instruments GmbH & Co. KG, Schwabach, Germany
Phero-Shaker	Biotec-Fischer GmbH, Reiskirchen, Germany
Sterile bench, Heraeus® HeraSafe®	Thermo Fisher Scientific, Waltham (MA), USA
Tecan infinite 500	Tecan Group Ltd., Maennedorf, Switzerland
VorTemp 56 shaking incubartor	Labnet International Inc., Ediaon (NJ), USA
Ventana Symphony slide stainer	Roche Diagnostics GmbH, Mannheim, Germany
Vacuum pump	Thermo Fisher Scientific, Waltham (MA), USA
Vortex Genie 2	Scientific Industries Inc., Bohemia (NY), USA
Waterbath 1002	GFL Gesellschaft für Labortechnik mbH, Burgwedel, Germany
Weighing machine, special accuracy	Sartorius AG, Goettingen, Germany

2.1.8 Software

Name	Manufacturer, Corporate headquarters
CellF	Cell Software Services Ltd., Brighton, UK
Graphpad Prism	Graphpad Software Inc., San Diego (CA), USA
icontrol	Tecan Group Ltd., Maennedorf, Switzerland
ImageJ	Wayne Rasband (NIH)
Lumistar Galaxy	BMG labtech, Ortenberg, Germany

Luminex	Luminex corporation, Austin (TX), USA
Microsoft office	Microsoft Corporation, Redmont (WA), USA
SnagIt	TechSmith, Okemos (MI), USA

2.2 Methods

2.2.1 Cell culture techniques

In the presented work different cell culture formats were used, namely 2D monolayers, 3D speroids as well as a pump-driven microfluidic system (Kirkstall Quasi-vivo). Since media formulations and thawing procedures as well as seeding procedures for monolayers did not differ so they are described first for each cell system used and subsequently the seeding procedures for 3D and the microfluidic format as well as media changes and treatments are described in separate subchapters.

2.2.1.1 *Collagen-coating of cell culture surfaces*

Extracellular matrices such as collagen help cells maintaining overall health and enhanced functionality when compared to maintenance on plain plastic surfaces (Michalopoulos and Pitot, 1975). All experiments in this study using 2D monolayers and quasi-vivo were conducted on collagen-coated surfaces. Collagen type IV lyophilisate from rat tail was reconstituted overnight in 0.2% acetic acid in a stock concentration of 1mg/mL. The stock solution was further diluted to 50µg/mL in 0.2% acetic acid and transferred into the respective plastic ware at type specific volumes described in table 2.1. Plastic ware was incubated for 1h at RT and subsequently washed twice with PBS -/- before use.

Table 2.1: Voumes used for collagen coating of cell culture surfaces.

Surface type	Coating volume [µL]
96-well plates	100
24-well plates	500
Glass coverslips*	500

*Glass coverslips were placed separately in 24-well plates for collagen coating.

2.2.1.2 *Determination of cell number and viability*

Determination of total cell number and percentage of viable cells was performed via trypan blue exclusion in a Fuchs-Rosenthal counting chamber. 50µL cell suspension were mixed with each 500µL of respective media and 0.5% trypan blue solution and incubated for 5min at RT. 20µL of the mixture were then loaded into each chamber and both total cells and dead cells, which appear blue were counted in at least 3 squares. The averages of both counts

were calculated and subsequently dilution factor (1:21) and square volume (0.2µL) were offset to the total number of cells per mL as follows:

$$total\,\frac{cells}{mL} = x * 5000 * 21$$

Percentage of viability was calculated and suspensions below 80% viability were not used for further experiments.

2.2.1.3 *Cryopreserved HepaRG cells*

2.2.1.3.1 Media formulations

Cryopreserved HepaRG cells were used in all cell culture formats using the media formulations below.

Table 2.2: Media formulations used for general Cell Culture of HepaRG cells.

Name	Formulation
HepaRG thaw/seed	500mL Williams Medium E 5mL L-glutamine 5mL Penicillin/Streptomycin 67mL HepaRG thaw/seed supplement (proprietary formulation, standard serum)
HepaRG TOX	500mL Williams Medium E 5mL L-glutamine 5mL Penicillin/Streptomycin 67mL HepaRG tox supplement (proprietary formulation, standard serum)

2.2.1.3.2 Thawing and 2D seeding

HepaRG cells (10mio/vial) were taken out of the liquid nitrogen tank and thawed in a water bath until small ice crystals were left. The vial content was then transferred into 50mL of prewarmed thaw medium and the vial was rinsed twice with 1mL thawing medium each in order to maximize the yield. Cells were then centrifuged for five minutes at RT (500xg). The supernatant was aspirated except for about 500µL, in which the cell pellet was gently resuspended. Subsequently, 10mL of prewarmed thaw medium was added and total cells and viability was determined via Trypan blue exclusion as described in section 2.2.1.2 and further diluted according to the different culture formats (see sections 2.2.1.1, 2.2.1.6 and 2.2.1.7).

For monolayer cultures, cell suspension was diluted in thaw media according to the plate type/well surface as described in table 8 and subsequently precultured for 96h prior to treatments (37℃/5%CO_2). Monolayers were always seeded in collagen-coated plates (section 2.2.1.1).

Table 2.3: Seeding densities for HepaRG monolayers.

Plate type	Volume per well	Cells per well
96-well	100µL	70,000
24-well	500µL	300,000

2.2.1.4 *Cryopreserved primary human hepatocytes*

Primary human hepatocytes were thawed and maintained in the media below.

Table 2.4: Media formulations used for PHH cell culture.

Name	Formulation
Cryo hepatocyte recovery medium (CHRM)	Proprietary (Invitrogen CatNo CM7000)
PHH culture medium	500mL Williams Medium E (50mL fetal bovine serum (FBS))[1)] 5mL L-glutamine 5mL Penicillin/Streptomycin 5mL Insulin-Transferrin-Selenium (ITS) 0.5mL Dexamethasone

1) FBS only supplemented during spheroid formation

2.2.1.4.1 Thawing and 2D seeding

Primary human hepatocytes (KaLy cell/ Invitrogen) were taken out of the liquid nitrogen tank and thawed in a water bath until small ice crystals were left. The vial content was then transferred into 50mL of prewarmed CHRM and the vial was rinsed twice with 1mL thawing medium each in order to maximize the yield. Cells were then centrifuged for five minutes at RT (100xg). The supernatant was aspirated except for about 500µL, in which the cell pellet was gently resuspended. Subsequently, 10mL of prewarmed culture medium was added and total cells and viability was determined via Trypan blue exclusion and further diluted according to the different culture formats.

For monolayer cultures, cell suspension was diluted in culture medium according to the plate type/well surface as described in table 2.5 and subsequently precultured for 24h prior to treatments (37℃/5%CO_2). Monolayers were always seeded in collagen-coated plates.

Table 2.5: Seeding densities for PHH monolayers.

Plate type	Volume per well	Cells per well
96-well	100µL	35,000
24-well	500µL	150,000

2.2.1.5 *HepG2 cell line*

In this study, HepG2 cells were maintained and passaged in culture medium. Cytotoxicity assessment was performed in HepG2 TOX medium according to the media formulations below.

Table 2.6: Media formulations used for HepG2 cell culture.

Name	Formulation
HepG2 culture	500mL DMEM 50mL FBS 5mL Penicillin/Streptomycin (100U/ 100µg/mL) 5mL L-Glutamine (200mM) 5mL non- essential amino acids (NEAA)
HepG2 TOX	500mL DMEM 5mL Penicillin/Streptomycin (100U/ 100µg/mL) 5mL L-Glutamine (200mM) 5mL non- essential amino acids (NEAA)

2.2.1.5.1 Thawing, maintenance and passaging of HepG2

HepG2 cells were taken out of the liquid nitrogen tank and thawed in a 37℃ water bath until small ice crystals were left. The content was quickly transferred into a 175cm^2 cell culture flask with 20mL prewarmed HepG2 culture medium. Cells were allowed to attach for 24h until media was renewed in order to remove the DMSO containing freezing medium. Cells were maintained until 75-90% confluency before passaging, thereby renewing the culture medium every 2-3 days.

Passaging of HepG2 was performed by aspirating the medium, washing once with 10mL PBS -/- and adding 2.5mL trypsin-EDTA. Flasks were then gently rotated to distribute trypsin and subsequently incubated for 5 minutes at 37℃/5% CO_2. The detached cells were then resuspended in culture medium into a fresh, prefilled cell culture flask in a splitting rate of 1:6 to 1:10 depending on previous confluency.

2.2.1.5.2 Seeding of HepG2

HepG2 cells were seeded in white 96-well plates for every experiment conducted. Therefore, confluent cell culture flasks were trypsinized (section 2.2.1.5.1) and subsequently counted via Trypan blue exclusion and diluted in culture medium to a concentration of 200,000 cells/mL. Cells were then seeded in 100µL per well (20,000 cells per well) into collagen-coated 96-well plates and preincubated for 48h (37°C/5%CO_2) to allow attachment and recovery prior to treatment.

2.2.1.6 *Spheroid cell culture*

Spheroid cell culture was conducted using 96-well ultra-low attachment plates (ULAP) with U-bottom. The surface of those plates is treated so that cells are not able to attach to the plastic and cells consequently attach to each other, thus forming a single spheroid per well in 4 to 7 days. The seeding procedure is similar to that of monolayers, only the total cell number per well is much less. Additionally, the plates containing PHH were centrifuged in order to shorten spheroid formation time. Details for seeding both cell systems are listed in table 2.7.

Table 2.7: Seeding densities, formation time and centrifugation steps for HepaRG and PHH spheroid culture.

Cell type	Cells/ well (spheroid)	Spheroid formation time	centrifugation
HepaRG	1,800	4 days	No
PHH	1,500	4-10 days	10min, 90xg, RT

Figure 2.1: Microscopic overview of spheroid formation of PHH Lot HU4197 over time. Single cells accumulate at the well bottom and form compact spheroids within 5 days. 4x magnification, bars = 200µm.

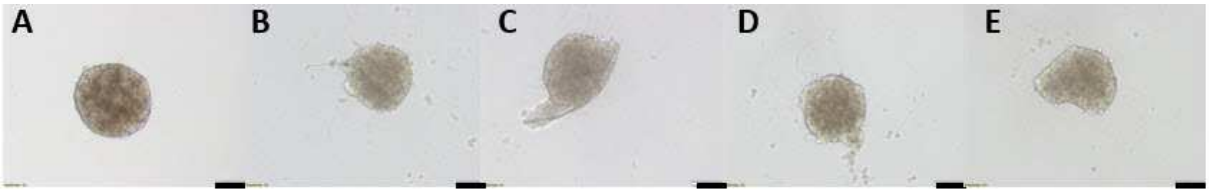

Figure 2.2: Examples of valid/ invalid HepaRG spheroids. A: valid spheroid with distinct lining showing no visible inclusions. B+C: invalid spheroids due to foreign material (e.g. fibres) leading to irregular shapes. D+E: invalid spheroids either without distinct lining (D) or too irregular in shape (E). 10x magnification, bars = 100µm

Spheroid formation time was determined empirically for both cell systems by daily microscopy. Spheroids were ready to use as soon as the outer lining appeared tight and not bubbly. Before starting any experiment, every single spheroid was checked regarding gross morphology and shape and approved as either “valid” or “invalid”. For every experiment 5 spare plates were seeded in order to replace invalid spheroids with valid ones. Therefore, all invalid spheroids were marked and aspirated and valid spare spheroids were transferred (100µL) into the empty wells. Spheroid formation as well as examples for valid/invalid spheroids is given in the following figures 2.1 and 2.2, respectively.

2.2.1.6.1 Medium change and compound treatment

Medium change was not performed before day 4 after seeding in order to not perturb the aggregation/spheroid formation process. Depending on the aggregation state on day four post seeding, cells were either treated (HepaRG) or maintained longer until compact spheroids were obtained (PHH, up to 7 days).

Medium change was performed by replacing 50µL of respective media (HepaRG thaw/ PHH culture medium) per well using an electronic pipet set to the lowest possible speed to avoid both spheroid aspiration and perturbation of the formation process. Once spheroids were compact and invalids were replaced, a medium change to HepaRG tox was performed twice before dosing HepaRG spheroids; PHH spheroids were kept in culture medium.

Dosing solutions were prepared by further dilution of the 200x DMSO stock solutions in the respective media. Since it is not possible to remove the total volume in this culture format due to spheroid loss, two different approaches have been used for compound treatment.

The first treatment was performed by diluting the 200x stocks in a 1:100 ratio resulting in 2x end concentration and replacement of 50µL leading to a further 1:2 dilution in the well.

Every subsequent treatment was performed using washing steps with the final end concentrations (1:200 stock dilution) in order to keep the concentration bias as low as possible. Thereby, 90µL were replaced three times as slowly as possible, resulting in a 1:1,000 dilution of the old dosing solution.

Medium change and/or compound treatment were performed every 2 to 3 days and with every treatment, vehicle (DMSO) controls were carried out.

2.2.1.7 *Quasi-vivo*®

The quasi-vivo system from Kirkstall Ltd. is a pump-driven microfluidics system that displays the option to manipulate the flow, thus enabling to setup the optimal flow rate for different cell systems. The introduction of flow to a cell population introduces shear forces and shear stress to the cells, which may enhance physiologically relevant functions *in vitro*. Additionally, the flow allows a more dynamic exchange capacity than under static culture conditions.

The 6-head pump allows testing six different conditions at a time, each head is connected to a reservoir bottle containing medium or dosing solution via tubing and pumps volume through the further connected cell culture chambers and finally back to the pump. Thereby, the amount of cell culture chambers per condition is variable and only limited by the incubator size. Figure 2.3 shows a picture of the system as well as schematic principle of how it works.

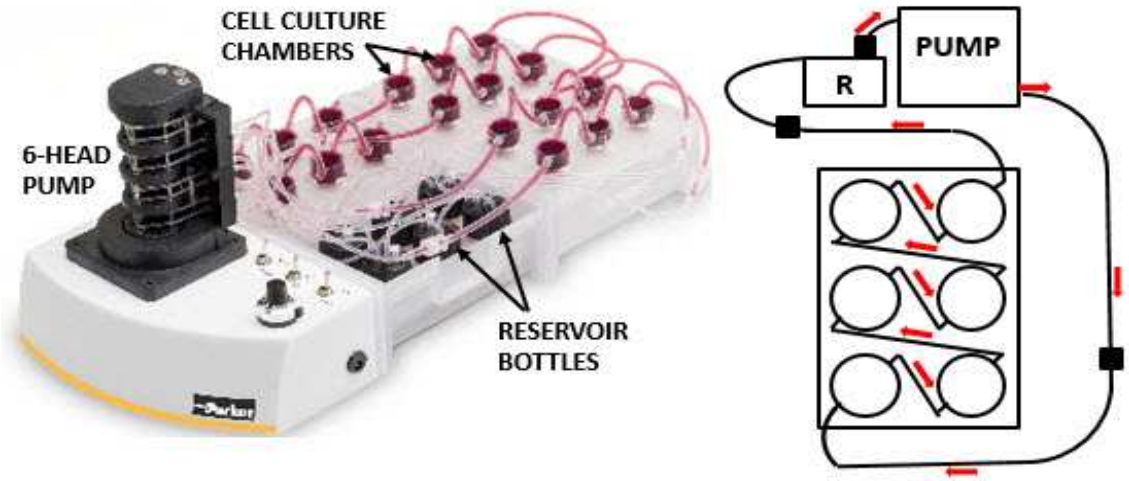

Figure 2.3: Overview of the quasi-vivo system. Left: Representative picture of the readily assembled system as it was used. Right: Schematic overview of the connecting tubing and flow direction (arrows) from reservoir (R) to plates and back. Interconnected luerlocks (black cubes) allow to short ciruit during sampling without the need to disassemble the tubing.

2.2.1.7.1 Pump calibration

Before any experiment, pump calibration was performed in order to validate the flow rate. For this, one head of the pump was connected to a reservoir bottle prefilled with water. An empty plastic weighing dish was weighed and subsequently the pump was started and let run for five minutes whereby the pumped water was collected in the dish and weighed again. The average in µL/min was calculated and adjustment was done if necessary, subsequently the procedure was repeated twice in order to ensure a constant flow rate. Note that the pump heads are not capable of independent flow rates since the peristaltic backbone of the pump is a single unit for all heads.

2.2.1.7.2 Cell seeding and maintenance

Since cells first need to attach before starting any flow, static preculture was required. Cells were seeded onto round, collagen-coated glass coverslips by transferring the single coverslips into the wells of a 24-well plate using sterile forceps. Cells were seeded according to monolayer protocol (section 2.2.2.3) and precultured for 96h (HepaRG) to allow attachment and recovery. On day 0, the coverslips were transferred into the QV 900 plates using sterile forceps and were directly covered with fresh medium or dosing solution to prevent drying out until all units were prepared. Subsequently, the culture chambers were closed connected using pre-sterilized tubing including luerlocks according to the scheme in

figure 8. every condition thereby resembles one closed unit including one reservoir bottle and one pump head. Reservoir bottles were prefilled with 25mL of cell type dependent medium or dosing solution units were then connected with their respective reservoir and head. All previous steps were performed under sterile conditions and as soon as every unit was closed the complete system was connected to the power supply and prefilled using the “prime” button, which pumps at maximum speed. After priming, the system was kept in an incubator at 37℃/5% CO_2.

For medium change and re-dosing, the system was taken out of the incubator and tubing was emptied using both the “reverse” and “prime” button until the total volumes were in the reservoirs. The system was put under a sterile bench and the respective media was replaced by 25mL of fresh, pre-warmed medium or dosing solution without the need of opening chambers or disconnect tubing. Subsequently, the system was primed again and placed in the incubator as described above. Medium change was performed twice a week and the system was checked daily on any leaking.

2.2.2 Molecular biological methods

In this thesis, different cell culture formats were used and compared to each other as far as possible. The different formats show substantial differences in i.e. required cell amounts, treatment and maintenance time as well as applicability to molecular biological methods. In the following subchapter, the formats that were applied to each method are noted separately for each section and possible format-depending differences in processing are described in detail.

2.2.2.1 *Experimental schedules*

Timeline for experiments with the endpoints viability, proteinalysis, and histopathological applications

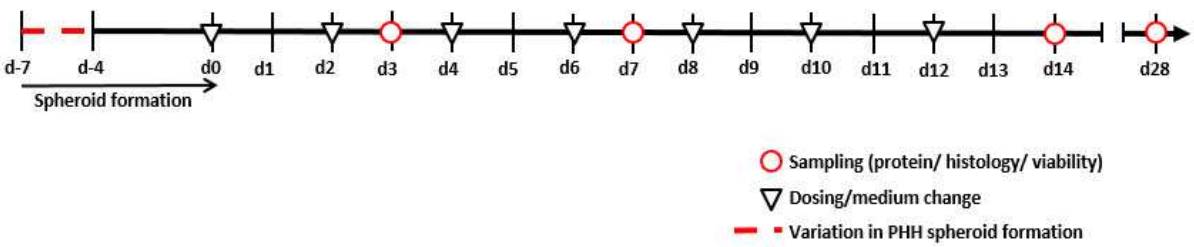

Figure 2.4: Timeline for long-term experiments in 2D, 3D and QV culture formats. Endpoints/ samples covered were viability, protein isolation and spheroid fixation for paraffin and cryoblocks.

Timeline for CYP induction experiments in HepaRG cells.

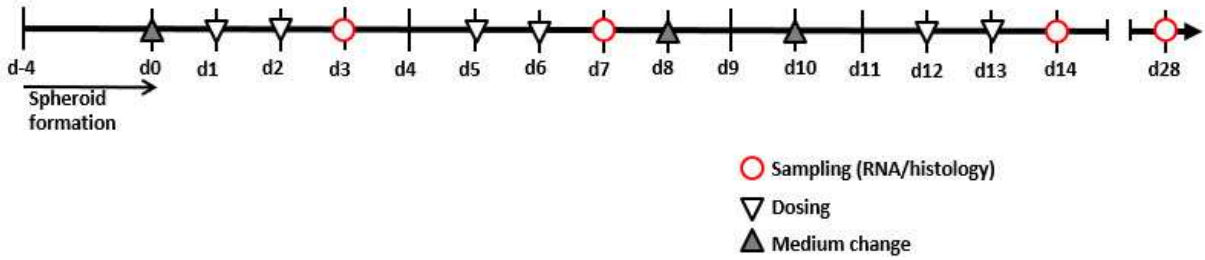

Figure 2.5: Timeline for long term CYP induction studies in both 2D and 3D cell culture in HepaRG cells. Samples covered by this schedule were RNA (for branched DNA) and spheroid fixation for cryoblocks (immunofluorescent staining).

2.2.2.2 *Compound concentrations*

In this study, 13 MIP-DILI training compounds as well as 4 model CYP inducers were used at various concentrations. Overall dose ranges of each compound are listed in table 2.8 and the compounds and concentrations for each experiment are listed in the respective subchapters of the results and discussion section. Compound concentrations for each experiment were defined depending on the compound-specific EC_{50} values as well as on experimental setup and duration.

Generally, MIP-DILI training compounds were prepared as 200x stock solutions in DMSO or water, CYP inducers were prepared as 1,000x stock solutions in DMSO and stored as aliquots at -20°C until use. Each aliquot was thawed once to avoid stability issues by freeze-thaw cycles.

Table 2.8: Compounds and overall dose ranges that were used in this study.
Specific dose ranges are described for each experiment in the results section.

Compound name (code)	Dose range [µM]	Solvent
Acetaminophen (APAP)	30.0 – 30,000	DMSO
Amiodarone (AMI)	3.0 – 300	DMSO
Bostentan (BOS)	3.0 – 300	DMSO
Buspirone (BUS)	3.0 – 300	DMSO
Diclofenac (DCF)	5.0 – 500	DMSO
Entacapone (ENT)	10.0 – 1,000	DMSO
Metformin (MET)	10.0 – 1,000	H_2O
Nefazodone (NEF)	3.0 – 300	DMSO
Perhexiline (PER)	3.0 – 300	DMSO
Pioglitazon (PIO)	3.0 – 300	DMSO
Tolcapone (TOL)	10.0 – 1,000	DMSO
Troglitazon (TRO)	3.0 – 300	DMSO
Ximelagatran (XIM)	3.0 – 300	DMSO
Omeprazole (OMEP)	1.55 – 100.0	DMSO
Phenobarbital (PB)	31.0 – 1,000	DMSO
Rifampicin (RIF)	0.1 – 50.0	DMSO
Flumazenil (FLU)	0.003 – 30.0	DMSO

2.2.2.3 *CellTiter-Glo® assay*

Viability was measured using CellTiter-Glo® assay, at which the total amount of ATP in the cell population disposes the limiting agent of a light emitting reaction described in figure 2.6. Emitted light was measured using a luminometer.

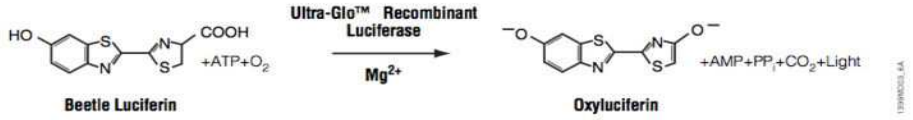

Figure 2.6: Assay principle of CellTiter-Glo®. Beetle luciferin undergoes oxidation to oxyluciferin in the presence of Mg^{2+} and ATP, the reaction thereby emits light. ATP poses the limiting reagent so that the amount of emitted light is directly proportional to the ATP content of the sample (Figure taken from www.promega.de).

Aliquoted CellTiter-Glo® substrate was dissolved in 10mL CellTiter-Glo® buffer and processed differently for 2D and 3D:

Table 2.9: Format-specific differences for viability measurements using CellTiter-Glo.

Monolayer	Spheroids
• 1part medium and 1part CellTiter-Glo® solution were mixed • Every condition was conducted in triplicates • Medium was aspirated and 100µL/well of the mixture was added • Plates were incubated protected from light for 2min while shaking and additional 10min without shaking • Luminescence was measured using a Luminometer	• Every condition was conducted in hexaplicates • 75% Medium (75µL from 100µL) was removed using an electronic pipette set at very low speed • 25µL/well of the CellTiter-Glo® solution was added and mixed thoroughly by pipetting up and down 10 times • Plates were incubated for 20min at 37℃ • Luminescence was measured using a Luminometer

The raw data was analyzed by generating mean and standard deviation. After subtracting the blank mean, the values were divided by the control and displayed as percent of control. EC_{50} values were calculated using non-linear regression analysis and plotted as mean and standard deviation summarizing the single experiments.

2.2.2.4 *Resazurin assay*

A second and multiplexable option for viability measurement was conducted by Resazurin or Alamar blue assay, at which viable cells reduce the blue, non-fluorescent Resazurin into pink and fluorescent Resorufin and viability can be measured either colorimetrically or fluorometrically. In this study, fluorescence was measured due to being the more sensitive option.

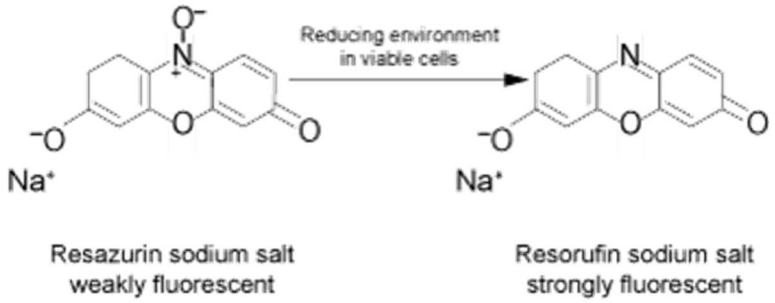

Figure 2.7: Resazurin assay principle. Blue and weakly fluorescent Resazurin is reduced by viable cells to pink and strongly fluorescent Resorufin. (Figure taken from www.promega.de)

A sterile 4.5 mM resazurin in PBS solution was added as 10% of total volume and incubated at 37℃ for 1-2 hours. Subsequently, the supernatant (100µL/well) was transferred into black/clear bottom 96-well plates and protected from light until measurement. Plates were measured using Tecan infinite F500 fluorescent reader (λ excitation: 571nm; λ emission: 585nm).

The raw data was analysed by generating mean and standard deviation. After subtracting the blank mean, the values were divided by the control and displayed as percent of control.

2.2.2.5 *Isolation of total Protein*

Total protein from the different culture formats was isolated using CytoBuster Protein extraction reagent, freshly supplemented with protease inhibitor cocktail set III (dilution 1:200) and phosphatase inhibitor set II (dilution 1:100) and chilled down to 4℃ before use.

QV samples were taken out of the system by emptying the system through reversing the flow, opening the chambers and transferring the glass coverslips into 24well plates using sterile forceps (triplicates per condition). Samples were the processed like static monolayers (duplicates per condition) and 3D samples were processed differently:

Table 2.10: Format-specific differences for isolation of total protein. Spheroids have to be treated with accutase in order to break up the tight structure and obtain higher yields.

2D and QV	3D
• Cells were washed twice with cold PBS and 400µL/well (2D) and	• 480 spheroids per condition were harvested and pooled in an 2mL

200µL/well (QV) of the supplemented Cytobuster reagent was added and incubated at RT for 10min • The well bottoms were gently scraped using a cell scraper in order to maximize the yield • The samples were transferred into reaction tubes and centrifuged at 4℃ and 16,000rpm for 10min • The supernatants were transferred into fresh reaction tubes and either kept on ice until use or stored at -80℃	reaction tube • Medium was aspirated and the spheroid pool was washed twice with cold PBS by spinning down and resuspension • 2mL accutase was added and spheroids were incubated for 20min at 37℃ • Spheroids were spun down and washed twice again with PBS • 400µL of supplemented Cytobuster was added and incubated for 15min at RT while vortexing quickly every few minutes • The samples were centrifuged at 4℃ and 16,000rpm for 10 minutes • The supernatants were transferred into fresh reaction tubes and either kept on ice until use or stored at -80℃

2.2.2.6 *Determination of total Protein via Bradford*

The Bradford protein assay is a colorimetric method for the determination of total protein content of samples in a microgram range by an absorption shift of Coomassie brilliant blue G-250 when forming complexes with proteins in solution. The preparation of a standard curve was performed by diluting a 2mg/mL protein standard solution according to the scheme in table 16. Samples were thawed on ice and quickly vortexed before use. 10µL per well of either standard or sample was transferred in a clear 96-well plate in quadruplicates and 200µL per well of 1x Bradford Reagent was added. The plate was incubated while shaking for 10min and optical density was subsequently measured.

Table 2.11: Preparation of Protein standard series for calculation of total protein in the samples.

standard	final concentration [µg/mL]	Vol Cytobuster [µL]	Vol standard 2mg/mL [µL]
1	0	100	0
2	100	950	50
3	250	350	50
4	400	200	50
5	500	150	50

OD means of the standards were plotted against the concentration and a linear trend line was added. The slope equation was used to determine the protein content [µg/mL] of the samples by resetting the equation to x and inserting the mean OD (= y) of each sample.

2.2.2.7 *SDS page gel-electrophoresis*

Samples were thawed on ice and 1x MES-SDS running buffer was prepared by diluting 50mL 20x MES-SDS running buffer in 950mL deionized water. For all electrophoreses performed, 5µg total sample protein was loaded to the gels resulting in different sample volumes according to their respective concentration. Samples were prepared by adding 4x sample buffer and 10x reducing agent according to the desired total volume (adjustment to end volume with deionized water if needed). Table 2.12 exemplifies the preparation scheme using HepaRG day3 control samples of different culture formats.

Table 2.12: Example of sample preparation for SDS-Page gel-electrophoresis. **A total amount of 5µg Protein per load was needed so that sample volume varied depending on the amount of protein in each sample.**

Reagents	Samples; total Volume= 200µL (10 loads)		
	HRG ctrl day3 2D	HRG ctrl day3 3D	HRG ctrl day3 QV
10x5µg Sample [µL]	36	76	63
10x reducing agent [µL]	20	20	20
4x sample buffer [µL]	50	50	50
Deionized water [µL]	94	54	67

The samples were subsequently denaturated for 10min at 70℃ and stored on ice until use. Ready to use 4%-12% Bis-Tris gels were unpacked and fixed in an electrophoresis chamber, which were then filled with running buffer and combs were removed. The gel pockets were then loaded with either 20µL sample or 10µL pre-stained protein marker. Chamber lids were put on and connected with power supply set to 200V and 125mA for 45min. Gels were subsequently blotted onto nitrocellulose membranes.

2.2.2.8 *Protein transfer via iBlot semi dry blotting system*

The iBlot device was opened and after removing the sealing, the anode stack was placed bottom with the tray directly on the blotting surface, nitrocellulose membrane facing up. The pre-run gel was taken out of its disposable plastic tray and transferred directly onto the membrane and the pre-soaked (deionized water) filter paper was placed on the gel and bubbles were gently removed using the Blotting Roller. Subsequently, the cathode stack was placed on top with the electrode side facing up and air bubbles were again rolled out. Lastly, the disposable sponge was placed into the lid with the metal contact in the upper right corner, the system was the closed and blotting was started (20V, 10min).

After Blotting, the membrane was taken out carefully and stored dry and light protected until use (up to 4 weeks).

2.2.2.9 *Western Blotting*

Table 2.13: Buffers used for Western Blotting.

Wash buffer	0.5% Triton x-100 in deionized water
Blocking buffer	5% nonfat dried milk powder in wash buffer

The membranes were placed in clean plastic trays and 15mL/ tray Blocking buffer was added and incubated at RT for one hour while shaking. Subsequently, the blocking buffer was discarded and respective antibodies were added (diluted in blocking buffer, 15mL per tray, dilutions see table 18) and incubated for 1-2 hours at RT while shaking. The antibody dilutions were then discarded and membranes were rinsed on with 25mL wash buffer per tray and then washed three times by adding 15mL wash buffer per tray and shaking for 10min and discarding wash buffer.

After washing, the respective secondary antibody (anti-mouse/anti-rabbit) was diluted 1:2,000 in blocking buffer and 15mL per tray were added and membranes were again incubated at RT for 1h while shaking. Membranes were then rinsed and washed again as described above and transferred into clean trays.

Western Blot detection reagents were mixed 1:2 and 2mL of the mixture was pipette directly on each membrane and incubated for 2min. excess detection reagent was carefully dripped off using a tissue and membranes were then transferred into a film cassette between two layers of transparent foil and air bubbles were removed. Further processing took place in a darkroom by putting the light sensitive film into the cassette and after an antibody-dependent exposure time (2-10min) the film was developed using the Amersham Hyperprocessor developer.

2.2.2.10 *Preparation of Paraffin sections*

6-12 spheroids per condition were harvested in a reaction tube and as much medium as possible was removed before 500µL 4% Formaldehyde solution was added and incubated at RT for 30min. Subsequently, as much volume as possible was removed and spheroids were washed once with PBS and spheroids were processed through the alcohol series by each adding 500µL, incubating for 2min at RT and removing as much volume as possible (~480µL). Alcohol series was performed as follows:

50% EtOH → 70% EtOH →96%EtOH →Isopropanol → Isopropanol: Xylene (1:2) → Xylene

The spheroids were then aspirated using a pipette and after they settled down at the tip opening, spheroids were transferred into a biopsy cryomold by dipping the tip onto the mold.

Subsequently, one drop Paraffin was added and cooled down to fix the spheroids at the mold bottom before the mold was filled completely. Molds were then frozen at -20℃ before sectioning.

Sections were obtained by using a rotational microtome set to 1.5µm thickness and put onto glass slides after stretching in warm water (42℃). Sections were stored at RT until use.

2.2.2.11 *H&E staining*

The hematoxylin and eosin (H&E) staining is the gold standard histologic staining method for the pathological assessment of tissue samples. Since spheroids can be described as microtissues, they are applicable to histological tissue processing in a modified way as described in section 2.2.2.10.

H&E staining of paraffin-embedded spheroid sections was performed as quality control to ensure general cell health and the absence of necrotic cores on the one hand as well as for histopathologic examination of treated spheroids to assess whether H&E stained sections pose a possible endpoint when using 3D cell culture for early safety assessment.

Staining was performed using the Ventana Symphony automated stainer (Roche) with the staining program “C43”, which stains according to the following protocol:

Table 2.14: Staining procedure for H&E staining of paraffin-embedded spheroid sections. Staining was performed using the Ventana Symphony automated stainer (protocol C43).

Step	Reagents and incubation time
Deparaffinization	Xylene, 2x2min
Rehydration	Isopropanol, 3min
	96% EtOH, 3min
	70% EtOH, 3min
	50% EtOH, 3min
	dH_2O, 3min
Stain with hematoxylin	Hematoxylin, 4min
Wash	Tap water, 3x2min
Stain with eosin	Eosin, 1min
Dehydrate	96% EtOH 2x10sec
	Isopropanol, 2x1min
	Isopropanol/Xylene, 2min
	Xylene, 2x2min
Mount	Entellan

The sections were subsequently evaluated microscopically and photos were taken exemplarily for each time point/ condition.

2.2.2.12 *Preparation of cryosections*

6-12 spheroids per condition were harvested in a reaction tube and as medium as possible was removed before 500µL 4% Formaldehyde solution was added and incubated at RT for 30min. Subsequently, as much volume as possible was removed and spheroids were

washed once with PBS before 500µL of a 30% (w/v) glucose solution was added and incubated for 30min. Spheroids were then aspirated in 20µL and transferred into the center of a biopsy cryomold and the mold was filled with O.C.T. compound and incubated for 1h at room temperature. After incubation, the samples were frozen and stored at -20℃.
Sections were prepared using a cryostat precooled at -20℃ and set to 3µm thickness and put onto glass slides by dipping the slide (RT) onto the section. Sections were stored at RT until use.

2.2.2.13 *Immunofluorescent staining*

Table 2.15: Buffers used for immunofluorescent staining of spheroid cryosections.

Blocking buffer	PBS with calcium and magnesium 0.3% Triton x-100 7.5% normal goat serum
Wash buffer	PBS with calcium and magnesium 0.02% Tween 20

Specimen position on each slide was labeled using a hydrophobic barrier pen in order to both avoid drying and minimizing needed volumes. Specimen were permeabilized and blocked for 30 min at RT using blocking buffer. Blocking buffer was discarded and primary antibodies in the desired dilutions were added and incubated at RT in respective times. Subsequently, the slides were washed twice with washing buffer and the respective secondary antibody, depending on the host species of the primary antibody, was added in a 1:2,000 dilution in blocking buffer supplemented with the counterstains Hoechst (nuclear stain, dilution 1:1,000) and Rhodamine-Phalloidin (membrane counterstain, dilution 1:100). Slides were incubated light protected for 1h at RT, washed twice in wash buffer and once in PBS and stored in PBS at 4℃ protected from light u ntil microscopy.

2.2.2.14 *CYP-450 induction*

The inducibility of specific CYP enzymes accounting for xenobiotic metabolism was used to characterize HepaRG per se as well as to compare CYP induction HepaRG cells in 2D and 3D cell culture format by model inducers. The quantification of the different target mRNAs was performed with the QuantiGene Plex Assay from Panomics (Plex Set 11563, Affymetrix) containing a target-specific mixture of Probe Set and Capture beads was used to detect 10 targets.

The assay is based on hybridization of the target sequence to magnetic beads (xMAP Luminex) and signal amplification via branched DNA technology. The technology principle is

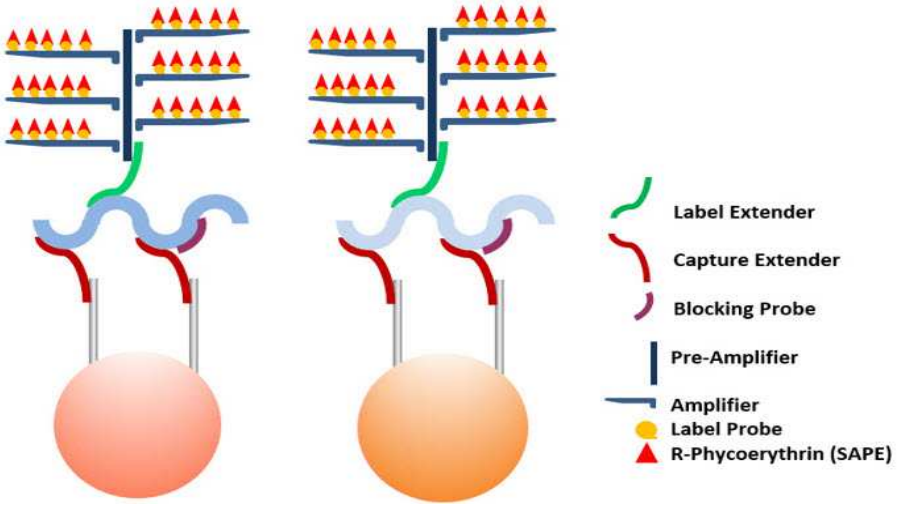

Figure 2.8: principle of the measurement of two target genes using the QuantiGene Plex 2.0 assay. After sample preparation and hybridization of the bead-bound capture extender to the target sequence, the signal amplification tree is built in sequential hybridization steps (see text for detailed description). Finally, phycoerythrin (SAPE) is exploited as fluorescence-based indicator for signal generation, which allows the quantification of target RNA present in the sample.

explained in figure 2.8 and signal detection was performed using the Luminex 200 system. HepaRG cells were seeded and precultured in 2D and 3D as described in sections 2.2.1.3 and 2.2.1.6 and subsequently treated with three model inducers and one negative control, namely Phenobarbital (PB), Omeprazol (OMEP), Rifampicine (RIF) and Flumazenil (FLU) in 7-8 different concentrations plus vehicle control (see table 2.7). Compound treatment was performed as described in 2.2.1.3 for 2D and 2.2.1.6 for 3D, using three replicates per condition for 2D and 12 spheroids per condition for 3D. In total, samples were taken at days 3, 7 and 14 for both formats and compound treatment was performed twice before sample processing as described in figure 2.5. After 48h of compound treatment, the respective samples were lysed by replacing the medium with a working lysis mixture composed of 1 part lysis mixture supplemented with 5microL/mL proteinase K (both included in the QGP 2.0 kit) and 2 parts HepaRG tox medium. For 2D, medium was aspirated and replaced by 90µL of working lysis mixture per well, whereas for 3D, each spheroid was taken up in 12µL medium and spheroids were pooled in one well of a 96 well plate resulting in 12 spheroids in 144µL and 72µL of supplemented lysis mixture were added. Subsequently, the samples were incubated at 37℃/5%CO_2 for 1h, lysis was checked microscopically and samples were snap frozen at -80℃ until further processing.

2.2.2.14.1 Hybridization (Day1)

Samples were thawed at RT and stored on ice until use. The appropriate probe set was thawed on ice before denaturation at 95℃ for 5min and put back on ice again. For the hybridization of the target RNAs to the corresponding capture beads, the working plex sets were prepared as described in table x for both samples and total liver RNA, which serves as quality control to confirm assay linearity. A standard curve of total liver RNA ranging from 0.78ng/µL to 25ng/µL was prepared using nuclease free water in two-fold dilutions and six concentrations. A volume of 80µL working plex set for total liver RNA and 20µL of corresponding total liver RNA as well as 20µL of working plex set for samples and 80µL sample plus blank were added to each well of a 96 well round bottom plate. The plate was sealed using self-adhesion foil and incubated at 600rpm and 54℃ for 16h using a VorTemp 56 shaking incubator.

2.2.2.14.2 Signal amplification (Day2)

Following target-to-bead hybridization, sequential hybridization steps were performed to amplify the signal to enable detection of low abundance molecules via the branched DNA technology (Ureda et *al.*, 1987). The wash buffer was prepared according to table 20 and prefilled into the 405TS microplate washer, which was set up by rinsing once with DEPC treated water.

After hybridization, the adhesive foils were removed and plates were placed in the automated washer using the washing program (3x 200 µL wash buffer). The magnetic plate tray of the washer keeps the magnetic beads at the well bottom so that no losses occur during the washing step. The plates were then further processed by adding 100µL/well pre-Amplifier and sealed again before quickly shaken at 800rpm and RT to resuspend the beads. Subsequently, the plates were incubated for 1h at 50℃ and 600rpm, washed again as described before and 100µL/well amplifier were added and plates were again resuspended and incubated at the same conditions.

2.2.2.14.3 CYP induction data analysis

The Luminex 200 measurement principle is comparable to FACS technology, only with beads instead of cells. The different target-specific beads contain different amounts of phycoerythrin, which result in a unique bead pigmentation for each target, thus allowing tracking of various analytes within one sample. The signal itself is fluorescent and the xPonent software calculates the median from the data range as “median fluorescence intensity (MFI)” values, which were used for further analysis. The assay quality was assessed by evaluating the housekeeping gene expression against the total liver RNA

standard curve. The blank-corrected averages of the measured duplicates were plotted against the applied total liver RNA concentrations.

3 Results and Discussion

This thesis primarily deals with the assessment and comparison of HepaRG cells in various cell culture formats and was performed as part of the IMI MIP-DILI project. In this section, the results from different endpoints including viability, protein expression, morphology and CYP induction are presented and discussed. Data analysis, illustrations and comprehensive interpretation of the results represent my own work and results and interpretations from collaborative experiments within MIP-DILI are clearly labeled. A detailed overview of the personal contributions within the MIP-DILI project is given in section 1.6 personal contributions.

3.1 Assessment of current hepatic cell culture models

3.1.1 Multicenter cytotoxicity ring trial

The starting point for MIP-DILIs *in vitro* work package was an unbiased assessment of hepatic cell culture models that are widely used in early safety assessment test batteries of the pharmaceutical industry. The focus was on whether simple cell models that are applied using simple endpoint measurements can distinguish between compounds that have the potential to cause DILI in man and those that are considered non-hepatotoxic.

A ring trial among seven MIP-DILI partners was performed, in which a small panel of DILI (9) and non-DILI (4) compounds was tested in monolayers of four hepatic cells systems: PHH, HepaRG, HepG2 and Upcyte hepatocytes. The cells were treated with the 13 compounds at 7 concentrations each (table 3.1) for 24h and 72h and two simple viability endpoints, ATP and Resazurin assay were conducted. Training compound selection was based on literature seach (performed by AstraZeneca) with focus on the selection of well-studied compounds that, taken together, sufficiently cover the five main mechanisms leading to DILI alongside four non-hepatotoxic compounds. Concentration ranges were selected on existing cytotoxicity data as well as on displaying a renge, which is broad enough to cover different increments on the severity of cytotoxic effects (performed by AstraZeneca and University of Liverpool). Detailed materials and methods are described in Sison-Young, Lauschke and Johann et *al.*, 2016.

Inter and intra-laboratory reproducibility was calculated as well as analysis of differences between the cell systems with respect to their ability to distinguish between DILI and non-DILI compounds. Additionally, differences between fresh and cryopreserved cells of two cell types (PHH and HepaRG cells) and also differences between two HepG2 clones were investigated statistically. Assay performance, dose-response curves and calculation of EC_{50} values was performed by each partner with the respectively generated data sets, final

analyses and statistics were performed at the University of Liverpool, Karolinska Institutet Stockholm and Merck KGaA Darmstadt.

Due to the lack of significant variation between the ATP and Resazurin assay, only the ATP data is presented (Resazurin and ATP viability data see Appendix 1).

Table 3.1: Selected training compounds and final dose ranges.

Compound (code)	Hepatotoxic/ non-hepatotoxic	Final dose range [μM]
Amiodarone (AMI)	Hepatotoxic	3; 5; 10; 30; 50; 100; 300
Bosentane (BOS)	Hepatotoxic	3; 5; 10; 30; 50; 100; 300
Buspirone (BUS)	Non-hepatotoxic	3; 5; 10; 30; 50; 100; 300
Diclofenac (DCF)	Hepatotoxic	10; 30; 50; 100; 300; 500; 1000
Entacapone (ENT)	Non-hepatotoxic	10; 30; 50; 100; 300; 500; 1000
Metformin (MET)	Non-hepatotoxic	30; 50; 100; 300; 500; 1000; 3000
Nefazodone (NEF)	Hepatotoxic	3; 5; 10; 30; 50; 100; 300
Paracetamol (APAP)	Hepatotoxic	30; 100; 300; 1000; 3000; 10,000; 30,000
Perhexiline (PER)	Hepatotoxic	3; 5; 10; 30; 50; 100; 300
Pioglitazone (PIO)	Non-hepatotoxic	3; 5; 10; 30; 50; 100; 300
Tolcapone (TOL)	Hepatotoxic	10; 30; 50; 100; 300; 500; 1000
Troglitazone (TRO)	Hepatotoxic	3; 5; 10; 30; 50; 100; 300
Ximelagatran (XIM)	Hepatotoxic	3; 5; 10; 30; 50; 100; 300

The EC_{50} values (effective concentration 50%) for the response in ATP content to each compound in the tested cell systems are shown in figure 21 for 24h (left) and 72h (right). The figure shows that none of the tested cell systems was able to reliably distinguish between DILI (red dots) and non-DILI (green dots) compounds at either time point.

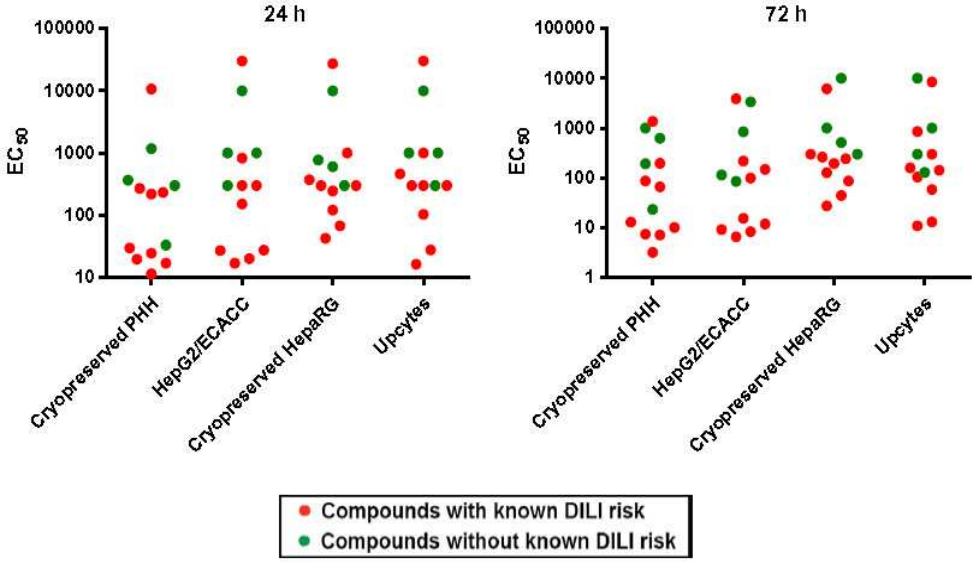

Figure 3.1: Scattergram of EC_{50} values derived from ATP content measurements after exposure to the training compounds of each cell type for 24h (left) or 72h (right). Data is expressed as mean from multiple measurements across test sites for each compound. Hepatotoxicants (red dots) and non-hepatotoxicants (green dots) are not clearly segregated in any of the cell models tested. (Figure taken from Sison-Young, Lauschke, Johann et *al.*, 2016)

When assessing the single EC_{50} values alone, as would occur in the early stages of drug discovery, these simple cell models were not able to predict a compound's potential to cause hepatotoxicity based on the primary EC_{50} values alone. Therefore, the EC_{50} values were corrected with *in vivo* exposure levels by integrating the clinically relevant peak plasma concentrations (C_{max}) for each compound in each cell model at both 24h and 72h as the EC_{50}/C_{max} ratio. Because no definite EC_{50}/C_{max} ratio is established as critical in the literature, a range of values has been tested in terms of how many hepatotoxicants are recognized.

Using an EC_{50}/C_{max} value of 20, all DILI positive compounds with the exception of XIM were detectable as such in PHH after 72h. Eight out of 9 DILI risk compounds were detected in PHH after 72h, but not after 24h (figure 3.2). The only DILI compound that was not identified was XIM, which was negative across all cell models tested. Additionally, one DILI negative compound was identified as positive in PHH after 72h, namely ENT. HepG2 cells showed a similar profile to PHH by identification of 7 out of 9 DILI compounds after 72h (except for APAP and XIM). At 24h, both PHH and HepG2 also showed similar profiles detecting 4 (PHH) and 3 (HepG2) out of 9 DILI compounds. In comparison, both HepaRG and Upcyte cells showed less accuracy for the indication of DILI risk at 24h (both 2 out of 9 hepatotoxicants) or 72h (both 4 out of 9 hepatotoxicants).

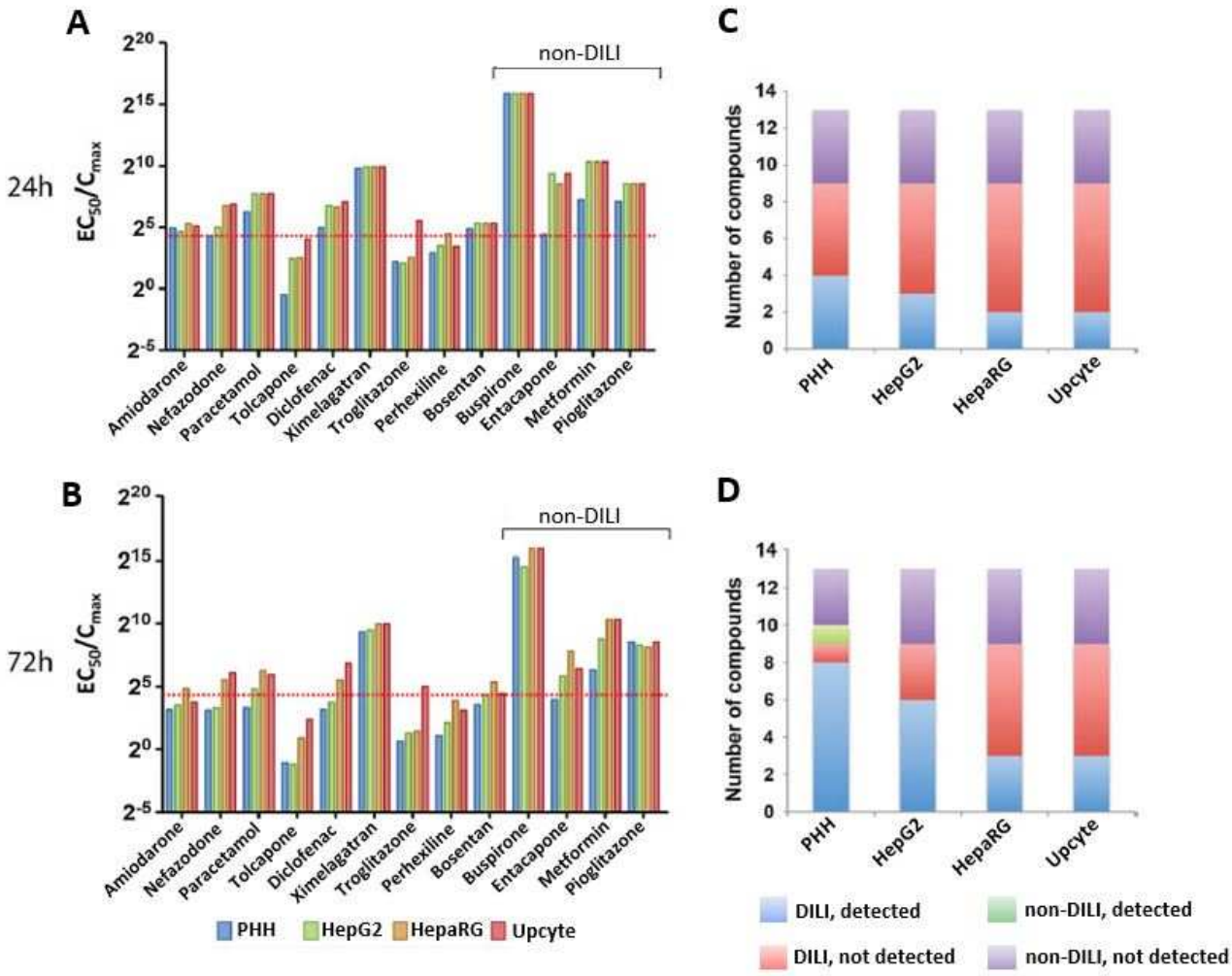

Figure 3.2: A and B are clustered column plots showing the EC_{50}/C_{max} values for thirteen compounds tested, as detected by the four cell models that have been tested by at least two partners (cryoPHH, HepG2 ECCAC, cryoHepaRG and Upcyte cells) after 24h (A) and 72h (B). The cutoff value for the EC_{50}/C_{max} ratio of 20 is indicated as red dotted line (represents 2^4 on the y-axis). The four non-hepatotoxic compounds are indicated as such. C and D show stacked column plots visualizing the number of compounds classified as toxic by the different cell models with an EC_{50}/C_{max} at or below 20 after 24h (C) and 72h (D). Primary human hepatocytes recognized more hepatotoxicants after both time points than the other cell systems tested, indicated by the blue columns in C and D. Following 72h, all cell models detected more DILI compounds as such compared to 24h. (Figure taken from Sison-Young, Lauschke and Johann et al., 2016, modified)

Another aim of this ring trial was the assessment of differences at both the inter- and intra-laboratory level, between fresh and cryopreserved cells (PHH and HepaRG) as well as between the two different HepG2 clones (the ECCAC[1] clone that is used for all MIP-DILI studies and the TS[2] clone, which is an in-house clone from one test site). Therefore, at least two different partners performed experiments for each cell system to allow pairwise comparison. Statistically significant inter-laboratory differences were detectable in the cytotoxic response of PHH, HepG2 and Upcyte hepatocytes, but not for HepaRG cells. The inter-laboratory differences range from minor variation in Upcyte cells (12.3%) to higher variation in HepG2 cells (23.4%) and PHH (48.5%) and also seems to be compound

[1] European Collection of Authenticated Cell Cultures
[2] Test Site

dependent (except for XIM - data not shown, see Sison-Young, Lauschke and Johann et *al.*, 2016). Interestingly, intra-laboratory variations also occurred, especially in HepG2 (15.4%) and upcyte cells (11.5%), whereas differences in HepaRG (5.7%) and PHH (2%) were negligible. These intra-laboratory variations also seem to be compound-specific, i.e. varying from 21.1% for the replicates of PIO to no significant differences for APAP and DCF across the cell models.

Furthermore, pairwise comparisons were also performed for fresh vs. cryopreserved HepaRG cells and statistically significant differences were found for only 3 of 13 compounds for both time points (TRO, AMI and TOL, data see Sison-Young, Lauschke and Johann et *al.*, 2016), showing that cryopreservation does not massively impact the cytotoxic response. Inter-donor variability between 5 donors of cryopreserved PHH was detected for 5 compounds, of which 3 compounds showed differences at 24h (APAP, DCF and MET) and 4 compounds varied at 72h (APAP, BOS, BUS and MET), resulting in an average of only 8.1% variation of the pairwise comparisons (Sison-Young, Lauschke and Johann et *al.*, 2016). Two different HepG2 clones were compared, since clone dependent differences in basal expression of phase I and II DMEs have been reported (Hewitt and Hewitt, 2004). The HepG2/ECCAC clone is commercially available and was the clone that was used for all MIP-DILI related HepG2 studies and was compared here with the HepG2/TS clone, which was routinely used in one participating laboratory. The pairwise comparison revealed statistically significant differences for 4 out of 13 compounds (AMI, NEF and TOL at 24h and NEF and BUS at 72h, data see Sison-Young, Lauschke and Johann et *al.*, 2016).

Predicting the hepatotoxic potential of drug candidates remains challenging and this short-term toxicity comparison using i) the most widespread hepatic cell models and ii) a set of well-known DILI/non-DILI training compounds, was conducted to define the current status as a basis for how these cell systems can be further developed and improved with respect to their ability to predict hepatotoxicity. By the implication of a drug´s C_{max} value, PHH and HepG2 were able to detect the majority of the used hepatotoxicants as such.

However, none of the simple cell models could distinguish between DILI and non-DILI drugs when comparing the compound-specific EC_{50} values alone, concluding that simple monolayer cultures are not capable of predicting whether a new chemical entity (NCE) is likely to cause DILI in man in the absence of human exposure data. Generally, no human pharmacokinetic data is available at the early developmental stages of hit-to-lead and lead optimization phases and this study showed that in the absence of known human C_{max} and area under curve (AUC) data, the basic cell models assessed here are unsuitable for DILI prediction, thus being limited to simple and rapid early discovery screens. Nevertheless, cytotoxicity screening remains an essential component at early developmental stages as the assessment of drug-induced changes on cell health are routinely used for a first-line ranking

of drug candidates (Weaver et *al.*, 2017). Although viability displays the simplest endpoint, it indicates the potential of a drug candidate to elicit intrinsic toxicity, which helps to rank drug candidates according to the concentration at which cytotoxic effects occur and sort out compounds with unfavorable cytotoxicity profiles. Additionally, cytotoxicity assays pose essential advantages in terms of simplicity in both performance and analysis, low cost as well as rapid data generation according to the fast pace of early development (Benbow et *al.*, 2010).

The importance of chronic exposure, which is more representative for the clinical setting in the majority of cases, was evident in this study. Following compound exposure for 72h, PHH could clearly segregate between DILI and non-DILI compounds, which was not observable following compound exposure for 24h. the time-dependent effects that were observable give evidence that it may be useful to include long-term studies in order to investigate whether the cell models tested here are able to better distinguish between hepatotoxicants and non-hepatotoxicants under repeated exposure. This may also enable the detection of hepatotoxic events with a slow onset.

The determination of variations at different levels, i.e. inter- and intra-laboratory variation, inter-donor and inter-clonal variation as well as variations between fresh and cryopreserved cells, enables to estimate the robustness of the generated dataset in order to use it as a reliable reference tool. Inter-laboratory variation was detected at different degrees across the cell types with the highest variation observed in PHH (48.5%), followed by HepG2/ECCAC (23.4%), whereas both Upcyte cells and HepaRG only showed marginal variations. PHH display the most complex, sophisticated and sensitive cell model used here, thus the high degree of variation between laboratories is not surprising, despite the use of harmonized protocols. In contrast, the high degree of variation in HepG2 is somewhat surprising, especially in the context of the reproducibility that cell lines offer in general and a notable intra-laboratory variation of 11.5 % under the conditions of this study. Those differences show that, although harmonized protocols have been used for each cell model, how important it is to work as stringently as possible according to a specific protocol. Despite relatively high degree of variation, both cell models were still relatively accurate in the discrimination of DILI risk when human exposure levels are taken into account.

The analysis of variance between fresh and cryopreserved cells showed only marginal effects in the response of both HepaRG cells and PHH. Overall, the very low levels of the analyzed variances (inter- and intra-laboratory as well as between fresh and cryopreserved cells) that have been observed for HepaRG in this study suggest that this cell line delivers robust and reproducible data. The effects of cryopreservation in PHH observed here are in agreement with other reports (Richert et *al*., 2006), but more pronounced differences between fresh and cryopreserved PHH have been reported as well (Gouillouzo et *al.*, 2007;

Madan et *al.*, 2003). However, it is noteworthy that in this study only one donor of fresh PHH was included and that the effect of cryopreservation may also be secondarily related to the inter-donor variability of PHH.

Finally, two different HepG2 clones (ECCAC and TS clone) have been compared in order to determine clonal differences in response to compound exposure, which have been reported in the literature (Hewitt and Hewitt, 2004; Gerets et *al.*, 2012). The variations between the clones were only minor under the conditions of the study, but however, as only two different clones have been included here, no statement can be made regarding the inter-clonal differences of all available HepG2 clones.

For the further improvement of the cell models tested here, it becomes evident that the cells should be cultured in a format that allows a stable and more physiologically relevant phenotype. In addition, the application and development of more sophisticated endpoints, which allow to monitor the initial events leading to specific forms of DILI outcome, is urgently needed. This however, requires the stable expression of physiologically relevant levels of drug metabolizing enzymes, thus emphasizing the indispensable necessity to improve cell culture conditions for each cell system.

Several approaches are available in terms of improving hepatocyte physiology *in vitro* with regard to organ-specific microarchitecture:

- First, a monolayer is very limited in terms of cell-cell contact, meaning that the contact surface of a cell to the surrounding cells is marginal when compared to the whole cell surface. This is given by the culture format itself as it forces a cell to attach and become more flattened, and this is clearly not the case *in vivo* where the cells are of cuboidal shape, thus resulting in an enormous discrepancy of the cytoskeletal organization. Improvements addressing this issue, such as the well-established sandwich culture method (Tuschl and Müller, 2005; Kienhuis et *al*, 2007; Rowe et *al*., 2010) prove that cell physiology can be improved by improving the cell shape and enable increased cell-cell contact by culturing the cells between two hydrated layers of collagen. However, even though this cell culture method does improve a stable expression of drug metabolizing enzymes (DME) in hepatocytes and hepatocyte-like cells, it is not compatible to high throughput screening methods required in the early drug discovery phase. Therefore, improvement towards a three-dimensional cell culture format would greatly extend the cell-cell contact without the necessity of large cell numbers.
- Second, when taking the sinusoidal microarchitecture into account, it becomes clear that flow and consequently shear forces are essential aspects which have an important impact on physiology, i.e. the zonal differences in hepatocyte performance due to flow-dependent gradients (nutrients, xenobiotics, gases and waste products).

This leads to the assumption that hepatocyte function may be improved *in vitro* when culturing cells under flow conditions.

- Third, although hepatocytes account for about 80% of the total liver mass, other cell types, such as cholangiocytes, Kupffer cells and Ito cells, are crucial for hepatic physiology and by incorporation of these in to *in vitro* systems. For example, the involvement of an immune component (Kupffer cells) or the incorporation of bile duct cells (cholangiocytes) is suggested to improve the physiology of the model and subsequently an increased relevance for safety testing. The latter becomes especially clear in the case of XIM, which is known to elicit immune-mediated hepatotoxicity under long-term administration and was therefore withdrawn in 2006 (Keisin and Andersson, 2010). XIM was not recognized by any cell model in this study, thus emphasizing the need for co-cultures with non-parenchymal cells (NPCs).

Taking the above aspects into account, a variety of options and combinations exist to develop more sophisticated hepatic *in vitro* models towards physiological relevance and thus potentially improving early safety assessment during drug development.

3.1.2 Comparative proteomic characterization

As the cytotoxicity ring trial revealed clear different sensitivities of the different cell models to be able to recognize potential DILI risk compounds, a global proteomic analysis was performed in order to determine whether these differences in sensitivity were related to a loss of hepatophysiologic function. The comparison of the proteomic profiles will enable to both understand what each model is able to perform and thus what each cell model is fit for.

In this study, the global protein expression profiles of the human-derived hepatic cell lines HepG2, HepaRG and Upcyte hepatocytes were compared to cryopreserved PHH with a focus on proteins in drug metabolism as well as on the expression on cytoprotective proteins. The cell culture work for this experiment was performed by five MIP-DILI partners (University of Liverpool, KaLy-Cell, Servier, Merck and Karolinska Institutet) and both sample processing and measurement was conducted at the University of Liverpool (for detailed methods see Sison-Young and Mitsa et *al.*, 2015).

PHH, HepG2, Upcyte and HepaRG cells were thawed and seeded into collagen-coated 24-well plates as monolayer culture in the cell type specific seeding density and media. Protein was isolated from 10 million cells each following a cell type specific pre-incubation period (24h for PHH and HepG2; 72h for HepaRG and Upcytes) and processed for nanoLCMS/MS measurement using the iTRAQ (isobaric tags for relative and absolute quantification) technology as described detail in Sison-Young and Mitsa et *al.*, 2015.

3.1.2.1 *Global protein expression*

Protein profiles of the four cell types were generated for a total of 4696 proteins, of which 2722 proteins were quantified in all cell types. The overall protein profile for PHH was clearly separated from all other cell types, the expression profiles for HepG2 and Upcyte cells showed the highest differences and the expression profile of HepaRG was closer to that of PHH. Hierarchical clustering of the 2722 common proteins indicates clearly that PHH separate from all cell lines (figure 3.3). the expression profile of HepaRG cells showed the least differences compared to PHH as indicated in the heat map (figure 3.3). Protein expression of both HepG2 and Upcyte cells cluster closely together and expression levels differ clearly to those of PHH. A heat map was generated to compare the overall profile and a large number of proteins showed significantly lower expression in all cell lines compared to PHH, with differences being less pronounced in HepaRG compared to Upcyte and HepG2 cells as indicated by the color increments in each row (figure 3.3).

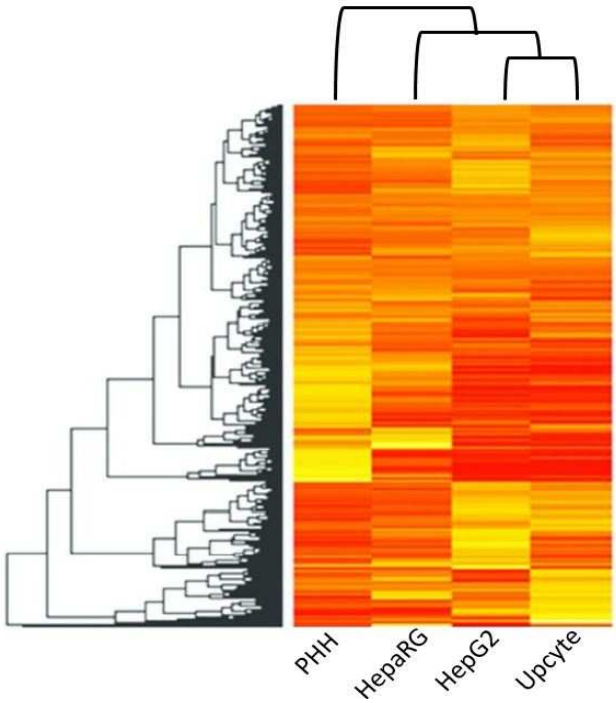

Figure 3.3: Heat map representation of the 2722 common proteins identified in all cell systems including hierarchical clustering. Columns represent the different samples analyzed and rows represent protein IDs. Values range from low (red) to high (yellow). All three cell lines segregated from PHH with the least pronounced difference in HepaRG cells. Figure taken from Sison-Young and Mitsa et *al.*, 2015.

Table 3.2: Average magnitude of change in protein expression of the cell lines related to cryopreserved PHH of the 20 top canonical pathways. 14 out of 20 pathways are downregulated across all cell lines, with the least difference in HepaRG cells.

	HepG2 vs cPHH	**HepaRG vs cPHH**	**Upcyte vs cPHH**
Pathway	Mean Log_2 Fold Change	Mean Log_2 Fold Change	Mean Log_2 Fold Change
EIF2 signalling	1.54	0.68	1.12
Mitochondrial Dysfunction	-2.92	-1.00	2.79
Oxidative Phosphorylation	-2.89	-1.19	-3.06
Regulation of eIF4 and p70S6K Signalling	1.44	0.81	1.19
tRNA charging	0.83	0.34	0.51
Serotonin Degradation	-4.46	-1.79	-4.95
Ethanol Degradation II	-3.27	-1.41	-4.29
mTOR Signalling	1.36	0.67	0.98
Fatty acid β-oxidation	-3.57	-1.56	-3.6
Noradrenaline and Adrenaline degradation	-3.85	-1.57	-4.46
TCA Cycle II	-3.4	-0.76	-3.29
Xenobiotic metabolism signaling	-2.61	-0.97	-2.92
Cholesterol biosynthesis	-1.49	-0.16	-0.75
Valine Degradation I	-4.65	-1.56	-4.47
Nrf-2-mediated oxidative stress response	-1.18	-0.22	-1.32
Nicotine Degradation II	-5.37	-2.19	-5.20
Methionine Degradation	-2.23	-1.20	-2.66
Remodelling of epithelial adherens Junctions	0.69	0.61	1.28
Bile acid Biosynthesis neutral pathway	-4.30	-1.24	-5.04
Protein ubiquitination pathway	0.84	0.12	0.40

Table 3.2 shows the 20-top canonical based on the total protein group analyzed and includes the log2 fold change in expression for each of these pathways, of which 14 were downregulated in HepaRG, HepG2 and Upcyte cells in comparison to PHH (table 3.2), e.g. pathways involved in drug metabolism (xenobiotic metabolism signaling, table 3.2), mitochondrial metabolism (oxidative phosphorylation) and steroid metabolism (cholesterol biosynthesis).

Few pathways also show a slight upregulation in the cell lines in when compared to PHH, i.e. proteins involved in cell motility and proliferation (Remodelling of epithelial adherens junctions).

3.1.2.2 *Expression profiles of drug metabolizing enzymes*

The determination of expression levels of proteins that are involved in xenobiotic metabolism is of crucial value in the context of hepatotoxicity testing *in vitro* and helps to identify the

suitability of a cell model to a specific purpose. It is well-known that toxic effects are not only related to a parent compound but may also occur through the metabolic generation of reactive species, which is mainly mediated by CYP450 functionalization reactions (Antoine et *al.*, 2008; McGill and Jaeschke, 2013). Therefore, a subset consisting of 128 drug metabolizing enzymes and transporter (DMET) proteins has been investigated and expression levels in HepG2, HepaRG and Upcyte cells were compared to expression in PHH. Figure 3.4 shows a heat map representing the expression levels of the DMET subset in the four cell models.

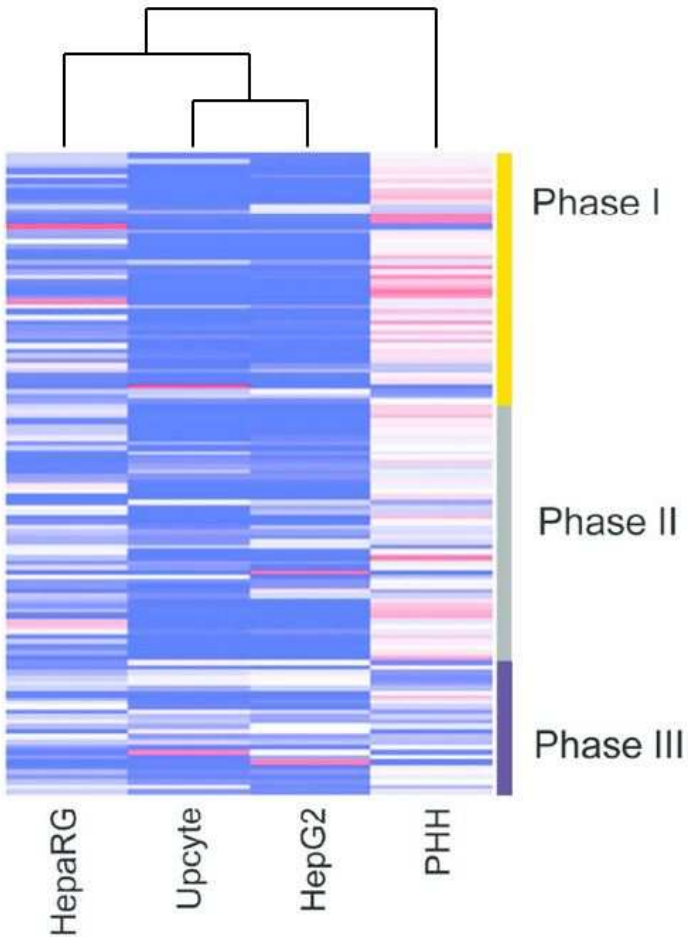

Figure 3.4: Heat map representing the hierarchical clustering of the four cell models in the basal expression levels of drug metabolizing enzymes and transporters (DMET). The colored side bar divides the heat map into phase I (yellow), phase II (grey) and phase III (purple) proteins. Upcytes and HepG2 cells cluster together whereas expression levels of HepaRG and PHH differ less. The highest difference is given for phase I expression levels and the least for phase III members. Values range from low to high using colour increments of pink and blue, respectively. Figure taken from Sison-Young and Mitsa et al., 2015, modified.

This protein set is composed of 50 phase I, 51 phase II and 27 phase III proteins and in consistency with the global expression profile PHH were clearly segregated from the other cell systems, again with less divergence in HepaRG cells. Based on phase I enzyme

expression the cell types were ranked regarding their metabolic capacity. Analysis of 15 CYP members proteins showed lower expression in the HepG2, Upcyte and HepaRG cells compared to PHH with a less pronounced difference for HepaRG cells (figure 3.4). For HepaRG cells, one exception was observed with the expression level of CYP3A4, that was calculated as 2.5-fold higher in basal expression than in PHH, which is in agreement with previous reports (Guillouzo et *al.*, 2007, Aninat et *al.*, 2005). In contrast, Rogue et *al.* (2012) compared the gene expression levels of DMETs in HepaRG and PHH of six donors, four of which expressed higher levels of CYP 3A4 compared to HepaRG, thus emphasizing the importance of including several PHH donors in comparative studies, independent from the investigated endpoint.

Regarding the expression of phase II enzymes, a lower expression of glutathione S-transferases (GSTs) and uridine diphosphate glucuronosyltransferases (UDPGTs) was observed in HepG2, Upcyte and HepaRG cells in comparison to PHH (figure 3.4). HepaRG cells showed higher expression of 3 isoenzymes of the GST and UDPGT families when compared to PHH. HepG2 cells showed higher expression of 5 phase II enzymes, i.e. N-acetyltransferase 10 (NAT10), glutathione S-transferase M3 (GSTM3), thiopurine S-methyltransferase (TPMT) and sulfotransferases 1A3 and 1A4 (SULT1A3 and 1A4) (see Sison-Young and Mitsa et *al.*, 2015).

The cell lines also showed lower expression levels of phase III transporters when compared with PHH and again HepaRG expression levels were closer to those of PHH than HepG2 and upcyte cells. All cell lines expressed higher levels of multidrug resistance protein1 (MRP1) expression and expression of multidrug resistance protein 3 (MRP3) and P-glycoprotein (P-gp, MDR1) was higher in HepaRG cells compared to PHH, which agrees with other studies (Jennen et *al.*, Rogue et *al.*, 2012).

The closer similarity of HepaRG cells to PHH in the responsiveness of xenobiotic metabolism has also been reported on the gene expression level (Lambert et *al.*, 2009; Jennen et *al.*, 2010; Rogue et *al.*, 2012, Gerets et *al*., 2012).

3.1.2.3 *Expression of cytoprotective proteins of the Nrf2/Keap1 pathway*

The outcome of a chemical insult is not only determined by the abundance and activity of DMETs, but also by the ability of a cell to defend itself against such insults, e.g. through the presence of antioxidants like glutathione or peroxiredoxins. A key regulator of the expression of proteins involved in the detoxification of reactive species is the Nrf2/Keap1 signaling pathway (Copple et *al.*, 2010) and the expression levels of HepG2, HepaRG and Upcyte cells relative to PHH are summarized in figure 3.5.

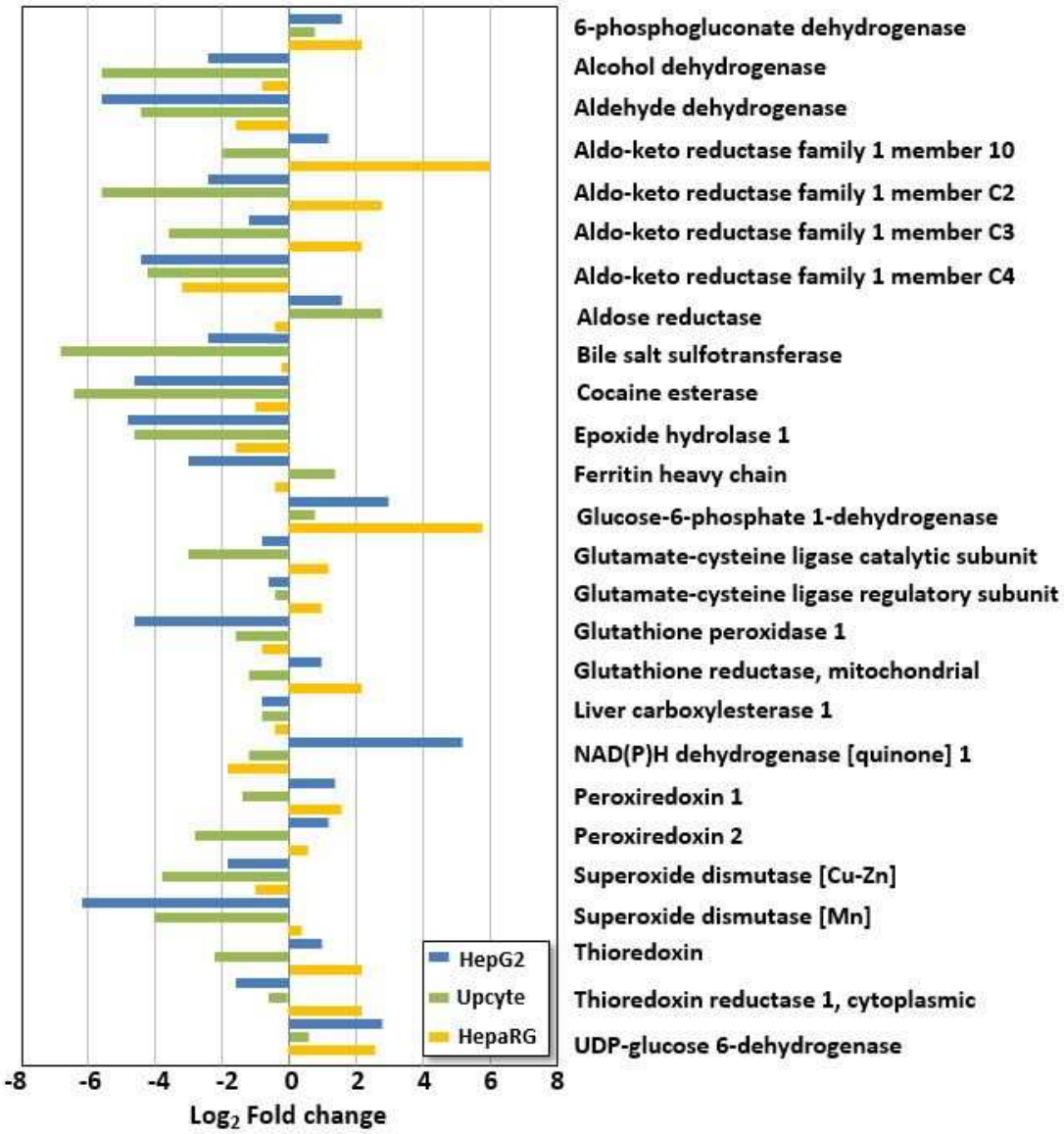

Figure 3.5: Expression levels of Nrf2-regulated proteins in HepG2 (blue), Upcyte (green) and HepaRG cells (yellow) relative to PHH expressed as log2 fold change. HepG2 and Upcyte cells show both the highest degree of downregulation, whereas in HepaRG cells the highest proportion of higher expression levels is observable, followed by HepG2. Figure taken from Sison-Young and Mitsa et al., 2015.

As shown in figure 3.5, the majority of the Nrf-2 regulated proteins contributing to cellular defense showed lower expression in both HepG2 and Upcyte cells and, to a lesser extent in HepaRG cells, which showed a more uniform distribution of either lower or higher abundance. Additionally, the two cancer-derived cell lines HepG2 and HepaRG both have a higher proportion of proteins that are more highly expressed relative to PHH than in the PHH-derived Upcyte cell line.

Given the inherent limitations that are present in single cells models with respect to their ability to predict clinically relevant DILI, many different approaches in developing more complex and physiologically relevant models have been initiated. These include the incorporation of non-parenchymal cells, three-dimensional cell culture approaches such as

spheroids or scaffold-based cultures, microfluidic and microphysiological models (Jiang et *al.*, 2015; Bale et *al.*, 2014; Brushan et *al.*, 2013; Wu et *al.*, 2010). However, independent from the complexity of those sophisticated *in vitro* approaches, they all rely on a hepatocyte or hepatocyte-like cell as the underlying basis. Indeed, the selection of a suitable cell model for the further development of liver cell models is of crucial importance as physiologically relevant cell-cell communication and -contact is likely to pose the fundament for the faithful development of a liver-like microarchitecture. It is therefore beneficial to characterize the cell models that are currently commonly used in early drug safety programmes with respect to the metabolic performance of each cell system and subsequently this helps to define suitable applications for each cell system.

The proteomic analysis was performed to understand the differences between commonly used cell systems in order to define what cell system is fit for what purpose. Primary human hepatocytes are considered the “gold standard” in *in vitro* hepatotoxicity testing strategies due to the closest relation to their native counterparts. But, due to the scarce availability, donor-to-donor variability and high costs associated with PHH, they are commonly not used in early screening approaches. Cancer cell lines, such as HepG2 and HepaRG, are routinely used in the pharmaceutical industry for a first estimation of cytotoxicity in the very early phases of drug development. These cell systems, although limited in their predictive value, are still beneficial as they are low cost, easily available, and display good reproducibility in comparison to primary human hepatocytes. However, in order to further develop more physiologically relevant hepatic *in vitro* systems, the proteomic signatures that were generated here using PHH as comparator may help to decide the appropriate cell source for a certain purpose.

In this comprehensive study, all tested cell systems clearly segregated from PHH in their protein expression profiles. The expression of key enzymes involved in xenobiotic metabolism is crucial for the assessment of hepatotoxic events that are not related to parent compounds. Therefore, the predictive value for hepatotoxicities that are mediated by reactive metabolites is limited in conventional monolayer cultures of cell lines. However, other phase I key enzymes were present in all cell lines but expressed significantly less when compared to PHH. It is known that manipulating the cell culture conditions, may lead to an enhanced expression of DMETs through a physiologically more appropriate microenvironment (Guillouzo and Guguen-Guillouzo, 2008; Prestwich et *al.*, 2008).

In addition to the overall low expression levels in the three cell lines compared to PHH, some proteins involved in cellular defense against toxic insults were expressed at higher levels. The Nrf2/Keap1 signalling pathway is a key pathway involved in the regulation of both constitutive and inducible cytoprotective proteins, such as peroxiredoxins and antioxidants, which are able to detoxify different reactive species. The expression of the Nrf2/Keap1

regulated cytoprotective proteins was the highest in the two cancer derived cell lines HepaRG and HepG2, which is in agreement with other studies that have shown the elevated cytoprotective capacity of cancer cells (Ganan-Gomez et *al.*, 2013; Shibata et *al.*, 2008; Ohta et *al.*, 2008). In Upcyte hepatocytes, which have been induced the proliferation by the introduction of "proliferative genes" by a viral vector (Burkard et *al.*, 2012), the expression of cytoprotective proteins was higher than in PHH, but less pronounced than in the cancer cell lines.

The proteomics data revealed that HepaRG cells have less pronounced differences compared to PHH than HepG2 and Upcyte cells, thus making them the most attractive model for further development. Interestingly, although HepaRG cells were the closest to PHH in the proteomic assessment, they have been shown to be the least sensitive cell system in the simple viability measurements as reported in section 3.1. A possible explanation for this discrepancy may be related to the increased susceptibility in HepG2 as the only proliferating cell line used here. Moreover, HepaRG was the only cell model for which serum supplemented media was used, which may affect the actual compound concentration due to serum protein binding of compounds.

The protein expression profile of Upcyte hepatocytes was closely to that of HepG2, thus not resembling the reported phenotype of 5-day old PHH (Burkhard et *al.*, 2012) under the conditions of this study. However, a second generation of Upcytes have been reported to express CYP activities equivalent to PHH and high CYP inducibility in initial studies. (Ramachandran et *al.*, 2015). Further studies, e.g. a genome-wide comparison between those cells and PHH or liver tissue would clarify the usefulness of 2nd generation upcytes in early drug safety assessment *in vitro.*

Overall, the low protein expression levels of the majority of DMETs alongside the overexpression of protective proteins in the cell lines, compared to PHH, may explain the underlying lower sensitivity of these commonly used cell systems towards toxic insult (section 3.1.1).

Moreover, it should be emphasized that only a small panel of hepatic cell models were included in this proteomic comparison and other hepatic cell lines that are in widespread use such as Hep3B, THLE or HuH-7 were not included. Additionally, the more and more emerging approach of stem cell derived hepatocytes, either from hESC[3] or iPSCs[4] have been shown to potentially provide a complementary tool to PHH (Chen et *al.*, 2012; Ware, Berger and Khetani, 2015) and should be further included in such comparative studies.

Taken together, the cell models tested do not reflect the native human liver physiology, but the possibility to improve this physiology by modulating cell culture conditions is worthwhile investigating. Due to the advantages of HepaRG cells in terms of protein expression levels

[3] Human embryonic stem cells
[4] Induced pluripotent stem cells

as well as HepaRG being a well-defined co-culture, this cell line, alongside PHH, was chosen for further studies.

3.2 Initial characterization of hepatic spheroids

Hepatocyte cellular polarity and differentiation are lost when cells are removed from their native configuration and cultured as monolayers (Levine and Stockdale, 1985). One option to culture cells with a higher morphologic relevance to the *in vivo* state is by introducing three-dimensionality, which dramatically changes cell shape in comparison to conventional monolayers. Three-dimensional cell culture (e.g. spheroids) is suggested to have a positive effect on overall cell health and physiologic functions since this culture format is more related to a native cell configuration. Spheroids display microtissues, thus they are amenable for histological applications enabling to get an overview of spheroid morphology.

In this section, spheroids of both PHH and HepaRG cells were investigated by different histological methods in order to assess general cell health and expression of DMEs over time. Cell culture techniques, molecular biological techniques, the preparation and staining of sections as well as image analysis represent my own work unless otherwise stated.

3.2.1 Spheroid morphology

The H&E (hematoxylin and eosin) staining is the gold standard method in pathology and was used to initially investigate spheroids from two different cell sources. The focus was on the cellular organization and morphological features associated with health and physiological functions of the spheroids. Trained pathologists confirmed all observations that are described in the following. Additionally, ATP content as well as the presence of Albumin were investigated in order to estimate overall cell health and physiologic function. Spheroid formation is mediated by self-assembly and whereas HepaRG speroids were reproducibly formed within four days, the formation time for PHH varied markedly depending on the donor (figure 3.6). Therefore, a cutoff of 7 days for spheroid formation was used for PHH and spheroid culture was performed for 14 days.

HepaRG and PHH spheroids were maintained in culture for 28 and 14 days, respectively, and samples were processed at days 3, 7, 14 and 28 for HepaRG spheroids and at days 3, 7 and 14 for PHH spheroids. Paraffin-embedded sections were prepared and stained with H&E (see section 2.2.2.11) in order to assess overall health and reveal intra-spheroidal microarchitecture.

Specific parameters were assessed, which are listed in table 3.3 and figure 3.7 shows an example of these parameters in a stained section.

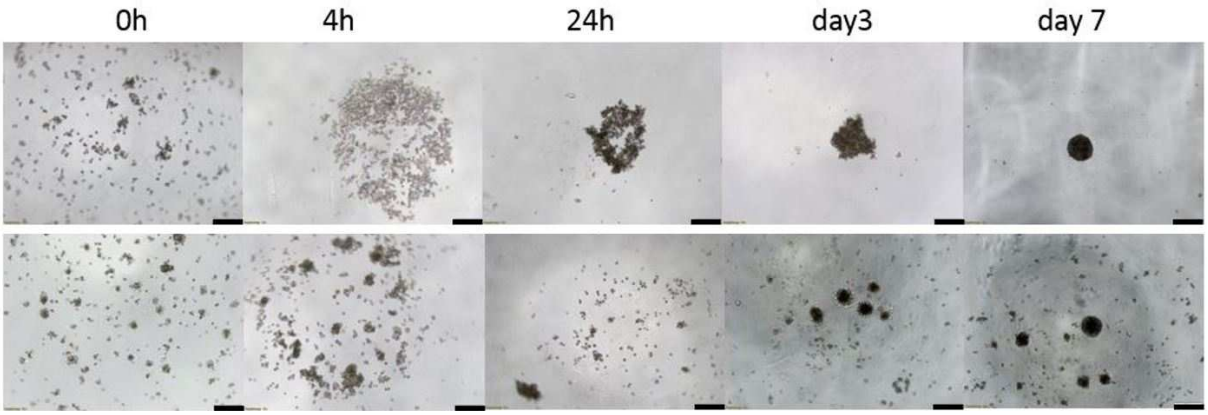

Figure 3.6: Time-dependent spheroid formation of PHH from two different donors. Donor-specific differences in spheroid formation time were observable and whereas PHH from one donor formed compact spheroids within seven days (upper row), those of a second donor formed multiple small spheroids or even no spheroids or loose aggregates (lower row). 4x magnification, bars = 200µm.

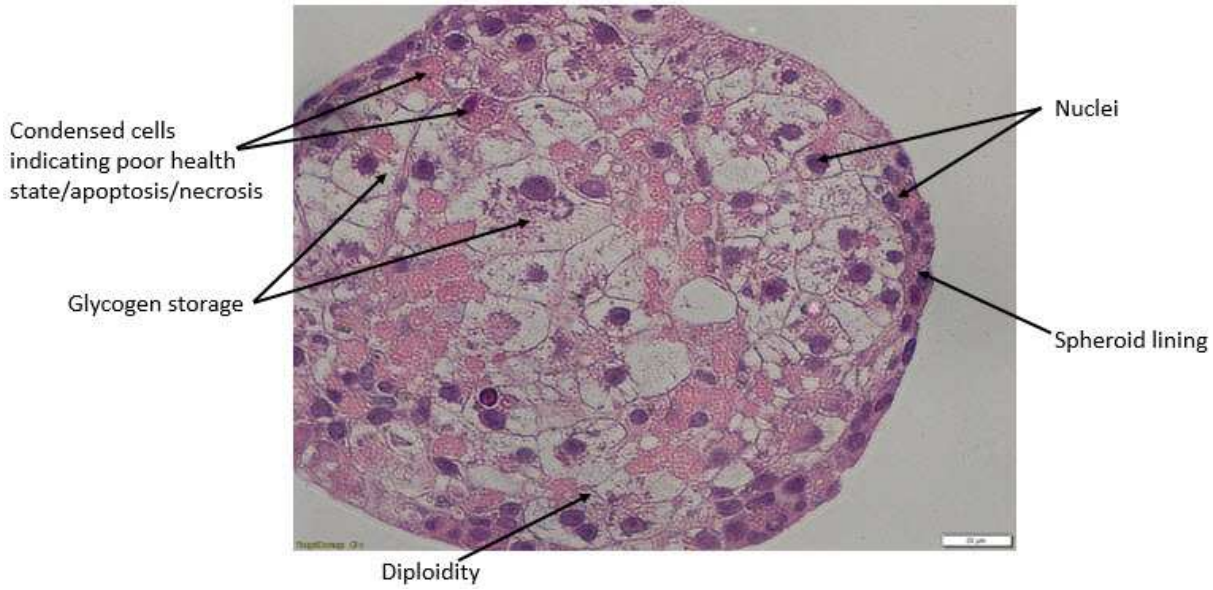

Figure 3.7: Overview of an H&E stained HepaRG spheroid microdissection. Arrows indicate the investigated parameters for basic cell health. HepaRG spheroid at day 7, 40x magnification, bar = 20 µm.

Table 3.3: Characteristic parameters used for the determination of spheroid health using H&E stained, paraffin embedded microdissections.

Parameter	Observational focus
General appearance	Cell shape and size, differences between center and lining
Nuclei	Size and shape, visibility of nucleoli, appearance and number of diploid cells
Glycogen	Dimension of glycogen storage, localization of glycogen storing cells
Cell death	Condensed and/ or fragmented cells, localization of apoptosis/ necrosis

3.2.1.1 *HepaRG spheroids*

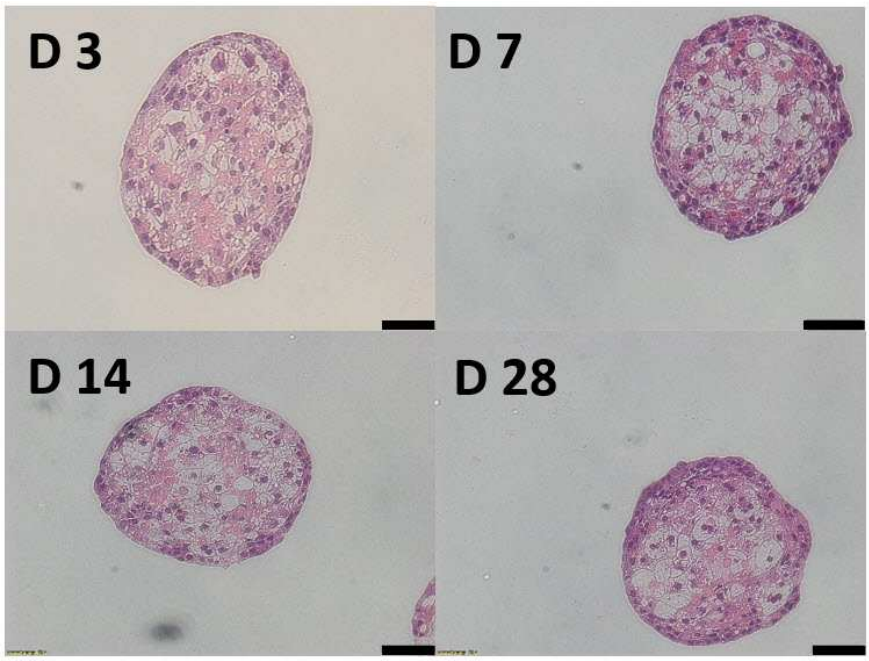

Figure 3.8: Paraffin embedded, H&E stained microdissections of HepaRG spheroids at different time points up to 28 days. HepaRG spheroids stayed viable for up to 28 days and showed two distinct cell morphologies: central cells with cuboidal shape and glycogen storage and flattened cells in the outer lining area. Additionally, overall spheroid size enables nutrition of central cells, indicated by the absence of necrotic cores. 20x magnification, bars = 50 µm.

Figure 3.8 shows representative images of H&E stained HepaRG spheroid sections over a cultivation period of 28 days. HepaRG spheroids showed well organized nuclei and cytoplasm without signs of necrotic or apoptotic centers (e.g. due to insufficient nutrition) at any time point. Intact nuclei are visible throughout the spheroid at every time point, defined by a regular purple staining and clearly visible nucleoli in the majority of cells. Differences in the shape of the nuclei were seen, ranging from spherical nuclei to more flattened and cigar-shaped nuclei. The shape seemed to depend on the localization within the spheroid, indicated by the fact that spherical nuclei were mostly located centrally, whereas the flattened appearance was restricted to the peripheral cells that line the spheroid. This distribution was consistent over time as seen in figure 3.8. Diploid cells were observable in most of the sections, but with a low frequency of approximately three to five diploid cells per section.

At the periphery, an irregular thickness of the lining layer was observed, ranging from one to five cell layers and characterized by small and flattened morphology in comparison to central cells with cuboidal shape. The lining was generally present at all time points in the complete

periphery and only a few single spots without this lining were observed (see fig 3.8, day 14 in the upper right quarter of the spheroid). Peripheral cells generally showed a different morphology, as well as much less glycogen storage capacity in comparison to central cells, suggesting two different cell types within the spheroid. As commercially available, differentiated HepaRG cells are a co-culture of hepatocyte-like cells and cholangiocyte-like cells (Jackson et *al.*, 2016), the two morphologies suggest that the central cells represent the hepatocyte-like population and the lining cells represent the cholangiocyte-like population, indicating a certain degree of organization in HepaRG spheroids.

An important function of hepatocytes in the liver is the storage of glycogen, which is essential for energy metabolism. HepaRG spheroids showed a robust capacity for glycogen storage from day 3, characterized by white intracellular areas interstratified with pink cytoplasm, which is subsequently referred to as “cloddy”. Other studies have reported a positive staining with periodic acid-Schiff (PAS) in cryosections of HepaRG spheroids (Ramaiahgari et *al.,* 2017), which corroborates the observed appearance in the paraffin-embedded sections used here. Glycogen storage capacity seemed to be restricted more centrally to the cuboidal cells, whereas the flattened lining appeared to contain either no or very little glycogen, thus confirming the localization of cholangiocyte-like cells in the peripheral area. The amount of glycogen per cell increased over time in most of the sections and individual cells stored large amounts of glycogen, indicated by increased cell size and rather white than cloddy appearance of the cytosol.

Condensed cytoplasm and chromatin, characterized by an increase of the staining intensity, and nucleic fragments indicate a poor health state that mostly results in cell death. These events were observable very infrequently and seemed to appear randomly distributed throughout the spheroids. This suggests that the apoptotic/ necrotic observed reflect a normal physiological turnover and were not a result of insufficient nutrient supply.

In order to estimate spheroid health on a molecular basis, HepaRG spheroid sections were additionally stained for Albumin and ATP content was measured in order to confirm the morphological results on a molecular level (figures 3.9 and 3.10).

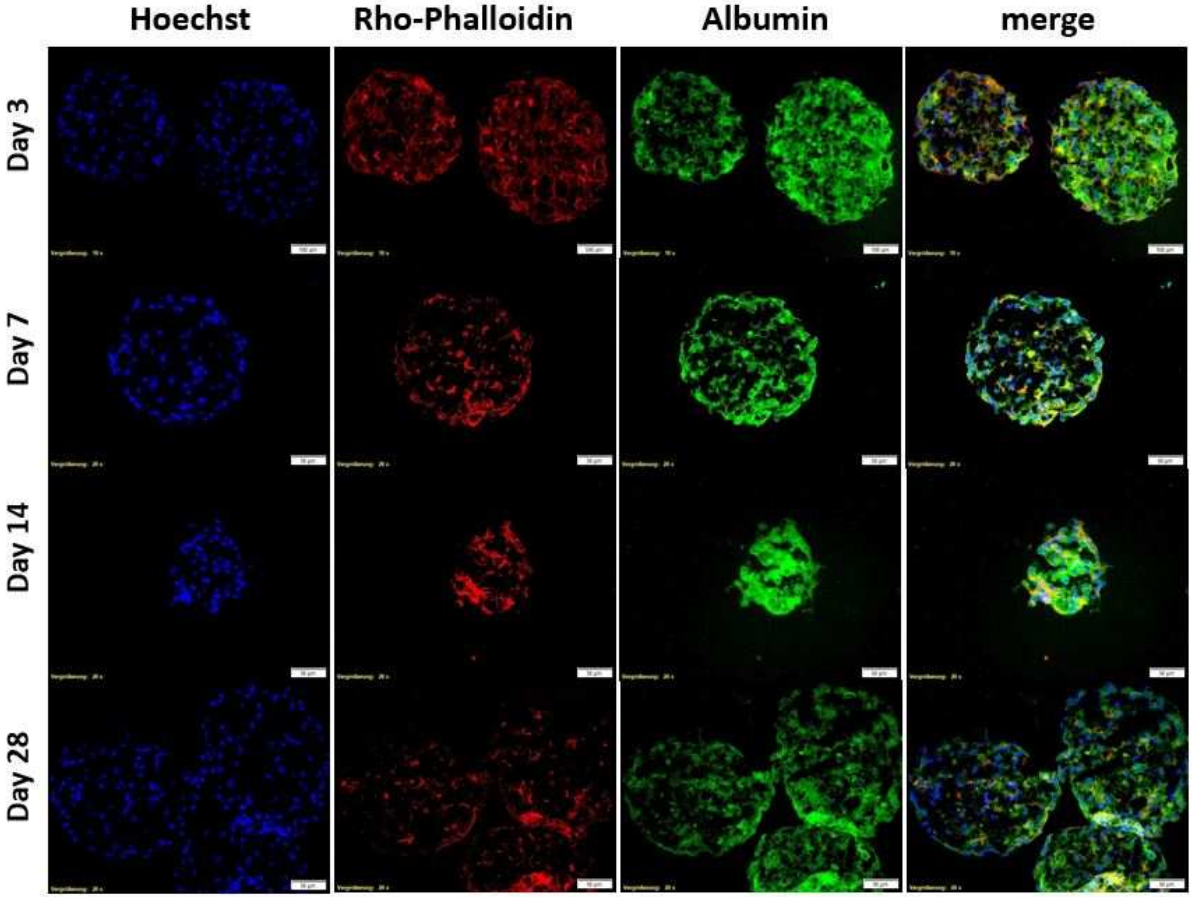

Figure 3.9: Expression of Albumin (green) in HepaRG spheroids at days 3, 7, 14 and 28 including double counterstain of nuclei (blue) and cytoskeleton (red). Albumin is clearly abundant in HepaRG spheroids throughout all time points at comparable levels. Note that the smaller spheroid size is related to the section plane and not to the overall spheroid size. 20x magnification, bars = 50µm.

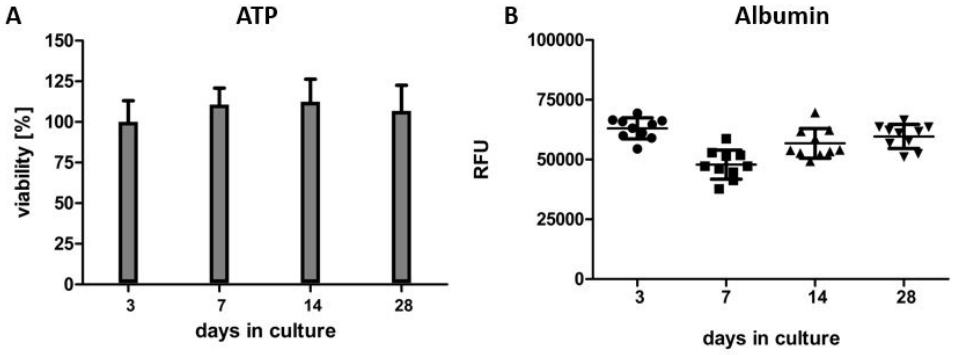

Figure 3.10: ATP (A) and Albumin (B) content in HepaRG spheroids at days 3, 7, 14 and 28. Both ATP and Albumin are clearly abundant in HepaRG spheroids throughout all time points without statistically significant differences. RFU = relative fluorescent units.

Figure 3.9 shows the immunofluorescent staining of albumin in HepaRG spheroids at different time points. Albumin was detectable at every time point and visual differences between time points as well as between spheroids at one time point were observable in single sections (fig 3.9, day 3), but overall intensities were not significantly different in the image analysis data as shown in figure 3.10 B. Additionally, the ATP content was at comparable levels over time without significant differences, thus confirming the microscopic observations.

3.2.1.2 *PHH spheroids*

Primary human hepatocytes spheroids were also investigated using the H&E staining and compared to HepaRG spheroids. Due to the extended spheroid formation time required for PHH, only three time points, namely days 3, 7 and 14, were compared.

Figure 3.11 shows representative PHH spheroid sections at days 7 and 14 (H&E stained sample of day 3 is not available).

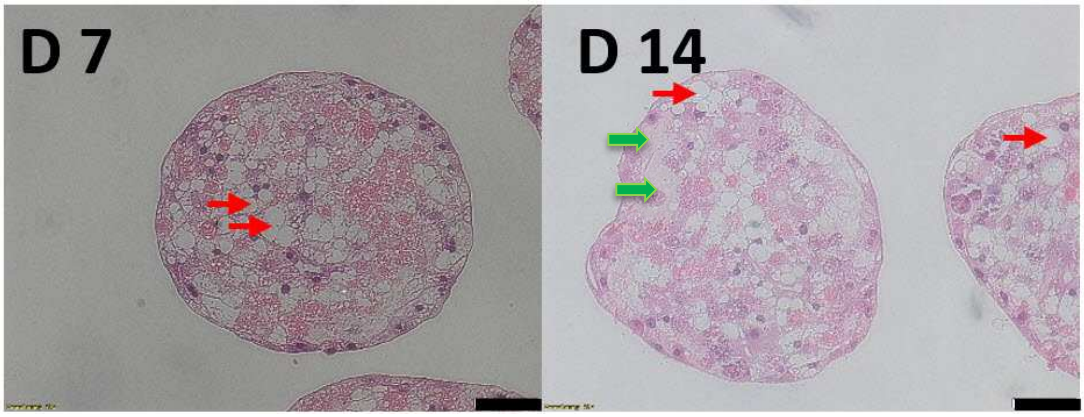

Figure 3.11: Paraffin-embedded, H&E stained microdissections of PHH spheroids at two different time points. The spheroids stayed viable for at up to 14 days showing one cell morphology as well as a thick lining which is suggested to be composed of extracellular matrix (ECM). 20x magnification, bars = 50 µm.

In general, PHH were viable for at least 14 days and showed a more uniform appearance in comparison to HepaRG spheroids. The most obvious difference was the absence of lining cells and the outer cells appeared much less flattened and showed moderate to high glycogen contents. PHH spheroids had a lining that was not built up of flattened cells, but they seemed to have a thickened membrane, suggesting the production of extracellular matrix components of the peripheral cells, potentially in order to enhance stability of the microtissues. The uniform appearance was also visible by the morphology of the nuclei, which were observable as round nuclei with clearly visible nucleoli, similar to those observed for the hepatocyte-like cells in the centers of HepaRG spheroids.

The glycogen content appeared to be uniform throughout the spheroid with the majority of cells showing moderate glycogen content.

Interestingly, PHH spheroids seemed to store a noticeable amount of lipids, visible as round inclusions with sharp borders and no visible cytosolic fractions compared to the glycogen, indicated by the red arrows in figure 3.11. These lipid droplets were consistent at both time points, suggesting that there is no time-dependent accumulation. Cryopreservation of PHH has been reported to alter lipid metabolism (Godoy et *al.*, 2013), which may be the underlying reason for this effect.

Similar to HepaRG spheroids, cell death was observed infrequently and independent from any localization within the spheroid so that an insufficient nutritional state could be excluded. Although apoptosis was responsible for the majority of cell death events, few necrotic cells were observable, which could have an impact on the health state of surrounding cells. An example for this is given in the day 14 section in figure 3.11, indicated by the green arrows. Since necrosis is defined as an uncontrolled event at which cell death is not regulated, the necrotic cells burst and cellular content is released in the interstitial area. This affects the surrounding cells and may also lead to further necrotic, areas, indicated by amorphous structures and a pale pink staining in the size range of 2-5 cells.

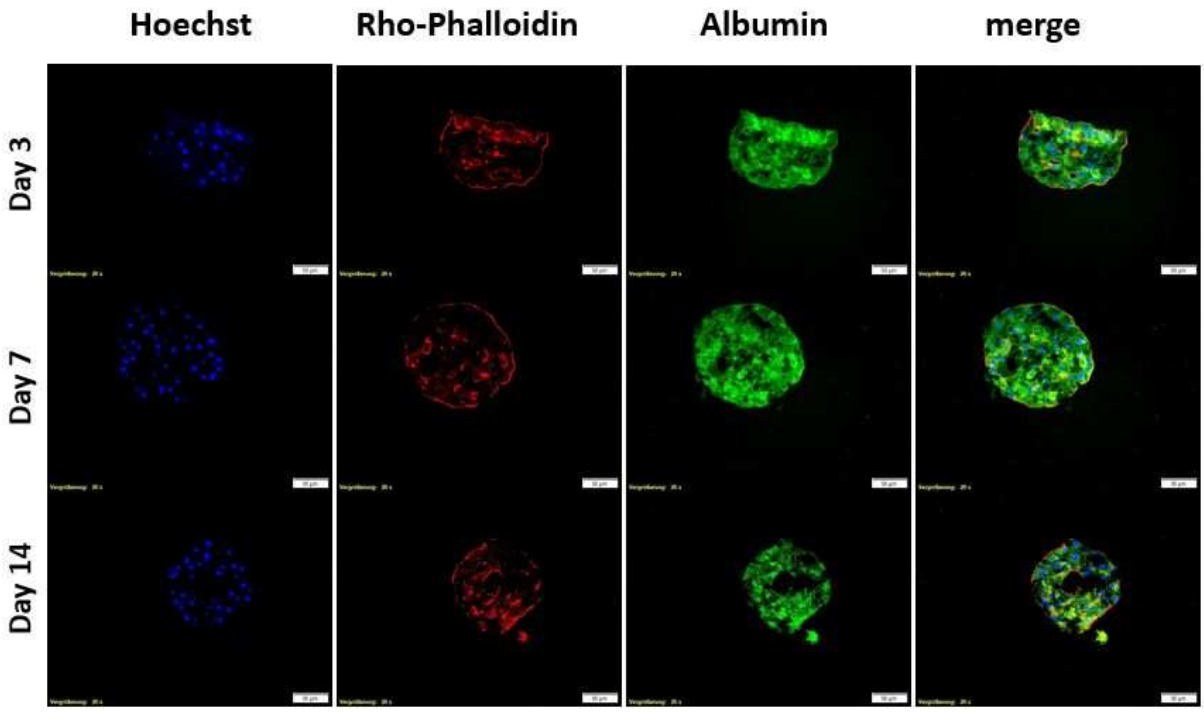

Figure 3.12: Expression of Albumin (green) in PHH spheroids at days 3, 7 and 14 including double counterstain of nuclei (blue) and cytoskeleton (red). Albumin is clearly abundant in PHH spheroids throughout all time points at comparable levels. Note that differences in size are related to the section plane. 20x magnification, bars = 50µm.

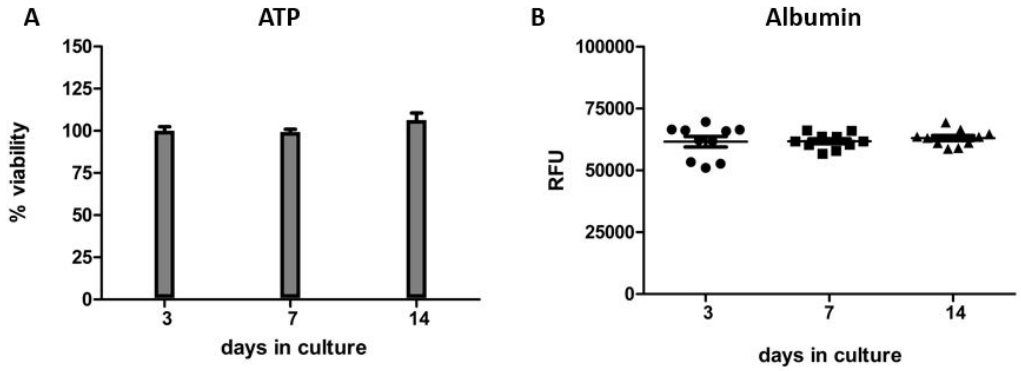

Figure 3.13: ATP (A) and Albumin (B) content in PHH spheroids at days 3, 7 and 14. Both ATP and Albumin are clearly abundant in PHH spheroids throughout all time points without statistically significant differences. RFU = relative fluorescent units.

Next to the morphological checkpoints, the determinations of albumin and ATP content were used as molecular markers for overall cell health (ATP) and hepatocyte physiology (albumin). Figure 3.12 shows the immunofluorescent staining of albumin (green) in PHH spheroids at days 3, 7 and 14. Albumin was present at every time point in comparable intensities as shown in figure 3.13 B, indicating that hepatocyte-specific functions are maintained during prolonged culture. Secondly, cell viability was assessed by quantification of ATP levels, which remained constant over time as visible in fig 3.13 A, thus indicating no decrease in viability in long-term culture.

The microscopic observation of spheroid sections over time showed that spheroids stay viable over a period of at least four weeks in HepaRG and two weeks in PHH spheroids, indicated by intact nuclei and membranes, storage capacity as well as the absence of necrotic areas. Additionally, the temporal stability of both albumin and ATP content further confirm the morphological observations.

In HepaRG spheroids, the abundance of two different cell morphologies suggest a certain organization of cholangiocyte-like cells and hepatocyte-like cells within the spheroid. Indeed, Ramaiaghari et *al*. (2017) found that cytokeratin 19 (ck19), a cholangiocyte-specific marker, was only expressed in the lining cells in HepaRG spheroids. This organization does not reflect the hepatic microarchitecture *in vivo* and the impact of this morphology on the physiologic relevance of HepaRG spheroids needs to be further analyzed. Visually, the lining cells were observed in a lower proportion as the central cells, which may hypothesize a potentially culture-dependent shift in the ratio of both cell types since the ratio commercially available HepaRG cells is approximately 1:1. In contrast, some reports with HepaRG spheroids generated in hanging-drop or spinner flask culture formats have observed an opposite localization, in which cholangiocyte-like cells were located centrally (Gunness et *al.,*

2013; Leite et *al*., 2012). This emphasizes that further studies are required in order to understand the dynamics of cellular reorganization in three-dimensional space as well as the impact of culture conditions on cell signaling mechanisms in hepatic spheroid models.

However, the simple H&E stain was an initial step to prove whether spheroid cell culture is capable of being cultivated for a certain period of time by monitoring cell health. But, obtaining organized, viable cells do not necessarily imply that the expression of DMETs is enhanced in this cell culture format or that this model has a higher physiological relevance.

Moreover, it has to be noted that the single sections investigated here only represent snapshots and do not reflect the spheroid as a whole, which would be possible by confocal microscopy.

However, the overall stable cell health and the maintenance of physiologic functions such as glycogen storage show a clear indication for long-term applications with a physiologically relevant hepatic *in vitro* model.

As primary human hepatocytes show a wide inter-donor variability (Hewitt et *al.*, 2015; Elaut et *al*., 2006), this variability somewhat seemed to be reflected in terms of the ability to form spheroids as well as the spheroid formation time, which varied markedly among donors (figure 3.6). This is currently hampering the applicability of PHH spheroids for routine use. A possible option to address this issue may be the use of pooled PHH, which has already been established by generating spheroids from 10 PHH donors (5 male and 5 female donors) (InSphero AG, Switzerland, www.insphero.com). Additionally, the optimization of protocols could also reduce spheroid formation time, e.g. by extending centrifugation steps in order to speed up cell aggregation.

3.2.2 Expression of drug metabolizing enzymes

As hepatocyte morphology and longevity in spheroid cultures was shown in the initial assessment, it was important to investigate whether spheroids have an improved metabolic capacity.

H&E staining of paraffin-embedded spheroid sections is an attractive option to monitor spheroid health and quality over time, but this method does not allow any assessment of the expression of DMETs, which play a major role in the initiation of metabolite-metiated hepatotoxicity. To address this issue, immunofluorescent (IF) staining of cryosections were performed in order to assess the general expression of DMETs, as well as to monitor expression over time. Therefore, representative members of each phase of xenobiotic metabolism were chosen (table 3.4).

Table 3.4: selected antibodies against phase I, II and III DMETs for the initial assessment of spheroids over time with respect to metabolic capacity.

Antigen, host, clonality	Dilution
Phase I	
CYP1A2, mouse monoclonal	1:200
CYP2B6, mouse monoclonal	1:200
CYP3A4, mouse monoclonal	1:500
Phase II	
NAT1/ 2, mouse monoclonal	1:200
SULT1A1, rabbit polyclonal	1:200
Phase III	
BSEP, rabbit polyclonal (ABCB11)	1:100
Mdr1, mouse monoclonal (ABCB1)	1:200
MRP2, rabbit polyclonal (ABCC2)	1:200

3.2.2.1 *Expression of Phase I isoenzymes*

Phase I DMEs (e.g., CYPs) are the first step in drug metabolism and are responsible for the introduction of functional groups in to the molecular structure of a compound. Although the biological intention of this step is the detoxification of a parent compound, the generation of toxic metabolites may also occur. These are often not formed in early *in vitro* hepatic cell systems due to lacking Phase 1 DME expression, resulting in false negative results. Thus, it is important to investigate whether a hepatic cell system expresses these enzymes in order to be capable of xenobiotic metabolism.

Figure 3.14 shows the localization of CYPs within the spheroids in detail using the example of CYP 3A4 and figures 3.15, 3.16 and 3.17 show the expression patterns of CYP1A2, CYP2B6 and CYP3A4, respectively, in HepaRG spheroids at days 3, 7, 14 and 28.

CYP3A4 appeared as moderate to strong cytoplasmic staining with an overlap to the outer border of the nuclei (blue), which was observed as a white “halo” in the merged channels (figure 3.14). This overlap in the merged picture suggested that the white areas resemble the endoplasmic reticulum (ER), to which CYP enzymes integrate as transmembrane proteins. The cytoplasmic staining appeared cloddy, which was consistent with the observations of glycogen storage leading to a cloddy appearance of the cytoplasm in H&E stained sections.

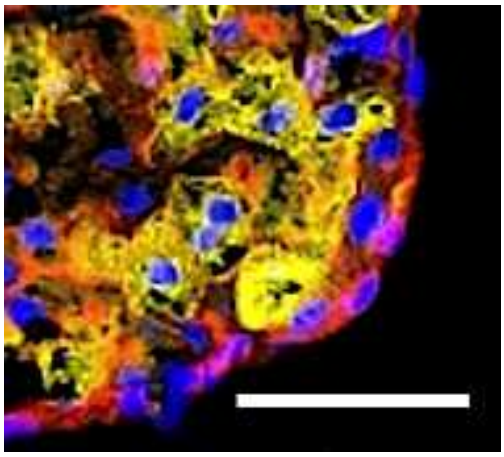

Figure 3.14: CYP3A4). CYPs are located in the cytoplasm as well as in the endoplasmic reticulum around the nuclei (yellow/white). Cutout from CYP3A4 staining in HepaRG spheroids at day 3. 40x magnification, bar = 20 µm

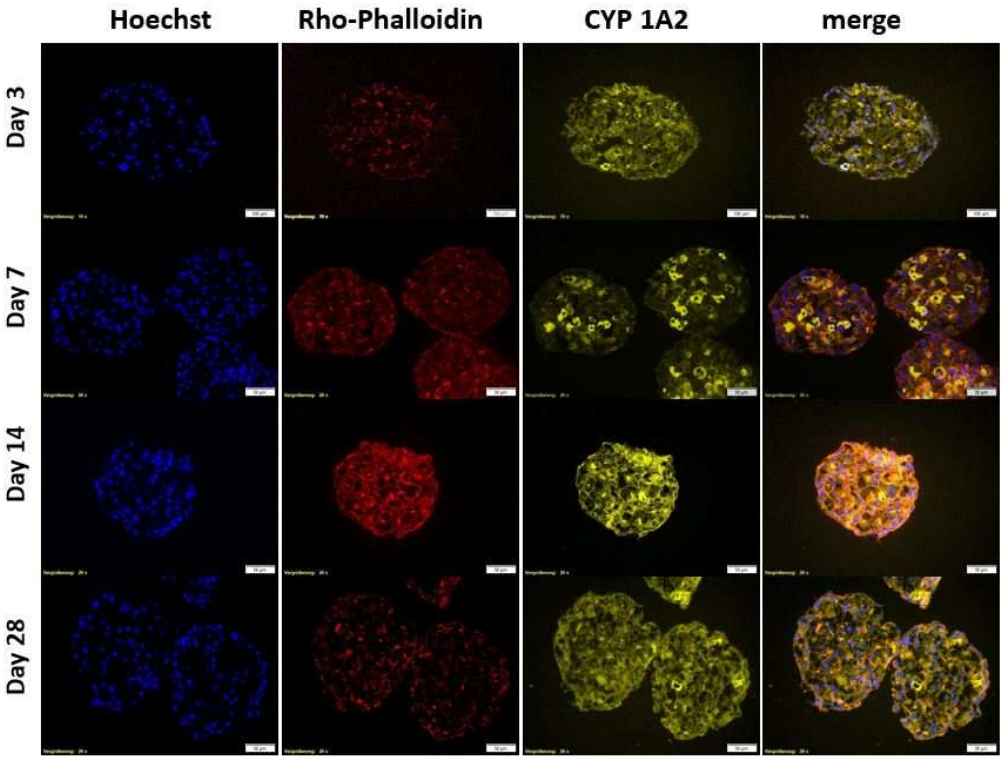

Figure 3.15: Expression of CYP 1A2 (yellow) in HepaRG spheroids at days 3, 7, 14 and 28 including double counterstain of nuclei (blue) and cytoskeleton (red). HepaRG spheroids express CYP 1A2 throughout all time points with varying intensities amongst single cells, resulting in a patchy expression pattern. 20x magnification, bars = 50µm.

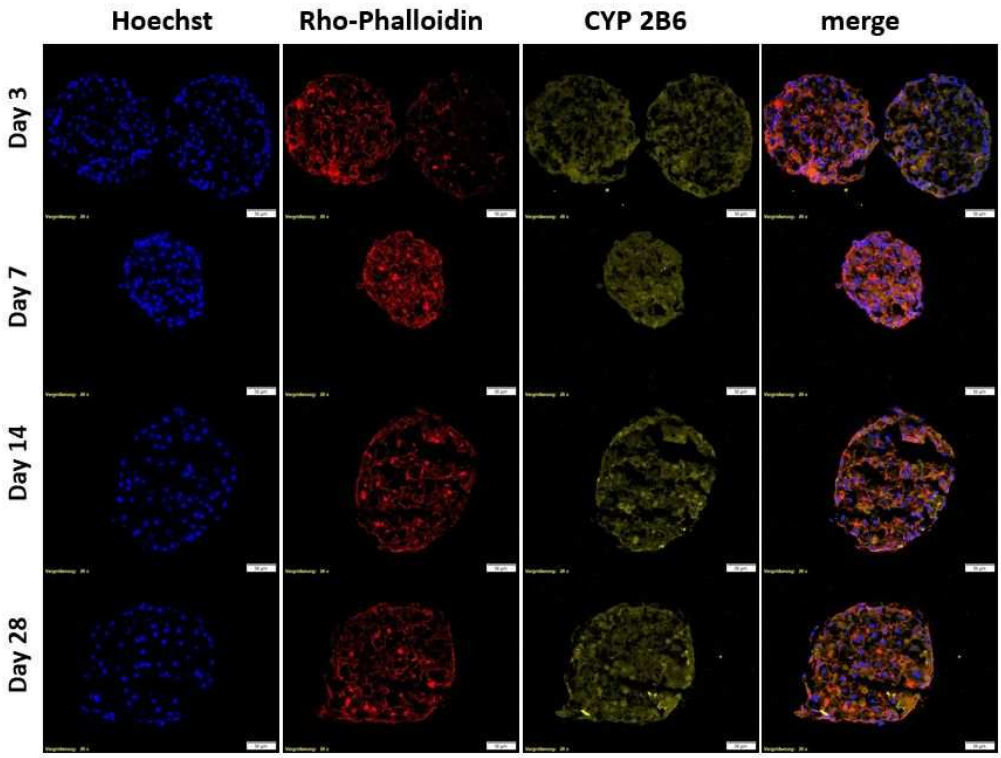

Figure 3.16: Expression of CYP 2B6 (yellow) in HepaRG spheroids at days 3, 7, 14 and 28 including double counterstain of nuclei (blue) and cytoskeleton (red). HepaRG spheroids weakly express CYP 2B6 throughout all time points. 20x magnification, bars = 50µm.

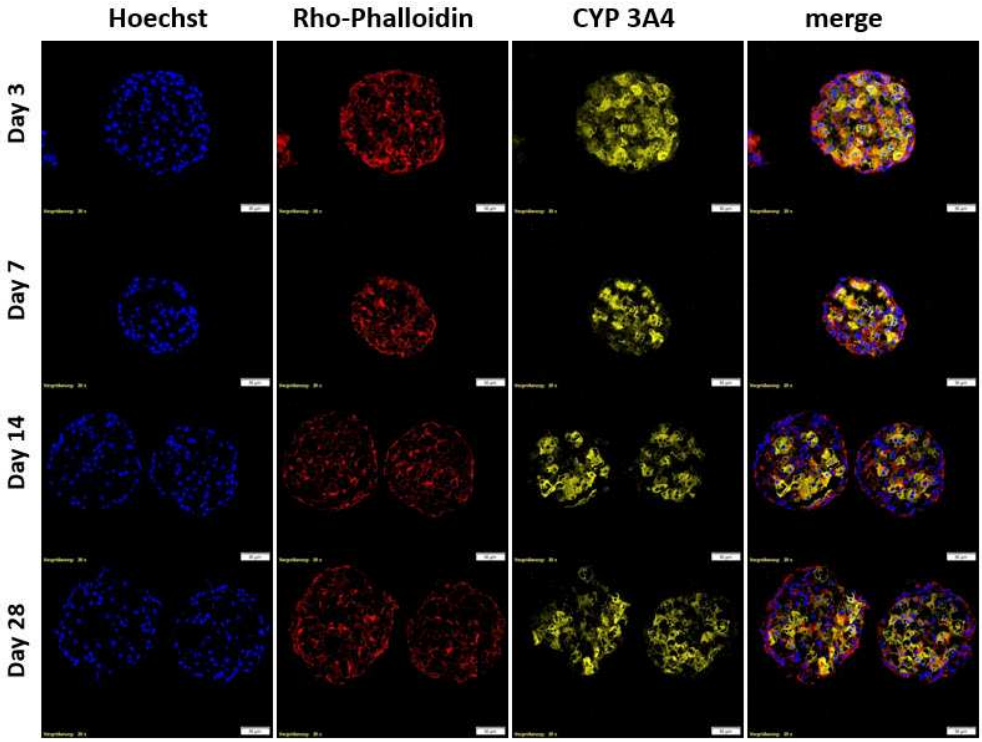

Figure 3.17: Expression of CYP 3A4 (yellow) in HepaRG spheroids at days 3, 7, 14 and 28 including double counterstain of nuclei (blue) and cytoskeleton (red). HepaRG spheroids express CYP 3A4 throughout all time points with varying intensities amongst single cells, resulting in a patchy expression pattern. A slight decrease in CYP 3A4 over time was observed. 20x magnification, bars = 50µm.

When looking at the overall distribution of both CYP 1A2 and CYP 3A4 expressing cells within the spheroid, it was observable that single cells expressed different enzyme levels, thus leading to a patchy appearance. It was also observed that the lining layers expressed no or very little levels of CYP 3A4.

In figure 3.14, HepaRG spheroids clearly expressed CYP 3A4 at all time points but seemed to decrease slightly over time. Therefore, the mean “area x intensity” of at least 10 sections per target protein was calculated in order to reveal whether the observed differences were significant or not. Figure 3.18 shows scatter plots of the relative fluorescent units per 1,000 pixels for all phase I enzymes investigated in HepaRG spheroids at all time points.

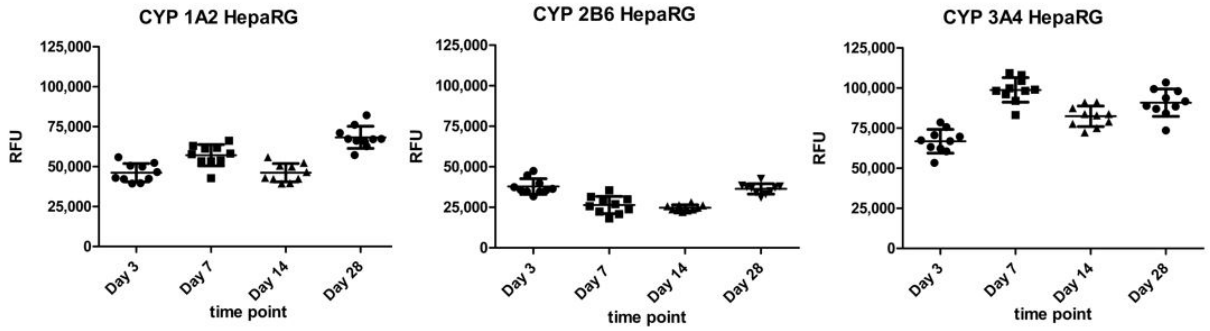

Figure 3.18: Scatter plots of CYP protein expression levels in HepaRG spheroids over time, expressed as the mean of area x intensity (relative fluorescent units per 10,000 pixels) of CYP 1A2 (left), CYP 2B6 (middle) and CYP 3A4 (right). Time-dependent differences were observable for every CYP without any general trend observed. Relative fluorescent unit values on the y-axis also indicate different basal expression levels for each isoenzyme with the highest expression levels for CYP 3A4. RFU = relative fluorescent units. (Turkey´s multiple comparisons test; α = 0.05, no significant differences)

The scatter plots revealed different expression levels for CYPs 1A2, 2B6 and 3A4 over time. The expression patterns also differed for each isoenzyme, showing increased expression of CYP1A2 at day 28, whereas the expression pattern of CYP2B6 was the highest at days 3 and 28 and seemed to drop in between and also CYP3A4 showed a different pattern with the lowest expression at day 3. Statistically significant differences were not measurable, suggesting an overall temporal stability of the CYPs investigated here. The intensity measurements also revealed different basal expression levels between isoenzymes. The highest expression was observed for CYP3A4, ranging from 60,000 to 100,000 RFU/1,000 pixels, whereas, in comparison, CYPs 1A2 (40,000-70,000 RFU) and 2B6 (20,000-40,000 RFU) were significantly lower expressed.

A second question that was addressed was the comparison of CYP expression levels in PHH compared to HepaRG spheroids. Figures 3.19, 3.20 and 3.21 show representative pictures of CYPs 1A2, 2B6 and 3A4 in PHH spheroids at days 3, 7 and 14, respectively.

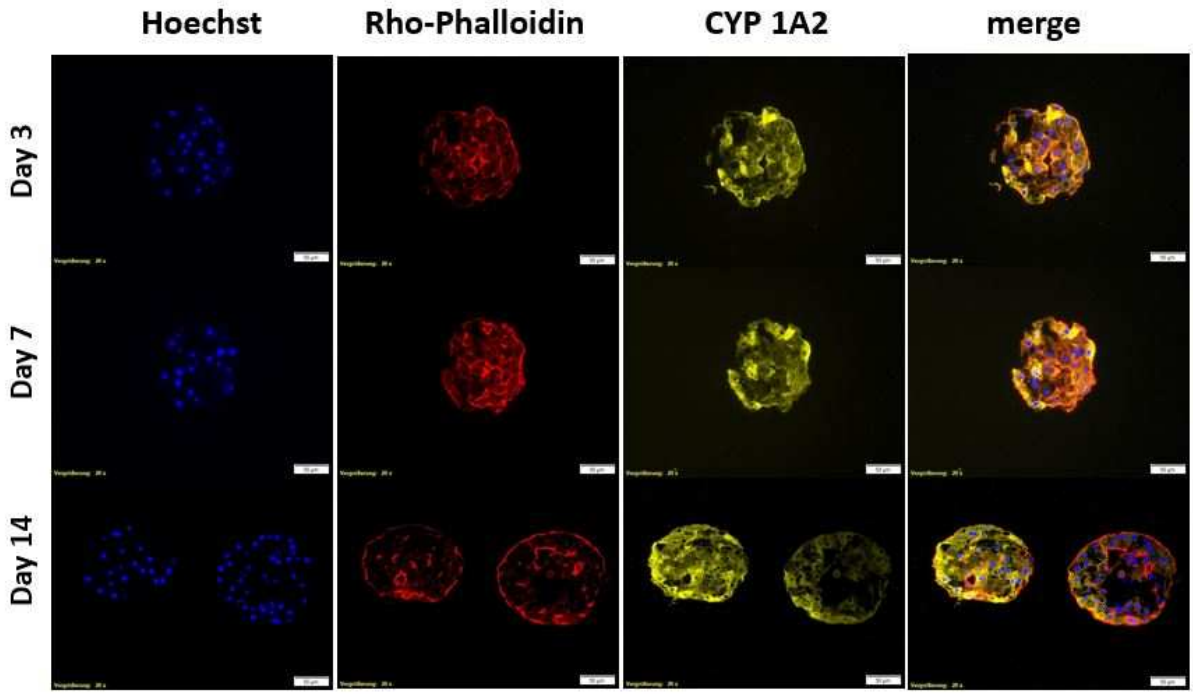

Figure 3.19: Expression of CYP1A2 (yellow) in PHH spheroids at days 3, 7 and 14 including double counterstain of nuclei (blue) and cytoskeleton (red). CYP1A2 expression was at comparable levels throughout all time points but differences between sections of one time point were observable as indicated at day 14, where spheroids showed different expression levels. Overall, peripheral cells appeared to express higher CYP1A2 levels. 20x magnification, bars = 50µm.

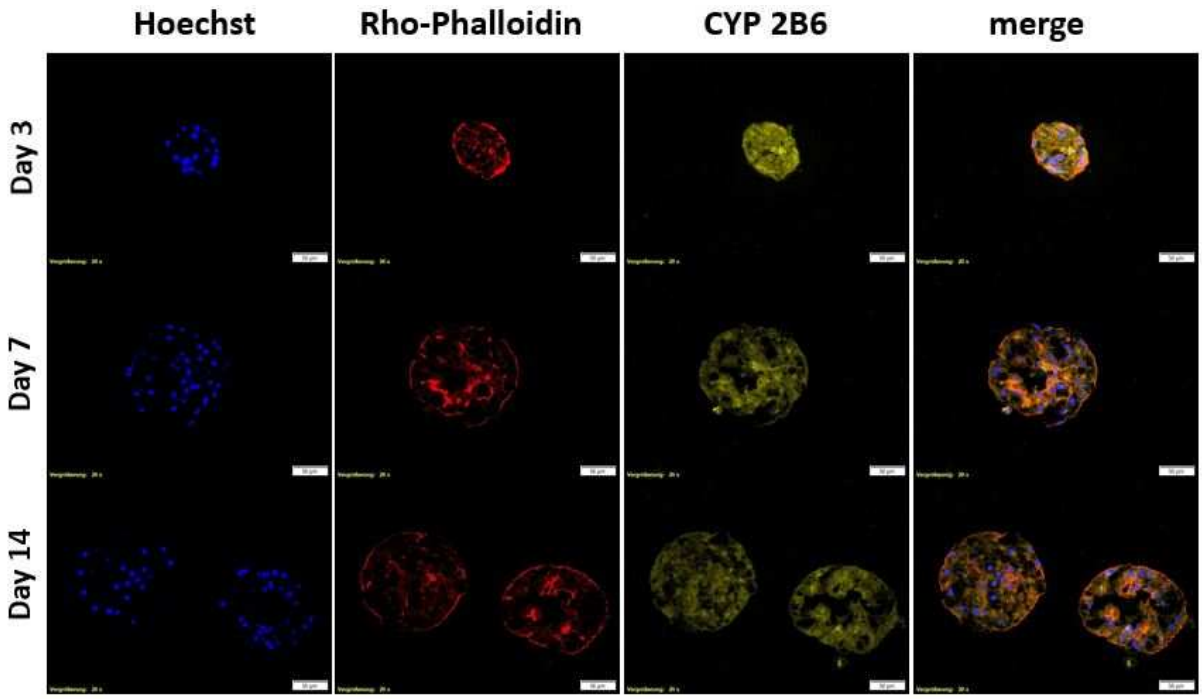

Figure 3.20: Expression of CYP 2B6 (yellow) in PHH spheroids at days 3, 7 and 14 including double counterstain of nuclei (blue) and cytoskeleton (red). CYP2B6 is weakly abundant in PHH spheroids throughout all time points in a patchy distribution pattern. Note that differences in size are related to the section plane. 20x magnification, bars = 50µm.

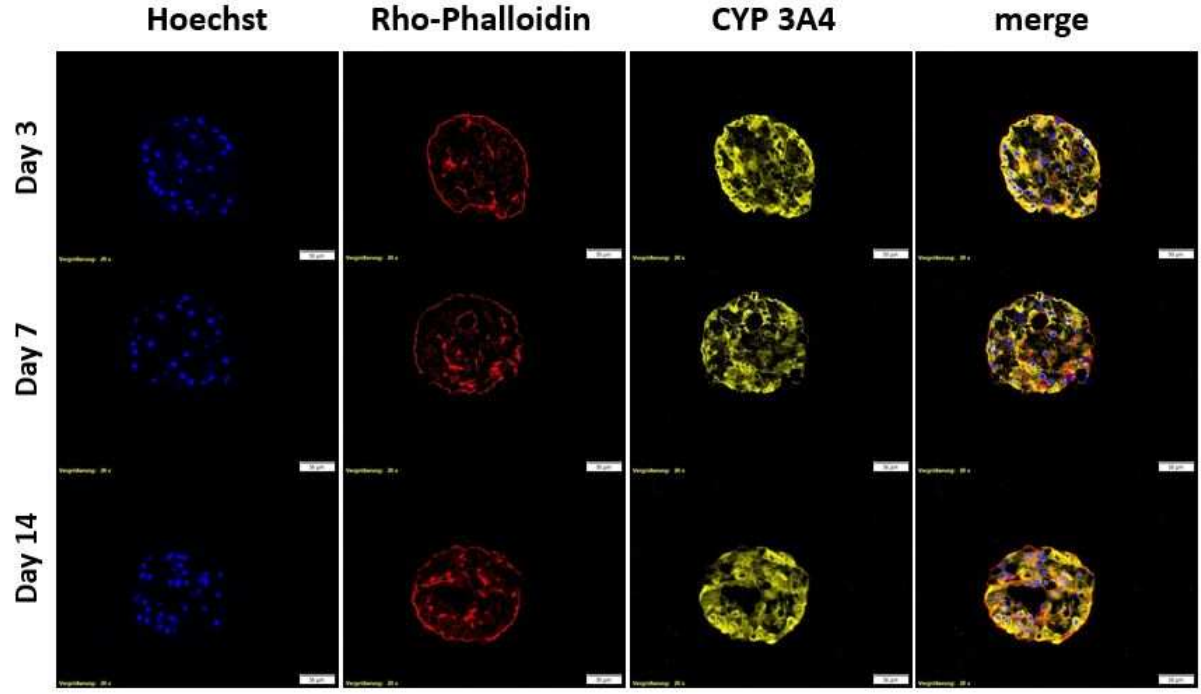

Figure 3.21: Immunofluorescent staining of CYP 3A4 in PHH spheroids at days 3, 7 and 14. CYP 3A4 (yellow) was expressed at both time points in most of the cells, but at different levels and peripheral cells appeared to express higher CYP3A4 levels. 20x magnification, bars = 50 µm.

In PHH spheroids, the CYP isoenzymes 1A2, 2B6 and 3A4 were expressed for at least 14 days in culture. The overall distribution appeared consistent and in comparison to the majority of HepaRG sections, the peripheral cells also expressed CYPs. Interestingly, CYP expression levels differed less over time in PHH than in HepaRG spheroids. Furthermore, expression levels of CYP 1A2 and 2B6 were significantly ($\alpha = 0.05$) higher in PHH compared to HepaRG, whereas CYP3A4 expression did not differ significantly between the cell models at either time point (Figure 3.21).

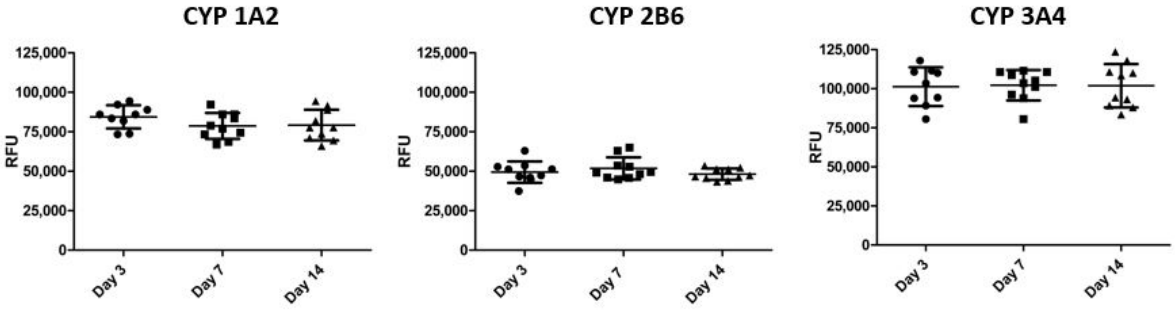

Figure 3.22: Scatter plots of CYP protein expression levels in PHH spheroids over time, expressed as the mean of area x intensity (relative fluorescent units per 10,000 pixels) of CYP 1A2 (left), CYP 2B6 (middle) and CYP 3A4 (right). No time-dependent differences were observable for every CYP isoenzyme. Relative fluorescent unit values on the y-axis also indicate different basal expression levels for each isoenzyme with the highest expression levels for CYP 3A4. RFU = relative fluorescent units. (Turkey´s multiple comparisons test; α = 0.05, no significant differences)

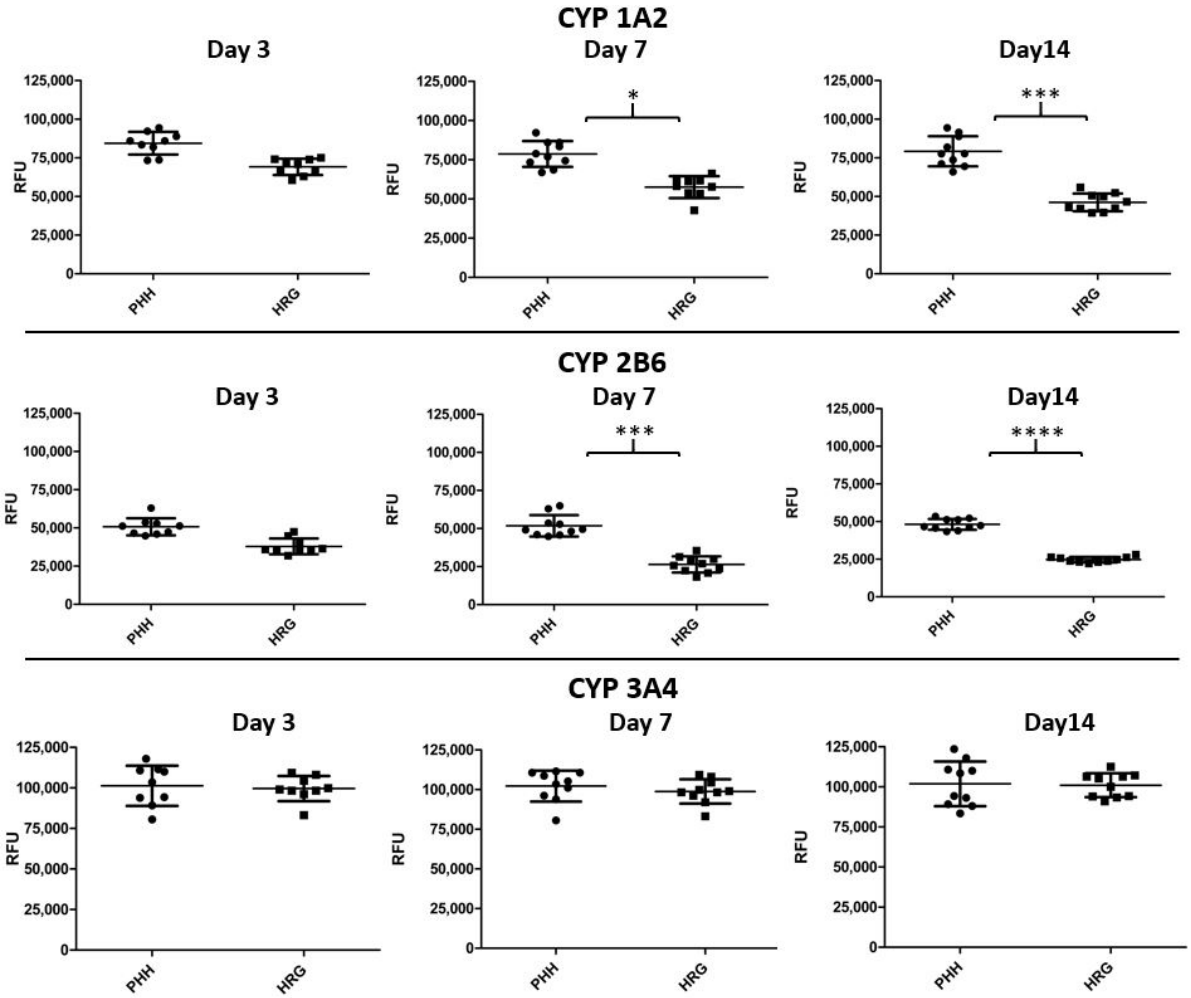

Figure 3.23: Comparative scatter plots of the expression levels of CYP 1A2 (top row), 2B6 (mid row) and 3A4 (bottom row) at days 7 (left) and 14 (right) in PHH and HepaRG (HRG) spheroids, expressed as means of area x intensity (relative fluorescent units per 10,000 pixels). The expression levels of both CYP 1A2 and CYP 2B6 were lower in HepaRG spheroids compared to PHH spheroids at both time points. For CYP 3A4, the expression levels were comparable regardless of the time point. Additionally, CYP 3A4 showed a higher variance in both cell systems. (unpaired t-test (α = 0.05; * = p < 0.05; ** = p < 0.01; *** = p < 0.005; **** = p < 0.0001). RFU = relative fluorescent units.

3.2.2.2 *Expression of Phase II isoenzymes*

Following the initiation of drug metabolism by phase I enzymes, phase II enzymes (mostly transferases) link drug metabolites to endogenous molecules in order to facilitate a more efficient excretion. HepaRG and PHH spheroids were immunofluorescently stained for two phase II enzymes, N-acetyltransferase 1/2 (NAT1/2) and sulfotransferase 1A1 (SULT1A1, only available for HepaRG) in order to assess their expression over time and also to

compare both spheroid models. Figures 3.24 and 3.25 show NAT 1/ 2 and SULT1A1 expression in HepaRG spheroids over time.

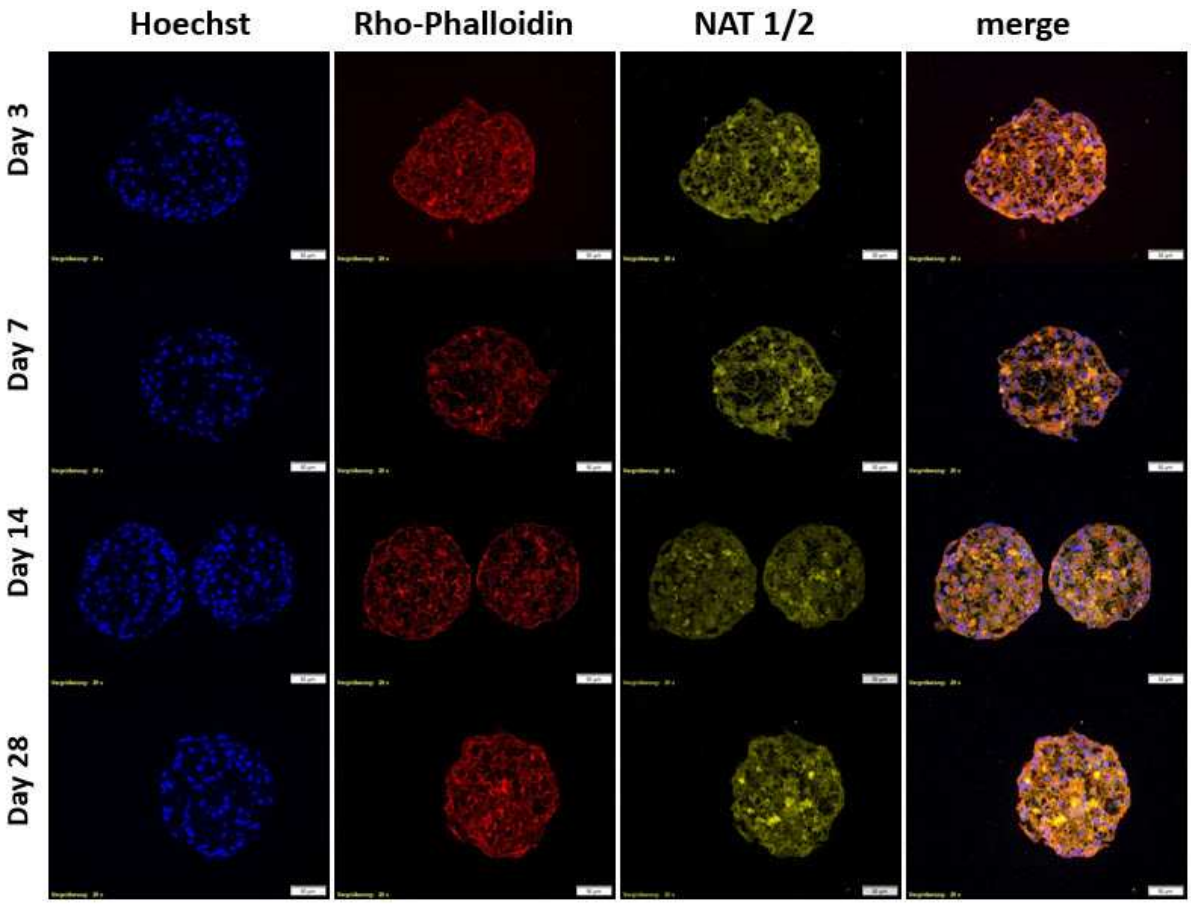

Figure 3.24: Expression of NAT 1/2 (yellow) in HepaRG spheroids at days 3, 7, 14 and 28 including double counterstain of nuclei (blue) and cytoskeleton (red). HepaRG spheroids weakly expressed NAT 1/ 2 at all time points, with the lowest level observed at day 14. NAT 1/2 was expressed diffusely with few focal spots showing a higher expression level. 20x magnification, bars = 50µm.

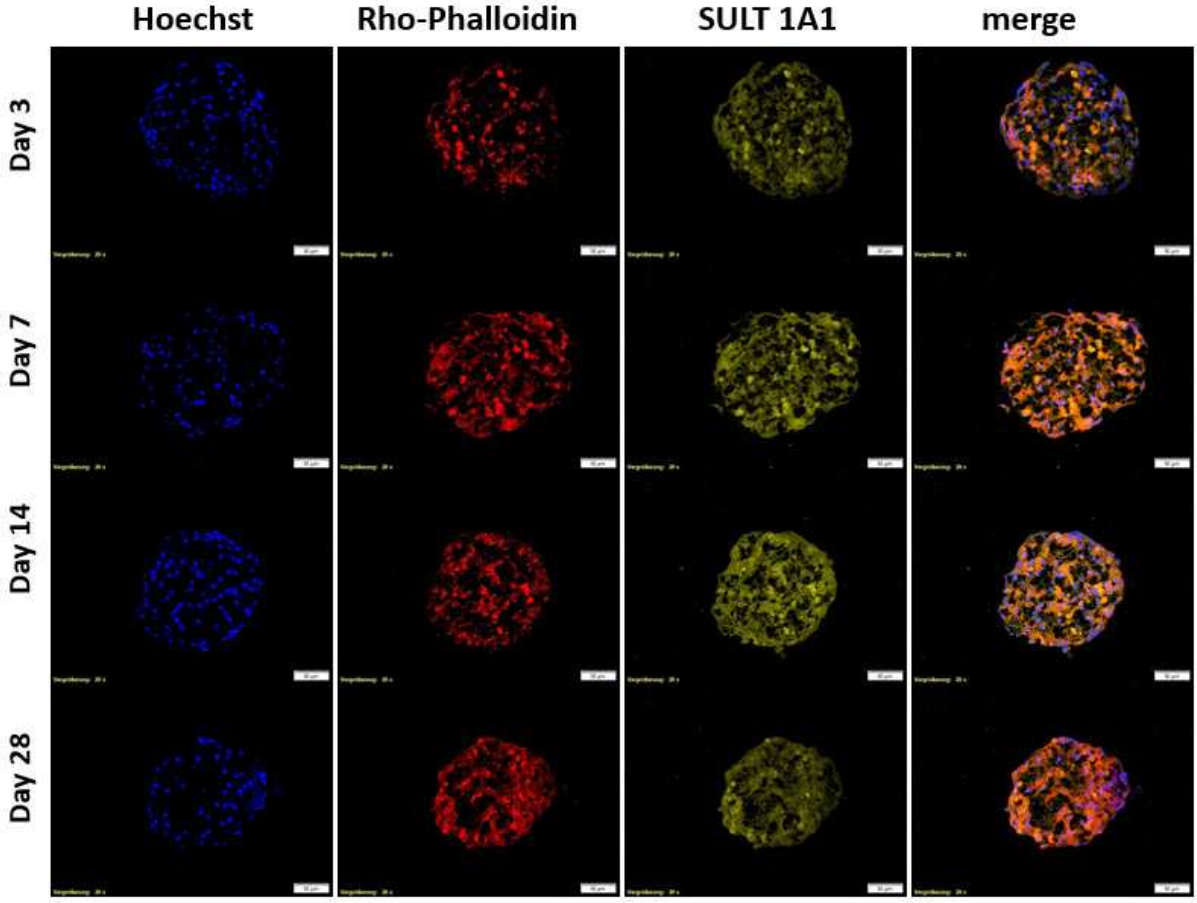

Figure 3.25: Expression of NAT 1/2 (yellow) in HepaRG spheroids at days 3, 7, 14 and 28 including double counterstain of nuclei (blue) and cytoskeleton (red). HepaRG spheroids weakly expressed NAT 1/ 2 at all time points, with the lowest level observed at day 14. NAT 1/2 was expressed diffusely with few focal spots showing a higher expression level. 20x magnification, bars = 50µm.

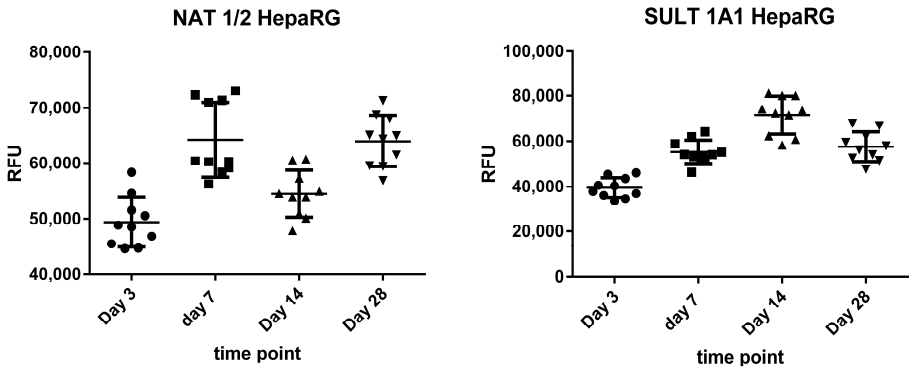

Figure 3.26: Scatter plots of phase II expression levels in HepaRG spheroids over time, expressed as means of area x intensity (relative fluorescent units per 10,000 pixels) of NAT 1/2 (left) and SULT 1A1 (right). Time-dependent differences were observable for both members without any general trend. RFU = relative fluorescent units. (Turkey´s multiple comparisons test; α = 0.05, no significant differences)

HepaRG spheroids expressed NAT 1/2 over a period of at least 28 days at equally low levels, showing diffuse cytoplasmic staining. At each time point, spots with a higher expression were visible, which appeared randomly distributed without any distinct distribution within the spheroid, as it was also observed for the CYP enzymes in spheroid centers. In contrast to the localization of the phase I members, both, NAT1/2 and SULT1A1 were detectable in HepaRG spheroid centers and linings at every time point investigated. When regarding the expression levels over time (figure 3.26), NAT 1/2 showed comparable levels at day 3 and 14, which were lower than those of day 7 and 28. In contrast, the expression of SULT 1A1 increases significantly over time until day 14 and slightly decreased at day 28, showing a similar level to day 7.

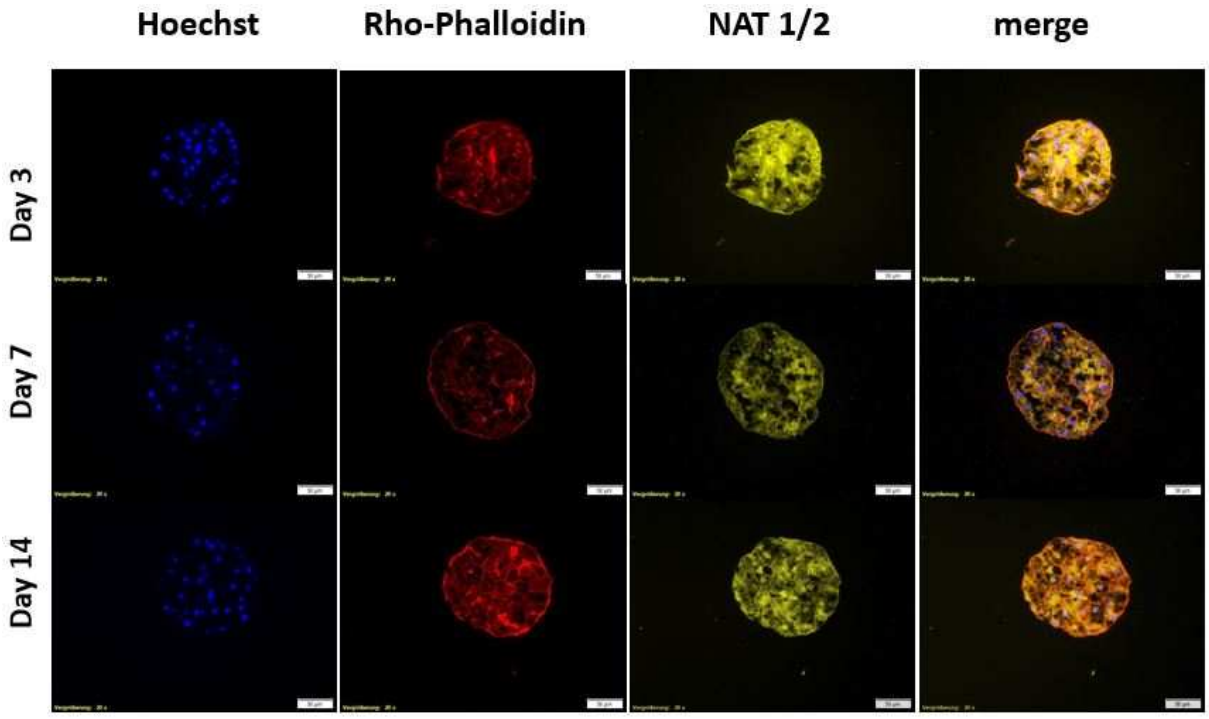

Figure 3.27: Immunofluorescent staining of NAT 1/ 2 in PHH speroids at days 3, 7 and 14. NAT 1/ 2 (yellow) was expressed at both time points in most of the cells, but at different levels and seemed to increase from day 7 to day 14. 20x magnification, bars = 50 µm.

In comparison to HepaRG, figure 3.27 shows NAT 1/2 expression in PHH spheroids at days 7 and 14 (data on SULT1A1 expression is not available for PHH spheroids). The localization of NAT 1/2 was cytoplasmic and not restricted to any area within the spheroid and appeared higher at day 14, which suggests a time-dependent variation of NAT 1/2 expression in PHH spheroids and, to a lesser extent, in HepaRG spheroids.

Intensity differences in PHH revealed a higher expression at day 14 so that time-dependent differences seemed to exist for both cell systems, but a different pattern was obtained

comparted to HepaRG spheroids. This time-dependent variation also seemed to vary for the different enzymes when comparing NAT 1/2 and SULT 1A1 expression patterns in HepaRG cells (figure 3.26). When comparing the expression levels of NAT 1/2 in PHH and HepaRG spheroids, a higher NAT 1/2 exppression was observable in PHH spheroids. It is well known that for both NAT isoenzymes (NAT1 and NAT2) as well as for SULT1A1 polymorphisms exist, which lead to slow, intermediate and rapid phenotypes of the respective catalyzed reactions, i.e. acetylation and sulfation (Wang et *al.*, 2002; Nagar et *al.*, 2006; Walker et *al.*, 2009; Hein et *al.*, 2006). The differences in NAT 1/2 expression levels may therefore not necessarily be due to the higher complexity of primary cells *per se*, but could also be related to different polymorphisms of the donors. While the expression of GSTs and UGTs has been well studied in HepaRG cells (Aninat et *al.*, 2005), the donor-specific polymorphisms of NATs and SULTs have not been addressed and were beyond the scope of this work. In general, the role of conjugating enzymes is underestimated in comparison to the functionalization enzymes of phase I (i.e. CYPs) and should be thoroughly investigated in the future as highly recommended by regulatory authorities (FDA, 2017).

3.2.2.3 *Expression of Phase III transporters*

The final step for an effective hepatic clearance of xenobiotics is performed by phase III members, which are mostly transporters of the ABC binding cassette transporter family. Among these are so-called multidrug resistance proteins (MDRs) and multidrug resistance related proteins (MRPs), which facilitate the excretion of conjugated metabolites out of the hepatocyte. A total of three transporters of the ATP-binding cassette transporter superfamily, MDR1 (ABCB1), MRP-2 (ABCC2) and bile salt export pump BSEP (ABCB11) were investigated in spheroids of both cell types. Figure 3.28 shows MDR1 expression in HepaRG spheroids over time.

MDR1 showed a high abundance in HepaRG spheroids at every time point investigated. Two different expression patterns were detectable: one fraction appeared yellow in the merged pictures, meaning that f-actin (red) and MDR1 (green) are co-localized, mostly restricted to cell borders in general, but not restricted to any specific area within the spheroid. This co-localization was clearly visible at every time point investigated. The second pattern appeared green without any co-localization and was located diffusely in the cytoplasm, but not restricted to any area within the spheroid. Whereas the expression of both the co-localized and the cytoplasmic fraction did not differ significantly over time, suggesting a stable expression of MDR1 over the prolonged cultivation period.

MDR1 staining in PHH spheroids led to similar observations, where also two different expression patterns were observed (figure 3.29). Neither fractions show any major differences between the time points, but clear differences in the co-localized fractions

between the two cell systems were observed. PHH spheroids showed a distinct co-localization in the outer lining of the spheroid next to the cell borders, whereas MDR1 in HepaRG spheroids was localized with a higher abundance in the inner areas. A detailed comparison is given in figure 3.30.

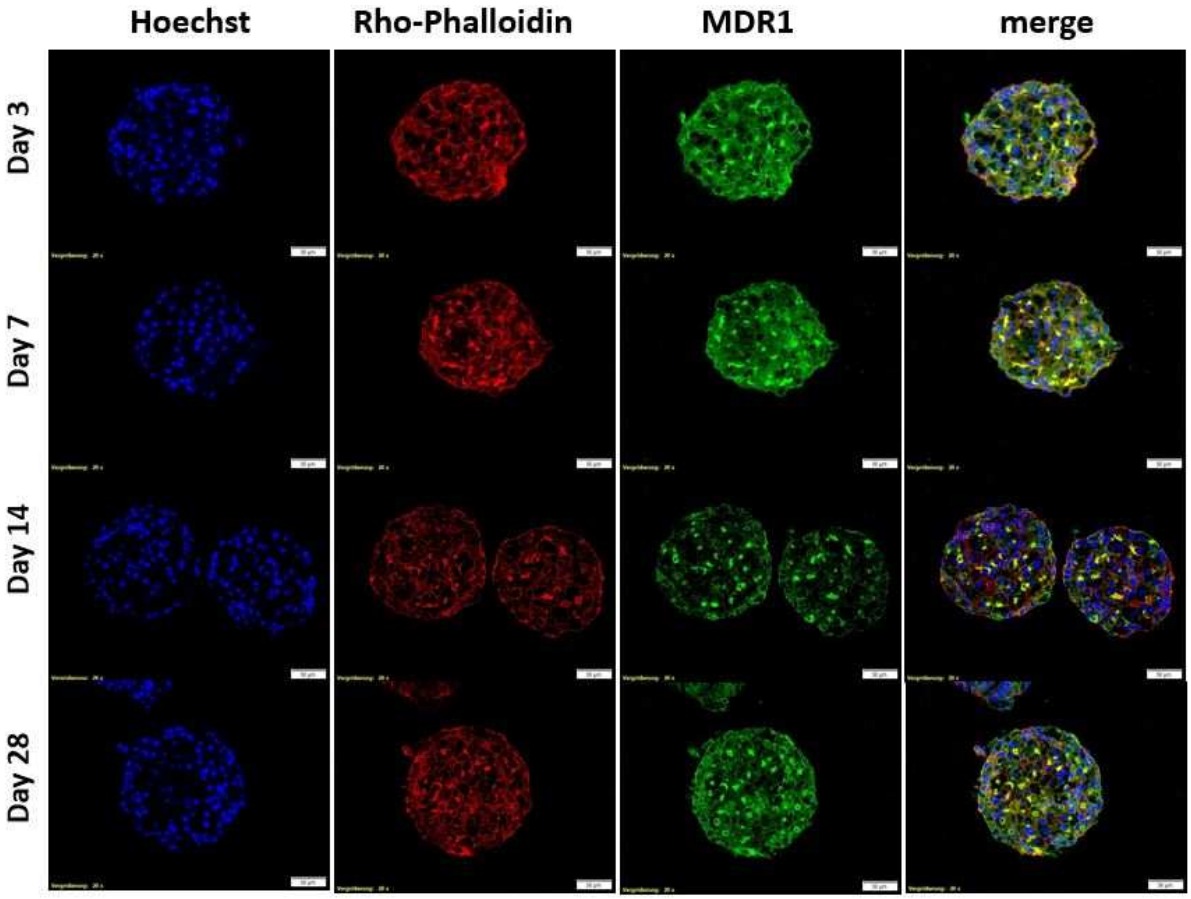

Figure 3.28: Expression of MDR1 (ABCB1, green) in HepaRG spheroids at days 3, 7, 14 and 28 including double counterstain of nuclei (blue) and cytoskeleton (red), visualized by immunofluorescent staining. HepaRG spheroids expressed MDR1 at all time points. MDR1 was expressed in two distinct patterns, which was observed as a green fraction as well as yellow fraction due to co-localization with the membranes (red) in the merged figures (right). 20x magnification, bars = 50µm.

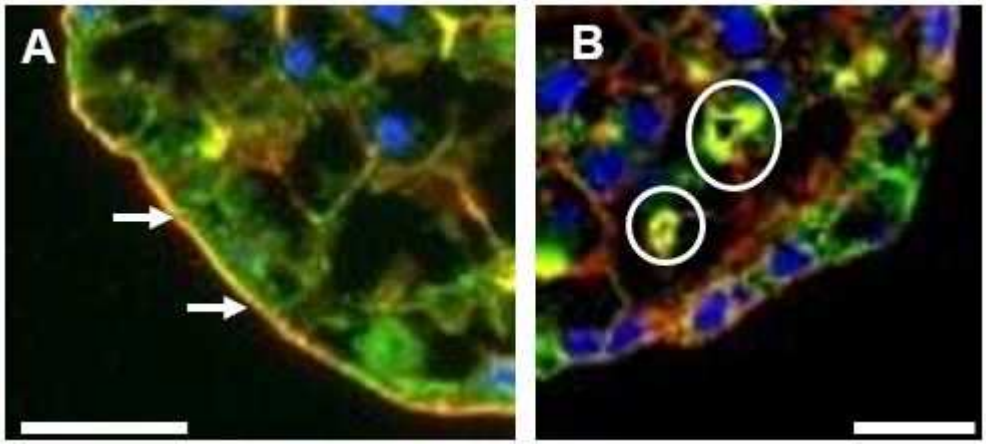

Figure 3.30: Detailed view of the co-located staining of MDR1 (yellow) in PHH spheroids (A) and HepaRG spheroids (B). In PHH spheroids, the co-localization was observable at the borders between cells as well as very distinct at the outer lining layer (arrows). In contrast, the yellow staining was only sporadically detectable in the lining cells and much more present between the cells. Frequently, a clear lumen was observable in HepaRG spheroids. Cutout from 40x magnification, bar = 20 µm

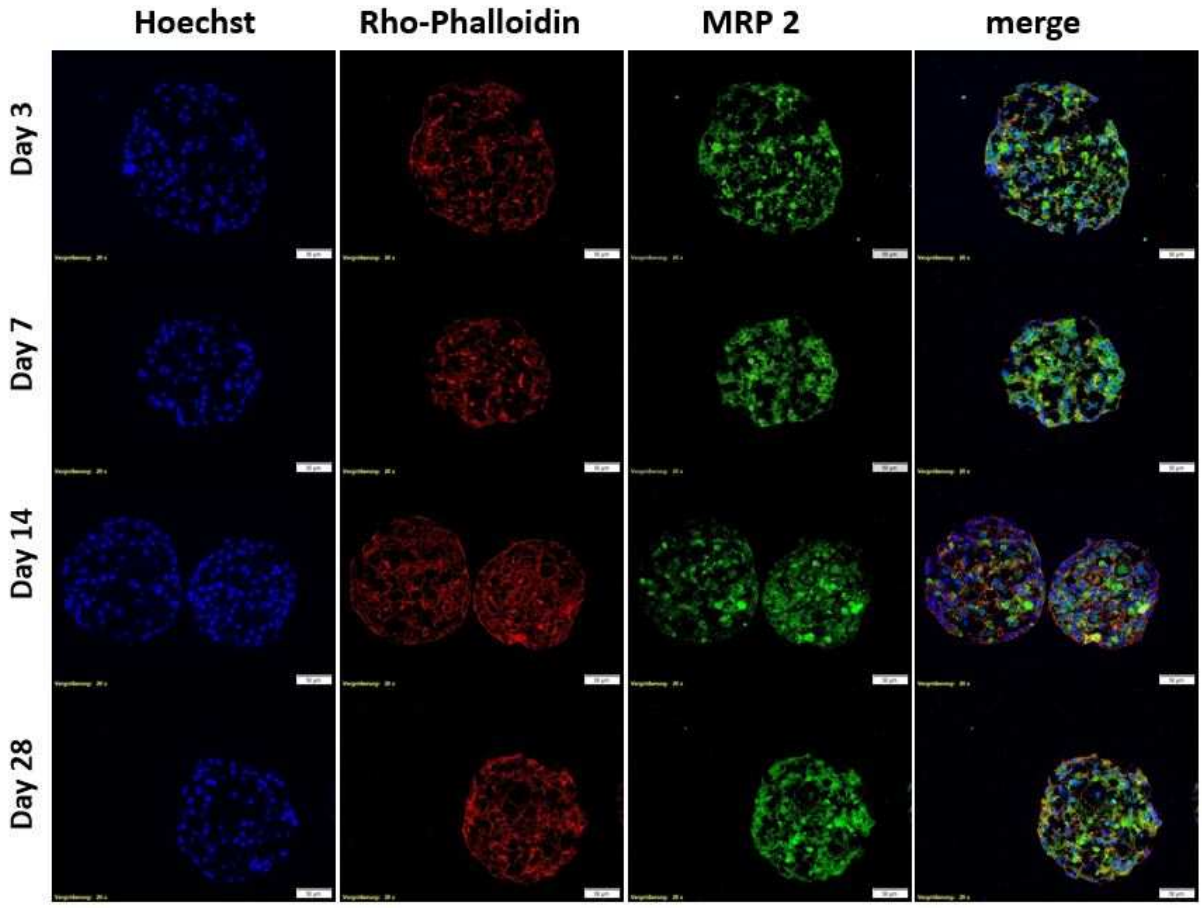

Figure 3.31: Expression of MRP2 (ABCC2, green) in HepaRG spheroids at days 3, 7, 14 and 28 including double counterstain of nuclei (blue) and cytoskeleton (red), visualized by immunofluorescent staining. HepaRG spheroids expressed MRP2 at all time points. MRP2 was expressed in two distinct patterns, which was observed as a green fraction as well as yellow fraction due to co-localization with the membranes (red) in the merged figures (right). 20x magnification, bars = 50µm.

For MDR1, MRP-2 and BSEP expression in both cell systems, it is evident that the yellow fraction is functionally integrated in the membranes, as co-localization is expected for transmembrane proteins. In addition, the green fraction is suggested to be either MDR1 substructures, e.g. single domains carrying the antigen or fully assembled MDR1, which is not yet integrated in to the membrane. Therefore, these fractions are non-functional as a result of either synthesis or degradation processes. The yellow fraction was detectable in two distinct areas: the border area between two or more cells and the outer lining. Whereas in HepaRG spheroids the majority of co-localized MDR1 was the borders between cells (figure 3.30 A). Interestingly, the border areas between cells appeared frequently with a clearly visible lumen, suggesting that both PHH and HepaRG spheroids formed a type of canalicular system in order to facilitate excretion of waste products, in part due to active transport.

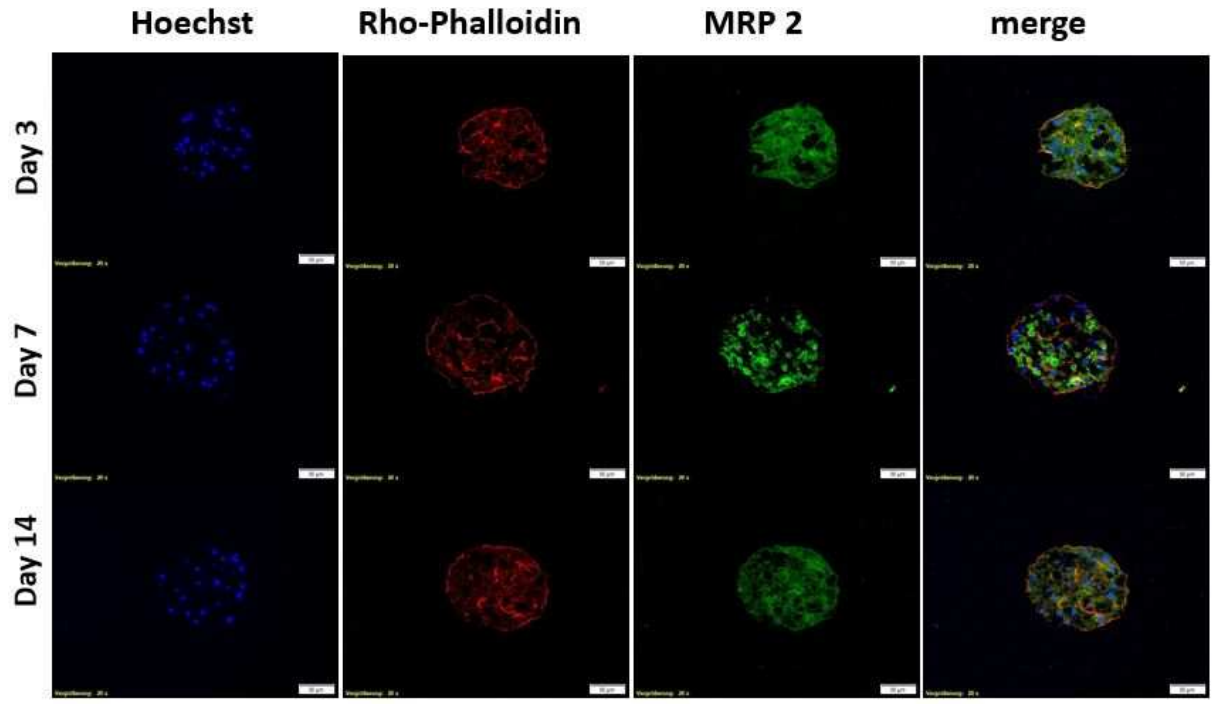

Figure 3.32: Expression of MRP2 (ABCC2, green) in PHH spheroids at days 3, 7 and 14 including double counterstain of nuclei (blue) and cytoskeleton (red), visualized by immunofluorescent staining. PHH spheroids expressed MRP2 at all time points. Mdr-1 was expressed in two distinct patterns, which was observed as a green fraction as well as yellow fraction due to co-localization with the membranes (red) in the merged figures (right). 20x magnification, bars = 50µm.

Figures 3.33 and 3.34 show the expression and localisation of BSEP in HepaRG and PHH spheroids. As with MDR1, but to a lesser extent, BSEP was expressed as two different patterns, and the co-localization of transporter and membrane.

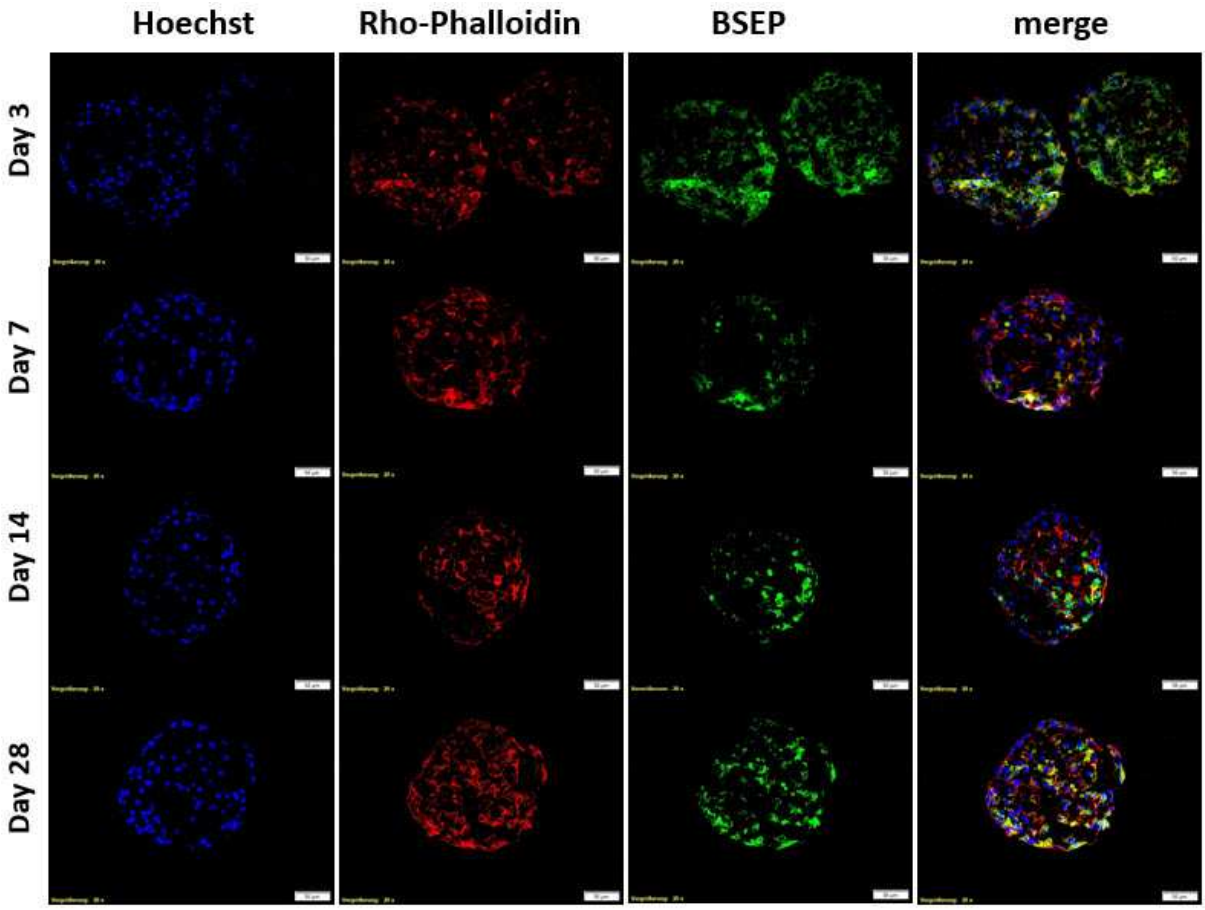

Figure 3.33: Expression of BSEP (ABCB11, green) in HepaRG spheroids at days 3, 7, 14 and 28 including double counterstain of nuclei (blue) and cytoskeleton (red), visualized by immunofluorescent staining. HepaRG spheroids expressed BSEP at all time points, visible as spots. BSEP was expressed in two distinct patterns, which was observed as green fraction as well as yellow fraction due to co-localization with the membranes (red) in the merged figures (right). Thereby, the yellow fraction is suggested to be the fully integrated membrane protein whereas the green fraction is suggested to represent synthesis and/or degradation of BSEP. 20x magnification, bars = 50µm.

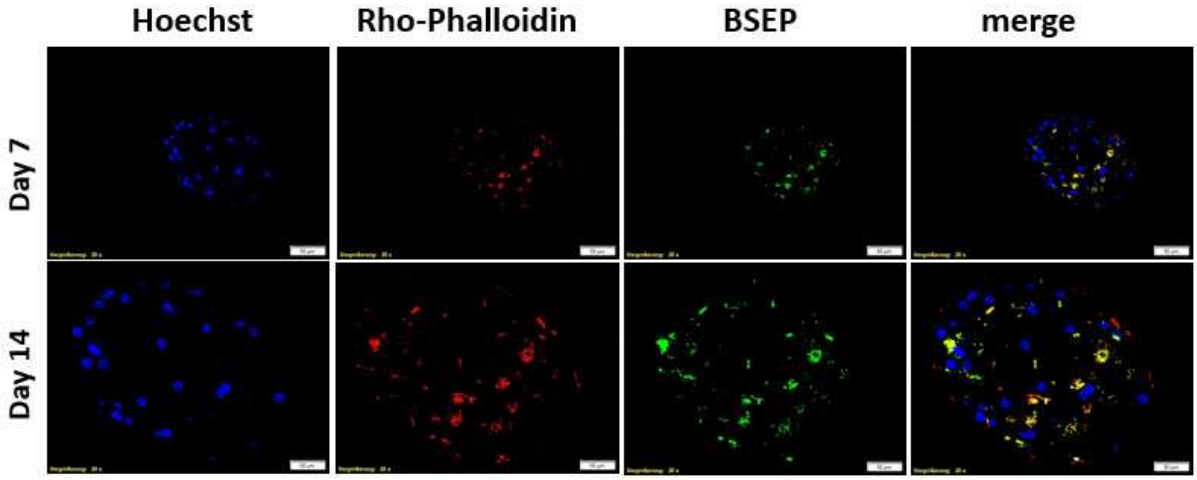

Figure 3.34: Immunofluorescent staining of BSEP (ABCB11, green) in PHH spheroids at days 7 and 14 (day 3 not available) including double counterstain of nuclei (blue) and cytoskeleton (red), visualized by immunofluorescent staining. BSEP was expressed in two distinct patterns at both time points, which was observed as green fraction as well as yellow fraction due to co-localization with the membranes (red) in the merged figures (right). Thereby, the yellow fraction is suggested to be the fully integrated membrane protein whereas the green fraction is suggested to represent synthesis and/or degradation of BSEP. 20x magnification, bars = 50µm.

It is well established that cells adapt to their surrounding environment by responding to local signals and cues, which in turn has consequences for physiological parameters such as differentiation and function (Baker and Chen, 2012). One of the major differences is related to the shape that cells acquire when cultured in a certain format, thus impacting the cytoskeleton, which has been shown to alter gene expression (Vergani et *al.*, 2004; Thomas et *al.*, 2002). The cultivation in standard 2D monolayers is far from the complexity that cells encounter in native tissue, which is partially due to the altered shape. Consequently, the cell-cell contacts are substantially reduced in monolayer culture. The introduction of a third dimension offers cells to retain a shape that is closer to that *in vivo* and dramatically increases cell-cell contact surface, which is suggested to improve intercellular signaling that allows a greater physiological relevance in comparison to 2D culture.

In order to estimate whether spheroid cell culture has an influence on the metabolic capacity of both HepaRG cells and PHH, a selection of phase I, II and III members were chosen in order to visually monitor expression in this three-dimensional cell culture system. This study was conducted to address several questions: Firstly, do cell models express DMET when cultured three-dimensionally and if so, is the expression pattern stable or variable over time? Secondly, is there a specific expression pattern within the spheroid and thirdly, are there differences in the above aspects when HepaRG spheroids and PHH spheroids are compared?

The immunofluorescent staining of the DMETs investigated showed overall stable expression levels of CYP isoenzymes that play major roles in drug metabolism (Zanger and Schwab, 2013), over a prolonged cultivation period.

For both phase I and II members, the overall expression was stable for the prolonged cultivation period in both cell systems, which is in agreement with other reports: Gunness et *al* (2013) observed a stable expression of CYP 2E1 and several UDP glucuronosyltransferases (UGTs) and the basal CYP activity of CYPs 1A2, 2B6 3A4 was found to be stable and far exceeded those observed in HepaRG monolayers (Ramaiaghari et *al.*, 2017). For the sake of completeness, it should be noted that HepaRG monolayers are also capable of enhanced CYP expression when cultured under 2% DMSO (Cerec et *al.*, 2007; Jackson et *al.*, 2016), but high DMSO concentrations cause i) cell death (Nibourg et *al.*, 2012) and i) constitutively induce CYP expression, which may further limit inducibility during compound testing. The above aspects therefore limit the reliability of HepaRG monolayers in high-DMSO culture approaches and the HepaRG spheroid model offers the advantage to achieve high levels of metabolic competence without requiring high DMSO concentrations. This has also been reported for HepaRG cells cultured in a bioreactor approach (Hoekstra et *al.*, 2012). The enhanced and stable metabolic phenotype in PHH spheroids was also observable in a proteomics approach, in which spheroids were compared

to liver tissue and 2D monolayers of the same donor (Bell et *al.*, 2016). While massive rearrangements of the molecular signatures, including a significant reduction in DMET expression, were observed in monolayers, PHH spheroids maintained a phenotype that was close to the liver tissue. Although the overall expression levels of the DMETs investigated here can be considered stable, differences in spheroids of both cell systems were observable that were sporadically statistically significant. Those differences seemed to be isoenzyme-dependent as the expression patterns did not reveal any general trend. This assumption is strengthened by other reports, e.g. Bell et. *al* (2016) found that the activities of most CYPs in PHH spheroids were overall stable over time, but differences were seen for CYP2C8, which significantly decreased over time as well as for CYP2C9, which showed a time-dependent increase in activity. Interestingly, whereas the expression levels of CYP2B6 were clearly lower than those of CYP1A2 and 3A4 in both cell systems, Ramaiaghari et *al.* (2017) reported the opposite observation in HepaRG spheroids, which showed higher abundance of CYP2B6 compared to CYP1A2. This, however, emphasizes the need for further studies that address the time-dependent differences in order to benchmark the metabolic performance a spheroid model is able to provide over a prolonged cultivation time. More time points need to be included to better understand the temporal dynamics of phase I and II expression patterns in hepatic spheroid models and thus help to define the purpose(s) for which they are applicable.

In vivo, the apical surfaces of adjacent hepatocytes form luminal cavities called bile canaliculi into which the bile is secreted. In their native state, hepatocytes are arranged in chords and lumen from adjacent hepatocytes form canalicular networks that transport bile into bile ducts (Treyer and Musch, 2013). In order to visualize the extent to which spheroid cultures model these features, three members of the canalicular efflux transporters that are mainly involved in drug and bile salt/acid transport (Kullack-Ublick et *al.*, 2002) have been fluorescently stained. MDR1, MRP2 and BSEP are apical surface markers located at the bile canalicular regions of hepatocytes and are involved in the secretion of bile acids as well as in detoxification of xenobiotics. Furthermore, the drug-induced inhibition of these transporters is known to cause cholestatic DILI as bile acids consequently accumulate in hepatocytes (Bell et *al.*, 2017).

All three transporters were expressed along the three-dimensional structures of both PHH and HepaRG spheroids in pockets and channel-like structures with the highest abundance of MDR1, followed by MRP2 and BSEP. Functional bile canalicular structures were also observed in bioreactor-generated PHH spheroids (Tostoes et *al.*, 2012), which showed a pronounced intracellular bile acid accumulation following treatment with the known cholestatic drug chlorpromazine. In HepaRG spheroids, transporter activity was visualized by the transport of cholyl-lysyl-fluorescein (CLF), a fluorescent bile acid analogue, which was

localized in the bile canalicular regions at the luminal surface of the spheroids by live cell imaging (Ramaiaghari et *al.*, 2017). Taken together, the consistent data clearly show the presence of extensive bile canalicular networks that are stably expressed over several weeks, indicating phase III metabolic competence and thus suggesting hepatic spheroids as a potential *in vitro* model for the prediction regarding the cholestatic potential of drug candidates in early drug development.

In this study, the expression of DMETs in hepatic spheroids in prolonged cultivation periods could be shown for the first time using several time points throughout the cultivation time, which proves the usefulness of 3D cell culture as a model for long term toxicity testing, hence bridging the physiological gap of 2D *in vitro* models by regaining a stable steady-state of hepatocyte differentiation. Moreover, the abundance of a three-dimensional canalicular network could be shown in both PHH and HepaRG spheroids over prolonged cultivation times, which endorses hepatic spheroids as a useful model for transporter induction/ inhibition studies *in vitro* that are highly recommended by regulatory authorities (Zhang et *al.*, 2009). This is especially useful since the methods for *in vitro* evaluation of transporter induction are less well understood compared to e.g. CYP induction and are mainly evaluated *in vivo*, the use of spheroids would add great value to early drug developmental phases.

3.2.3 CYP induction in HepaRG spheroids

During drug development, it is essential to assess whether a drug candidate has the potential to impact drug metabolism by either inhibition or induction, which can have fundamental clinical consequences. The induction of drug metabolizing enzymes, such as the CYP family, is known to cause drug-drug interactions (DDIs) (Sinz, Wallace and Sahi, 2008). This interaction can have substantial effects on co-administered drugs or the inducer itself (autoinduction) and may lead to a decreased or complete loss of efficacy due to increased elimination (Hewitt, LeCluyse and Ferguson, 2007). Additionally, CYP inducers can lead to an increased bioactivation of drugs that are metabolized to reactive (adverse) intermediates and thus trigger adverse effects (Park et *al*., 2005). Due to the significance of such DDIs and the fact that multiple drug therapy is more prevalent nowadays (Zhang et al., 2009), the screening of drug candidates with respect to their ability to induce CYPs is required by regulatory authorities, usually prior to the start of clinical trials (Chu et *al.*, 2009; EMA, 2012; FDA, 2017). Therefore, a hallmark of highly differentiated hepatocyte functionality in physiologically relevant hepatic cell culture models is the ability to respond to xenobiotic activation and induce liver enzyme expression. The most common mechanism of CYP induction is transcriptional gene activation, which is mediated by hepatic receptor activators such as Aryl-hydrocarbon receptor (AhR), constitutive androstane receptor (CAR) and

pregnane x receptor (PXR), which function as transcription factors (Levy et *al.,* 2015; Mandal et *al.*, 2005; Tirona and Kim, 2005; Honkakoshi et *al.*, 1998).

Therefore, the ability of HepaRG spheroids to respond to clinically relevant activators of AhR, CAR and PXR receptor pathways to induce expression of sentinel gene targets CYP 1A (AhR), 2B (CAR), 2C and 3A (PXR), respectively, is of major importance.

3.2.3.1 *Immunofluorescence*

In this section, the inducibility of CYPs in HepaRG cells in the 3D configuration was assessed by two different methods, immunofluorescent staining and mRNA expression. Additionally, the CYP induction in HepaRG monolayers was investigated on the mRNA level in order to compare both culture formats. For this purpose, HepaRG spheroids and monolayers were exposed to three different model inducers: Omeprazole, Rifampicine and Phenobarbital. Omeprazole (OMEP) is a model inducer for the CYP1A family through the activation of the Aryl hydrocarbon receptor (AhR) (Yoshinari et *al.*, 2008) and is in widespread use as positive control for CYP induction studies in preclinical drug development. Rifampicin (RIF) has been used as model inducer for both CYP 2B6 and CYP 3A4 and Phenobarbital (PB) was used to investigate the inducibility of two members of the CYP2C subfamily, namely CYPs 2C9 and 2C19.

The induction of CYP1A2 and 3A4 at day 3 is shown in figures 3.35 and 3.36 and a summary is given in figure 3.37.

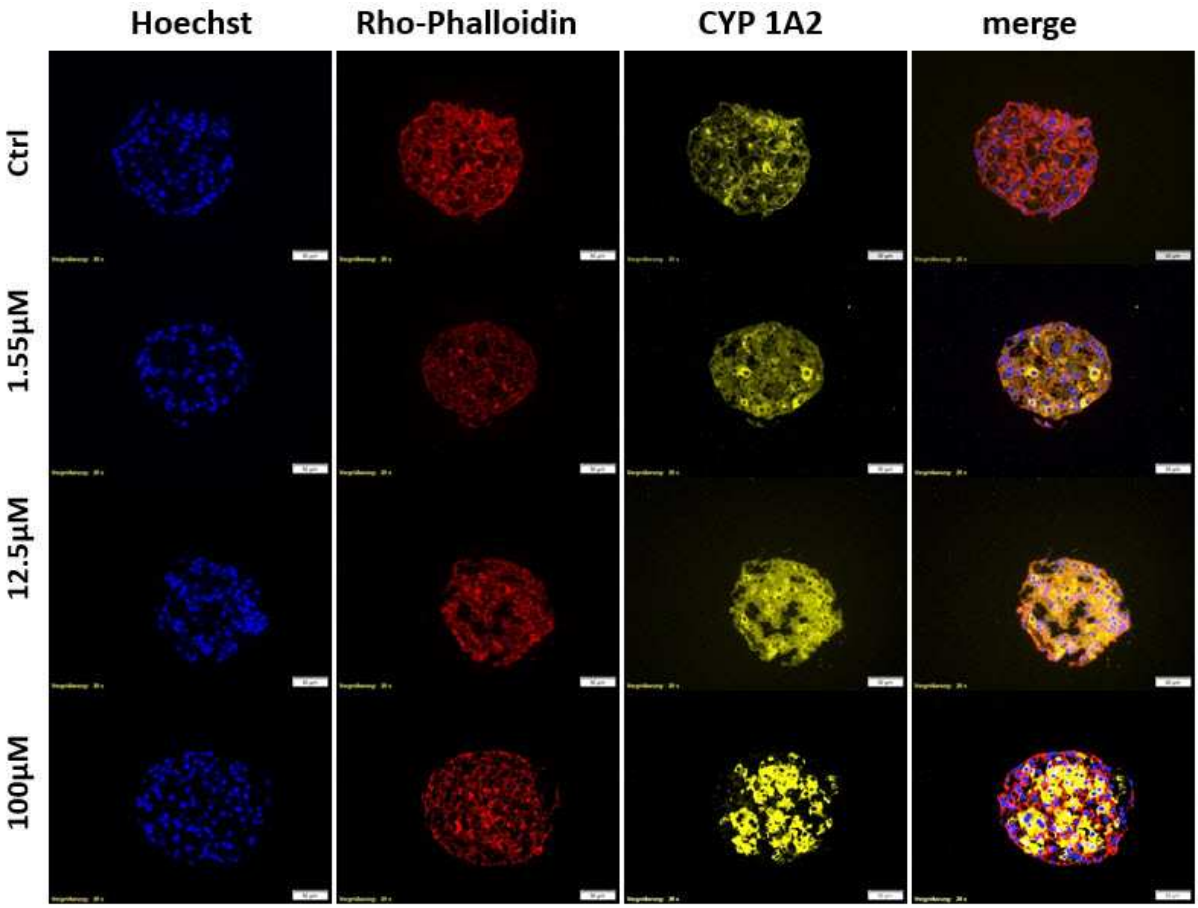

Figure 3.35: Induction of CYP 1A2 (yellow) in HepaRG spheroids treated with increasing concentrations of Omeprazole at day 3. By increasing dose, the expression increased dose-dependently in terms of both number of expressing cells and intensity of the staining. 20x magnification, bars = 50 µm.

Figure 3.35 shows the induction of CYP1A2 by Omeprazole at three different concentrations on day 3 and a clear concentration -dependent induction was observed. Already at 1.55 µM, which was the lowest concentration tested, randomly distributed single cells with a more intensive staining were detected at all time points investigated. With increasing

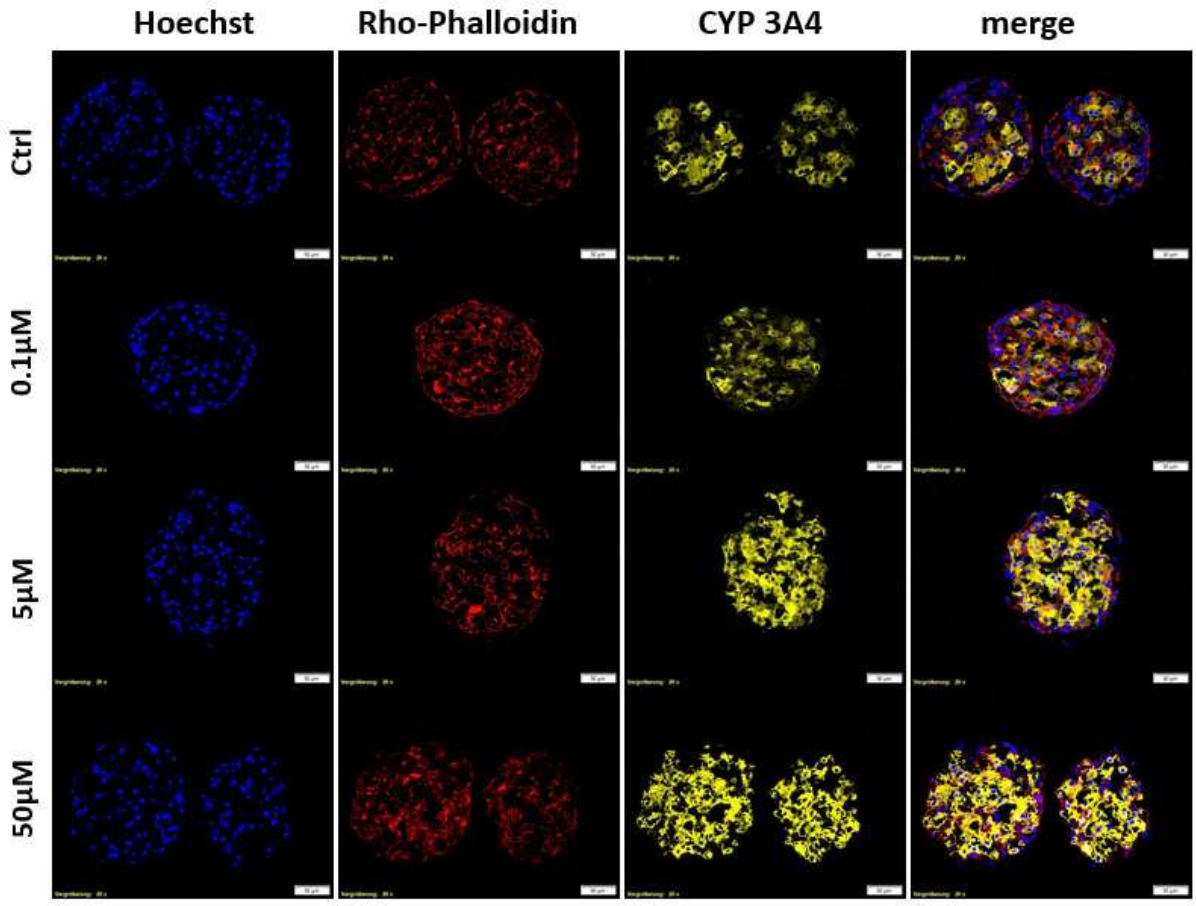

Figure 3.36: Induction of CYP 3A4 (yellow) in HepaRG spheroids treated with increasing concentrations of Rifampicin at day 3. By increasing dose, the expression increased dose-dependently in terms of both, number of expressing cells and intensity of the staining. 20x magnification, bars = 50 µm.

concentration, the percentage of highly expressing cells increased markedly, with variable expression patterns. Whereas the intermediate concentration (12.5 µM) was characterized by an equally distributed and moderate CYP1A2 expression, the expression in the top concentration spheroids showed a more binary pattern with cells either highly expressing CYP1A2 and cells that express no or very low levels of CYP1A2. Interestingly, the percentage of induced cells in the top concentration was localized centrally, as it was observed in control spheroids. This effect was not observed at the intermediate concentration at any time point.

Figure 3.36 shows the induction of CYP3A4 by Rifampicin at three concentrations on day 3 CYP3A4 is known to have a high basal expression in HepaRG cells (Guillouzo et *al.*, 2004), which was observed in the expression patterns of untreated HepaRG spheroids at all time

points tested. Rifampicin had a clear concentration-dependent effect on CYP3A4 expression in HepaRG spheroids. At the lowest concentration of 0.1 µM, induction was not detectable in comparison to the control spheroids. In contrast, the intermediate concentration of 5 µM and the top concentration of 50 µM led to a clear induction of CYP3A4, indicated by both the intensity of the staining and the percentage of intensively stained cells.

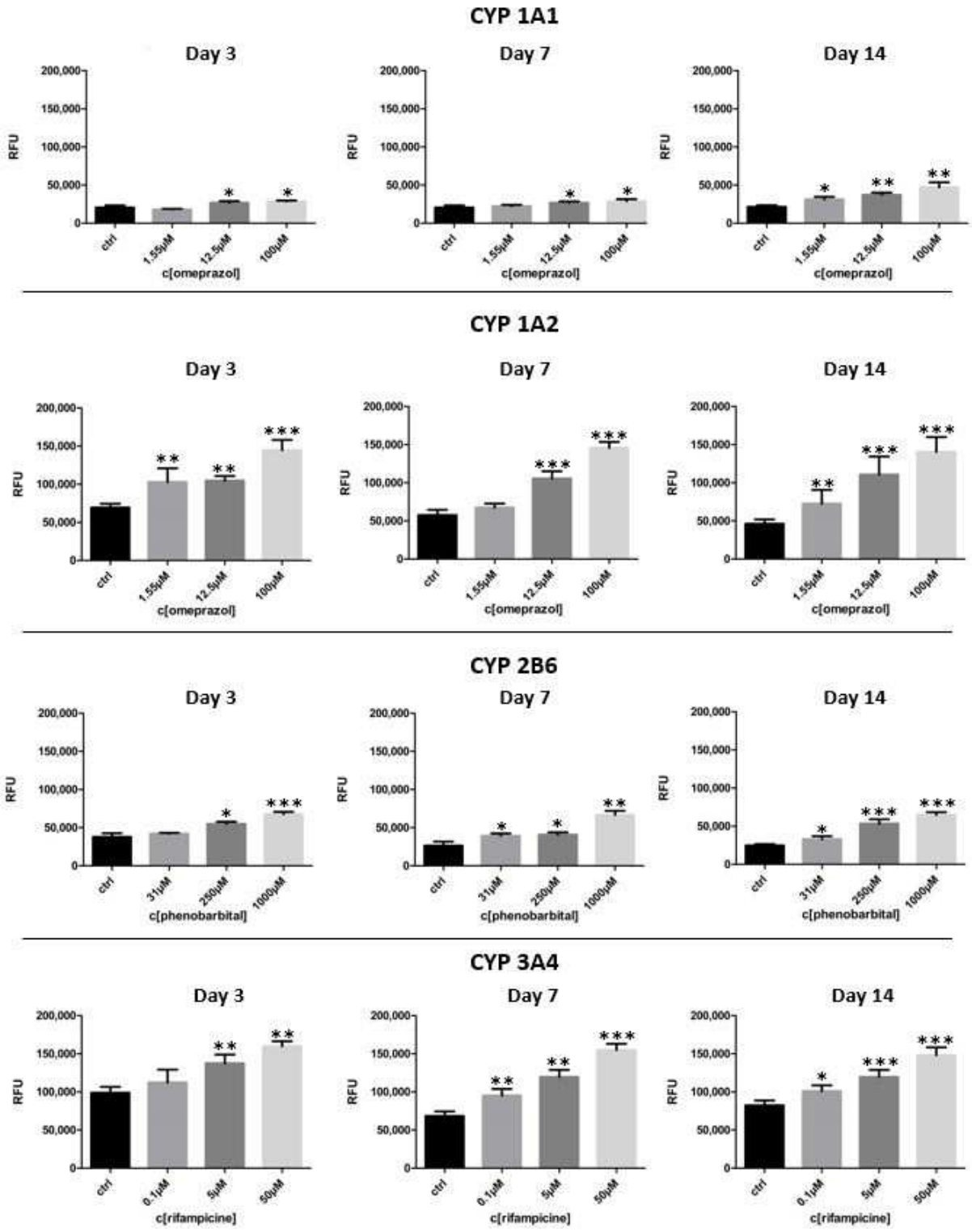

Figure 3.37: Column plots of CYP induction in HepaRG spheroid sections of CYPs 1A1, 1A2, 2B6 and 3A4 at days 3 (left column), 7 (mid column) and 14 (right column), expressed as relative fluorescent units per 1,000 pixels. All CYPs were inducible in a dose-dependent manner, indicated as increased mean RFU by increasing dose. Significance levels refer to control values. (Dunnett´s multiple comparisons test, α = 0.05; * = p < 0.05; ** = p < 0.01; *** = p < 0.005; **** = p < 0.0001; RFU = relative fluorescent units)

Figure 3.37 summarizes the induction of the four CYPs investigated at day 3 (left), day 7 (middle) and day 14 (right). Overall, CYPs 1A1, 1A2, 2B6 and 3A4 were inducible in HepaRG spheroids in a concentration-dependent manner over a prolonged cultivation period of 14 days.

Although it could be clearly shown that CYP inducibility occurs in HepaRG spheroids, the stained sections only display snapshots of certain areas, meaning that it remains difficult to extrapolate the expression pattern of a section to that of a whole spheroid. Therefore, the inducibility of these CYP enzymes was investigated by a more sensitive method (mRNA expression) again comparing HepaRG spheroids and monolayers (method see section 2.2.2.14).

3.2.3.2 *mRNA levels*

The inducibility of CYP enzymes in HepaRG spheroids was clearly observed in a dose dependent manner by immunofluorescent staining.

HepaRG cells cultured in 2D and 3D format have been treated for 3, 7 and 14 days with three model inducers (Omeprazole (OMEP), Rifampicin (RIF) and Phenobarbital (PB)) and one negative control (Flumazenil (FLU)) and CYP induction was investigated over time as well as both cultivation formats were compared to each other (induction levels see Appendixx).

Figure 3.38 a) shows the induction profile of CYP 1A1 in OMEP-treated HepaRG cells cultured as monolayers (shades of red) and as spheroid (shades of blue) at three different time points. OMEP highly induced CYP 1A1 in both formats up to values of over 400-fold induction in a concentration-dependent fashion. The induction was clearly more pronounced in monolayer cultures across the time points investigated (shades of red). In HepaRG spheroids, the fold changes were low, but were comparable across the three time points investigated. For CYP 1A1, the OMEP-mediated inducibility did not decrease over the time of culture regardless of the culture format.

The induction pattern of CYP 1A2 is shown in figure 3.38 b). Omeprazole-mediated CYP 1A2 induction is higher in HepaRG spheroid cultures (shades of blue) in comparison to monolayers (shades of red) at every time point investigated. In both culture formats, the induction of CYP 1A2 was clearly concentration-dependent at every time point. In monolayers, the highest fold changes were observed at day 3 (light red) with a trend to decrease over time, indicated by the lowest fold change at day 14 (dark red). The same effect was observed in spheroid cultures but was less pronounced.

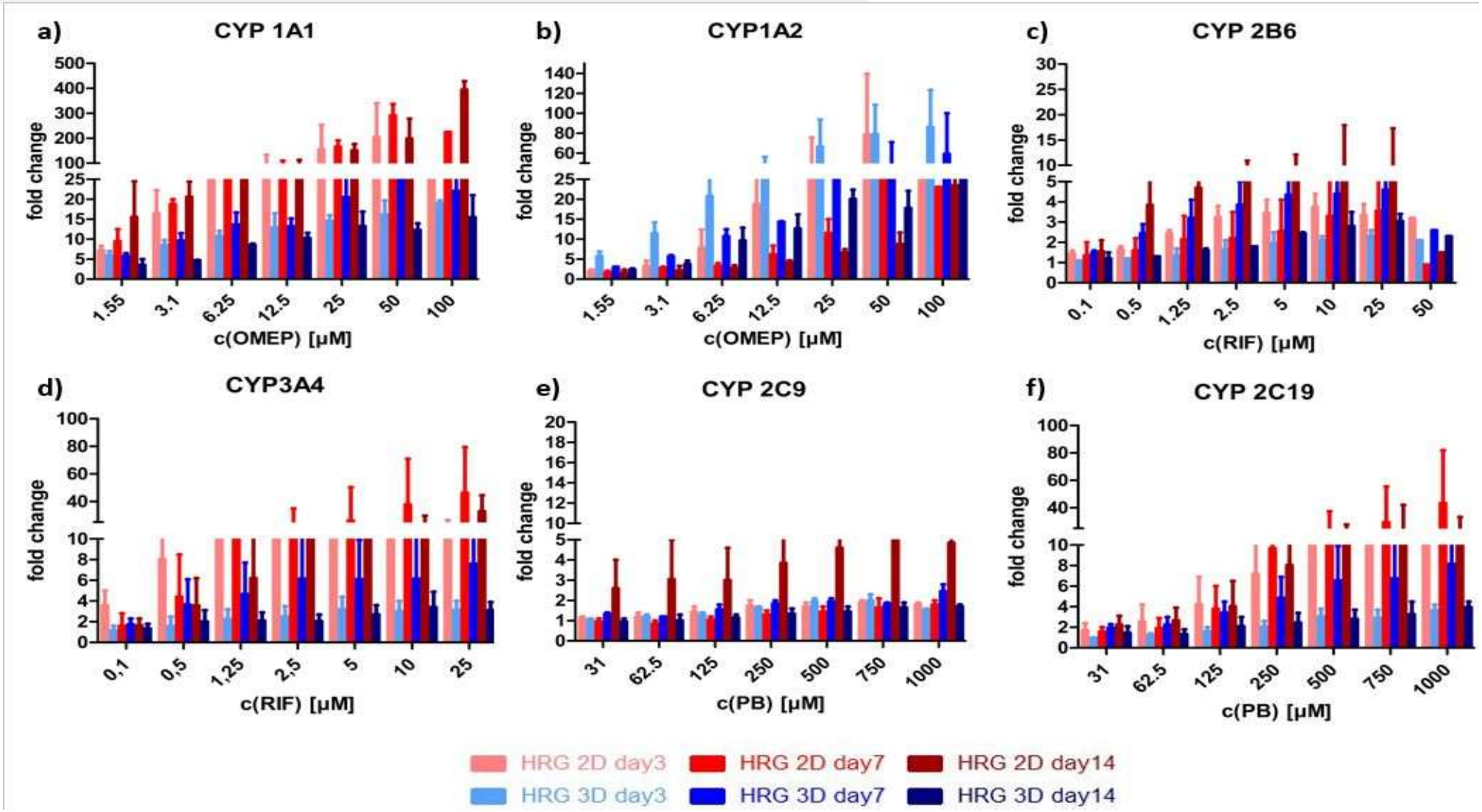

Figure 3.38: Grouped column plots of CYP induction in HepaRG cells cultured as monolayers (shades of red) and as spheroids (shades of blue) after treatment with prototypical inducers at days 3, 7 and 14. Data is expressed as fold change compared to normalized vehicle control. For CYP 1A1 (a), CYP 2C9 (e) and CYP 3A4 (f), the induction in HepaRG monolayers was detectable in a clearly concentration-dependent manner at every time point. In HepaRG spheroids, only the induction of CYP 1A2 was clearly observed, with a decreasing trend over time. All other CYP isoenzymes of the panel were not substantially induced in HepaRG spheroids.

The induction of CYP 2B6 in HepaRG cells following RIF treatment is shown in figure 3.38 c), which generally showed a low to moderate induction in both culture formats. For both culture formats, dose dependency was less pronounced as was observed for OMEP. In spheroid cultures (shades of blue), the highest induction was observed at day 7 (blue). Interestingly, the inducibility of CYP 2B6 in monolayers was the highest on day 14 (dark red) and comparably lower on days 3 (light red) and 7 (red).

Rifampicin-mediated induction of CYP 3A4 (figure 3.38 d)) was clearly dose-dependent in HepaRG monolayers (shades of red) compared to spheroids (shades of blue) which showed the strongest effect at day 7 (red). In HepaRG spheroids, the highest inducibility was observed at day 7 (blue) and the induction patterns at days 3 (light blue) and 14 (dark blue) were comparably low independent from the dose.

As shown in figure 3.38 e), CYP 2C9 was only inducible in HepaRG monolayers on day 14 (dark red), although not in a dose-dependent manner. No induction of CYP 2C9 above 2-fold was observed at any other condition.

In contrast, PB clearly induced CYP 2C19 with a higher inducibility in monolayers than in spheroids. Regardless of the cell culture format, the inducibility was the highest at day 7 (red and blue) and both days 3 and 14 showed lower induction levels in 3D cultures (light blue and dark blue). In HepaRG monolayers, a concentration-dependent increase in CYP 2C19 expression was present at all time points (shades of red), whereas in spheroids a clear dose-dependency was only observed at day 7 (blue).

The CYP induction study shows that the drug metabolizing enzymes CYP 1A1, 1A2, 2B6, 2C19 and 3A4 are inducible in HepaRG cells in both culture formats investigated.

CYP induction in HepaRG monolayers is known as an appropriate model for CYP induction studies routinely performed in early drug development with regulatory acceptance (Kanebratt and Andersson, 2007).

Both CYP 1A1 and 1A2 were highly inducible in monolayer and spheroid cultures at every time point investigated, with a higher inducibility of CYP 1A1 and a lower inducibility of CYP 1A2 in monolayers in comparison to spheroids, overall suggesting that HepaRG cells in both formats express a functional Aryl hydrocarbon receptor (Persson et *al.*, 2006). CYP 2B6 as well as CYP 3A4 were moderately inducible by Rifampicin in both culture formats with a more pronounced effect in monolayers and a slight CYP 3A4 induction was also observable following PB treatment at higher doses (data not shown, see appendix 3). Rifampicin is considered to be a selective activator of PXR, whereas PB activates both PXR and CAR (Kanebratt and Andersson, 2007; Wang et *al.*, 2004; Moore et *al.*, 2000), thus suggesting that CYP induction in HepaRG cells occurs in a physiologically relevant fashion via receptor mediated induction.

The induction of CYP 2C19 by PB was also clearly observed in a dose-dependent fashion independent from the culture format but with a more pronounced effect in monolayers. In contrast, CYP2C9 was only inducible in monolayers at day 14. However, this effect is consistent with other reports stating that the induction of CYP2C9 occurs at very low levels in HepaRG as well as in PHH (Kanebratt and Andersson, 2007; Gerbal-Chaloin et *al.*, 2001).

In this study, HepaRG spheroids showed much lower inducibility in comparison to monolayers for most of the CYPs investigated, which could have several reasons.

In spheroid cell culture, only a small proportion of cells are in direct contact with the surrounding media, whereas in monolayers each cell is in direct contact with the cell culture medium. This may result in lower exposure levels than desired, which would consequently lead to lower response levels in spheroids. Hampered compound transport has been reported as underlying reason for the lower sensitivity towards chemical insult of certain compounds (Walker et *al*., 2000). Secondly, the expression of the receptors could be lower in 3D compared to 2D, which would explain the lower induction levels of 3D compared to 2D observed in the branched DNA approach although a dose dependent induction was observed in the IF staining. The very low induction levels of CYP 2C members could be explained by the low expression levels of CAR in HepaRG monolayers compared to PHH (Aninat et *al.*, 2005). Additionally, both PXR and CAR are regulated by the glucocorticoid receptor (GR, Richert and Tuschl et *al.*, 2009) and the investigation of GR expression in HepaRG 2D and 3D cultures may help to clarify the low inducibility of CAR and PXR-regulated CYP subfamilies. GR itself can be upregulated by submicromolar concentrations of Dexamethasone and is routinely supplemented in PHH culture media (Richert and Tuschl et *al.*, 2009) and could be also used to enhance GR expression in HepaRG cells.

Other studies reported a clear concentration-dependent inducibility of CYPs in HepaRG spheroids (Gunness et *al.*, 2013; Ramaiaghari et *al.*, 2017), which is in agreement with the imaging data presented here. However, those studies were only conducted in 3D and no comparison to 2D was addressed.

Although the dosing regimen was identical for both CYP induction studies, a certain discrepancy was also observable when comparing the OMEP-mediated CYP induction in HepaRG spheroids across both methods: whereas CYP 1A2 was strongly induced by OMEP in the branched DNA approach, showing values up to 100-fold over control (day 3, figure 3.38), the imaging data only approximates a threefold induction as indicated by the RFU values (figure 3.36). For CYP 1A1, the dose-dependency was much less pronounced in the imaging data compared to the branched DNA data. These effects could be explained by the different methods per se: whereas the imaging data gives insight on a protein level, the branched DNA method monitors the induction on the mRNA level and the differences observed here may display a delayed induction on the protein level as mRNA needs to be

translated into protein first. Moreover, measuring CYP induction on the mRNA level is much more sensitive compared to the protein level (Richert and Tuschl et *al.*, 2009; Zhang et *al.*, 2006).

Additionally, the method used here is optimized for monolayers and requires further optimization for spheroid cultures. Therefore, an optimized robust protocol for spheroid samples, especially in terms of the low number of cells in comparison to 2D culture, needs to be established.

However, those studies were only conducted in 3D and no comparison to 2D was addressed. The imaging data clearly evidences the overall stable concentration-dependent inducibility of CYP1A1, 1A2, 2B6 and 3A4 in HepaRG spheroids over several weeks in culture, but further studies are required in order to elucidate the underlying reasons for the lower inducibility in HepaRG spheroids compared to monolayers. Therefore, the usefulness of HepaRG spheroids in CYP induction studies remains questionable.

Nonetheless, hepatic spheroids may display a useful tool in DDI studies, especially regarding their longevity that enables to investigate induction and inhibition processes with a slow onset and could help to predict potential DDIs of drugs intended for chronic administration, which is appreciated by regulatory authorities (FDA, 2017).

3.3 Comparative cytotoxicity study

Many chemical entities are either detoxified or converted into toxic metabolites by xenobiotic metabolizing enzymes. Both PHH and HepaRG spheroids were proven to exhibit stable levels of pharmacologically important DMETs over a period of at least 14 and 28 days, respectively. Therefore, the utility of the spheroid cell culture model was tested by a simple viability assay following compound treatment to address whether spheroids exhibit greater sensitivity to chemical insult compared to the corresponding monolayers (described in section 3.1). The clinical outcome of a hepatotoxic response in humans is often observed following subchronic or chronic administration, which remains undetected in short-term in vitro testing strategies that are routinely used in early drug development, resulting in EC_{50} values far exceeding C_{max} levels that elicit toxic response in man.

Therefore, HepaRG cells were cultured in both formats and treated with 6 of the MIP-DILI training compounds, five hepatotoxicants (APAP, BOS, DCF, FIA and TRO) and PIO (non-hepatotoxic compound) (table 3.4). The cells were treated every other day at seven concentrations per compound and viability was assessed via ATP measurement on days 3, 7 and 14.

Additionally, spheroids of two different PHH donors were treated simultaneously in order to compare inter-donor variability in 3D culture (due to the limited availability of cells from both spheroid forming donors, PHH monolayers were not included in this study). The compounds display a subset of the training compound set and were chosen to cover the DILI mechanisms except immune-mediated DILI. Concentration ranges were selected in order to cover several increments of cytotoxic effects at each time point.

PIO, however, could not be used as negative control due to heavy precipitation in 3D cultures because of the format-specific dosing procedure (no precipitation occurred in 2D monolayers).

Table 3.4: Selected compounds and final concentration ranges for the cytotoxicity comparison of monolayers and spheroids.

Compound (Code)	Hepatotoxic/ non-hepatotoxic	Final concentration range [µM]
Acetaminophen (APAP)	hepatotoxic	100, 200, 500, 1,000, 2,000, 5,000, 10,000
Bosentan (BOS)	hepatotoxic	4, 10, 20, 40, 100, 200, 400
Diclofenac (DCF)	hepatotoxic	5, 10, 25, 50, 100, 250, 500
Fialuridine (FIA)	hepatotoxic	0.3, 1, 3, 10, 30, 100, 300
Troglitazone (TRO)	hepatotoxic	0.4, 1, 2, 4, 10, 20, 40
Pioglitazone (PIO)	Non-hepatotoxic	0.4, 1, 2, 4, 10, 20, 40

Dose-response curves have been generated for each compound/ time point and EC_{50} values were calculated as shown in the following.

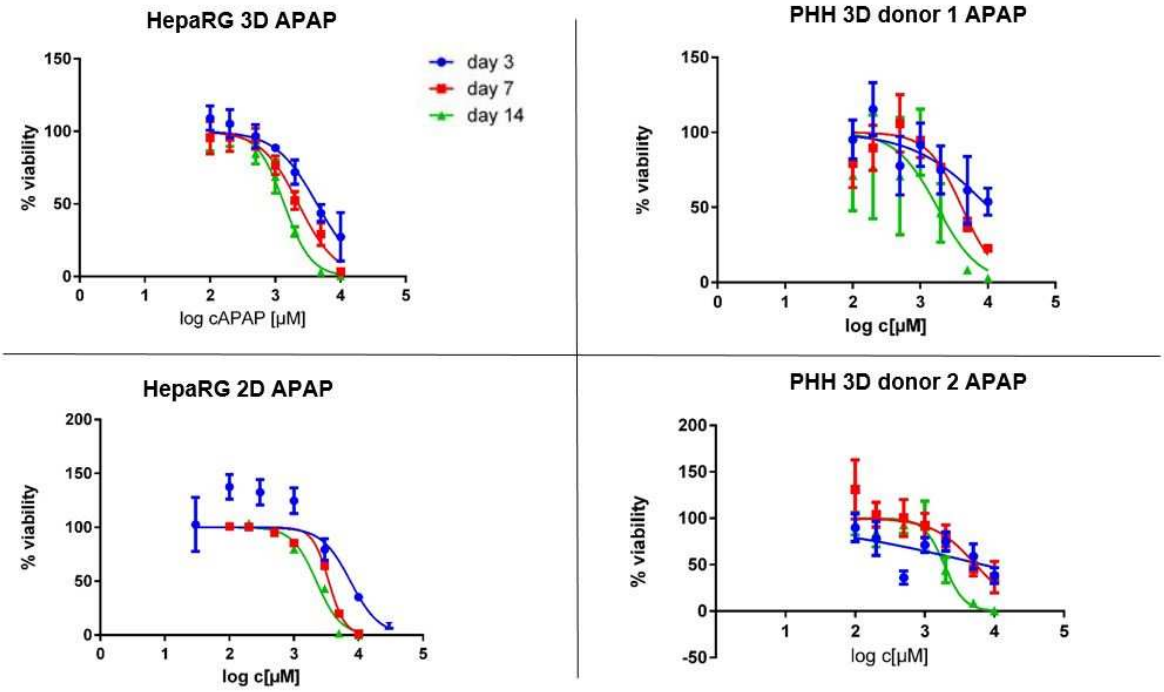

Figure 3.39: Dose-response curves of APAP treated HepaRG cells in 2D and 3D culture (left) and PHH spheroids from two different donors (right) at days 3, 7 and 14. Data expressed as nonlinear regression curves from mean viability values of three independent experiments. HepaRG cells cultured in both formats showed both, a clear dose- and time dependent response with a time-dependent shift of the curve towards lower concentrations. This effect was less clear in both PHH donors, especially in spheroids from donor 2.

Table 3.5: Mean EC_{50} values of cell models following APAP treatment for up to 14 days generated from three independent experiments.

Cell model	EC_{50} [µM]		
	Day 3	Day 7	Day 14
HepaRG 2D	7,512	3,462	2,227
HepaRG 3D	4,352	2,269	1,367
PHH 3D donor 1	6,915	5,419	1,905
PHH 3D donor 2	10,386	4,152	1,794

A clear dose-dependent decrease in the ATP content was observed following APAP treatment in all conditions tested. Additionally, it was shown that the cytotoxic effects occurred in a time dependent manner, evident by the shift of the dose response curves towards lower concentrations by increasing treatment duration (table 3.5). APAP caused lower EC_{50} values after repeated exposures, indicated by and EC_{50} of 4 - 10 mM at day 3 compared to 1.3 - 2.2 mM after 14 days. The latter is approximately tenfold of the clinically relevant C_{max} (149 µM; Villeneuve, Gosselin and Whyte, 2014). Following APAP treatment, HepaRG spheroids were the most sensitive cell model and showed EC_{50} values that were approximately half of those in monolayers. Additionally, HepaRG spheroids were more sensitive in comparison to PHH spheroids on days 3 and 7, whereas EC_{50} values at day 14 were in a comparable range for all spheroid models. PHH spheroids donor-to-donor variability was clearly present on day 3, indicated by the substantial difference in APAP induced EC_{50} values, but were comparable after 14 days.

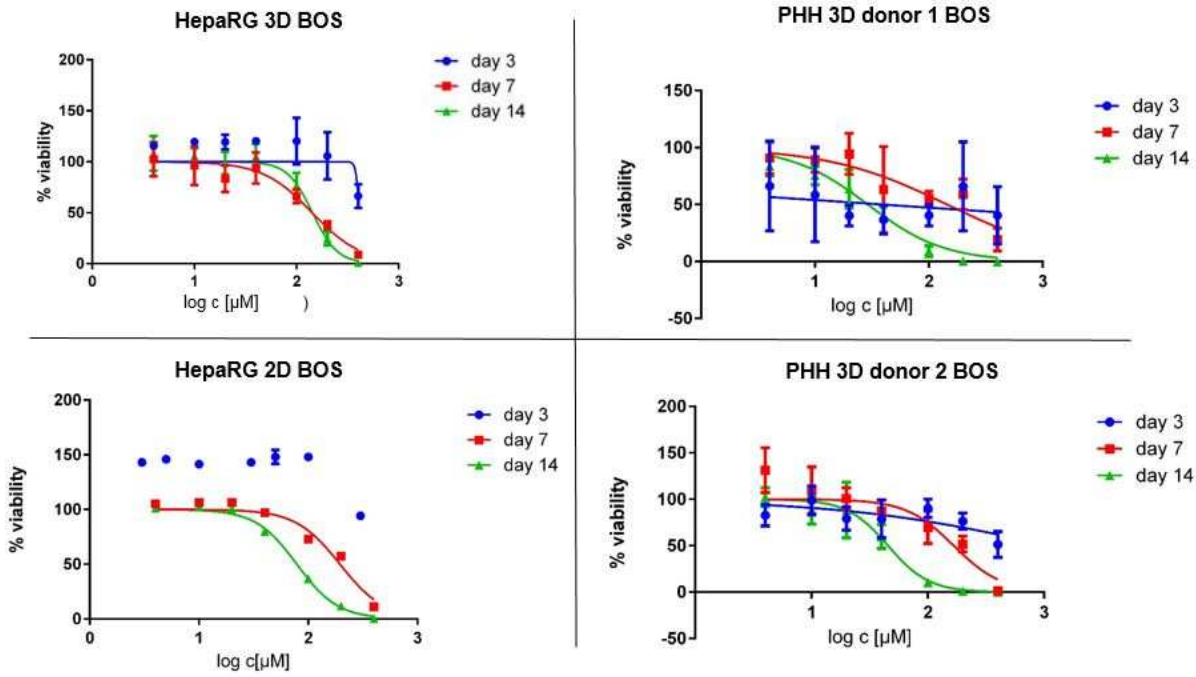

Figure 3.40: Dose-response curves of BOS treated HepaRG cells in 2D and 3D culture (left) and PHH spheroids from two different donors (right) at days 3, 7 and 14. Data expressed as nonlinear regression curves from mean viability values of three independent experiments. HepaRG cells cultured in both formats showed a clear dose- and time dependent response with a time-dependent shift of the curve towards lower concentrations. This effect was less clear in both PHH donors, especially in spheroids from donor 2.

Table 3.6: Mean EC_{50} values of cell models following BOS treatment for up to 14 days generated from three independent experiments.

Cell model	EC_{50} [µM]		
	Day 3	Day 7	Day 14
HepaRG 2D	>400	195.5	78.75
HepaRG 3D	>400	142.3	143.2
PHH 3D donor 1	>400	144.9	29.11
PHH 3D donor 2	>400	167.4	45.57

Dose response curves following BOS treatment showed a clear time-dependent decrease in EC_{50} values. At day 3, BOS did not elicit cytotoxic response in any of the cell systems an EC_{50} values were not determinable. In contrast, EC_{50} values at day 7 were in a comparable range for all cell systems, which further decreased with increasing treatment duration in HepaRG 2D and PHH spheroids from both donors, whereas the EC_{50} value in HepaRG spheroids at day 14 was similar to that of day 7 (142.3 µM vs. 143.2 µM).

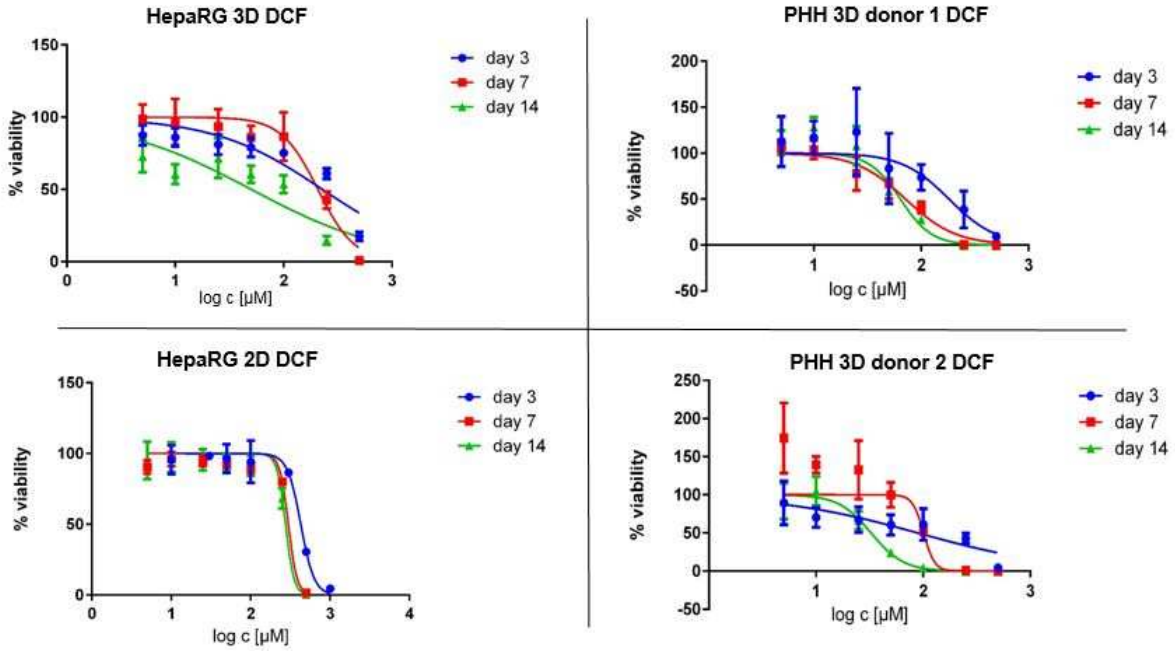

Figure 3.41: Dose-response curves of DCF treated HepaRG cells in 2D and 3D culture (left) and PHH spheroids from two different donors (right) at days 3, 7 and 14. Data expressed as nonlinear regression curves from mean viability values of three independent experiments. HepaRG cells cultured in both formats showed both, a clear dose- and time dependent response with a time-dependent shift of the curve towards lower concentrations. This effect was less clear in both PHH donors but was still clearly detectable.

Table 3.7: Mean EC_{50} values of cell models following DCF treatment for up to 14 days generated from three independent experiments.

Cell model	EC_{50} [µM]		
	Day 3	Day 7	Day 14
HepaRG 2D	427.8	298.5	274.8
HepaRG 3D	229.0	207.6	50.58
PHH 3D donor 1	89.38	101.0	32.69
PHH 3D donor 2	181.9	71.68	63.97

Following DCF treatment, EC_{50} values decreased in a time-dependent manner in all cell models. HepaRG were less sensitive in 2D than 3D, with the most pronounced effect at day 14 as indicated by a fivefold higher EC_{50} value in 2D compared to 3D (274.8 µM vs. 50.58 µM). Spheroids from both PHH donors were more sensitive in comparison to HepaRG spheroids at days 3 and 7, respectively, but EC_{50} values were in a comparable range after 14 days of treatment. cell models and a greater sensitivity in HepaRG spheroids was observed (table 3.7).

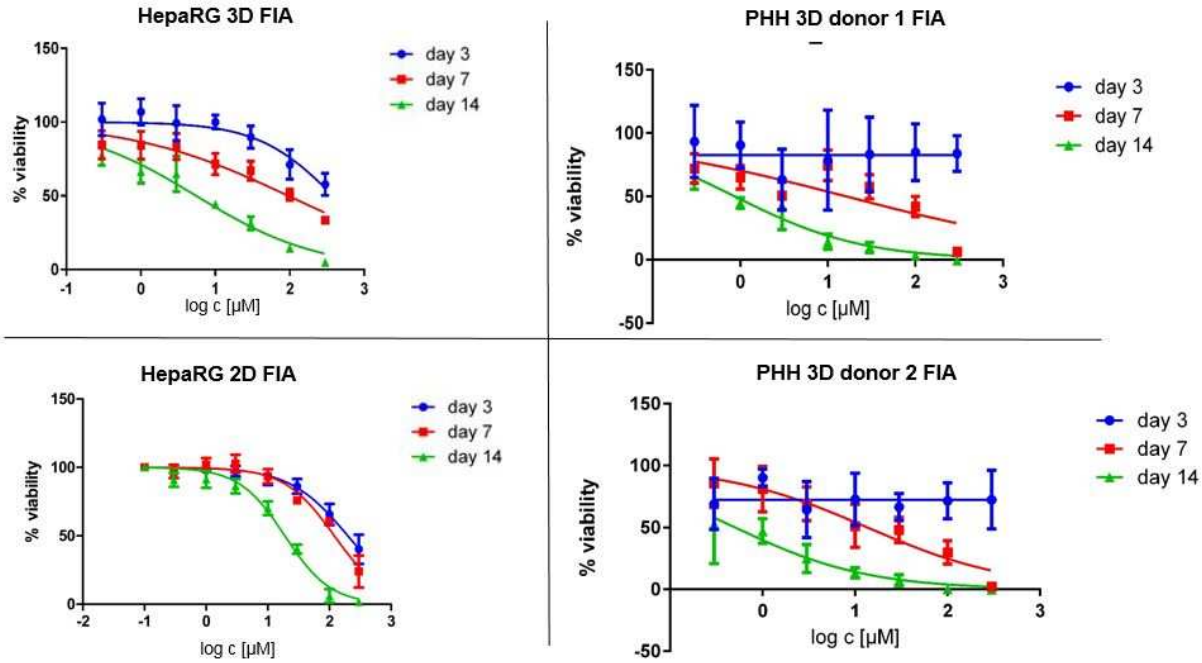

Figure 3.42: Dose-response curves of FIA treated HepaRG cells in 2D and 3D culture (left) and PHH spheroids from two different donors (right) at days 3, 7 and 14. Data expressed as nonlinear regression curves from mean viability values of three independent experiments. HepaRG cells cultured in both formats as well as PHH spheroids showed, a clear dose- and time dependent response with a time-dependent shift of the curve towards lower concentrations.

Table 3.8: Mean EC_{50} values of cell models following FIA treatment for up to 14 days generated from three independent experiments.

Cell model	EC_{50} [µM]		
	Day 3	Day 7	Day 14
HepaRG 2D	>300	>300	17.5
HepaRG 3D	>300	95.69	5.54
PHH 3D donor 1	>300	16.43	0.87
PHH 3D donor 2	>300	13.69	0.51

The effect of increased susceptibility upon repeated exposure was most prominent for FIA and whereas at day 3 no EC_{50} value could be established in any cell model, a strong cytotoxic effect was observable at day 14, indicated by the low EC_{50} values. Interestingly, HepaRG cell in both 2D and 3D showed a dose-dependent decrease in viability already at day 3, whereas in PHH spheroids, the overall viability was somewhat decreased independent from the dose. Again, HepaRG monolayers were much less sensitive compared to spheroids. EC_{50} values were very close in PHH spheroids of both donors at every time point.

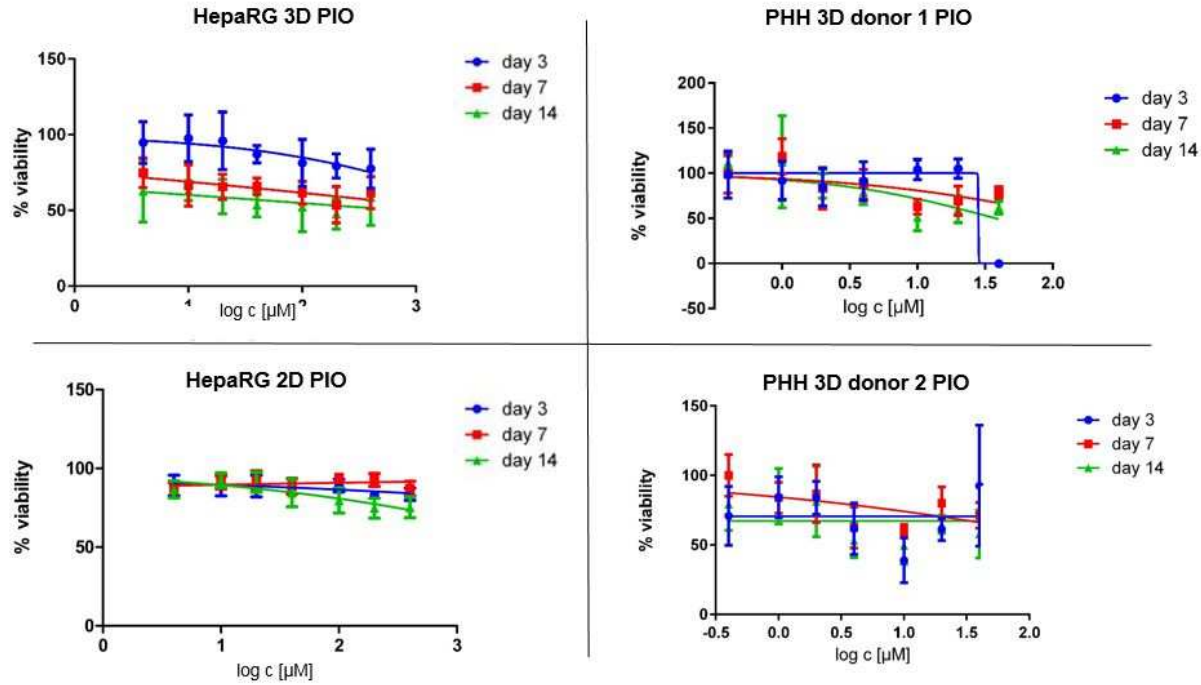

Figure 3.43: Dose-response curves of PIO treated HepaRG cells in 2D and 3D culture (left) and PHH spheroids from two different donors (right) at days 3, 7 and 14. Data expressed as nonlinear regression curves from mean viability values of three independent experiments. No dose-dpendent cytotoxicity was observable in either condition, the decrease in overall viability in spheroids refers to compound precipitation.

None of the cell models showed a clear response to the non-DILI compound PIO as expected (figure 3.43). However, in 3D culture models, precipitation was observed as a

consequence of the dosing regimen, which subsequently led to the inclusion of precipitate in spheroids, resulting in an overall decreased viability (figure 3.44).

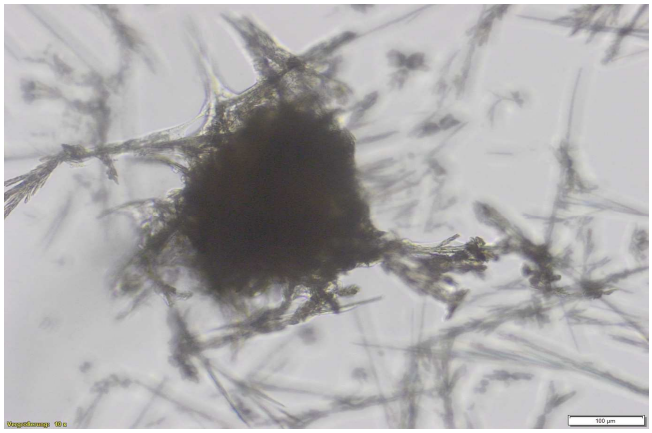

Figure 3.44: Precipitation of PIO as a consequence of the dosing regimen in spheroid culture. Spheroids incorporated the precipitate, which led to an overall lower viability by increasing duration. HepaRG spheroid treated with 40 µM PIO at day 7. 10x magnification, bar = 100 µm.

TRO-mediated cytotoxicity was clearly dose- and time dependent in PHH spheroids of donor 1 as indicated by a time-dependent decrease of EC_{50} values (table 3.9). in contrast, spheroids of donor 2 showed similar EC_{50} values at day 3 and 7, but a clear decrease at day 14. Interestingly, no cytotoxic effect of TRO was observable in HepaRG cells in either cell culture format at any time point.

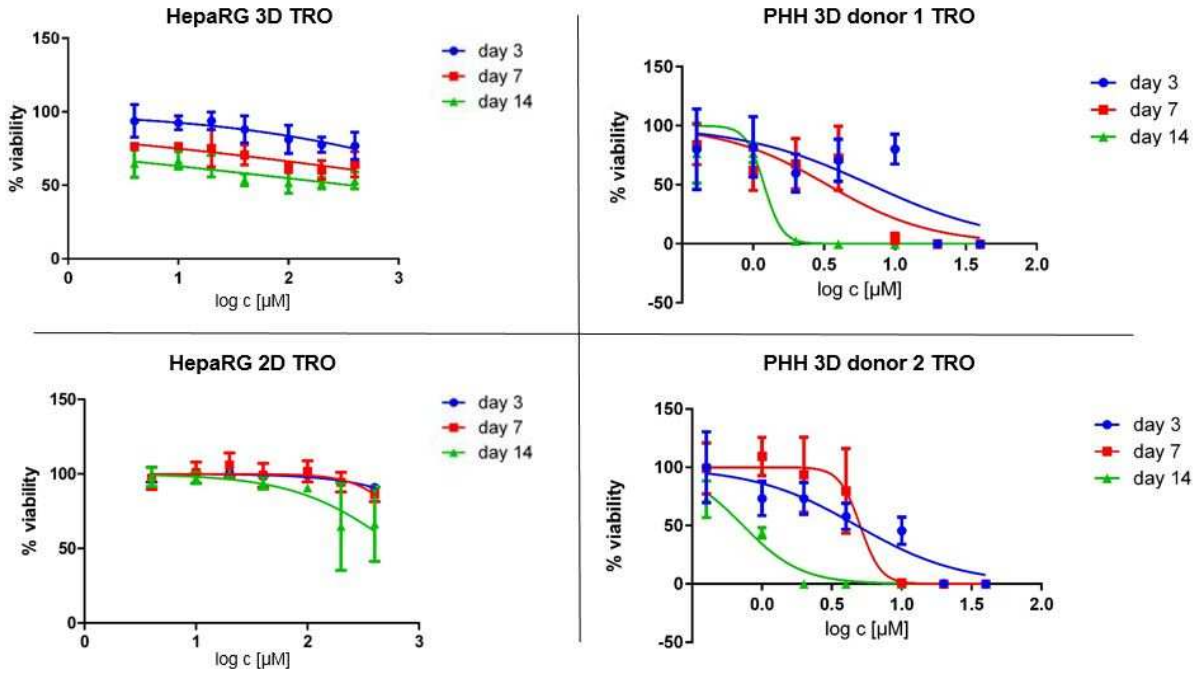

Figure 3.45: Dose-response curves of TRO treated HepaRG cells in 2D and 3D culture (left) and PHH spheroids from two different donors (right) at days 3, 7 and 14. Data expressed as nonlinear regression curves from mean viability values of three independent experiments. HepaRG cells cultured in both formats showed no response to TRO at either time point in either format, whereas TRO clearly induced cytotoxicity in PHH spheroids of both donors.

Table 3.9: Mean EC_{50} values of cell models following TRO treatment for up to 14 days generated from three independent experiments.

Cell model	EC_{50} [µM]		
	Day 3	Day 7	Day 14
HepaRG 2D	>40	>40	>40
HepaRG 3D	>40	>40	>40
PHH 3D donor 1	6.77	3.34	1.19
PHH 3D donor 2	4.79	5.05	0.74

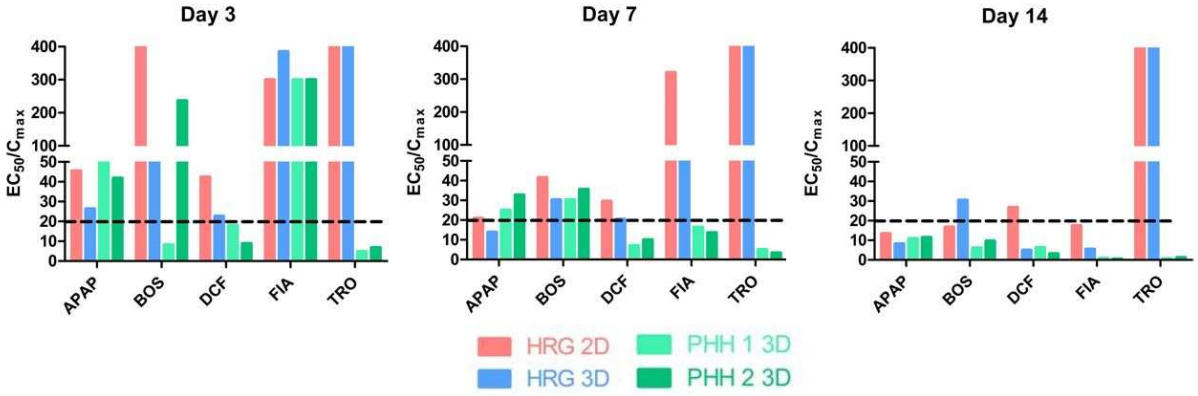

Figure 3.46: Clustered column plots showing the EC_{50}/Cmax values for the four hepatotoxicants by measurement of the ATP content in HepaRG (HRG) 2D (red), HepaRG 3D (blue) and PHH 3D in two different donors (shades of green) after treatment for 3 (left), 7 (middle) and 14 (right) days. The time-dependent decrease of EC_{50} values and thus the EC_{50}/Cmax value was clearly observed for most conditions.

Figure 3.46 shows the C_{max} correction of the EC_{50} values, which was performed for the 2D multicenter ring trial data (section 3.1.1). Following 3 days of treatment, the majority of cell models could not detect hepatotoxicity. Spheroids from PHH (donor 1) detected both BOS and DCF with EC_{50}/C_{max} values below 20. Additionally, PHH spheroids (donor 2) detected DCF as hepatotoxic.

After seven days of treatment, the EC_{50}/C_{max} ratio clearly decreased for all conditions, except for FIA in HepaRG monolayers, and no cell model could identify BOS as hepatotoxic.

The results shown for the 14-day treatment indicate a dramatic decrease in the EC_{50}/C_{max} ratio, suggesting a greater sensitivity to predict hepatotoxicity. The overall trend is that HepaRG spheroids were more sensitive under these conditions than HepaRG monolayers with only one exception (BOS day 14). In addition, although spheroid cultures of HepaRG were less sensitive compared to PHH spheroids, the EC_{50} values of both spheroid models were overall in a comparable range over prolonged exposure times, which is in contrast to that observed in monolayers, which were the least sensitive cell model under the conditions of this study. However, although hepatic spheroids showed an overall greater sensitivity,

some exceptions were observable that appeared to be compound specific and are discussed in the following.

Bosentan, a dual endothelin receptor antagonist which is known to cause hepatotoxicity (Simmoneau et *al.*, 2014), did not show a time dependent decrease of the EC_{50} in HepaRG spheroids from day 7 to day 14, whereas in both HepaRG monolayers and PHH spheroids, the effective concentration markedly decreased upon repeated exposure. BOS is mainly metabolized by CYP 2C9 and 3A4 into three major metabolites: Ro 48-5033; Ro 64-1056 and Ro 47-8634, of which Ro 47-8634 has been identified as hepatotoxic (Matsunaga et *al*., 2015). The formation of Ro 47-8634 is mainly mediated via CYP 2C9, whereas the formation of both Ro-48-5033 and Ro 64-1056 is CYP 3A4 mediated. Additionally, BOS is also strongly inducing both enzymes (Matsunaga et *al.*, 2015) and as CYP 2C9 inducibility was only observable following 14-day exposure in HepaRG monolayers as presented in section 3.2.3.2 (figure 3.38), a possible explanation for the low cytotoxic effect in HepaRG spheroids could be the absence of CYP 2C9 induction that would consequently lead to a much lower CYP2C9-mediated formation of the toxic Ro-47-8634 in comparison to monolayers.

Following DCF treatment, discrepancies in EC_{50} values were observable between HepaRG 2D and 3D after 14 days as well as between PHH from both donors (table 3.7 and figure 3.46). It is known that the metabolic activation of DCF to 5-hydroxy-DCF plays a major role in DCF-mediated DILI and both CYPs 2C8 and 3A4 are involved in the formation of 5-hydroxy-DCF (Shen et al., 1999; Naisbitt et al., 2007; Kishida et al., 2012). Therefore, different expression levels of those enzymes between the two PHH donors as well as between HepaRG monolayers and spheroids may be the underlying reason for those differences.

Another discrepancy that was observable was the absence of any TRO-mediated cytotoxicity in HepaRG cells of either format. TRO was approved for the treatment of type II diabetes by the FDA in 1997 and subsequently withdrawn from the market in 2000 due to severe hepatotoxicity in some patients (Gale, 2001). TRO elicited severe cytotoxicity in PHH spheroids from both donors as indicated by the very low EC_{50} values (4.79 µM, 5.05 µM and 0.74 µM in donor 2 at day 3, 7 and 14, respectively), no effect was observable in the HepaRG cell models due to the following potential reasons: Firstly, TRO is known to strongly bind to plasma proteins (99%, Loi et *al*., 1999; Kawai et *al*., 1997) and all experiments in HepaRG cells were conducted in serum-containing TOX medium for the sake of comparability, which subsequently leads to a decrease in the effective dose. Indeed, cytotoxicity was observed in HepaRG spheroid cultures maintained under low-serum conditions (Bell et *al.*, 2017). Secondly, the metabolism of TRO is complex and various intermediates are known, of which those generated by both CYP3A4 and SULT1A1 are associated with toxicity, but remain controversial. CYP 3A4 metabolizes TRO to a quinone, which is suggested to cause hepatotoxicity through oxidative stress and covalent binding to

subcellular molecules (Smith, 2003). The SULT-mediated formation of the TRO-sulfate is known to cause moderate cholestasis through the inhibition of bile acid export and was shown to be tenfold more potent than TRO itself (Funk et *al*., 2001). However, the TRO-quinone was found to be less toxic than expected and Hewitt et *al*. (2002) found that high CYP 3A4 activity correlated with high EC_{50} values in TRO treated PHH of 27 donors. The combination of both, the serum-dependent decrease of the effective dose and the high expression level of CYP 3A4 alongside the low SULT1A1 levels as detected in section 3.2.2.2 in HepaRG cells likely contribute to the absence of TRO-mediated toxicity, independent from the culture format.

In the context of the observed lining morphology in HepaRG spheroids, an impaired drug uptake may also contribute to lower sensitivities compared to PHH in 3D. Although no TRO-mediated toxicity was detected in HepaRG monolayers as well, an altered expression pattern of uptake transporters in 3D may contribute to the absence of toxicity when considering the overall higher sensitivity of HepaRG spheroids compared to their 2D counterparts. An efficient drug uptake mediates the initial step of hepatic elimination and for HepaRG monolayers functional levels of uptake transporters have been reported (Le Vee et al., 2006), but the expression of those needs to be set in relation to exporter expression. For example, as the investigated phase III transporters showed different expression levels in spheroid configuration as described in section 3.2.2.3, differences in the expression of uptake transporters such as OCTs[5] or OATPs[6] may contribute to a preferred or impaired uptake of a compound, depending on its physicochemical properties. Thus, it would be important to further investigate the expression and activities of both uptake and export transporters as well as the ratio between the respective capacities in HepaRG spheroid configuration in order to define the exact usefulness of this model for toxicity studies.

The heavy precipitation that was observed for PIO addresses a question that is superordinated in terms of the shortcomings that are associated with spheroid cell culture:

Due to the inability to remove the complete dosing solution in ultra-low attachment plates, in which spheroids are suspended, PIO precipitate residues could not be efficiently removed and with each subsequent dosing an increased amount of precipitate was observed. This finally led to the attachment of spheroids (and growth) to the precipitate. As a secondary effect, the overall health of PIO treated spheroids was impaired and PIO was excluded as a negative control under the conditions of this study. The effect that was seen for PIO visualizes the issue of inaccurate dosing in spheroid cell culture upon repeated dosing regimen, which is in fact mitigated by washing steps with the dosing solution but those inaccuracies cannot be fully avoided by the applied methodology, which may also be the underlying reason for the high standard deviations observed in spheroids from both PHH

[5] Organic cation transporter
[6] Organic anion transporting polypeptides

donors. This emphasizes the need for further studies in order to define a more robust and less error-prone 3D culture protocol that displays the premise for industrial routine use.

DILI in humans at therapeutic doses often requires cumulative exposure to manifest clinical signs (Roberts et *al*., 2014). Consequently, common cell culture approaches in early drug development, which mostly include monolayer cultures and a maximum exposure time approximately 72 hours, are simply not able to predict a clinically relevant outcome that requires multiple doses. This was clearly shown by the data presented from the cytotoxicity ring trial (section 3.1). Although differences in the sensitivity towards chemical insult existed across the different cell models assessed, none were able to distinguish between compounds that are associated or not associated with DILI (Sison-Young, Lauschke and Johann et *al*., 2016).

Spheroid cell culture offers the ability to maintain stable physiology and expression levels of DMETs for several weeks, which is consistent with other reports (Ramaiahgari et *al*., 2017, Noor et *al*., 2015, Gunness et *al*., 2013) and for PHH spheroids, a stable physiology has been reported for up to 35 days (Bell et *al*., 2016). Therefore, spheroids provide an appropriate basis for the application of multiple dosing that will enable investigations of repeated exposure scenarios that are more reflective of human exposures to assess cumulative and/ or slower developing adverse effects.

In this work, long-term dosing enhanced the sensitivity of HepaRG cells to a panel of six hepatotoxicants in both cell culture formats, but with greater sensitivity in spheroids compared to monolayers. However, as only PHH spheroids were included, no conclusion on whether PHH spheroids are more sensitive compared to their 2D counterparts can be made for this study. This question was addressed by Bell et *al*. (2017), who compared PHH spheroids to 2D sandwich cultures of the same donors in a cytotoxicity study. In this study, PHH spheroids detected toxicity of all compounds at clinically relevant concentrations following repeated exposure, whereas PHH cultured in 2D sandwich configuration exhibited substantially lower sensitivities for most of the compounds.

The study conducted here initially reflects the delayed onset of many DILI compounds in vivo (Kaplowitz, 2004), showing a significant reduction in the EC_{50} values for all compounds tested, which is in agreement with other studies (Bell et *al*., 2016 and 2017). This effect was most prominent for fialuridine, for which cytotoxicity was exclusively detected upon long-term dosing (e.g. EC_{50} >300µM at day 3 vs. EC_{50} = 0.51 µM at day 14 for PHH spheroids from donor 2). Fialuridine caused severe hepatotoxicity in 7 of 14 patients in clinical trials, 5 of whom died, (McKensie et *al.*, 1995) and no indication of fialuridine hepatotoxicity was observed in any preclinical testing strategy. FIA mediated DILI occurs via intrahepatic accumulation through hENT1[7] (Zhang et al., 2016), which accounts for the slow onset of

[7] Human equilibrative nucleoside transporter 1

cytotoxicity as observed in this study. For hENT1, different genetic variants exist (Zhang et *al.*, 2016), which could be the underlying reason for the different sensitivities in HepaRG and PHH. In this study, it could be successfully shown that the ability to treat hepatic spheroids over prolonged cultivation periods can dramatically decrease the concentration at which chemical insult occurs, which would add great value in the development of drugs that are indicated for subchronic to chronic administrations. Whereas HepaRG showed some limitations (i.e. no TRO-mediated cytotoxicity), PHH spheroids were shown to display a very sensitive and useful *in vitro* tool for long-term cytotoxicity studies.

But, although spheroids showed applicability for long-term testing as well as a greater sensitivity towards chemical insult in comparison to conventional monolayer cultures, only a small panel of compounds was tested and a proper validation using a large panel of both DILI and non-DILI compounds is necessary in order to benchmark spheroid cell culture applicability in the drug developmental process.

Both, spheroid culture per se and repeated dosing regimens require much more resources than conventional short-term tests in monolayers, thus the application of spheroid cell culture as a screening tool is unlikely and spheroids will rather be applied in a tiered approach as a potential *in vitro* application for subsequent investigations.

3.4 Comparative protein expression in HepaRG cells cultured in three different formats

Given the inherent deficiencies of organ-specific microenvironmental properties in conventional 2D monolayer culture, the possibilities to emulate relevant physiological aspects in hepatic in vitro systems are manifold. In the previous chapters, the effect of three-dimensionality on hepatocyte longevity, DMET expression and CYP inducibility has been thoroughly investigated, but not compared to the respective levels in 2D. Moreover, spheroid cell culture displays only one option to modulate a hepatocyte´s phenotype towards higher physiological relevance. For example, the role of fluid transport is fundamental for cell signaling (Mammoto and Ingber, 2010) and physiologic patterns of organ function (Hahn and Schwartz, 2009; Hildebrandt et *al*., 2011). Living cells possess the ability to sense mechanical forces and transduce those into biological responses (Bao and Suresh, 2003; Freund et *al*., 2012) and the mechanisms that modulate cell behavior by fluid shear are diverse, e.g. through cell surface receptors (Tzima et *al*., 2005) and cell adhesion molecules (Tzima et *al*., 2005). In hepatocytes, shear stress has been reported to modulate viability (Park et *al*., 2008) and alter gene expression levels (Mufti et *al*., 1995; Mufti and Shuler, 1996; Shvartsman et *al*., 2009; Vinci et *al*., 2011).

One option to introduce shear stress to hepatocytes through medium flow is the pump-driven quasi-vivo (QV) system (Kirkstall Ltd., Sheffield, UK), which enables an adjustable medium flow over monolayer culture in a standard multiwell approach (detailed description in section 2.2.1.7).

In this section, the expression patterns of CYP1A2, CYP3A4 and NAT1/2 were compared in HepaRG cells cultured in 2D monolayers, 3D spheroids and QV flow culture over a prolonged cultivation period of 14 days in order to initially elucidate the effects that different environmental cues may have on the same cell model. An overview of the used culture system specific requirements is given in table 3.8.

Table 3.10: Cell culture format specific parameters for 2D monolayers, 3D spheroids and QV microfluidic cell culture system. Substantial differences in seeding densities and subsequently replicates for common applications impact the selection of feasible comparative endpoints.

HepaRG	2D monolayers	3D spheroids	QV fluidic
Plate format	96; 24	96	6 (48)
Seeding densities	72,000; 300,000	1,800	300,000[3)]
	Required minimum replicates		
Viability	3 (96)	6	2
Protein	2 (24)	≥500	2
RNA	3 (96); 2 (24)	≥12[1)]; ≥500[2)]	2 (48)
IF	3 (96)	8 (96)	NA

1) replicates required for Luminex branched DNA
2) replicates for RNA isolation
3) seeding and preculture in 24-well plates

The well-established protocols for monolayers needed modification to be applicable to the tight microtissues in 3D as well as of the relatively low cell number per spheroid. For example, standard lysis protocols are not applicable to the spheroids and therefore lysing of microtissue needs other requirements. In contrast, the QV system is designed in a 6-well plate format and each well has the growth surface of a well of a 48 well plate (0.75 cm^2) and a static preculture on glass coverslips is required. The 6-well plate format of QV limits scalability and the six independent heads of the pump only allows testing of six conditions at once, thus only low throughput is possible using this system.

Optimized protein isolation protocols for each cell culture format were established, therefore a comparison of the different cell models was performed via Western Blotting. Due to the large number of spheroids needed for protein isolation, as well as the limited number of conditions that can be tested in QV, only basal expression levels were investigated.

Several DMETs were investigated previously in spheroids by immunofluorescent staining (section 3.2.2), but no comparison between the culture systems per se has been performed so far. Therefore, expression of CYP1A2, CYP3A4 (Phase I) and NAT 1/ 2 (Phase II) were compared in the three different cell culture formats.

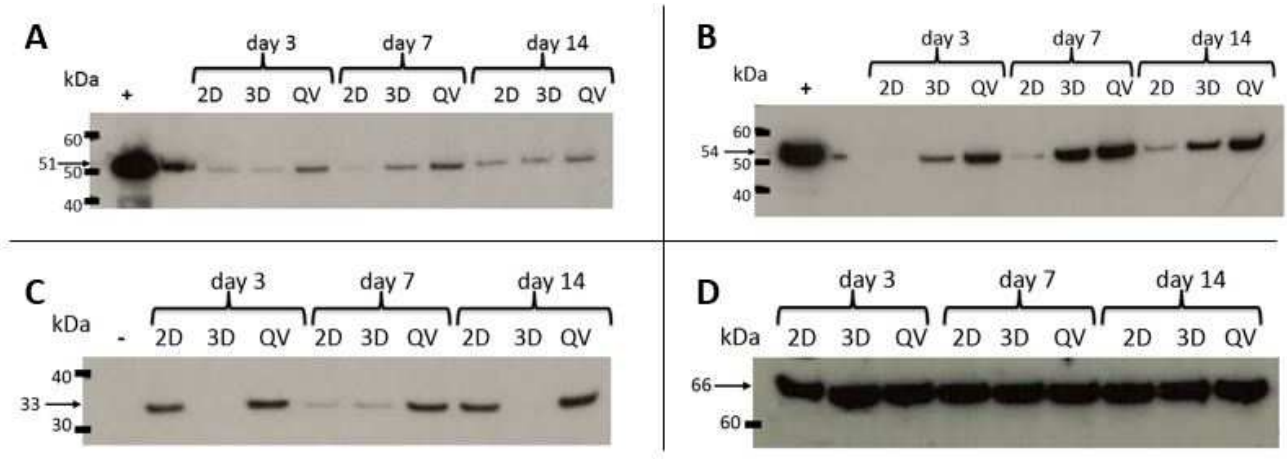

Figure 3.47: Comparative protein expression levels of DMEs in HepaRG cells cultured in three different formats at three different time points. Both culture format and time-dependent differences in the expression of CYP 1A2 (A), 3A4 (B) and NAT 1/ 2 (C) were clearly visible. A clear inducing effect of the flow conditions was observed for QV. In contrast, only CYP 3A4 expression was higher in spheroids at all time points compared to 2D, whereas CYP 1A2 expression did not substantially differ from expression levels in monolayers. Interestingly, NAT 1/ 2 expression was only weakly visible in 3D at day 7 and was not expressed at days 3 and 14, whereas NAT 1/ 2 was clearly expressed in 2D and QV at all time points investigated. As a quality control, D shows the expression of albumin, which was not substantially affected by the culture format. kDa = kilo Dalton.

Figure 3.45A shows the expression levels of CYP1A2 in HepaRG cells cultured in the different formats on days 3, 7 and 14. At day 3, expression was generally low and no substantial difference in CYP1A2 expression was observed between 2D and 3D. In contrast, HepaRG cultured in the QV clearly showed a higher expression. Following 7 days of culture, the expression pattern changed and monolayers expressed very low CYP1A2 levels,

whereas the expression in spheroids increased, again the highest expression level was observed under flow conditions, with increased expression observed compared to day 3. After 14 days of culture, CYP1A2 expression increased in 2D and decreased in 3D and observable under flow conditions, although expression was still higher in the QV format.

In contrast, the expression pattern of CYP 3A4 was more consistent over time (fig 3.47 B). At every time point, HepaRG monolayers expressed lower levels compared to both 3D and QV culture conditions, but with an increased expression from day 3 to day 14. As observed for CYP 1A2, the expression levels under flow conditions were clearly the highest at each time point, with the lowest level at day 3 and the highest level at day 7. A similar pattern was observable in HepaRG spheroids, but at a lower level when compared to QV conditions. This comparative expression study shows that the expression of phase I enzymes (CYP1A2 and CYP3A4) is more stable when cultured in 3D and expression improved further under flow conditions. Interestingly the expression levels of both CYPs in 2D was the highest at day 14, suggesting that some degree of physiological recovery is happening and that standard monolayers may be applicable for specific subacute experiments. Although the expression patterns of HepaRG cultured in both 3D and QV were overall higher at time points, a decrease from day 7 to day 14 was observed for both CYPs investigated. This clearly shows that for any cell model applied to prolonged cultivation and treatment periods it is essential to investigate physiological function at more time points in order to generate a relevant profile over time.

NAT 1/ 2 (Phase II) has been comparatively investigated across the three culture formats, and protein is shown in figure 3.30.

Figure 3.47 C shows the expression patterns of NAT 1/ 2 in HepaRG cells cultured in the different formats. Here, the expression patterns were similar at days 3 and 14 with comparable bands for 2D and QV with a slightly higher expression in QV. Interestingly, HepaRG cells did not express NAT 1/ 2 at these time points in 3D culture. On day 7, both 2D and 3D cultured HepaRG expressed NAT 1/ 2 at a similar, low level, whereas the expression in QV was consistent over time.

Additionally, as a technical control for total protein, albumin expression was compared across the culture formats (fig 3.47 B). No relevant difference in the expression pattern of albumin was observed between the culture formats or time points.

These data clearly show that by modulating the cell culture conditions for the same cell, the degree of DME expression is highly manipulatable. The three DME proteins tested here showed different expression patterns at each time point investigated, thus not allowing a general statement of the influence of the cell culture system itself on DME expression.

In HepaRG spheroids, the expression levels showed time-dependent differences with the highest levels at day 7, whereas those of both day 3 and 14 were comparably lower. In

spheroids, the degree of cell-cell interaction is much higher compared to 2D, and the abundance of various junctions is known to be beneficial on hepatocyte functionality and drug metabolism (Hamilton et *al.*, 2001). A possible explanation for the lower expression levels at day 3 would be that the junctional network may be in a set-up period and thus not yet fully established, which may result in lower expression levels at day 3 and an enhanced expression at day 7 due to a higher degree of intercellular crosstalk.

In contrast, the decreased expression levels at day 14 may relate to the diffusion-driven gas transport: A sufficient oxygen supply is crucial for hepatocyte functionality since a high metabolic capacity results in a high oxygen turnover (Cho et *al.*, 2007). The transport of gases in spheroid configuration is mediated by passive diffusion due to the absence of a vascular system. This diffusion is directly linked to the spheroid diameter, which should not exceed 200 µm in order to prevent critical O_2 concentrations in the spheroid core (Curcio et *al.*, 2007). Although the spheroids generated here did not exceed this critical diameter, the oxygen supply may have an impact over prolonged cultivation time as the oxygen saturation in the surrounding media is decreased under static conditions (Vinci et *al.*, 2011). Additionally, it has been suggested that the penetration of compounds is limited in spheroid configuration (Walker et *al.*, 2000), an effect that can also occur for certain nutrients and subsequently may alter a spheroid´s expression DME pattern. As metabolism is in general a delicate interplay of nutrient uptake and waste product excretion, the above aspects are also applicable to the transport of CO_2 and catabolites, which affect the microenvironment within the spheroid over time.

Only the QV system showed an overall greater abundance of the investigated proteins, with the highest expression observed for CYP 3A4, followed by NAT 1/ 2 and CYP 1A2. This suggests that the introduction of flow and shear forces have a beneficial effect on the DME expression in HepaRG cells, which is in agreement with other reports: Vinci et *al.* (2011) evaluated the influence of medium flow in PHH in comparison to monolayers of the same donor and found a much higher expression of DMETs such as CYPs, UGTs and MRP2 in PHH exposed to shear stress. Additionally, CYP1A expression was increased by increasing flow rates, whereas the expression levels of other CYPs (2B6, 3A4) decreased again by increasing shear stress. This emphasizes how specific a certain stimulus influences expression of individual proteins. For example, both CYP1A1 and 1A2 are also highly expressed in arterial and venous endothelial cells (Han et *al.*,2008) which are continuously exposed to high shear stress *in vivo*, thus high flow rates may enhance their expression in hepatocytes under hydrodynamic culture conditions as well. In contrast, CYP3A4 expression is mostly restricted to liver (and gastrointestinal, the human protein atlas, www.proteinatlas.org) tissue and native hepatocytes are exposed to low shear stress due to the sinusoidal microarchitecture, which may lead to the guess that the stimuli to which a CYP

isoenzyme responds or not are a result of the stimuli that are given in the respective expressing tissues. Overall, the results obtained here alongside other studies demonstrate that hepatocytes and hepatocyte-like cells respond to hydrodynamic stimuli by greater metabolic capacity. But additionally, the indicated relation of CYP expression and flow rate (Vinci et *al.*, 2011) emphasize how delicately the modulation of cell culture conditions affect the hepatocyte phenotype. This becomes especially clear by considering that a change in culture conditions reflects a multifactorial change on many levels. For example, when introducing medium flow, cells are not only exposed to the mechanical shear stimulus but also to convection-aided turnover in the form of increased oxygen and nutrient supply as well as a higher catabolite removal (Sbrana et *al.*, 2010). Moreover, additional factors such as the choice of the construction material (e.g. polydimethylsiloxanes, silicones or Teflon) as well as the underlying technology to introduce flow (e.g. gravity-driven, pump-driven or syringe-driven) highly contribute to the multitude of phenotype-affecting stimuli that cells perceive (Wu et *al.*, 2010). To date, a myriad of publications on physiologically relevant improvements in cell culture exist, which all pursue the same goal, namely emulating liver biology, and all show evidence for improved hepatocyte phenotypes over conventional methods, they all differ in their respective setup, highlighting how difficult it remains to define an optimal culture condition for a specific purpose. From an industry perspective, the application of any novel in vitro approach remains a huge challenge since, despite the increased physiological relevance that those models offer, they have to be thoroughly benchmarked in order to be able to define the purpose each specific model is fit for and to find acceptance.

4 Conclusion and future perspectives

Undetected drug-induced liver injury (DILI) displays one of the leading causes of drug candidate termination in late developmental phases and post-marketing withdrawal (Kenna, 2018; Kaplowitz et *al.*, 2013) and remains a serious challenge for the pharmaceutical industry given the limited predictive value of currently applied preclinical testing strategies. Whilst preclinical animal models are essential for the detection of adverse drug reactions (ADRs), species-specific differences in drug metabolism pathways and pharmacokinetics lead to a predictivity of only 50% for human DILI (Olson et *al.*, 2000). Moreover, animal models are not capable of reflecting the broad diversity of human population including factors such as age, sex, co-morbidity and lifestyle since relatively low numbers of young animals with limited genetic diversity under standardized conditions are routinely used. The aforementioned factors contribute to the many cases of idiosyncratic DILI that occurs unpredictably in a small number of patients, which may be mediated by both the innate and adaptive immune system when triggered by hepatocyte injury. Eventually, the interplay between injurious and adaptive cellular response to chemical insult determines whether the liver of a certain patient adapts to a mild injury or proceeds to severe liver injury. The pharmaceutical industry is therefore seeking for well-characterized human hepatic *in vitro* models in order to reliably characterize a drug candidate for its potential to cause DILI in man at the earliest possible developmental stage. In this work, hepatic cell models have been assessed in different culture formats with respect to their ability to emulate relevant hepatophysiology in the context of possibly improving preclinical toxicity testing strategies. The usefulness, advantages and shortcomings as well as possible applications in the early drug development pipeline are summarized for each cell culture format in the following.

4.1 Applicability of 2D monolayer cultures

Hepatic cell models in simple 2D monolayer cultures are in routine use as first-line approach for the assessment of drug candidates, which directly injure hepatocytes in a dose-dependent fashion without the contribution of external molecular factors that may be required for hepatotoxicity to occur. This type of hepatotoxicity is commonly referred to as intrinsic hepatotoxicity and is often reliably detectable in preclinical *in vitro* and *in vivo* testing strategies. Two-dimensional hepatic monolayers have been successfully used for the detection and ranking of drug candidates that cause intrinsic cytotoxicity, which often occurs at very high doses, usually at the multiple of clinically relevant human plasma concentrations. The comprehensive cytotoxicity study described in section 3.1.1 emphasizes the shortcomings of 2D monolayers in terms of predicting DILI at relevant doses, which is due to several reasons:

- In early cytotoxicity studies, broad concentration ranges are used as a conservative approach since human pharmacokinetics data of newly synthesized drug candidates is yet unknown. The EC_{50}/C_{max} correction that was used in this study is therefore only useful as a validation approach for novel *in vitro* assays using well-studied training compound sets. Nonetheless, cytotoxic EC_{50} values initially enable a ranking of drug candidates according to unfavorable cytotoxicity profiles.
- Cytotoxicity assays are not capable of providing any information on the underlying mechanisms leading to DILI.
- Classic 2D cytotoxicity assays are, due to limited longevity in a differentiated state, normally performed in a short-term setup with incubation times between 24 and 72 hours, thus they are not able to recognize hepatotoxicities with a slow onset.

Despite the limitations described above, the usefulness of those assays is not negligible since cytotoxicity is in accordance with systemic tolerance and general organ toxicity in preclinical animal models (Benbow et *al*., 2010). Although these assays may not provide a mechanistic understanding of multifactiorial hepatotoxicity, the essential advantages are simplicity, low cost, rapid data generation and high throughput, which fits well to the fast paced early developmental stages. Taken together, these data can provide an estimation of potentially safe C_{max} values by e.g. comparing the EC_{50} values of cytotoxicity to that of the *in vitro* pharmacologically effective dose at the target, which then helps to identify candidates with the widest margin between effectivity and toxicity. Ultimately, while lacking both complexity and sensitivity, simple cytotoxicity assays serve as an early filter for drug candidates or compound series due to inacceptable or unfavorable intrinsic toxicity profiles.

Nevertheless, further improvement of cytotoxicity assessments may add essential value to the early ranking of drug candidates. For example, the short-term applicability of hepatic monolayer models is mostly due to the poor metabolic capacity in this culture format, either because cancer cell lines are inherently lacking physiological relevance as it was observable in the proteomic profiles compared to PHH in section 3.1.2, or because PHH suffer from rapid dedifferentiation when cultured as monolayers, thus hampering a physiologically relevant outcome with prolonged incubation times. The loss of hepatophysiologic functions in 2D culture is mainly a consequence of the unphysiologic shape that cells acquire in 2D formats. The attachment on plasticware leads to a flattened cell morphology, which in turn has substantial consequences on cellular polarity on the one hand and leads to a massive decrease of intercellular contact surface on the other hand, both substantially contributing to altered cell signalling and loss of hepatocyte-specific functionality.

Nonetheless, simple 2D monolayers are applicable to various other endpoints that further help to rank and flag compounds with respect to the underlying mechanisms of DILI, such as mitochondrial impairment. The primary function of mitochondria is the production of the cell´s

energy in the form of ATP alongside the regulation of major cellular functions including cell death signaling pathways (McBride et al, 2006). Given the myriad of metabolic tasks of the liver, hepatocytes have a high energy demand, thus they are rich in mitochondria rendering the liver more susceptible to mitochondrial toxicants. Mitochondrial dysfunction has become increasingly implicated in the etiology of drug-induced toxicities (Dykens and Will, 2007), which consequently increases the demand for preclinical mitochondrial toxicity assays. In order to avoid mitochondrial liabilities, routine screens can be performed in the drug discovery process and several *in vitro* models exist for the evaluation of mitochondrial toxicity, which differ in readout complexity (Dykens and Will, 2007). For example, the glucose galactose assay (glu-gal assay) compares the cytotoxicity profile of a compound in hepatocyte cell models, usually HepG2, when cultured in either glucose-rich or galactose-rich media. HepG2 cells are able to cover their energy demand through glycolysis alongside oxidative phosphorylation (the crabtree effect, Marroquin et *al.*, 2007), a metabolic feature which is not given in primary hepatocytes (Kamalian et *al.*, 2015). When cultured under galactose-rich conditions, HepG2 cells metabolically switch to oxidative phosphorylation, which makes them more susceptible to mitochondrial impairment and the ratio of EC_{50} values of glucose and galactose conditions can indicate a compound´s potential to cause mitochondrial toxicity. This assay is applicable as an early screening approach in order to flag compounds, but it is not capable of revealing insight of the exact underlying mechanism. Another option that displays more mechanistic understanding, is the measurement of the oxygen consumption rate (OCR) and/or extracellular acidification rate (ECAR) with the XF96 extracellular flux analyzer (Seahorse biosciences). Here, it is possible to measure specific mechanistic endpoints such as spare respiratory capacity, ATP production or uncoupling (Nadanaciva et *al*., 2012; Eakins et *al*., 2016). Moreover, since mitochondria contain their own genome, the measurement of drug-induced alterations of mtDNA also displays another option for the detection of mitochondrial toxicants, especially since certain liver pathologies such as diabetes or non-alcoholic fatty liver disease (NAFLD) are known to change mtDNA levels (Fromenty et *al*., 2013; Massart et *al*., 2012; Aubert et *al*., 2012), thus patients with preexisting indications may be more susceptible to mitochondrial toxicity. The development of *in vitro* disease models with clinically relevant alterations of mtDNA may therefore be useful to identify susceptible subpopulations. However, in currently applied short term assays, changes in mtDNA remain unrecognized and to date little is known about the *in vitro-in vivo* correlation of mitochondrial toxicants, mostly due to the low specificity associated with high compound concentrations used in early toxicity studies.

As the ultimate advantage of monolayer cultures is their ease of use alongside the applicability to high throughput and the rapid data generation, they are suitable for high content screening assays. High content screening (HCS) of multiplexed fluorescent readouts

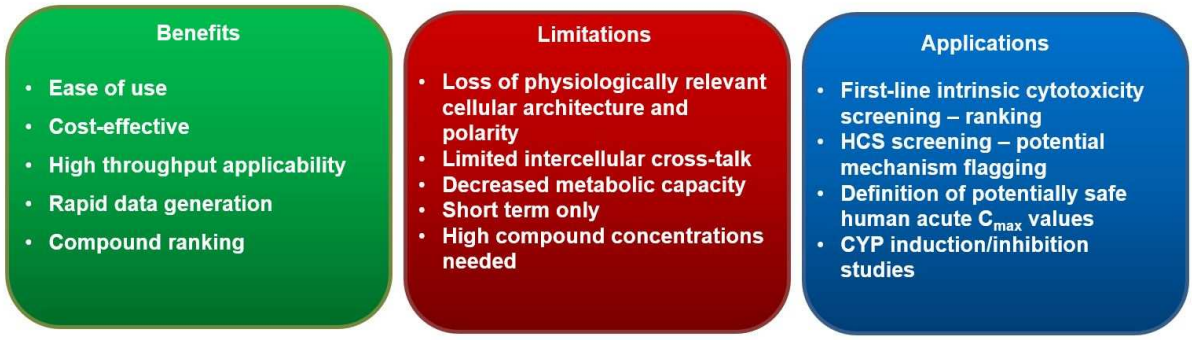

Figure 4.1: Summary of Benefits, limitations and applications of hepatic 2D monolayers in early drug development. Ease of use and screening applicability enable monolayers to display the first-line screening for intrinsic toxicity, which allows a ranking of compounds or compound series. Furthermore, HCS approaches enable the indication of possible underlying mechanisms and compounds can be flagged. Due to the poor metabolic capacity, monolayers are only applicable to short-term experiments, which in turn require high doses that may not reflect plasma concentrations in animal models and humans. HCS = high content screening; CYP = cytochrome P-450; Cmax = peak plasma concentration.

can be used as a rapid approach to obtain an understanding of mechanisms underlying DILI at the organelle levels. HCS systems couple automated fluorescent microscopy with software for real-time analysis of fluorescent intensities and area measurements within individual cells. For example, Garside et *al*., (2014) used a 384-well plate format to investigate the effects of 144 drugs on HepG2 cells cultured in the absence or presence of rat liver S9 mix to enhance drug metabolites as well as on PHH in a high content screening assay. The parameters assessed covered several mechanisms of DILI such as reactive oxygen species, mitochondrial membrane potential, apoptosis, cell cycle arrest cell stress response, phospholipidosis and neutral lipid accumulation. Persson et *al*. (2013) validated a multiparametric HCS method in HepG2 cells including six parameters (nuclei count, nuclear area, plasma membrane integrity, lysosomal activity, mitochondrial membrane potential and mitochondrial area) using a training set of 102 compounds and reported 50% sensitivity and 90% specificity in DILI prediction. Despite the relatively low sensitivity, HCS approaches help in early hazard identification, risk assessment and -avoidance as HCS assays are cost-effective and allow high throughput, which makes them amenable as a first-line safety screening assay in drug discovery projects that allows for decision making through enabling prioritization between compounds or compound series during the hit-to-lead process and to assess the DILI risk towards candidate selection and provide guidance of safe exposure levels in humans. Figure 4.1 summarizes the benefits, limitations and applications of hepatic monolayer models within the drug development pipeline.

4.2 Applicability of 3D spheroid cell culture

As the cellular microarchitecture is clearly connected to physiologic functionality and differentiation, the recapitulation of both cellular polarity and cell-cell contact surface would lead to an improved physiologic relevance in hepatic *in vitro* models. By introducing a third dimension to cell culture, a cell model is enabled to reconstitute a more native shape which allows cellular polarity and massively extended contact surface. HepaRG showed two distinct cell morphologies, which are believed to be the hepatocyte-like cell population in the spheroid centers and the cholangiocyte-like cell population in the periphery. Although a certain degree of organization is indicated, it does not necessarily reflect a liver-like organization and the exact role of this type of cell distribution in the context of physiological relevance is yet unknown and needs to be further investigated. Spheroids of both HepaRG cells and PHH have been shown to display longevity for several weeks (section 3.2.1) and display the expression of DMETs, which makes them amenable to prolonged cultivation and compound exposure times. In the context of cytotoxicity, it could be shown that EC_{50} values substantially decrease over time in both HepaRG and PHH spheroids as summarized in section 3.3. The same effect was observable in HepaRG monolayers, but to a lesser extent, initially showing that spheroids are more sensitive towards chemical insult compared to their monolayer counterparts. The time-dependent effect was especially observable for FIA, which was not detected as hepatotoxicant in any cell model after three days, whereas after 14 days the EC_{50} values decreased to levels comparable to human plasma concentrations. Fialuridine toxicity remained undetected in preclinical development, which is emphasizing the value that long-term compound exposure *in vitro* may add in early developmental stages, thus the application of prolonged compound exposure in hepatic spheroid models would further help to identifiy toxicities with a slow onset and the estimation of 'safe' C_{max} values. However, although spheroids showed an overall higher sensitivity in the cytotoxicity assessment, further investigations are necessary to thoroughly estimate the usefulness of spheroids in the context of cytotoxicity assessment strategies. Following treatment with troglitazone, HepaRG cells did not show any response in either format, which may be due to serum containing media or high CYP3A4 activity or both, but also may indicate a decreased compound penetration. For example, Walker et *al*. (2000) found that hepatic spheroids did not respond to metothrexate treatment, whereas the corresponding monolayer did. Hampered compound penetration may also be the underlying reason why HepaRG spheroids responded less to some CYP model inducers in comparison to their 2D counterparts, suggesting that compound-specific penetration could display a potential drawback in the routine applicability of spheroids in the drug development pipeline. This effect may be more pronounced when regarding the morphology of HepaRG spheroids, which showed a tight lining layer that might have an isolating effect and such morphologies

have also been observed in PHH spheroids cocultured with non-parenchymal cells (NPC), thus emphasizing that the certain degree of organization in hepatic spheroids may neither necessarily reflect *in vivo* physiology nor that this type of organization is mandatory beneficial for the prediction of clinically relevant hepatotoxic outcomes. Additionally, the expression of DMETs was detectable over prolonged cultivation periods in 3D but showed time-dependent differences which were much more pronounced in the western blot analysis compared to IF stained sections (sections 3.2 and 3.4). The expression levels of DMETs in PHH spheroids observed in this study display a huge step towards the long-term use of primary cells in a physiological consensus, thus overcoming one major limitation of hepatic monolayer culture. However, the extension of culture duration also introduces time as parameter that needs to be addressed. Further investigation of the time-dependent dynamics on cell signaling in 3D configuration is therefore crucial for a proper validation process prior to industrial application as it defines what purpose hepatic spheroid models are fit for.

Another outcome of drug-induced liver injury is cholestasis, which is defined as an impairment of bile flow that can manifest as jaundice or icterus. The detection of a compound´s potential to cause cholestasis remains challenging in preclinical species as it is mostly of slow onset and often occurs following (sub)chronic dosing and can be species-specific (Hailey et *al.*, 2014). Additionally, no reliable and well-correlating markers exist to date, hence drug-induced cholestasis is often only detected histopathologically in preclinical species. To date, no reliable *in vitro* test system exists that is able to identifiy cholestatic liabilities in early developmental stages and effective *in vitro* models of translational relevance would provide substantial advantages to the lead optimization process. On major issue in common 2D culture is the absence of an extensive canalicular system as a consequence of the limitations due to monolayer configuration, thus most 2D systems are not allowing the proper assessment of a drug´s cholestatic potential. Additionally, the various underlying mechanisms leading to cholestasis are poorly understood. Nonetheless, a number of *in vitro* approaches are available to study compound effects on hepatobiliary transporters and bile acid uptake and -excretion. For example, the HepaRG cell line displays several physiological characteristics of human hepatocytes that are essential for the study of hepatobiliary transporter function such as the polarity of transporters, well-defined bile canaliculi and bile acid production (Antherieu et *al.*, 2006). The use of bile salt export pump (BSEP, ABCB11) inhibition has been proposed as a tool for detecting drug-induced hepatobiliary transport and may be employed in early development to identify cholestatic liabilities (Morgan et *al.*, 2013; Atienzar et *al.*, 2016). This approach, however, has been associated with a poor specificity when only screening BSEP inhibition (Atienzar et *al.*, 2016) and improvements have been reported when other biliary transporter proteins such as MRPs and Mdrs are included (Köck et *al.*, 2014; Morgan et *al.*, 2013). Measuring transporter

inhibition displays only one mechanism associated with cholestasis and a deeper understanding of the manifold mechanisms that contribute to cholestasis is essential for the development of predicitive preclinical testing strategies. Recent development has been made using hepatocyte sandwich cultures, which allow a more comprehensive assessment of the cholestatic risk of drug candidates (Chatterjee et *al.*, 2014; Oorts et *al.*, 2016). Yet, hepatocyte sandwich cultures require complex handling and high cell numbers resulting in low-throughput applicability and high costs. Furthermore, drug exposure is generally limited to 72 hours, which is questioning the ability of sandwich cultures to assess the slow onset of most cholestatic liabilities. Both HepaRG and PHH spheroids express stable levels of the aforementioned transporters over prolonged cultivation periods (section 3.2.2.3) and additionally, the development of bile canalicular systems in three-dimensional space may better recapitulate the *in vivo* situation, thus suggesting that hepatic spheroid models may be amenable for studying cholestatic liabilities *in vitro*. Hendriks et *al.* (2016) repeatedly co-exposed PHH and HepaRG spheroids to a non-toxic bile acid mixture and a set of cholestatic and non-cholestatic drugs for up to 14 days and reported a pronounced intracellular accumulation of bile acids when spheroids were treated with cholestatic drugs, whereas the non-cholestatic drugs did not lead to bile acid accumulation. Moreover, the ability to induce cholestatic events in spheroids might allow the further development of 3D cholestatic disease models and enable the assessment of DILI in the context of co-morbidity (Bell et *al.*, 2016). Moreover, other pathologies such as steatosis and phospholipidosis may be integrated in the spheroid model in order to potentially investigate possible predisposisition to DILI in early

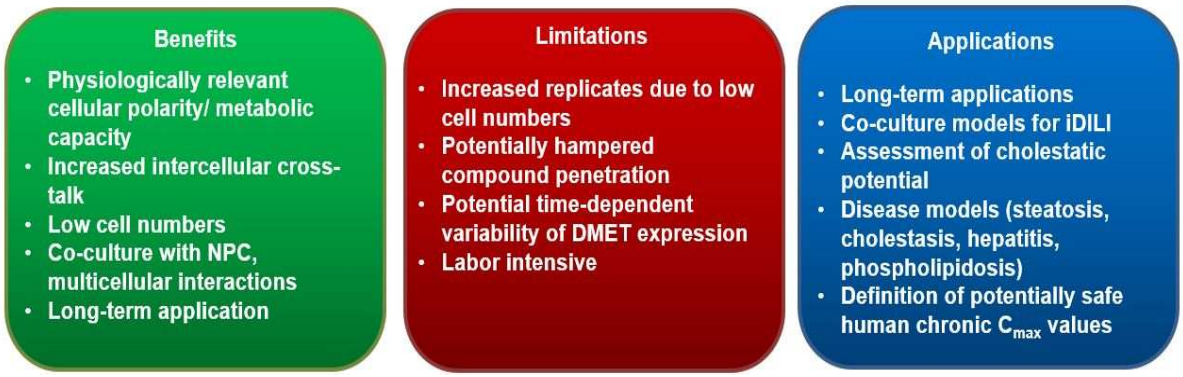

Figure 4.2: Summary of benefits, limitations and applications of hepatic 3D cell culture formats in early drug development. The introduction of a third dimension allows cells an improved phenotype through increased cell-cell contact surface and cellular polarity. This leads to longevity, which makes 3D cell culture systems applicable for repeated dosing regimen to elucidate potential hepatotoxicities with a slow onset. Through co-cultivation with NPCs, the contribution of non-parenchymal factors to hepatotoxic events can be assessed and the development of disease models may help to define susceptible subpopulations prior to clinical trials. Increased replicates and labor time suggest those culture formats to be applied as a second tier following initial assessment in 2D. Moreover, the potentially hampered compound penetration as well as time-dependent variability in DME expression levels need to be thoroughly investigated in order to define the exact performance of a certain model. NPC = non-parenchymal cells; DMET = drug metabolizing enzymes and transporters; iDILI = immune-mediated drug-induced liver injury; Cmax = peak plasma concentration.

developmental phases prior to the clinic. Idiosyncratic DILI is often mediated through the immune system as it is highly implicated in most cases of unpredictable hepatotoxicities. In comparison to the intracellular events that contribute to the previously discussed DILI mechanisms, immune-mediated DILI (iDILI) is a complex association of both intra- and extrahepatic signaling (Stephens et *al.*, 2014). Hepatocellular injury and the hepatic microenvironmental dysregulation are thus believed to play a crucial role in the initiation of an immune response. The progression of an immune response attributes to both resident innate immune cells and infiltrating lymphocytes (Racanelli and Rehermann, 2006). The contribution of the adaptive immune system is defined by a delayed onset of symptoms following first exposure and a rapid onset upon rechallenge (Papay et *al.*, 2009), next to the clear association with certain human leukocyte antigens (HLAs) (Ogese et *al.*, 2017). Certain HLA alleles have been identified to be associated as predisposition factor for establishing iDILI of drugs such as flucloxacillin and ximelagatran (Monshi et *al.*, 2013; Daly et *al.*, 2009; Keisu and Andersson, 2010). However, the exact mechanism by which the presence of certain HLA alleles may increase a patient's susceptibility to iDILI remains poorly understood, which is further evidenced by the fact that some individuals that express the implicated HLA alleles do not develop iDILI. These gaps need to be investigated first before the application of HLA typing as potential predictive marker for the identification of susceptibilities. Given the unpredictable nature of immune-mediated idiosyncratic DILI, there is an urgent need for early *in vitro* and preclinical approaches for the detection of iDILI prior to clinical development and appropriate *in vitro*-based models are currently unavailable. *In vitro* models that identify

potential chemical liabilities such as covalent binding or glutathione (GSH) depletion may help to sort out unfavorable candidates, but they are limited by poor sensitivity and low predictive value. The development of co-cultures with non-parenchymal cells (NPC) such as Kupffer cells or hepatic stellate cells is offering the potential to assess the role of innate immune response to chemical insult. Spheroid cultures of PHH and NPC have been shown an increased susceptibility towards DILI compounds, which are known to cause immune-mediated hepatotoxicities (Bell et *al.*, 2016). Moreover, PHH spheroids could be efficiently infected by recombinant adenovirus prior to aggregation in order to mimic viral hepatitis *in vitro*. Subsequent treatment of infected PHH spheroids with trovafloxacin, whose hepatotoxicity is amplified by inflammatory stimuli, enhanced toxicity was observable, indicating that virus-mediated inflammatory responses are triggering the toxic response. Simultaneously, no response was observed following the treatment with the non-hepatotoxic analogue levofloxacin (Bell et *al.*, 2016). However, the development of three-dimensional cell culture models, co-culture models and disease models has yet begun and further investigations and validation processes are necessary in order to properly understand those cell culture systems, which is the underlying basis for any purpose definition.

4.3 Applicability of microfluidic cell culture

Although hepatocytes cultured under flow conditions have only been initially investigated (section 3.4), some evidence is given that medium flow enhances the expression of DMETs, which is in agreement with other studies (Vinci et *al.*, 2011; Rennert et *al.*, 2015). Flow conditions introduce mechanical stimuli by shear force as well as molecular stimuli through the continuous supply of nutrients and removal of waste products, which impact cell signaling. The QV system used in this study is, due to the cell culture format and the need of an external pump, not applicable to higher throughput and initially showed higher metabolic capacity, but only three antigens were tested which do not allow an overall statement of the usefulness and possible applications of this system. However, the possibilities to introduce flow to cell culture are manifold, therefore the applicability of (micro)fluidic approaches in general is discussed in the following.

Even though hepatocytes are protected from flow induced shear stress by the endothelial fenestration in their native sinusoidal microenvironment, flow causes gradients of gases such as oxygen, nutrients and hormones, which have been shown to lead to zonation or differential functions in hepatocytes across the length of the sinusoid (Jungermann and Kietzmann, 1996). DILI can thus manifest with a zonal pattern dependent on the mechanism of action of a drug and its metabolism by specific isoenzymes within hepatocytes. The QV system used here introduces a pump-driven flow of culture media to monolayer cultures,

which resulted in a higher expression of some DMEs compared to both 2D and 3D spheroids over a cultivation period of 14 days (section 3.4). In addition to the mechanic stimuli that are introduced by medium flow, it has been postulated that flow can allow better nutrient exchange and removal of waste products, which may lead to higher hepatophysiologic functions compared to static cultures. Novik et *al.* (2010) observed higher rates of drug metabolite production in hepatocyte cultures subjected to flow in comparison to static cultures, which is further confirming the enhanced CYP expression observed in the QV model. Although enhanced expression of CYP1A2, 3A4 and NAT 1/2 was clearly detectable under flow conditions in comparison to both 2D and 3D, the applicability of the QV system remains questionable as it is of low throughput, requires high cell numbers and the need of an external pump. Moreover, the high media volume that is required in this system does not allow any metabolite profiling due to high dilution factors. Nevertheless, shear stress and medium flow have beneficial impact on hepatocyte physiology and recent advances of microscaled approaches offer several possibilities for DILI prediction *in vitro*. When downscaling the media to cell ration in microfluidic systems, very low media volumes can be used which then allow the analysis of metabolites and additionally, zonal hepatotoxicity patterns may be detectable. For example, a bioreactor plate with oxygen gradients has been used to introduce a zonal pattern of CYP450s in rat hepatocytes, which led to a zonal pattern of acetaminophen toxicity, particularly in low oxygen regions where CYP450 enzymes were expressed at higher levels than in regions with higher oxygen concentrations (Allen and

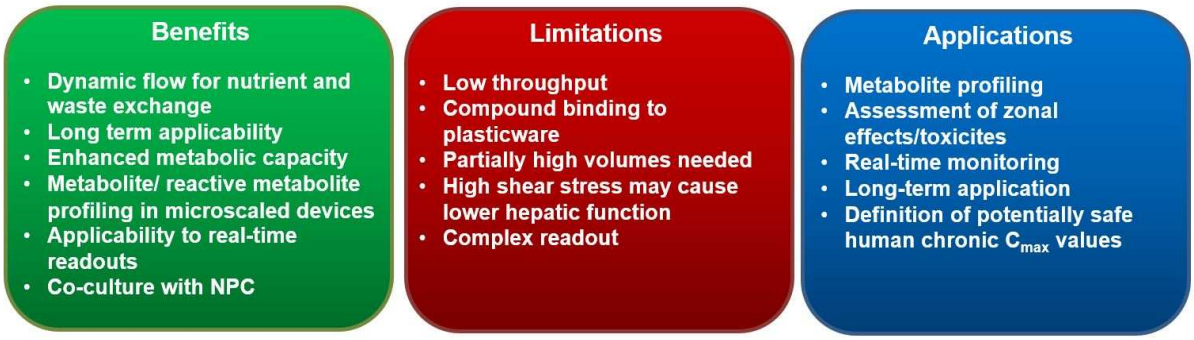

Figure 4.3: Summary of benefits, limitations and applications of hepatic microfluidic systems in early drug development. The dynamic flow enables an improved nutrient and metabolite exchange, resulting in longevity and higher metabolic capacity compared to static conditions. Depending on the device, the assessment of zonal hepatotoxicities, real time effects and the identification of potentially relevant metabolites may be possible. Nevertheless, the diversity of microfluidic approaches is manifold, thus further, platform-specific investigations are needed to validate the usefulness of a certain system within the developmental pipeline. NPC = non-parenchymal cells; Cmax = peak plasma concentration

Bhatia, 2003; Allen, Khetani and Bhatia, 2005). In addition to perfusion of culture medium, microfluidic models can also be utilized to control the arrangement of cells to yield a degree of microarchitecture with physiological relevance. For example, Kobayashi et *al.* (2013) used microfluidic devices to coculture HepG2 and Swiss 3T3 fibroblasts in a stripe-patterned

hydrogel, that enabled control for the formation of rod-like organoids inside the hydrogel. In another approach, HepG2 cells were mixed with a hydrogel that imitates extracellular matrix (ECM) and the mixture was then loaded into parallel channels of a microfluidic device. This model showed a greater sensitivity to ethyl alcohol-mediated effects in comparison to monolayers (Skardal et *al.*, 2015). Ma et *al.* (2016) used a microfluidics-based method to generate a 3D liver lobule-like microtissue consisting of HepG2 and immortal human endothelial cell line to mimic the presence of liver endothelial cells. In this configuration, HepG2 cells were able to metabolize acetaminophen, isoniazid and rifampicin.

Microfluidic devices are inherently of low throughput and are more difficult to set up and handle relative to standard multiwell plates commonly used in industry. Therefore, the incorporation of real-time monitoring of toxicity biomarkers in microfluidic devices can not only aid in ease of use, but also provide a more rapid assessment of drug effects in comparison to conventional assays. For instance, 3D aggregates of HepG2/C3A cells in a liver-on-a-chip device were exposed to rotenone and troglitazone for 24 hours (Bavli et *al.*, 2016). Real-time assessment of mitochondrial function and glucose metabolism was performed and oxygen uptake dropped within the first minutes upon drug exposure while the metabolic shift from oxidative phosphorylation to glycolysis was detected several hours later. Vernetti et *al.* (2016) co-cultured PHH, endothelial cells, monocytes and hepatic stellate cells in a continuously perfused device and the model was more sensitive when exposed to troglitazone, nimesulide and trovafloxacin. Moreover, susceptibility to trovafloxacin was further increased when cultures were coexposed to lipopolysaccharide (LPS) and the model also indicated fibrotic activation by an increase of stellate cell migration and expression of ECM components in response to metothrexate. All the aforementioned examples give evidence that multicellular cultures can greatly improve the outcome of more complex DILI events by allowing the cross-talk between hepatocytes and various NPCs that is necessary to elicit physiologically relevant responses.

4.4 Future perspectives

Drug-induced liver injury is a serious global health burden and the many late stage attritions and post-marketing withdrawals emphasize that current preclinical *in vitro* and *in vivo* test strategies are insufficient to fully predict and understand clinical outcomes (Olson et *al.*, 2000). Furthermore, the idiosyncratic nature of many DILI cases in the clinic is challenging the preclinical drug development even further (Kaplowitz, 2005). While the development of hepatic *in vitro* models was initiated many decades ago with the isolation and culture of PHH, the rapid functional decline of primary cells outside their native microenvironment substantially limits the prediction of human DILI (Xu et *al.*, 2008; Khetani and Bhatia, 2008). Additionally, the development of cell lines, which are predominantly obtained from cancerous

tissue, enables screening approaches on the one hand but suffer from poor metabolic capacity on the other hand, which limits their applicability for more physiologically relevant questions. In the last decade, many efforts have been made towards improved *in vitro* tools that allow more complex cell culture conditions leading to stable hepatophysiologic functions over several weeks. Over many years of research, the field of engineered liver models was able to realize several important considerations in the design of such models: Hepatic cell models can be functionally stabilized for weeks without the necessity for an exact emulation of the microarchitecture or composition of the liver (i.e. peripheral cholangiocytes in HepaRG spheroids, co-cultures of human hepatic cells with rodent fibroblasts or endothelial cells etc.) (LeCluyse et *al.*, 2012). Second, exercising control over cell-cell interactions, both homotypic or heterotypic with stromal cells in either cell culture format (monolayer, spheroids, bioprinted tissues etc.) is of utmost importance when recapitulating hepatophysiologic functions. Additionally, the incorporation of multiple liver cell types at physiological ratios *in vitro* can be useful for modeling certain types of DILI such as iDILI and fibrosis where heterotypic cell-cell communication between two or more liver cell types is important. For example, activation of Kupffer cells towards an inflamed state may downregulate certain CYPs in hepatic cell models, which can subsequently modulate the toxicity of drugs that are metabolized by those enzymes (Nguyen, Ukairo and Khetani, 2015). Additionally, drugs can activate hepatic stellate cells which can redifferentiate into myofibroblasts that deposit excessive amounts of ECM and secrete cytokines, thus impacting hepatocyte functions due to the changing microenvironment (Vernetti et *al.*, 2016). The aforementioned technological developments have already and will continue to highly improve the sensitivity of human DILI detection *in vitro* and provide further insights into the underlying mechanisms of different types of DILI. However, with several models that are already commercially available (e.g. *InSphero* spheroid culture, Hμrel and Hepregen microfluidic devices or Organovo bioprinting approaches), selection criteria need to be defined in order to select appropriate models for specific phases within the drug development process. In this context, the choice of the culture model is dependent on the hypotheses being addressed and the confidence that a certain *in vitro* model has acceptable levels of sensitivity and specificity for the desired type of application. For example, hepatic cell models that recapitulate improved functionality when cultured under more sophisticated culture conditions as shown in this thesis can be used to identify unfavorable compounds very early in the drug development pipeline. These compounds can then be re-subjected to medicinal chemistry for structural modifications in order to reduce or even eliminate severe toxicity. In the absence of pharmacokinetic data for a compound, it is important to determine a safety margin using *in vitro* toxicity data and binding affinity of the compound to the respective molecular target. In later stages of drug development, 3D spheroids and/or micropatterned cocultures in multiwell plates can be used

to further probe the toxic effects of lead candidate compounds following chronic exposure. According to the 3R principle, those long-term systems can also be frontloaded to animal toxicity studies using primary hepatocytes from the respective species in order to aid the definition of appropriate dosing regimen. As a lead candidate progresses through the pipeline, organs on chip platforms could be used to determine how different tissue types interact to produce toxicity in one or more tissue types. A proposal for the potential implementation of advanced cell culture formats in early drug development as a tiered approach from simple 2D cell screenings to complex, low throughput applications is given in figure 4.4.

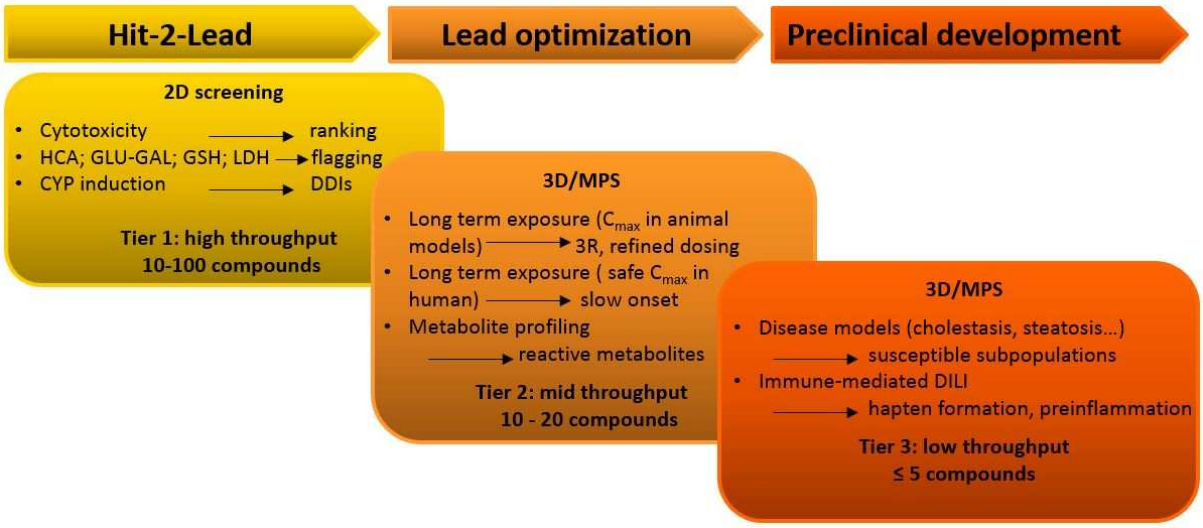

Figure 4.4: proposed application of conventional and novel *in vitro* assays in early drug development as a tiered approach. With progressing developmental stages, *in vitro* assays from simple to complex may be applied and tier 1 recapitulates simple, short term screening approaches that help to prioritize compounds according to their toxicity profile and may give indications for tier 2 experiments. Tier 2 applications increase in complexity and decrease in throughput, help to elucidate potential mechanisms (if flagged in tier 1) and may contribute to refine subsequent *in vivo* studies through the identification of hepatotoxicities upon repeated exposure. When compounds enter phase 0 development, sophisticated co-culture and disease models may be applied to define potentially susceptible subpopulations (preexisting disease) as well as a possible role of immune-mediated effects. HCA = high content aanalysis; GLU-GAL = glucose-galactose assay; GSH = Glutathione; LDH = lactate dehydrogenase; CYP = Cytochrome P-450; DDI = drug-drug interactions; Cmax = peak plasma concentration; 3R = reduce, refine, replace; MPS = microphysiological system; DILI = drug-induced liver injury).

If a low-throughput but highly complex model was used in the early stages of drug development, this may lead to bottlenecks in testing compound series in multiple concentrations. Thus, the needs for throughput and cost should be balanced with the sensitivity/specificity of the culture model applied. Even with the need for such a balance, the abovementioned iterative use of progressively more complex human liver models still provides a significantly faster and cheaper tiered testing strategy than afforded by the slow and sometimes misleading animal testing. Certainly, the expectation is that the integration of physiologically relevant models will reduce attrition in clinical trials, which constitute a main cost center that it takes to bring a successful drug to the market (Rawlins, 2004; Kaitin,

2010). Even with considerable progress in the development of increasingly complex human liver models, some key questions need to be addressed to move forward:

It is important to harmonize endpoints and data normalization schemes (i.e. based on cell number, protein and/or RNA levels) when analyzing functionality and stability of a certain in vitro system so that the data can be compared across laboratories using the same system and between different types of sophisticated models. Common markers such as albumin or CYP3A4 are routinely employed for the assessment of hepatophysiology, but the industrial community needs to agree on which markers are appropriate for which application and how to demonstrate the phenotype of other hepatic cell types.

It is important to compare gene expression profiles and functions of hepatocytes or hepatocyte-like cells in the different culture formats over time in order to determine the extent to which each culture format is impacting the expression signature of a certain cell model. In the case of PHH, it would be highly beneficial to compare the complex culture formats to fresh tissue or freshly isolated cell counterparts prior to plating from the same donors to determine deviations or similarities from the in vivo like phenotype and to elucidate pathways that are more affected by a certain culture configuration than others.

A proper validation across laboratories using many model hepatotoxicants and non-hepatotoxicants is of utmost importance in order to define the exact purpose of each system on the one hand and both the sensitivity and specificity each system is able to deliver within this purpose on the other hand.

In the end, any *in vitro* liver culture, independent from the culture format *per se*, is unlikely to mimic the *in vivo* situation perfectly, but the degree to which each system is able to will determine its usefulness for testing specific hypotheses in drug development. The overall advantage would be to reach a consensus as to which biomarkers are useful for validating the specific use of a certain platform for predicting a certain DILI outcome. Typically, endpoints such as resazurin, albumin secretion or lactate dehydrogenase release (LDH) can be used to assess hepatic injury nondestructively over time in the same culture. It has been shown that a combination of these endpoints in stable PHH cultures can provide approximately 70% sensitivity for the identification of drugs from several different drug classes as “toxic” (Khetani, Kanchagar and Ukairo et *al.*, 2013). High content approaches provide additional endpoints such as MMP[8], ROS[9] formation, phospholipidosis or lipid accumulation to better elucidate the mechanisms underlying DILI, thus aiding to flag possible liabilities of compounds or compound series in early developmental stages (Persson et *al.*, 2013; Xu et *al.*, 2008). Furthermore, -omics approaches can be used to provide indications of various molecular pathways that are affected by drug treatment prior to overt cell injury. However, which endpoints and data analysis strategies represents a reliable set for

[8] Mitochondrial membrane potential

[9] Reactive oxygen species

hepatotoxicity prediction in complex models during early drug development is not yet defined. By including more liver cell types in hepatic *in vitro* systems, a consensus also needs to be defined on cell-type specific endpoints that are important for the prediction of DILI forms in which heterotypic cell-cell communication plays an essential role.

Several studies have shown that *in vitro* systems can detect certain so-called “idiosyncratic” toxins such as troglitazone and diclofenac following extended dosing regimen (e.g. viability in PHH spheroids, section 3.3) or zafirlukast and clozapine using cellular stress markers (Xu et *al.*, 2008; O´Brien et *al.*, 2006), potentially because hepatic stress resembles the first step in the cascade of mechanisms that cause overt liver injury in specific patients with one or more genetic (e.g. DMET polymorphisms) and environmental (e.g. coadministered drugs) factors. However, it is currently not possible to predict which specific individuals will go on to adapt to cell stress and which individuals will develop severe DILI by using *in vitro* approaches. The creation of patient-derived cell models may be essential to fully understand those interindividual variations in DILI outcomes due to those factors. In this context, the use of *in vitro* models that emulate different diseased backgrounds such as steatosis, cholestasis or preinflammation could display the first step to provide information on patient-specific DILI.

Conclusively, the achievement of a productive drug discovery pipeline and addressing undesirable levels of safety-related, late stage attrition or withdrawal deserves continued efforts and resources to further develop predictive *in vitro* test systems for the hepatotoxic potential of NCEs will remain an essential part of this process. There is and obvious need for i) test systems with levels of sufficient sensitivity and specificity to detect compounds with the potential to induce moderate and low-level hepatotoxicities following prolonged exposure, ii) the definition of appropriate endpoints and data analysis strategies to obtain the highest possible predictive value of a certain model, and iii) a clear validation of existing systems robustly evaluated for performance. In early screenings, a stable cell phenotype permits consistent readouts which ensures that test systems are reproducibly applied within and across chemical series prior to preclinical candidate selection. Improvements in robustness and characterization of *in vitro* models are necessary alongside an in-depth mechanistic understanding and the identification of relevant biomarkers to define chemical risks and to use these for an accurate extrapolation to humans. The development and benchmarking of novel test systems for the risk assessment of drug candidates requires the selection of well-studied compounds which can be used as reference chemicals to validate readouts properly. Furthermore, it is important to avoid the development of systems that do not clearly outperform over the simplest functional test systems for risk assessment. In this thesis, PHH spheroids were shown to clearly outperform over monolayer culture in terms of stable DMET expression for several weeks, which subsequently enables long-term testing approaches that have shown a clear approximation of EC_{50} values towards clinically relevant plasma

concentrations, thus emphasizing the potential of this cell culture system to substantially narrow the gap between *in vitro* short-term and *in vivo* repeated-dose studies.

References

Allen JW and Bhatia, SN 2003: Formation of steady-state oxygen gradients in vitro: Application to liver zonation**.** Biotechnology and Bioengineering, Volume 82, Issue 3, pp 253–262

Allen JW, Khetani, SR and Bhatia, SN 2004**:** In Vitro Zonation and Toxicity in a Hepatocyte Bioreactor. *Toxicological Sciences*, Volume 84, Issue 1, pp 110–119

Alvarez-Sanchez R, Montavon F, HartungT, and Pähler A, 2006: Thiazolidinedione Bioactivation: A Comparison of the Bioactivation Potentials of Troglitazone, Rosiglitazone, and Pioglitazone Using Stable Isotope-Labeled Analogues and Liquid Chromatography Tandem Mass Spectrometry. *Chem. Res. Toxicol.*, Volume *19, Issue 9*, pp 1106–1116

Anderson N and Borlak J, 2006: Drug-induced phospholipidosis. FEBS letters, Volume 580, Issue 23, pp 5533–5540

Aninat C, A. Piton, D. Glaise, T. Le Charpentier, S. Langouët, F. Morel, C. Guguen-Guillouzo, A. Guillouzo: Expression of cytochromes P450, conjugating enzymes and nuclear receptors in human hepatoma HepaRG cells. Drug Metabolism and Disposition, 34 (2005), pp. 75-83

Antherieu S, Chesne C, Li R, Camus S, Lahoz A, Picazo L, Turpeinen M, Tolonen A, Uusitalo J, Guguen-Guillouzo C and Guillouzo A, 2009: stable expression, activity and inducibility of cytochromes p450 in differentiated HepaRG cells. Drug Metabolism and Disposition, Volume 46, Issue 4, pp 516-25

Antoine D. J. Williams D. P. Park B. K: Understanding the role of reactive metabolites in drug-induced hepatotoxicity: State of the science. Expert Opin. Drug Metab. Toxicol. Volume 4, pp 1415-1427

Armstrong RN, 1987: Enzyme catalyzed detoxication reactions: mechanisms and stereochemistry. CRC Crit. Rev. Biochem., 22 (1987), pp. 39-87

Arrowsmith J, 2011a/b: Phase III and submission failures: 2007-2010. Nature Reviews Drug Discovery volume 10, Issue 2, p 87

Asahina K, Tsai SY, Peng L, Ishii M, Maxson REJ, Sucov HM, Tsukamoto H, 2009. Mesenchymal origin of hepatic stellate cells, submesothelial cells, and perivascular mesenchymal cells during mouse liver development. Hepatology, Volume 49, Issue 3, pp 998–1011

Aubert J, Karima Begriche, Matthieu Delannoy, Isabelle Morel, Julie Pajaud, Catherine Ribault, Sylvie Lepage, Mitchell R. McGill, Catherine Lucas-Clerc, Bruno Turlin, Marie-Anne Robin, Hartmut Jaeschke and Bernard Fromenty: Differences in Early Acetaminophen Hepatotoxicity between Obese *ob/ob* and *db/db* Mice. Journal of Pharmacology and Experimental Therapeutics September 2012, 342 (3) 676-687

Baker BM and Chen CS, 2012: Deconstructing the third dimension – how 3D culture microenvironments alter cellular cues. J Cell Sci 2012 Volume 125, pp.: 3015-3024

Bale SS, Vernetti L and Senutovich N., 2014: *In vitro* platforms for evaluating liver toxicity. Experimental Biology and Medicine, Volume 239, Issue 9, pp. 1180-91

Baughman TM, Graham RA, Wells-Knecht K, Silver IS, Tyler LO, Wells-Knecht M and Zhao Z, 2005: metabolic activation of pioglitazone identified from rat and human liver microsomes and freshly isolated hepatocytes. Drug Metabolism and Disposition, Volume 33, Issue 6, pp 733-738

Bao G and Suresh S, 2003: Cell and molecular mechanics of biological materials. *Nature Materials* Volume 2, pp 715–725

Bavli D, Sebastian Prill, Elishai Ezra, Gahl Levy, Merav Cohen, Mathieu Vinken, Jan Vanfleteren, Magnus Jaeger and Yaakov Nahmias., 2016: Real-time monitoring of metabolic function in liver-on-chip microdevices tracks the dynamics of mitochondrial dysfunction. Biol. Sci. Volume 113, Issue 16, pp. 2231-2240

Bell CC, Hendriks DFG, Moro SML, Ellis E, Walsh J, Renblom A, Fredriksson-Puigvert L, Dankers ACA, Jacobs F, Snoeys J, Sison-Young RL, Jenkins RE, Nordling A et al., 2016: Characterization of primary human hepatocyte spheroids as a model system for drug-induced liver injury, liver function and disease. *Scientific Reports,* Volume 6, pp.

Bell CC, Lauschke VM, Vorrink SU, Palmgren H, Duffin R, Andersson TB and Ingelman-Sundberg M, 2017: Transcriptional, Functional, and Mechanistic Comparisons of Stem Cell–Derived Hepatocytes, HepaRG Cells, and Three-Dimensional Human Hepatocyte Spheroids as Predictive In Vitro Systems for Drug-Induced Liver Injury. Drug Metabolism and Disposition Volume 45, Issue 4, pp 419-429

Benbow JW, Aubrecht J, Banker MJ, Nettleton D and Aleo MD, 2010: Predicting safety toleration of pharmaceutical chemical leads: Cytotoxicity correlations to exploratory toxicity studies. Toxicology letters, Volume 197, Issue 3, pp. 175-182

Berson A, Descatoire V, Sutton A, Fau D, Maulny B, Vadrot N, Feldmann G, Berthon B, Tordjmann T and Pessayre D, 2001: Toxicity of Alpidem, a Peripheral Benzodiazepine Receptor Ligand, but Not Zolpidem, in Rat Hepatocytes: Role of Mitochondrial Permeability Transition and Metabolic Activation. Journal of Pharmacology and Experimental Therapeutics November 2001, Volume 299, Issue 2, pp 793-800

Bird TG, Lorenzini S and Forbes SJ, 2008: Activation of stem cells in hepatic diseases. Cell and Tissue Research, Volume 331, pp 283-300

Black M, 1984: Acetaminophen toxicity. Ann Rev Med, Volume 35, pp 577-93

Atienzar FA, Eric A. Blomme, Minjun Chen, Philip Hewitt, J. Gerry Kenna, Gilles Labbe, Frederic Moulin, Francois Pognan, Adrian B. Roth, Laura Suter-Dick, Okechukwu Ukairo, Richard J. Weaver, Yvonne Will, and Donna M. Dambach, 2016: Key Challenges and Opportunities Associated with the Use of In Vitro Models to Detect Human DILI: Integrated Risk Assessment and Mitigation Plans. BioMed Research International Volume 2016, pp.

Borzelleca JF, 2000: Paracelsus: Herald of Modern Toxicology. *Toxicological Sciences*, Volume 53, Issue 1, pp 2–4

Braet F and Wisse E, 2002: Structural and functional aspects of liver sinusoidal endothelial cell fenestrae: a review. *Comparative Hepatology*, Volume 1

Bhushan A, Senutovitch N, Bale SS, McCarty WJ, Hegde M, Jindal R, Golberg I, Usta OB, Yarmush ML, Vernetti L, Gough A, Bakan A, Shun TY, Biasio R and D Lansing Taylor, 2013: Towards a three-dimensional microfluidic liver platform for predicting drug efficacy and toxicity in humans. Stem Cell Research & Therapy Volume 4 (Suppl 1), p 16

Burkard A, Dähn C, Heinz S, Zutavern A, Sonntag-Buck V, Maltman D, Przyborski S, J. Hewitt NJ and Braspenning J, 2012: Generation of proliferating human hepatocytes using upcyte® technology: characterisation and applications in induction and cytotoxicity assays. Xenobiotica Volume 42, Issue 10, pp 939-56

Cerec V, Glaise D, Garnier D, Morosan S, Turlin B, Drenon B, Gripon P, Kremsdorf T, Guguen-Guillouzo C and Corlu A, 2007: Transdifferentiation of hepatocyte-like cells from the human hepatoma HepaRG cell line through bipotent progenitor. Hepatology Volume 45, Issue 4, pp 957–67

Chatterjee S, Richert L, Augustijns P and Annaert P, 2014: Hepatocyte-based in vitro model for assessment of drug-induced cholestasis. Toxicology and Applied Pharmacology Volume 274, Issue 1, 1 January 2014, Pages 124-136

Cho CH, Park J, Nagrath D, Tilles AW, Berthiaume F, Toner M and Yarmoush ML, 2007: Oxygen uptake rates and liver-specific functions of hepatocyte and 3T3 fibroblast co-cultures. Biotechnology and Bioengineering Volume 97, Issue 1, pp 188–199

Chu V, Heidi J. Einolf, Raymond Evers, Gondi Kumar, David Moore, Sharon Ripp, Jose Silva, Vikram Sinha, Michael Sinz and Andrej Skerjanec, 2009: In Vitro and in Vivo Induction of Cytochrome P450: A Survey of the Current Practices and Recommendations: A Pharmaceutical Research and Manufacturers of America Perspective. Drug Metabolism and Disposition July 2009, 37 (7) 1339-1354

Clement B and Katrin Lopian, 2003: Characterization of in Vitro Biotransformation of New, Orally Active, Direct Thrombin Inhibitor Ximelagatran, an Amidoxime and Ester Prodrug. Drug Metabolism and Disposition May 2003, 31 (5) 645-651

Cogger VC, McNerney GP, Nyunt T, DeLeve LD, McCourt P, Smedsrod B, Le Conteur DG and Huser TR, 2010: Three-dimensional structured illumination microscopy of liver sinusoidal endothelial cell fenestrations. J Struct Biol, Volume 171, Issue 3, pp 382-388.

Copple IM, Lister A, Obeng AD, Kitteringham NR, Jenkins RE, Layfield R, Foster BJ, Goldring CE and Park BK, 2010: Physical and Functional Interaction of Sequestosome 1 with Keap1 Regulates the Keap1-Nrf2 Cell Defense Pathway. J Biol Chem, Volume 285, pp 16782-88.

Court MH, Hao Q, Krishnaswamy S, Bekaii-Saab T, Al-Rohaimi A, von Moltke LL et al. (2004). UDP-Glucuronosyltransferase (UGT) 2B15 Pharmacogenetics: UGT2B15 D85Y Genotype and Gender Are Major Determinants of Oxazepam Glucuronidation by Human Liver J Pharmacol Exp Ther 310 Issue 2: 656–665

Curcio E, Salerno S, Barbieri G, De Bartolo L, Drioli E and Bader A, 2007: Mass transfer and metabolic reactions in hepatocyte spheroids cultured in rotating wall gas-permeable membrane system. Biomaterials, Volume 28, Issue 36, pp 5487-97

Daly AK, Donaldson PT, Bhatnagar P, Shen Y, Pe'er I, Floratos A, Daly MJ, Goldstein DB, John S, Nelson MR, Graham J, Park BK, Dillon JF, Bernal W, Cordell HJ, M, Aithal GP and Day CP, 2009: HLA-B*5701 genotype is a major determinant of drug-induced liver injury due to flucloxacillin. Nature Genetics Volume 41, pp 816–819

Darnell M, Karlsson JE, Owen A, Hidalgo IJ, Li J, Zhang W and Andersson TB, 2010: Investigation of the Involvement of P-Glycoprotein and Multidrug Resistance-Associated Protein 2 in the Efflux of Ximelagatran and Its Metabolites by Using Short Hairpin RNA Knockdown in Caco-2 Cells. Drug Metabolism and Disposition, Volume 38, Issue 3, pp 491-97

Darnell M, Ulvestad M, Ellis E, Weidolf L and Andersson TB, 2012: In Vitro Evaluation of Major In Vivo Drug Metabolic Pathways Using Primary Human Hepatocytes and HepaRG Cells in Suspension and a Dynamic Three-Dimensional Bioreactor System. Journal of Pharmacology and Experimental Therapeutics, Volume 343, Issue 1, pp 134-44

Deaciuc IV, D´Souza NB, Fortunato F, Hill DB, Sarphie TB and McClain CJ, 2001: Alcohol-induced sinusoidal endothelial cell dysfunction in the mouse is associated with exacerbated liver apoptosis and can be reversed by caspase inhibition. Hepatology Research Volume 19, Issue 1, 1 January 2001, Pages 85-97

DeLeve LD, Wang X, Hu L, Mc Cuskey MR and McCuskey SR, 2004: Rat liver sinusoidal endothelial cell phenotype is maintained by paracrine and autocrine regulation. Am J Phys Volume 287 Issue 4, pp G757-G763

DeLeve LD, 2007: Hepatic Microvasculature in Liver Injury. Semin Liver Dis Volume 27 Issue 4, pp 390-400

Dingemanse J and van Giersbergen PLM, 2004: Clinical Pharmacology of Bosentan, a Dual Endothelin Receptor Antagonist. Clin Pharmacokinetics, Volume 43, Issue 15, pp 1089-1115.
Donnelly PJ, Robin M. Walker, William J. Racz, 1994: Inhibition of mitochondrial respiration in vivo is an early event in acetaminophen-induced hepatotoxicity. Arch Toxicol 68: 110
Dykens JA and Will Y, 2007: The significance of mitochondrial toxicity testing in drug development. Drug Discovery Today Volume 12, Issues 17–18, September 2007, Pages 777-785

Eakins J, Bauch C, Woodhouse H, Park B, Bevan S and DilworthPaul C, 2016: A combined in vitro approach to improve the prediction of mitochondrial toxicants. Toxicology in Vitro, Volume 34, pp 161-170

Elaut G, Henkens T, Papeley P, Snykers S, Vinken M, Vanhaecke T and Rogiers V, 2006: Molecular Mechanisms Underlying the Dedifferentiation Process of Isolated Hepatocytes and Their Cultures. Curr Drug Metab Volume 7, Issue 6, pp 629-60

Elsherbiny ME, El-Kadi AOS and Brocks DR, 2008: the metabolism of amiodarone by various cyp isoenzymes of human and rat, and the inhibitory influence of ketoconazole. j Pharm Sci, Volume 11, Issue 1, PP 147-59.

EMA, 2012: Guidelines on the investigation of drug interaction. www.ema.europa.eu

Fava G, Glaser S, Francis H and Alpini G, 2005: The Immunophysiology of Biliary Epithelium. Semin Liver Dis, Volume 25, Issue 3, pp 251-64

FDA, 2017: In vitro metabolism and transporter mediated drug-drug interaction studies. Guidance for Industry. www.fda.gov

Ferri D, Moro L, Mastrodonato M, Capuano F, Marra E, Liquori GE and Greco M, 2005: Ultrastructural zonal heterogeneity of hepatocytes and mitochondria within the hepatic acinus during liver regeneration after partial hepatectomy. Biology of the Cell Volume 97, Issue 4, pp 277–288

Freund JB, Goetz JG, Hill KL and Vermot J, 2012: Fluid flows and forces in development: functions, features and biophysical principles. Development, Volume 139, pp 1229-1245

Friedmann SL, 2008: Hepatic Stellate Cells: Protean, Multifunctional, and Enigmatic Cells of the Liver. Phys Rev, Volume 88, Issue 1, pp 127-72

Fromenty B, 2013: Bridging the gap between old and new concepts in drug-induced liver injury. Clinics and Research in Hepatology and Gastroenterology, Volume 37, Issue 1, pp 6-9
Fromenty B and Pessayre D, 1995: Inhibition of mitochondrial beta-oxidation as a mechanism of hepatotoxicity. Pharmacology & Therapeutics, Volume 67, Issue 1, pp 101-54.

Funk C, Pantze M, Jehle L, Ponelle C, Scheuermann G, Lazendic M and Gasser R, 2001: Troglitazone-induced intrahepatic cholestasis by an interference with the hepatobiliary export of bile acids in male and female rats. Correlation with the gender difference in troglitazone sulfate formation and the inhibition of the canalicular bile salt export pump (Bsep) by troglitazone and troglitazone sulfate. Toxicology, Volume 167, Issue 1, pp 83-98

Gale EAM, 2001: Lessons from the glitazones. The Lancet, Volume Volume 357, Issue 9271,, pp 1870-75

Ganan-Gomez I, Wie Y, Yang H, Boyano-Adanez MC, Garcia-Manero G., 2013: Oncogenic functions of the transcription factor Nrf2. Free Radical Biol Med, Volume 65, pp 750-64.

Garside H, Marcoe KF, Chesnut-Speelman J, Foster AJ, Muthas D, Kenna JG, Warrior U, Bowes J and Baumgartner J, 2014: Evaluation of the use of imaging parameters for the detection of compound-induced hepatotoxicity in 384-well cultures of HepG2 cells and cryopreserved primary human hepatocytes. Toxicology in Vitro Volume 28, Issue 2, Pages 171-181

Gaudio E, Carpino G, Cardinale V, Franchitto A, Onori P and Alvaro D, 2009: New insights into liver stem cells. Digestive and Liver Disease, Volume 41, Issue 7, pp 455-62

Gebhardt R, 1992: Metabolic zonation of the liver: Regulation and implications for liver function. Pharmacology and Therapeutics, Volume 53, Issue 3, pp 275-354

Gerbal-Chaloin S, Jean-Marc Pascussi, Lydiane Pichard-Garcia, Martine Daujat, Felix Waechter, Jean-Michel Fabre, Nicolas Carrère and Patrick Maurel., 2001: Induction of CYP2C Genes in Human Hepatocytes in Primary Culture. Drug Metabolism and Disposition March 2001, 29 (3) 242-251

Gerets HHJ, Tilmant K, Gerin B, Chanteux H, Depelchin BO, Dhalluin S and Atienzar FA, 2012: Characterization of primary human hepatocytes, HepG2 cells, and HepaRG cells at the mRNA level and CYP activity in response to inducers and their predictivity for the detection of human hepatotoxins. Cell Biol Toxicol, Volume 28, Issue 2, pp 69–87

Glaser S, Francis H, DeMorrow S, LeSage G, Fava G, Marzioni M, Venter J, and Alpini G, 2009: Heterogeneity of the intrahepatic biliary epithelium. W J Gastroenterol, Volume 12, Issue 22, pp 3523-36

Godoy P, Nicola J. Hewitt, Ute Albrecht, Melvin E. Andersen, Nariman Ansari, Sudin Bhattacharya, Johannes Georg Bode, Jennifer Bolleyn, Christoph Borner, Jan Böttger, Albert Braeuning, Robert A. Budinsky, Britta Burkhardt, Neil R. Cameron, Giovanni Camussi, Chong-Su Cho, Yun-Jaie Choi, J. Craig Rowlands, Uta Dahmen, Georg Damm, Olaf Dirsch, María Teresa Donato, Jian Dong, Steven Dooley, Dirk Drasdo, Rowena Eakins, Karine Sá Ferreira, Valentina Fonsato, Joanna Fraczek, Rolf Gebhardt, Andrew Gibson, Matthias Glanemann, et al., 2013: Recent advances in 2D and 3D in vitro systems using primary hepatocytes, alternative hepatocyte sources and non-parenchymal liver cells and their use in investigating mechanisms of hepatotoxicity, cell signaling and ADME. Arch Toxicol Volume 87, Issue 8, pp 1315–1530.

Goldstein JA and Faletto MB, 1993: Advances in mechanisms of activation and deactivation of environmental chemicals. Environ Health Perspect. Volume 100, pp 169–176.

Govindarajan R, Endres CJ, Whittington D, LeCluyse E, Pastor-Anglada M, Tse CM and Unadkat JD, 2008: Expression and hepatobiliary transport characteristics of the concentrative and equilibrative nucleoside transporters in sandwich-cultured human hepatocytes. Am J Physiol, Volume 295, Issue 3, pp G570-G580

Guengerich FP, Liebler DC and Reed DL, 1985: Enzymatic activation of chemicals to toxic metabolites. Critical Reviews in Toxicology, Volume 14, Issue 3, pp. 259-307.

Guillouzo A, Corlu A, Aninat C, Glaise D, Morel F and Guguen-Guillouzo C, 2007: The human hepatoma HepaRG cells: A highly differentiated model for studies of liver metabolism and toxicity of xenobiotics. Chemico-Biological Interactions Volume 168, Issue 1, 20 May 2007, Pages 66-73

Guillouzo A and Guguen-Guillouzo C, 2008: Evolving concepts in liver tissue modeling and implications for *in vitro* toxicology. Exp Opin Drug Met Tox, Volume 4, Issue 10, pp. 1279-94.

Gunness P, Müller D, Shevchenko V, Heinzle E, Ingelman-Sundberg M and Noor F, 2013: 3D Organotypic Cultures of Human HepaRG Cells: A Tool for **In Vitro** Toxicity Studies. Toxicological Sciences, Volume 133, Issue 1, pp 67–78

Hailey JR, James B. Nold, Roger H. Brown, John M. Cullen, Julie C. Holder, Holly L. Jordan, Daniela Ennulat, Richard T. Miller ,2014: Biliary Proliferative Lesions in the Sprague-Dawley Rat Adverse/Non-adverse Volume: 42, Issue 5, pp 844-854

Halliwell et *al*., 1997: Antioxidants and human disease: A general introduction. Nutrition reviews Volume 55, Issue 1, pp 44-9; discussion pp 49-52

Haouzi D, Lekehal M, Moreau A, Moulis C, Feldman G, Robin MA, Letteron P, Fau D and Pessayre D, 2000: Cytochrome P450–generated reactive metabolites cause mitochondrial permeability transition, caspase activation, and apoptosis in rat hepatocytes. Hepatology Volume 32, Issue 2, pp 303–311

Hamilton GA, Jolley SL, Gilbert D, Coon JD, Barros S and LeCluyse EL, 2001: Regulation of cell morphology and cytochrome P450 expression in human hepatocytes by extracellular matrix and cell-cell interactions. *Cell and Tissue Research* Volume 306, Issue 1, pp 85–99

Han Z, Miwa Y, Obikane H, Mitsumata M, Takahashi-Yanaga F, Morimoto S and Sasaguri T, 2008. Aryl hydrocarbon receptor mediates laminar fluid shear stress-induced CYP1A1 activation and cell cycle arrest in vascular endothelial cells. Cardiovasc. Res. 77, 809–818.

Hatano E, Bradham CA, Stark A, Iimuro Y, Lemasters JJ and Brenner DA, 2000: The Mitochondrial Permeability Transition Augments Fas-induced Apoptosis in Mouse Hepatocytes. The Journal of Biological Chemistry Volume 275, pp 11814-11823.

Hein DW, 2006: *N*-acetyltransferase 2 genetic polymorphism: Effects of carcinogen and haplotype on urinary bladder cancer risk. Oncogene Volume 25, Issue 11, pp. 1649-58

Hendriks DFG, Fredriksson-Puigvert L, Messner S, Moritz W and Ingelman-Sundberg M, 2016: Hepatic 3D soheroid models for the detection and study of compounds with cholestatic liability. Scientific Reports Volume 6, article number 35434

Hewitt NJ, lloyd S, Hayden M, Butler R, Sakai Y, Springer R, Fackett A and Li AP 2002: Correlation between troglitazone cytotoxicity and drug metabolic enzyme activities in cryopreserved human hepatocytes. Chemico-Biological Interactions Volume 142, Issues 1–2, pp 73-82

Hewitt NJ and Li AP, 2015: Cryopreservation of hepatocytes. Protocols in In Vitro Hepatocyte Research Volume 1250, pp 13-26

Hewitt NJ and Hewitt P, 2004: Phase I and II enzyme characterization of two sources of HepG2 cell lines. Xenobiotica, Volume 34, issue 3, pp 243-56.

Hewitt NJ, LeCluyse EL and Ferguson SS, 2007: Induction of hepatic cytochrome P450 enzymes: methods, mechanisms, recommendations, and *in vitro–in vivo* correlations. Xenobiotica, Volume 37, Issue 10-11, pp. 1196-1224.

Yuriko Higuchi, Shigeru Kawakami, Fumiyoshi Yamashita and Mitsuru Hashida, 2007: The potential role of fucosylated cationic liposome/NFκB decoy complexes in the treatment of cytokine-related liver disease. Biomaterials Volume 28, Issue 3, pp 532-539

Hoekstra R, Nibourg GAA, van der Hoeven TA, Plomer G, Seppen J, Ackermans MT, Camus S, Kulik W, van Gulik TM, Elferink RPO and Chamuleau RAFM et *al.*, 2012: Phase 1 and Phase 2 Drug Metabolism and Bile Acid Production of HepaRG Cells in a Bioartificial Liver in Absence of Dimethyl Sulfoxide. Drug Metabolism and Disposition Volume 41, Issue 3, pp 562-567

Honkakoshi P, Moore R, Washburn K and Negishi M (1998) Activation by diverse xenochemicals of the 51-base pair phenobarbital-responsive enhancer module in the CYP2B10 gene. *Mol Pharmacol* Volume 53, pp 597-601.

Hosomi H, Tatsuki Fukami, Atsushi Iwamura, Miki Nakajima and Tsuyoshi Yokoi, 2011: Development of a Highly Sensitive Cytotoxicity Assay System for CYP3A4-Mediated Metabolic Activation. Drug Metabolism and Disposition August 2011, 39 (8) 1388-1395

Hubbard, A. L., Bartles, J. R. & Braiterman, L. T. (1985). Identification of rat hepatocyte plasma membrane proteins using monoclonal antibodies. *J. Cell Biol.* 100, 1115-1125.

Ingelman-Sundberg M, 2001: Genetic susceptibility to adverse effects of drugs and environmental toxicants. The role of the CYP family of enzymes. Mutat. Res., Volume 482, pp 11-19

Ingelman-Sundberg M, 2003: Human drug metabolising cytochrome P450 enzymes: properties and polymorphisms. Naunyn-Schmiedebergs Arcived of Pharmacology, vol 368, issue 1, pp 89-104

Jaakkola T, Laitila J, Neuvonen PJ and Backman JT, 2006: Pioglitazone is Metabolised by CYP2C8 and CYP3A4 in vitro: Potential for Interactions with CYP2C8 Inhibitors. Basic and Clinical Pharmacology and Toxicology Volume 99, Issue 1, pp 44-51

Jonathan P. Jackson, Linhou Li, Erica D. Chamberlain, Hongbing Wang and Stephen S. Ferguson, 2016: Contextualizing Hepatocyte Functionality of Cryopreserved HepaRG Cell Cultures. Drug Metabolism and Disposition September 2016, Volume 44, Issue 9, pp 1463-1479

Jaeschke H, 2007: Troglitazone Hepatotoxicity: Are We Getting Closer to Understanding Idiosyncratic Liver Injury? Toxicological Sciences, Volume 97, Issue 1, pp 1–3

Jennen DG, Magkoufopoulou C, Ketelslegers HB, van Herwijnen MH, Kleinjans JC, van Delft JH, 2010: Comparison of HepG2 and HepaRG by whole-genome gene expression analysis for the purpose of chemical hazard identification. Toxicol Sci 115:66–79

Jiang J, Wolters J, Van Breda S, et al. Development of novel tools for the in vitro investigation of drug-induced liver injury. Expert Opin Drug Metab Toxicol. 2015 Volume Issue 11, pp. 1523–1523.

Jungermann K, Kietzmann T, Freimann S and Bratke J, 1996: Regulation of the gluconeogenic phosphoenolpyruvate carboxykinase and the glycolytic aldolase A gene expression by O_2 in rat hepatocyte cultures. Involvement of hydrogen peroxide as mediator in the response to O_2. FEBS letters, Volume 388, Issue 2-3, pp 228–232.

Kalgutkar AS, Amit S, Gardner I Iain, Obach RS, Shaffer CL, Callegari E, Henne KR R, Mutlib AE, Dalvie DK, Lee JS, Nakai Y, O'Donnell JP, Boer J and Harriman, SP 2005: A Comprehensive Listing of Bioactivation Pathways of Organic Functional Groups. Current Drug Metabolism, Volume 6, Issue 3, pp. 161-225

Kaitin KI, 2010: Deconstructing the Drug Development Process: The New Face of Innovation. Clinical Pharmacology and Therapeutics Volume 87, Drug Discovery & Development, Pages 356–361

Kamalian L, Chadwick AE, Bayliss M, French NS, Monshouwer M, Snoeys J and Park BK, 2015: The utility of HepG2 cells to identify direct mitochondrial dysfunction in the absence of cell death. Toxicology in Vitro Volume 29, Issue 4, pp 732-740

Kanebratt KP and Andersson TB, 2007: Evaluation of HepaRG Cells as an *In Vitro* Model for Human Drug Metabolism Studies. Curr Drug Disp Metab Volume 36, Issue 7, pp 1444-52

Kaplowitz N, 2004: Drug-induced liver injury. Clinical Infectious Diseases, Volume 38, Issue Supplement 2, pp S44–S48

Kaplowitz N, 2005: idiosyncratic hepatotoxicity. Nature Reviews Drug Discovery Volume 4 pp 489-499

Kawai T, Izumi Takei, Yuko Oguma, Norimi Ohashi, Mikiya Tokui, Shuji Oguchi, Fuminori Katsukawa, Hiroshi Hirose, Akira Shimada, Kiyoaki Watanabe and Takao Saruta 1997: Effects of troglitazone on fat distribution in the treatment of male type 2 diabetes. Metabolism Volume 48, Issue 9, pp 1102-1107

Keisu M and Andersson TB, 2010: Drug-Induced Liver Injury in Humans: The Case of Ximelagatran. Adverse Drug Reactions, pp 407-418

Kenna JG, 2018: Integrating DILI hazards in predicting toxicity of drug candidates: Assessment and management of human risk in the pharmaceutical industry. Drug Metab Pharmacokin Volume 33, Issue 1, pp S3-S4

Khetani SR and Bhatia SN, 2008: Microscale culture of human liver cells for drug development. Nature Biotechnology Volume 26, pp 120–126

Khetani SL, Kanchagar C and Ukairo O, Moore A, Shi J, Gaffney J, Aoyama S, Rose K, Krzyzewski S, McGeehan J, Anderesen ME and LeCluyse EL et *al.*, 2013: Long-Term Stability of Primary Rat Hepatocytes in Micropatterned Cocultures. Journal of Biochemical and Molecular Toxicology, Volume 27, Issue 3, pp 204–212

Kienhuis AL, Wortelboer HM, Maas WJ, van Herwijnen M, Kleinjans JCS, van Delft JHM and Stierum JH, 2007: A sandwich-cultured rat hepatocyte system with increased metabolic

competence evaluated by gene expression profiling. Toxicology in Vitro Volume 21, Issue 5, pp 892-901

Kishida T, Tomoya Onozato, Toru Kanazawa, Satoru Tanaka, Junji Kuroda, 2012: Increase in covalent binding of 5-hydroxydiclofenac to hepatic tissues in rats co-treated with lipopolysaccharide and diclofenac: involvement in the onset of diclofenac-induced idiosyncratic hepatotoxicity. J Toxicol Sci Volume 37, Issue 6, pp 1143-1156

Klaassen CD and Aleksunes LM, 2010: Xenobiotic, Bile Acid, and Cholesterol Transporters: Function and Regulation. Pharmacological Reviews March 2010, Volume 62, Issue 1, pp 1-96

Klaassen CD and Rozman KK, 1991: Absorption, Distribution and Excretion of Toxicants. Casaretts and Doull´s Toxicology: The basic science of poisons. Chapter 5, ISBN 9780071054768

Klaassen and Watkins, 1984: Mechanisms of Bile formation, hepatic uptake and biliary excretion. Pharmacological Reviews Volume 36, Issue 1, pp 1-67

Kobayashi A, Yamakoshi K, Yajima Y and Seki M, 2013: Preparation of stripe-patterned heterogeneous hydrogel sheets using microfluidic devices for high-density coculture of hepatocytes and fibroblasts. J Biosci Bioeng Volume 116 Issue 6

Kodavanti UP and Mehendale HM, 1990: Cationic amphiphilic drugs and phospholipid storage disorder. Biochemical pharmacology, 1990, Volume 42, No. 4, pp. 327-48.

Köck K, Ferslew BC, Netterberg I, Yang K, Urban TJ, Swaan PW, Stewart PW, Brouwer KL (2014) Risk factors for development of cholestatic drug-induced liver injury: inhibition of hepatic basolateral bile acid transporters multidrug resistance-associated proteins 3 and 4. Drug Metab Dispos 42:665–674

Kola I and Landis J, 2004: Can the pharmaceutical industry reduce attrition rates? Nature Rev Drug discovery, vol 3, pp. 711-16.

Kolios G, Valatas V and Kouroumalis E, 2006: Role of Kupffer cells in the pathogenesis of liver disease. World J Gastroenterol. Volume 14 Issue 12 (Supplementary 46), pp 7413–7420

Kullack-Ublick GA., 2002: Regulation of Drug and Bile Salt Transporters in Liver and Intestine. Drug Metab Rev, Volume 35, Issue 4, pp. 305-17.

Kumar, S., Samuel, K., Subramanian, R., Braun, M.P., Stearns, R.A., Chiu, S.H.L., Evans, D.C., Baillie, T.A., 2002. Extrapolation of diclofenac clearance from in vitro microsomal metabolism data: role of acyl glucuronidation and sequential oxidative metabolism of the acyl glucuronide. J. Pharmacol. Exp. Ther. Volume 303, pp 969–978.

Lai, Y., Tse, C. M., Unadkat, J. D. (2004). Mitochondrial expression of the human equilibrative nucleoside transporter 1 (hENT1) results in enhanced mitochondrial toxicity of antiviral drugs. J Biol Chem 279:4490–4497

Laine JE, S. Auriola, M. Pasanen, R.O. Juvonen, 2009: Acetaminophen bioactivation by human cytochrome P450 enzymes and animal microsomes. Xenobiotica, Volume 39, pp. 11-21

Lambert CB, Spire C, Claude N, Gouillouzo A, 2009: Dose- and time-dependent effects of phenobarbital on gene expression profiling in human hepatoma HepaRG cells. Toxicol Appl Pharmacol Volume 234, pp 345–360

Lautala P, Ethell BT, Taskinen J and Burchell B, 2000: The Specificity of Glucuronidation of Entacapone and Tolcapone by Recombinant Human Udp-Glucuronosyltransferases. Drug Metabolism and Disposition Volume 28, Issue 11, pp 1385-1389

LeCluyse EL, Witek RP, Andersen ME and Powers MJ, 2012: Organotypic liver culture models: Meeting current challenges in toxicity testing. Crit Rev Toxicol, Volume 42, Issue 6, pp. 501-48.

Leite SB, Wilk-Zasadna I, Zaldivar JM, Airola E, Reis-Fernandez M, Mennecozzi M, Guguen-Gouillouzo C, Chesne C, Guillou C, Alves PM and Coecke S, 2012: Three-Dimensional HepaRG Model As An Attractive Tool for Toxicity Testing. Toxicological Sciences Volume 130, Issue 1, pp 106–116

Lemasters JJ, Nieminen AL, Qian T, Trost LC, Elmore SP, Nishimura Y, Crowe RA, Cascio WE, Bradham CA, Brenner DA and Herman B, 1998: The mitochondrial permeability transition in cell death: a common mechanism in necrosis, apoptosis and autophagy. BBA Bioenergetics, Volume 1366, Issues 1-2, pp 177-96.

Levine JF and Stockdale FE, 1985: Cell-cell interactions promote mammary epithelial cell differentiation. Journal of cell biology, Volume 100, Issue 5, pp-141-5
Levy R, 2015: Response to Chalassani et al. The American Journal of Gastroenterology Volume 110, p 471

Libbrecht L, De Vos R, Cassiman D, Desmet V, Aerts R, Roskams T, 2001: Hepatic progenitor cells in hepatocellular adenomas. Am J Surg Pathol 25:1388–1396

Lindros KO, 1997: Zonation of cytochrome P450 expression, drug metabolism and toxicity in liver. General Pharmacology: The Vascular System Volume 28, Issue 2, pp 191-196

Loi, CM., Young, M., Randinitis, E. 1999: Clinical Pharmacokinetics of Troglitazone. Clin Pharmacokinet Volume 37, p 91

Ma Q, L. Dong, J.P. Whitlock Jr., 2005: Transcriptional activation by the mouse Ah receptor. Interplay between multiple stimulatory and inhibitory functions. J. Biol. Chem., 270 (21) (1995), pp. 12697-12703

Madan A, Graham RA, Carroll KM, Mudra DR, Burton LA, Krueger LA, Downey AD, Czerwinski M, Forster J, Ribadeneira MD, et al, 2003: Effects of Prototypical Microsomal Enzyme Inducers on Cytochrome P450 Expression in Cultured Human Hepatocytes. Drug Metabolism and Disposition Volume 31, Issue 4, pp 421-431

Mammoto T and Ingber DE, 2010: Mechanical control of tissue and organ development. Development, Volume 137: 1407-1420

Mandal PK: Dioxin: a review of its environmental effects and its aryl hydrocarbon receptor biology. J. Comp. Physiol. B, 175 (4) (2005), pp. 221-230

Marzioni M, Glaser SS, Francis H, Phinizy JL, LeSage G and Alpini G, 2002: Functional Heterogeneity of Cholangiocytes. Semin Liver Dis Volume 22 Issue 3, pp 227-240

Marroquin L, Hynes J, Dykens J, et al. Circumventing the Crabtree effect: replacing media glucose with galactose increases susceptibility of HepG2 cells to mitochondrial toxicants. Toxicol Sci. 2007;97(2):539–547

Massart, M.A. Robin, F. Noury, A. Fautrel, P. Lettéron, A. Bado, P.A. Eliat, B. Fromenty, 2012: Pentoxifylline aggravates fatty liver in obese and diabetic ob/ob mice by increasing intestinal glucose absorption and activating hepatic lipogenesis. Br. J. Pharmacol., 165 (2012), pp. 1361-1374

Norikazu Matsunaga, Naomi Kaneko, Angelina Yukiko Staub, Takeo Nakanishi, Ken-ichi Nunoya, Haruo Imawaka and Ikumi Tamai, 2015: Analysis of metabolic pathway of bosentan and cytotoxicity of bosentan metabolites based on a quantitative modeling of metabolism and transport in sandwich-cultured human hepatocytes. Drug Metabolism and Disposition Volume 46, Issue 4

McBride HM, Neuspiel M and Wasiak S, 2006: Mitochondria: More Than Just a Powerhouse. Curr Biol Volume 16, Issue 14, pp R551-R560

McGill MR and Jaeschke H, 2013: Metabolism and Disposition of Acetaminophen: Recent Advances in Relation to Hepatotoxicity and Diagnosis. *Pharmaceutical* Research, Volume 30, Issue 9, pp 2174–2187.

McKenzie R, Fried MW, Sallie R, Conjeevaram H, M. Di Bisceglie AM, Park Y, Savarese B, Kleiner D, Tsokos M, Luciano C, Pruett T, Stotka JL, et *al.*, 1995: Hepatic Failure and Lactic Acidosis Due to Fialuridine (FIAU), an Investigational Nucleoside Analogue for Chronic Hepatitis B. N Engl J Med Issue 333, pp 1099-1105

Meyers LL, W.P. Beierschmitt, E.A. Khairallah, S.D. Cohen: Acetaminophen-induced inhibition of hepatic mitochondrial respiration in mice. Toxicol. Appl. Pharmacol., 36 (1988), pp. 1193-1196

Milles D, 1999: History of Toxicology. Toxicology, pp 11–23

Mitchell JR, Jollow DJ, Potter WZ, Davis DC, Gillette JR and Brodie BB, 1973: acetaminophen-induced hepatic necrosis. i. role of drug metabolism. Journal of Pharmacology and Experimental Therapeutics October Volume 187, Issue 1, pp 185-194

Moebs and Pfuetzner, 2017: Drug reactions. *Der Hautarzt* January 2017, Volume 68, Issue 1, p 4

Monshi MM, Faulkner L, Gibson A, Jenkins RE, Farrell J, Earnshaw CJ, Alfirevic A, Cederbrant K, Daly AK, French N, Pirmohamed M, Park BK and Naisbitt DL, 2013: Human leukocyte antigen (HLA)-B*57:01-restricted activation of drug-specific T cells provides the immunological basis for flucloxacillin-induced liver injury. Hepatology Volume 57, Issue 2 pp 727–739

Moore LB, Parks DJ, Jones SA, Bledsoe RK, Consler TG, Stimmel JB, Goodwin B, Liddle C, Blanchard SG, Willson TM, Collins JL and Kliewer SA, 2000: Orphan Nuclear Receptors Constitutive Androstane Receptor and Pregnane X Receptor Share Xenobiotic and Steroid Ligands. The Journal of Biological Chemistry Volume 275, pp 15122-15127.

Morgan RE, Trauner M, van Staden CJ; Lee PH, Ramachandran B, Eschenberg M, Afshari CA, Qualls CW, Jr, Lightfoot-Dunn R and Hamadeh HK, 2009: Interference with Bile Salt Export Pump Function Is a Susceptibility Factor for Human Liver Injury in Drug Development. Toxicological Sciences, Volume 118, Issue 2, 1 December 2010, Pages 485–500

Morgan RE, Goralski KB, Piquette-Müller M, Renton KW, Roberton GR, Chaluvadi MR, Charles KA, Clarke KA, Kacevska M, Liddle C, Richardson TA, Sharma R and Sinal CJ, 2013: Regulation of Drug-Metabolizing Enzymes and Transporters in Infection, Inflammation, and Cancer. Drug Metabolism and Disposition February 2008, 36 (2) 205-216

Mufti NA, Bleckwenn NA, Babish JG and Shuler ML, 1995: Possible Involvement of the AH Receptor in the Induction of Cytochrome P-450IA1 Under Conditions of Hydrodynamic Shear in Microcarrier-Attached Hepatoma Cell Lines. Biochem Biophys Res Com Volume 208, Issue 1, Pp 144-152

Mufti NA and Shuler ML, 1996: Possible Role of Arachidonic Acid in Stress-Induced Cytochrome P450IA1 Activity. Biotechnology Progress, Volume 12, Issue 6, Pages 847–854

Nadanaciva S, Rana P, Beeson GC, Chen D, Ferrick DA, Beeson CC and Will Y, 2012: Assessment of drug-induced mitochondrial dysfunction via altered cellular respiration and acidification measured in a 96-well platform. J Bioenergetics Biomembranes, Volume 44, Issue 4, pp 421-37.

Nagar S, Walther S and Blanchard RL, 2006: Sulfotransferase (SULT) 1A1 polymorphic variants *1, *2, and *3 are associated with altered enzymatic activity, cellular phenotype, and protein degradation. Mol Pharmacol Volume 69, Issue 6, pp. 2084-92

Naisbitt DJ, Fraser SG, Pirmohamed P and Park BK, 2000: Immunological Principles of Adverse Drug Reactions. The Initiation and Propagation of Immune Responses Elicited by Drug Treatment. Drug-Safety Volume 23, Issue 6, pp 483- 507

Naisbitt DJ, Pirmohamed P and Park BK, 2003: Immunopharmacology of hypersensitivity reactions to drugs. Curr Allergy Asthma Rep Volume 3, Issue 1, pp 22-29

Naisbitt DJ, Sanderson LS, Meng X, Stachulsky AV, Clarke SE and Park BK, 2007: investigation of the immunogenicity of diclofenac and diclofenac metabolites. Toxicol Lett Volume 168, Issue 1, pp 45-50

Nguyen TV, Okechukwu Ukairo, Salman R. Khetani, Michael McVay, Chitra Kanchagar, Wolfgang Seghezzi, Gulesi Ayanoglu, Onyi Irrechukwu and Raymond Evers, 2015: Establishment of a Hepatocyte-Kupffer Cell Coculture Model for Assessment of Proinflammatory Cytokine Effects on Metabolizing Enzymes and Drug Transporters. Drug Metab Dip, Volume 43, Issue 5, pp. 774-85.

Nibourg GAA, Boer JD, van der Hoeven TV, Ackermans MT, van Gulik TM, Chamuleau RAFM and Hoekstra R, 2012: Perfusion flow rate substantially contributes to the performance of the HepaRG-AMC-bioartificial liver. Biotechnology and Bioengineering Volume 109, Issue 12, pp 3182–3188

Noor F, 2015: A shift in paradigm towards human biology-based systems for cholestatic-liver diseases. J Physiol, Volume 593, Issue 23, pp 5043–5055

Novik E, Maguire TJ, Chao P, Cheng KC, Yarmush ML (2010) A microfluidic hepatic coculture platform for cell-based drug metabolism studies. Biochem Pharmacol 79(7):1036–1044

O'Brien PJ, W. Irwin, D. Diaz, E. Howard-Cofield, C.M. Krejsa, M.R. Slaughter, B. Gao, N. Kaludercic, A. Angeline, P. Bernardi, P. Brain, C. Hougham: High concordance of drug-induced human hepatotoxicity with *in vitro* cytotoxicity measured in a novel cell-based model using high content screening. Arch. Toxicol., 80 (2006), pp. 580-604

Ohta T, Iijima K, Miyamoto M, Nakahara I, Tanaka H, Ohtsuji M, Suzuki T, Kobayashi A, Yokota J, Sakiyama T, Shibata T, Yamamoto M and Hirohashi S, 2008: Loss of Keap1 Function Activates Nrf2 and Provides Advantages for Lung Cancer Cell Growth. Canc Res Volume 68, Issue 5, pp 1303-9

Ohyama K, Nakajima M, Nakamura S, Shimada N, Yamazaki H and Yokoi T, 2000: A Significant Role of Human Cytochrome P450 2C8 in Amiodarone *N*-Deethylation: An Approach to Predict the Contribution with Relative Activity Factor. Drug Metab Disp, Volume 28 Issue 11, pp 1303-1310

Olson H, Betton G, Robinson D,' Thomas K,' Monro A,' Kolaja G,' Lilly P,' Sanders J,' Sipes G,' Bracken W,' Dorato M,' Van Deun K,' Smith P,' Berger B, and Heller A, 2000: Concordance of the Toxicity of Pharmaceuticals in Humans and in Animals Regulatory Toxicology and Pharmacology Volume 32, Issue 1, August 2000, Pages 56-67

Ogese M, Ahmed S, Alferivic A, et al. New approaches to investigate drug-induced hypersensitivity. Chem Res Toxicol. 2017 November 2;30(1):239–259

Oorts M, Baze A,' Bachellier P', Heyd B,' Zacharias T,' Annaert P and Richert L, 2016: Drug-induced cholestasis risk assessment in sandwich-cultured human hepatocytes. Toxicology in vitro, Volume 34, pp 179-186

Padovan E, Bauer T, Tongia MM, Kalbacher H and Weltzien HU: Penicilloyl peptides are recognized as T cell antigenic determinants in penicillin allergy. Eur. J. Immunol., 27 (1997), pp. 1303-1307

Papay J, Clines D, Rafi R, et al. Drug-induced liver injury following positive drug rechallenge. Regul Toxicol Pharmacol. 2009; 54: 84–90

Park BK, Kitteringham NR, Maggs JM, Pirmohamed M and Williams DP: The role of metabolic activation in drug-induced hepatotoxicity. Annu. Rev. Pharmacol. Toxicol., 45 (2005), pp. 177-202

Parola M and Pinzani M, 2009: Hepatic wound repair. Fibrogenesis and tissue repair, Volume 2, Issue 4, pp.

Patel T, Roberts LR, Jones BA and Gores GJ: Dysregulation of apoptosis as a mechanism of liver disease: an overview. Semin. Liver Dis., 18 (2) (1998), pp. 105-114

Perri RE and Shah V, 2005: Hepatic Sinusoidal endothelial cells. Signaling Pathways in Liver Diseases, chapter 5, pp 53-62.

Persson M, Loye AF, Mow T and Hornberg JJ, 2006: A high content screening assay to predict human drug-induced liver injury during drug discovery. J Pharmacol Toxicol Methods, Volume 68, Issue 3, pp 302-313

Pessayre D, Mansouri A, Haouzi D, Fromenty B, 1999: Hepatotoxicity due to mitochondrial dysfunction. Cell Biology and Toxicology Volume 15, Issue 6, pp 367–373

Pichler WJ, 2002: Pharmacological interaction of drugs with antigen-specific immune receptors: the p-i concept. Current Opinion in Allergy and Clinical Immunology Volume 2, Issue 4, pp 301-305

Pichler WJ, 2008: The p-i Concept: Pharmacological Interaction of Drugs With Immune Receptors. World Allergy Organization Journal Volume Issue pp

Prestwich, G. D., Liu, Y., Yu, B., Shu, X. Z. and Scott, A. 2007. 3-D culture in synthetic extracellular matrices: new tissue models for drug toxicology and cancer drug discovery. Adv Enzyme Regul, 47: 196–207

Probst I, Jungermann K and Unthan K 1983: Short-term regulation of glycolysis by insulin and dexamethasone in cultured rat hepatocytes. FEBS Journal, Volume 135, Issue 1 Pages 151–156

Racanelli V and Rehermann B, 2006: the liver as an immunological organ. Hepatology Volume 43, Issue S1 Pages S54–S62

Ramadori G, Moriconi F, Malik I and Dudas J, 2008: Physiology and Pathophysiology of the Liver. Inflammation, Damage and Repair. J Physiol Pharmacol, Volume 59, Suppl 1, pp 107-17

Ramaiahgari SC, Waydianatha S, Dixon D, DeVito MJ, Paules RS and Ferguson SS 2017: Three-Dimensional (3D) HepaRG Spheroid Model With Physiologically Relevant Xenobiotic Metabolism Competence and Hepatocyte Functionality for Liver Toxicity Screening. Tox Sci, Volume 159, Issue 1, pp 124–136

Rawlins MD, 2004: Cutting the cost of drug development? Nature Reviews Drug Discovery Volume 3, pp 360–364

Reasor MJ and Kacew S, 2001: Drug-Induced Phospholipidosis: Are There Functional Consequences? Exp Biol Med, Volume 226, Issue 9, pp 825-30

Reid LM, Fiorino AS, Sigal SH, Brill S and Holst PA, 1992: Extracellular matrix gradients in the space of disse: Relevance to liver biology. Hepatology Volume 15, Issue 6, pp 1198–1203

Rennert K, Steinborn S, Gröger M, Ungerböck B, Jank AM, Ehgartner J, Nietzsche S, Dinger J, Kiehntopf M et al., 2015: A microfluidically perfused three-dimensional human liver model. Biomaterials Volume 71, pp. 119-31

Rhodes S, Otten J, Hingorani G, Hartley D, Franklin R. Simultaneous assessment of cytochrome P450 activity in cultured human hepatocytes for compound-mediated induction of CYP3A4, CYP2B6, and CYP1A2. J Pharmacol Toxicol Methods Volume 63, pp. 223–6

Richert L, Liguori MJ, Abadie C, Heyd B, Mantion G, Halkic N and Waring JF, 2006: gene expression in human hepatocytes in suspension after isolation is similar to the liver of origin, is not affected by hepatocyte cold storage and cryopreservation, but is strongly changed after hepatocyte plating. Drug Metabolism and Disposition Volume 34, Issue 5, pp 870-879

Richert L, Tuschl G, Abadie C, Blanchard N, Pekthong D, Mantion G, Wevber JC and Müller SO, 2009: Use of mRNA expression to detect the induction of drug metabolizing enzymes in rat and human hepatocytes. Toxicol Appl Pharmacol Volume 235, Issue 1, pp 86-96

Roberts RA, Ganey PE, Ju C, Kamendulis LM, Rusyn I and Klaunig JE, 2007: Role of the Kupffer Cell in Mediating Hepatic Toxicity and Carcinogenesis. Toxicological Sciences, Volume 96, Issue 1, 1 March 2007, Pages 2–15

Robinson RL, Visscher GE, Roberts SA, Engstrom RG, Hartman HA, Ballard FH. Generalized phospholipidosis induced by an amphiphilic cationic psychotropic drug. Toxicol Pathol. 1985;13(4):335-48.

Rodrigues CM, Fan G, Wong PY, Kren BT and Steer CJ, 1998: Ursodeoxycholic acid may inhibit deoxycholic acid-induced apoptosis by modulating mitochondrial transmembrane potential and reactive oxygen species production. Molecular Medicine Volume 4, Issue 3, pp 165–178

Rogue A, Lambert C, Spire C, Claude N, Gouillouzo A, 2012: Interindividual variability in gene expression profiles in human hepatocytes and comparison with HepaRG cells. Drug Metab Disp Volume 40, Issue 1, pp 151-8

Rowe C, Goldring CEP, Kitteringham NR, Jenkins RE, Lane BS, Sanderson C, Elliott V, Platt V, Metcalfe P and Park BK, 2010: Network Analysis of Primary Hepatocyte Dedifferentiation Using a Shotgun Proteomics Approach. *J. Proteome Res.* Volume *9, Issue* 5, pp 2658–2668

Sacerdoti D, Gatta A and McGiff JC, 2003: Role of cytochrome P450-dependent arachidonic acid metabolites in liver physiology and pathophysiology. Prostaglandins and other lipid mediators, Volume 72, Issues 1-2, pp 51-71.

Sudipta Saha S, New LS, Ho HK, Chui WK, Chun E and Chan Y, 2010: Direct toxicity effects of sulfo-conjugated troglitazone on human hepatocytes. Toxicology Letters Volume 195, Issues 2–3, pp 135-141

Santoni-Rugiu E, Jelnes P, Thorgeirsson SS and Bisgaard HC., 2005: Progenitor cells in liver regeneration: molecular responses controlling their activation and expansion. J Pathol Microbiol Immunol, Volume 113, Issue 11-12, pp 876–902.

Sbrana T and Ahluwalia A, 2010: Engineering Quasi-Vivo® in Vitro Organ Models. New Technologies for Toxicity Testing. Advances in Experimental Medicine and Biology, vol 745. ISBN 978-1-4614-3054-4

Schrenk D, Eisenmann-Tappe I, Gebhardt R, Mayer D, El Mouelhi M, Röhrdanz E, Münzel P and Bock KW, 1991: Drug metabolizing enzyme activities in rat liver epithelial cell lines, hepatocytes and bile duct cells. Biochem Pharmacol Volume 41, Issue 11, pp 1751-57.

Shayeganpour A, El-Kadi AOS and Brocks DR, 2006: determination of the enzyme(s) involved in the metabolism of amiodarone in liver and intestine of rat: the contribution of cytochrome p450 3a isoforms. Drug Met Dispos, Vol 34, Issue 1, pp 43-50.

Shen, S., Marchick, M. R., Davis, M. R., Doss, G. A., and Pohl, L. R. (1999): Metabolic activation of diclofenac by human cytochrome P450 3A4: Role of 5-hydroxydiclofenac. Chem. Res. Toxicol Volume 12, pp 214–222

Shibata T, Ohta T, Tong KI, Kokubu A, Odogawa R, Tsuta K, Asamura H, Yamamoto M and Hirohashi S, 2008: Cancer related mutations in NRF2 impair its recognition by Keap1-Cul3 E3 ligase and promote malignancy. PNAS Volume 105, Issue 36, pp 13568-13573

Shvartsman I, Dvir T, Harel-Adar T, Cohen S (2009) Perfusion cell seeding and cultivation induce the assembly of thick and functional hepatocellular tissue-like construct. Tissue Eng Part A 15(4):751–760

Simon-Hettich B, Rothfuss A and Steger-Hartmann T., 2006: Use of computer-assisted prediction of toxic effects of chemical substances. Toxicology, Volume 224, Issues 1-2, pp. 156-62.

Simmonneau G, Galie N, Jansa P, Bohns Meyer GM, Al-Hith H, Kusic-Pajic A, Lemarie JC, Hoeper M and Rubin LJ, 2014: Long-term results from the EARLY study of bosentan in WHO functional class II pulmonary arterial hypertension patients. Int J Cardiol, Volume 172, Issue 2, pp 332-9.

Simons K and Fuller SD, 1985: Cell Surface Polarity in Epithelia. Annual Review of Cell Biology Volume 1, pp.243-288

Sinz M, Wallace G and Sahi J, 2008: Current Industrial Practices in Assessing CYP450 Enzyme Induction: Preclinical and Clinical. AAPS Journal, Volume 10, Issue 2, pp. 391-400

Sipes I. G., Gandolfi A. J. Biotransformation of toxicants. Casarett and Doull's Toxicology. The Basic Science of Poisons, 4th edn, M. O. Amdur, J. Doull, C. D. Klaassen. Pergamon, New York 1991; 88–126

Sison-Young RL, Lauschke VM, Johann E, Alexandre E, Antherieu S, Aerts H, Gerets HJH, Labbe G, Hoet D, Dorau M, Schofield CA, Lovatt CA, Holder JC, Stahl SH, Richert L, Kitteringham NR, Jones RP, Elmasry M, Weaver RJ, Hewitt PG, Ingelmann-Sundberg M, Goldring CE and Park BK, 2016: A multicenter assessment of single-cell models aligned to standard measures of cell health for prediction of acute hepatotoxicity. Arch Toxicol, Volume 91, Issue 3, pp. 1385-1400.

Sison-Young RL, Mitsa D, Jenkins RE, Mottram D, Alexandre E, Richert L, Aerts H, Weaver RJ, Jones RP, Johann E, Hewitt PG, Ingelman-Sundberg M, Goldring CEP, Kitteringham NR and Park BK et *al.*, 2015: Comparative Proteomic Characterization of 4 Human Liver-Derived Single Cell Culture Models Reveals Significant Variation in the Capacity for Drug Disposition, Bioactivation, and Detoxication. Toxicological Sciences, Volume 147, Issue 2, pp 412–424

Skardal A and Atala A, 2015: Biomaterials for Integration with 3-D Bioprinting. Annals for Biomedical Engineering Volume 43, Issue 3, pp 730-46

Smith KS, Smith PL, Heady TN, Trugman JM, Harman WD, and Macdonald TL, 2003: In Vitro Metabolism of Tolcapone to Reactive Intermediates: Relevance to Tolcapone Liver Toxicity. *Chem. Res. Toxicol.*, 2003, *16* (2), pp 123–128

Strautnieks SS, Bull LN, Knisley AS, Kocoshis SA, Dahl N, Arnell H, Sokal E, Dahan K, Childs S, Ling V, Tanner MS, Kagalwalla AF, Nemeth A, Pawlowska J, Baker A, Mieli-Vergani G, Freimer NB, Gardiner RM and Thompson RJ, 1998: A gene encoding a liver-specific ABC transporter is mutated in progressive familial intrahepatic cholestasis. Nature Genetics, Volume 20, pp 233-38.

Stephens, C; Andrade, RJ and Lucena, M. I, 2014: Mechanisms of drug-induced liver injury. Current Opinion in Allergy and Clinical Immunology: August 2014 - Volume 14 - Issue 4 - p 286–292

Sunman JA, Hawke RL, LeCluyse EL and Kashuba ADM, 2004: kupffer cell-mediated IL-2 suppression of cyp3a activity in human hepatocytes. Drug Metabolism and Disposition Volume 32, Issue 3, pp 359-363

Thomas CH, Collier JH, Sfeir CS and Healy KE: Engineering gene expression and protein synthesis by modulating nuclear shape. Proc. Natl. Acad. Sci. USA, 99 (2002), pp. 1972-1977

Tietz PS and LaRusso NF, 2006: Cholangiocyte biology. Curr Opin Gastroent, Volume 22, Issue 3, pp 279-287.

Tirona RG and Kim RB, 2005: Nuclear Receptors and Drug Disposition Gene Regulation. J Pharm Sci, Volume 94, Issue 6, pp 1169-1186.

Tostoes RM, Leite SB, Serra M, Jensen J, Björquist P, Carrondo MJT, Brito C and Alves PM., 2012: Human liver cell spheroids in extended perfusion bioreactor culture for repeated-dose drug testing. Hepatology, Volume 55, Issue 4, pp 1227–1236.

Traber PG, Chianale J and Gunucio JJ, 1988: Physiologic significance and regulation of hepatocellular heterogeneity. Gastroenterology Volume 95, Issue 4, pp 1130-45

Treyer A and Musch A, 2013: Hepatocyte Polarity. Comprehensive physiology, Volume 3, pp 243-87.

Turner R, Lozoya O, Wang Y, Cardinale V, Gausio E, Alpini G, Mendel G, Wauthier E, Barbier C, Alvaro D and Reid LM, 2011: Human hepatic stem cell and maturational liver lineage biology. Hepatology Volume 53, Issue 3, pp 1035–1045

Tuschl G and Müller SO, 2006: Effects of cell culture conditions on primary rat hepatocytes-cell morphology and differential gene expression. Toxicology Volume 218, Issue 2-3, pp 205-15

Tzima E, Irani-Therani M, Kiosses WB, Dejana E, Schultz DA, Engelhardt B, Cao G, DeLisser H and Schwartz MA, 2005: A mechanosensory complex that mediates the endothelial cell response to fluid shear stress. Nature volume 437, pp 426–431

Tzvetkov MV, Vormfelde SV, Balen D, Meineke I, Schmidt T, Sehrt D, Sabolic I, Koepsell H and Brockmöller J, 2009: The Effects of Genetic Polymorphisms in the Organic Cation Transporters OCT1, OCT2, and OCT3 on the Renal Clearance of Metformin. Clinical Pharmacology and Therapeutics Volume 86, pp 299–306

van Montfoord JE, Hagenbuch B, Groothuis GMM, Koepsell H, Meier PJ and Meijer DKF, 2003: Drug Uptake Systems in Liver and Kidney. Curr Drug Metab, Volume 4, Issue 3, pp 185-211.

Vergani L, Grattarola M and Nicolini C, 2004: Modifications of chromatin structure and gene expression following induced alterations of cellular shape. The International Journal of Biochemistry & Cell Biology Volume 36, Issue 4, pp 1447-1461

Vernetti LA, Senutovitch N, Boltz R, DeBiasio R, Shun TY, Gough A and Taylor DL, 2016: A human liver microphysiology platform for investigating physiology, drug safety, and disease models. Experimental Biology and Medicine Vol 241, Issue 1

Vig P, Russo FP, Edwards RJ, Tadrous PJ, Wright NA, Thomas HC, Alison MR, Forbes SJ (2006) The sources of parenchymal regeneration after chronic hepatocellular liver injury in mice. Hepatology 43:316–324

Vignati L, Turlizzi E, Monaci S, Grossi P, de Kanter R and Monshouwer M, 2005: An in vitro approach to detect metabolite toxicity due to CYP3A4-dependent bioactivation of xenobiotics. Toxicology Volume 216, Issues 2–3, pp 154-167

Villeneuve E, Gosselin S and Whyte I, 2014: Four-hour acetaminophen concentration estimation after ingested dose based on pharmacokinetic models. Clin Toxicol, Volume 52, Issue 5, pp. 556-60.

Vinci B, Duret C, Klieber S, Gerbal-Chaloin S, Sa-Cunha A, Laporte S, Suc B, Maurel P, Ahluwalia A and Daujat-Charanieu M, 2011: Modular bioreactor for primary human hepatocyte culture: Medium flow stimulates expression and activity of detoxification genes. Biotechnology Journal Volume 6, Issue 5, pp 554–564

Von Moltke LL, Greenblatt DL, Granda BW, Grassi JM, Schmider J, Harmatz JS and Shader RI, 1999: Nefazodone, meta-chlorophenylpiperazine, and their metabolites in vitro: cytochromes mediating transformation, and P450-3A4 inhibitory actions. Psychopharmacology, Volume 145, Issue 1, pp 113-22.

Walker TM, Rhodes PC and Westmoreland C, 2000: The differential cytotoxicity of methotrexate in rat hepatocyte monolayer and spheroid cultures. Toxicology in vitro, Volume 14, Issue 1, pp 475-485.

Walker K, Ginsberg G, Hattis D, Johns DO, Guyton KZ and Sonawane B, 2009: Genetic polymorphism in N-Acetyltransferase (NAT): Population distribution of NAT1 and NAT2 activity. J Toxicol Environ Health B Crit Rev Volume 12, Issue 5-6, pp. 440-72

Wang H, Faucette S, Moore R, Sueyoshi T, Negishi M and LeCluyse EL, 2004: Human Constitutive Androstane Receptor Mediates Induction of CYP2B6 Gene Expression by Phenytoin. The Journal of Biological Chemistry Volume 279, pp 29295-29301.

Wang Y, Zhanhg D, Zhang J, Ma M and Jiang H, 2010: New insights into the antifibrotic effects of sorafenib on hepatic stellate cells and liver fibrosis. Journal of Hepatology Volume 53, Issue 1, Pages 132–144

Wang Y, Spitz MR, Tsou AM, Zhang K, Makan N and Wu X, 2002: Sulfotransferase (SULT) 1A1 polymorphism as a predisposition factor for lung cancer: a case-control analysis. Lung Cancer Volume 35, Issue 2, pp. 137-42

Weaver RJ, Betts C, Blomme EAG, Gerets HHJ, Jensen KG, Hewitt PG, Juhila S, Labbe G, Liguori MJ, Mesens N, Ogese MO, Persson M, Snoeys J, Stevens JL, Walker T and Park BK, 2017: Test systems in drug discovery for hazard identification and risk assessment of human drug-induced liver injury. Exp Opin on Drug Metabolism and Toxicology Volume 13, Issue 7, pp 767-782

Weber C, Gasser R and Hopfgartner G, 1999: Absorption, excretion, and metabolism of the endothelin receptor antagonist bosentan in healthy male subjects. Drug Metab. Dispos., 27 (1999), pp. 810-815

Wu L.Q · Zhang W.J · Niu J.X · Ye L.Y. · Yang Z.H. · Grau G.E. and Lou J.N, 2008: Phenotypic and Functional Differences between Human Liver Cancer Endothelial Cells and Liver Sinusoidal Endothelial Cells. J Vasc Res 2008; 45: 78–86

Wu MH, Huang SB and Lee GB**:** Microfluidic cell culture systems for drug research. Lab Chip, 10 (2010), pp. 939-956

Xia X, Francis H, Glaser S, Alpini G, and LeSage G, 2006: Bile acid interactions with cholangiocytes. World J Gastroenterol. 2006 Jun 14; 12(22): 3553–3563.

Xie G, Wang X, Wang L, Wang L, Atkinson RD, Kanel GC, Gaarde WA and DeLeve LD, 2012: Role of liver sinusoidal endothelial cell differentiation in progression and regression of rat hepatic fibrosis. *Gastroenterology.* 2012;142(4):918–927.

Xu JJ, P.V. Henstock, M.C. Dunn, A.R. Smith, J.R. Chabot, D. de Graaf, 2008: Cellular imaging predictions of clinical drug-induced liver injury. Toxicol. Sci., 105 (2008), pp. 97-105

Yamada M, Utoh R, Ohashi K, Tatsumi K, Yamato M, Okano T and Seki M, 2012: Controlled formation of heterotypic hepatic micro-organoids in anisotropic hydrogel microfibers for long-term preservation of liver-specific functions. Biomaterials Volume 33, Issue 33, pp. 8304-15

Yamamoto Y, Yamazaki H, Ikeda T, Watanabe T, Iwabuchi H, Nakajima M and Yokoi T, 2002: Formation of a Novel Quinone Epoxide Metabolite of Troglitazone with Cytotoxic to HepG2 Cells. Drug Metabolism and Disposition Volume 30, Issue 2, pp 155-160

Yoshikawa Y, M. Morita, H. Hosomi, K. Tsuneyama, T. Fukami, M. Nakajima, T. Yokoi, 2009: Knockdown of superoxide dismutase 2 enhances acetaminophen-induced hepatotoxicity in rat. Toxicology, 264 (2009), pp. 89-95

Yoshinari Y, Ueda R, Kusano K, Yoshimura T, Nagata K and Yamazoe Y, 2008: Omeprazole transactivates human CYP1A1 and CYP1A2 expression through the common regulatory region containing multiple xenobiotic-responsive elements. Biochemical Pharmacology Volume 76, Issue 1, pp 139-145

Zahno A, Brecht K, Morand R, Maseneni S, Török M, Lindinger PW and Krähenbrühl S, 2011: The role of CYP3A4 in amiodarone-associated toxicity on HepG2 cells. Biochemical Pharmacology Volume 81, Issue 3, pp 432-441

Zanger UM and Schwab M, 2013: Cytochrome P450 enzymes in drug metabolism: Regulation of gene expression, enzyme activities, and impact of genetic variation. Pharmacology and Therapeutics, Volume 138, Issue 1, pp 103-41.

Zhang L, Zhang Y, Zhao P and Huang SM, 2009: Predicting Drug-Drug interactions: An FDA perspective. AAPS Journal, Volume 11, Issue 2, pp 300-6

Zhang W, Suenaga M, Schirripa M, Chao S, Yang D, Berger MD et al., 2016: Genetic variants of hENT-1 to predict efficacy of TAS-102 in patients with refractory metatstatic colorectal cancer. J clin Onc Volume 34, Issue 15, p 3580

Zhu M, Weiping Zhao, Humberto Jimenez, Donglu Zhang, Suresh Yeola, Renke Dai, Nimish Vachharajani, and James Mitroka, 2005: cytochrome p450 3a-mediated metabolism of buspirone in human liver microsomes. Drug Metab Dispos. Volume 33, Issue 4:500-7

Ziegler DM, 1988: Flavin-containing monooxygenases: Catalytic mechanism and substrate specificities. Drug Metabolism Reviews Volume 19, pp 1-32

Zimmerman HJ, 1999: Hepatotoxicity: The Adverse Effects of Drugs and Other Chemicals on the Liver. Lipincott Williams and Wilkins, ISBN 0-7817-1952-6

Appendix

Appendix 1A: Mean EC_{50} values [µM] from all cell systems in response to the training compounds

A. ATP

COMPOUND	PHH: Fresh		PHH: Cryo		HepG2: ECACC		HepG2: TS clone		HepaRG: Fresh		HepaRG: Cryo		Upcytes	
	24 h	72 h	24 h	72 h	24 h	72 h	24 h	72 h	24 h	72 h	24 h	72 h	24 h	72 h
Amiodarone	43.29	18.16	24.64	7.18	20.2	9.26	22.58	23.07	31.85	23.12	67.81	44.39	27.9	10.91
Buspirone	249.7	261.3	>300	193.4	>300	115.4	>300	>300	>300	>300	>300	>300	>300	>300
Entacapone	41.52	35.34	33.34	23.43	>1000	85.45	>1000	26.18	560.6	336.5	771.9	514.7	>1000	129.2
Metformin	1289	680.5	1176	625.5	>10000	3351	>10000	2734	>10000	>10000	>10000	>10000	>10000	>10000
Nefazodone	19.36	13.68	17.11	7.43	27.61	8.38	37.79	28.05	95.14	39.12	121.6	86.71	103.4	58.77
Paracetamol	4971	1343	10669	1363	>30000	3897	>30000	3898	>30000	10768	27162	6141	>30000	8454
Tolcapone	17.64	10.99	19.8	13.06	152.2	11.98	149.8	5.15	156.5	51.83	372.7	127.5	462.5	143.7
Diclofenac	235.6	68.32	233	66.7	828.1	99.09	>1000	89.56	770	333.8	>1000	262.2	>1000	854.1
Pioglitazone	>1000	>1000	366.9	>1000	>1000	846	>1000	>1000	>1000	751.5	603.4	>1000	>1000	>1000
Ximelagatran	260.6	277.9	270.6	196	>300	217.9	>300	256	>300	>300	>300	243.1	>300	>300
Troglitazone	14.43	13.57	29.84	10.1	27.32	15.51	36.59	17.5	36.95	17.5	245.9	194.8	>300	204.7
Perhexiline	11.57	9.72	11.55	3.2	17.11	6.6	12.73	12.28	34.54	22.57	42.7	27.62	16.39	13.1
Bosentan	152.6	90.4	219	86.89	>300	149.3	>300	>300	>300	>300	>300	>300	>300	160

B. Resazurin

COMPOUND	PHH: Fresh		PHH: Cryo		HepG2: ECACC		HepG2: TS clone		HepaRG: Fresh		HepaRG: Cryo		Upcytes	
	24 h	72 h	24 h	72 h	24 h	72 h	24 h	72 h	24 h	72 h	24 h	72 h	24 h	72 h
Amiodarone	62.52	16.05	30.78	8.96	39.28	15.24	33.21	22.8	41.29	24.62	228.6	91.34	75.92	14.43
Buspirone	>300	>300	>300	230.4	>300	>300	>300	>300	>300	>300	>300	>300	>300	>300
Entacapone	52.69	30.64	44.71	29.31	>1000	342.8	>1000	46.87	>1000	482	>1000	919.9	>1000	235.6
Metformin	9068	1268	4609	794.5	>10000	>10000	>10000	>10000	>10000	>10000	>10000	>10000	>10000	>10000
Nefazodone	40.74	21.37	39.51	7.37	80.55	18.4	35.32	29.61	164.1	90.4	191.2	100.6	224.4	58.77
Paracetamol	3127	779.3	5558	3278	18644	6336	16659	6378	>30000	11997	>30000	9534	>30000	5010
Tolcapone	24.95	17.22	20.72	11.96	104.1	12.83	51.8	4.5	465.3	82.07	>1000	249.8	>1000	242.5
Diclofenac	567.6	78.52	287.4	72.11	273	89.85	412.4	65.47	>1000	428.6	>1000	>1000	>1000	>1000
Pioglitazone	>1000	>1000	>1000	>1000	>1000	718.1	>1000	>1000	>1000	>1000	>1000	>1000	>1000	>1000
Ximelagatran	251.6	216.2	243.8	154.6	>300	>300	>300	>300	>300	>300	>300	>300	>300	>300
Troglitazone	13.12	11.24	40.79	15.85	22.24	17.31	50.14	25.32	50.14	25.32	>300	>300	>300	289.8
Perhexiline	16.98	12.12	14.13	3.94	18.3	8.47	13.27	13.06	46.16	24.73	56.32	29.84	22.11	13.1
Bosentan	289.8	115.7	>300	159.3	>300	275.4	>300	>300	>300	>300	>300	>300	>300	232

Appendix 1b: Cytotoxicity ring trial viability data, expressed as % of control

APAP 24h

APAP [µM]	24h ATP					24h Resazurin				
HepG2										
	N=1	**N=2**	**N=3**	**mean**	**stDev**	**N=1**	**N=2**	**N=3**	**mean**	**stDev**
0	100.00	100.00	100.00	**100.00**	**5.72**	100.00	100.00	100.00	**100.00**	**3.86**
30	109.40	114.94	104.00	**109.45**	**4.47**	102.66	99.24	103.29	**101.73**	**1.78**
100	117.34	120.65	104.42	**114.14**	**7.00**	106.42	102.30	102.97	**103.90**	**1.80**
300	109.44	116.73	107.80	**111.32**	**3.88**	101.99	100.12	100.05	**100.72**	**0.90**
1,000	98.47	110.33	100.30	**103.04**	**5.21**	99.03	98.19	99.94	**99.06**	**0.71**
3,000	87.05	92.34	89.50	**89.63**	**2.16**	95.90	89.91	96.30	**94.04**	**2.92**
10,000	74.97	84.35	78.92	**79.41**	**3.85**	80.33	85.15	90.92	**85.47**	**4.33**
30,000	110.22	121.44	108.57	**113.41**	**5.72**	96.19	94.52	103.42	**98.04**	**3.86**
HepaRG										
	N=1	**N=2**	**N=3**	**mean**	**stDev**	**N=1**	**N=2**	**N=3**	**mean**	**stDev**
0	100.00	100.00	100.00	**100.00**		100.00	100.00	NA	**100.00**	
30	98.13	113.40	99.09	**103.54**	6.98	112.28	97.47	NA	**104.88**	10.47
100	97.80	118.45	104.56	**106.94**	8.60	109.11	98.32	NA	**103.72**	7.63
300	97.61	123.30	101.42	**107.45**	11.32	109.35	98.45	NA	**103.90**	7.71
1,000	97.41	125.13	97.41	**106.65**	13.06	116.58	96.28	NA	**106.43**	14.35
3,000	97.24	107.97	94.33	**99.84**	5.87	115.14	93.11	NA	**104.12**	15.58
10,000	86.54	89.76	90.64	**88.98**	1.76	105.10	81.75	NA	**93.43**	16.52
30,000	59.42	55.63	28.85	**47.97**	13.60	87.11	61.05	NA	**74.08**	18.43
Upcyte hepatocytes										
	N=1	**N=2**	**N=3**	**mean**	**stDev**	**N=1**	**N=2**	**N=3**	**mean**	**stDev**
0	75.68	87.16	100.00	81.42	8.11	92.88	103.29	NA	98.08	7.36
30	78.24	87.16	**87.16**	83.33	6.63	98.97	101.39	NA	100.18	1.71
100	78.16	94.33	**94.33**	88.97	9.29	89.92	110.30	NA	100.11	14.41
300	82.05	101.94	**101.94**	94.01	13.73	92.53	104.27	NA	98.40	8.30
1,000	73.50	98.41	**98.41**	92.96	9.45	112.60	107.53	NA	110.06	3.59
3,000	64.43	102.14	**102.14**	92.59	16.53	112.02	104.33	NA	108.17	5.43
10,000	51.66	74.87	**74.87**	71.39	6.03	132.46	93.68	NA	113.07	27.42
30,000	75.68	59.32	**59.32**	56.77	4.42	92.88	103.29	NA	98.08	7.36

APAP 72h

APAP [µM]	72h ATP					72h Resazurin				
HepG2										
	N=1	**N=2**	**N=3**	**mean**	**stDev**	**N=1**	**N=2**	**N=3**	**mean**	**stDev**
0	100.00	100.00	100.00	**100.00**	**0.00**	100.00	100.00	100.00	**100.00**	**0.00**
30	86.13	122.86	82.16	**97.05**	**22.44**	96.32	100.57	99.94	**98.94**	**2.29**
100	118.30	119.25	108.47	**115.34**	**5.97**	106.87	99.17	103.71	**103.25**	**3.87**
300	96.07	99.62	118.04	**104.58**	**11.79**	97.18	100.41	103.64	**100.41**	**3.23**
1,000	88.41	81.26	105.52	**91.73**	**12.47**	96.38	96.57	102.67	**98.54**	**3.58**
3,000	53.60	38.64	35.31	**42.52**	**9.74**	69.54	77.78	85.85	**77.72**	**8.16**
10,000	36.48	33.60	29.21	**33.10**	**3.66**	49.76	53.27	64.47	**55.83**	**7.68**
30,000	13.21	17.16	18.18	**16.18**	**2.62**	10.35	16.66	25.90	**17.64**	**7.82**
HepaRG										
	N=1	**N=2**	**N=3**	**mean**	**stDev**	**N=1**	**N=2**	**N=3**	**mean**	**stDev**
0	100.00	100.00	NA	**100.00**	**0.00**	100.00	100.00	100.00	**100.00**	**0.00**
30	91.21	102.64	NA	**96.92**	**8.08**	97.95	91.45	NA	**94.70**	**4.60**
100	99.28	137.62	NA	**118.45**	**27.11**	98.82	100.55	NA	**99.68**	**1.23**
300	97.21	132.63	NA	**114.92**	**25.05**	98.45	100.26	NA	**99.35**	**1.28**
1,000	94.27	124.69	NA	**109.48**	**21.51**	95.16	104.16	NA	**99.66**	**6.37**
3,000	72.73	79.47	NA	**76.10**	**4.76**	78.18	80.52	NA	**79.35**	**1.65**
10,000	35.44	35.23	NA	**35.33**	**0.15**	47.76	65.28	NA	**56.52**	**12.39**
30,000	6.14	14.17	NA	**10.16**	**5.68**	1.54	10.93	NA	**6.23**	**6.64**
Upcyte hepatocytes										
	N=1	**N=2**	**N=3**	**mean**	**stDev**	**N=1**	**N=2**	**N=3**	**mean**	**stDev**
0	100.00	100.00	NA	**100.00**	**0.00**	100.00	100.00	NA	**100.00**	**0.00**
30	92.17	90.27	NA	**91.22**	**1.34**	77.51	89.21	NA	**83.36**	**8.27**
100	102.31	113.55	NA	**107.93**	**7.95**	78.79	86.93	NA	**82.86**	**5.76**
300	103.33	121.96	NA	**112.65**	**13.17**	94.81	88.93	NA	**91.87**	**4.15**
1,000	100.69	131.48	NA	**116.09**	**21.78**	61.86	90.55	NA	**76.21**	**20.29**
3,000	85.46	133.06	NA	**109.26**	**33.66**	66.65	86.63	NA	**76.64**	**14.12**
10,000	28.35	58.30	NA	**43.33**	**21.18**	22.17	50.93	NA	**36.55**	**20.34**
30,000	17.88	7.85	NA	**12.86**	**7.09**	2.68	11.79	NA	**7.24**	**6.44**

Amiodarone 24h

AMI [µM]	24h ATP					24h Resazurin				
HepG2										
	N=1	**N=2**	**N=3**	**mean**	**stDev**	**N=1**	**N=2**	**N=3**	**mean**	**stDev**
0	100.00	100.00	100.00	**100.00**	**0.00**	100	100	100	**100.000**	**0.000**
3	109.71	78.21	54.33	**80.75**	**22.68**	105.91	96.68	100.65	**101.08**	**3.78**
5	92.84	12.18	5.24	**36.75**	**39.76**	100.56	96.62	95.01	**97.40**	**2.33**
10	38.78	0.66	0.55	**13.33**	**17.99**	81.44	59.83	59.24	**66.83**	**10.33**
30	27.48	0.17	0.17	**9.28**	**12.87**	87.56	10.23	5.27	**7.75**	**39.96**
50	8.97	0.01	0.04	**3.00**	**4.22**	81.44	6.10	1.03	**3.57**	**38.99**
100	3.44	-0.32	-0.25	**0.96**	**1.76**	53.19	4.56	-1.14	**1.71**	**25.84**
300	114.06	102.61	87.14	**101.27**	**11.03**	34.03	3.15	-3.06	**0.04**	**17.18**
HepaRG										
	N=1	**N=2**	**N=3**	**mean**	**stDev**	**N=1**	**N=2**	**N=3**	**mean**	**stDev**
0	100.00	100.00	100.00	**100.00**	**0.00**	100.00	100.00	NA	**100.00**	**0.00**
3	102.84	118.13	98.88	**106.62**	**8.30**	108.95	100.00	NA	**104.48**	**6.33**
5	102.21	116.41	103.27	**107.30**	**6.46**	115.01	103.52	NA	**109.26**	**8.12**
10	99.76	119.80	104.84	**108.13**	**8.51**	118.12	107.87	NA	**112.99**	**7.25**
30	94.26	113.83	89.76	**99.29**	**10.45**	118.28	110.46	NA	**114.37**	**5.52**
50	69.13	95.83	56.05	**73.67**	**16.56**	119.21	107.63	NA	**113.42**	**8.19**
100	1.18	0.73	0.21	**0.71**	**0.40**	30.09	5.65	NA	**17.87**	**17.28**
300	-0.10	0.14	-0.22	**-0.06**	**0.15**	5.58	5.68	NA	**5.63**	**0.07**
Upcyte hepatocytes										
	N=1	**N=2**	**N=3**	**mean**	**stDev**	**N=1**	**N=2**	**N=3**	**mean**	**stDev**
0	100.00	100.00	100.00	**100.00**	**0.00**	100	100	NA	**100.00**	**0.00**
3	91.88	102.82	102.82	**99.17**	**6.32**	122.49	97.66	NA	**110.08**	**17.56**
5	95.06	97.15	97.15	**96.45**	**1.21**	122.08	98.92	NA	**110.50**	**16.38**
10	66.45	63.09	63.09	**64.21**	**1.94**	135.98	97.28	NA	**116.63**	**27.37**
30	15.12	19.77	19.77	**18.22**	**2.68**	62.05	79.87	NA	**70.96**	**12.60**
50	6.56	12.28	12.28	**10.38**	**3.30**	46.67	85.69	NA	**66.18**	**27.59**
100	3.76	1.95	1.95	**2.55**	**1.05**	37.96	38.16	NA	**38.06**	**0.14**
300	0.26	0.82	0.82	**0.63**	**0.32**	20.52	27.11	NA	**23.81**	**4.66**

Amiodarone 72h

AMI [µM]	72h ATP					72h Resazurin				
HepG2										
	N=1	**N=2**	**N=3**	**mean**	**stDev**	**N=1**	**N=2**	**N=3**	**mean**	**stDev**
0	100.00	100.00	100.00	**100.00**	**0.00**	100.00	100.00	100.00	**100.00**	**0.00**
3	77.94	77.86	82.22	**79.34**	**2.49**	101.93	96.92	98.08	**98.98**	**2.62**
5	70.95	102.24	63.51	**78.90**	**20.55**	107.50	97.77	100.18	**101.81**	**5.07**
10	61.01	14.64	8.55	**28.07**	**28.69**	99.22	61.57	52.62	**71.13**	**24.73**
30	33.18	0.70	0.53	**11.47**	**18.80**	58.42	-1.97	1.30	**19.25**	**33.96**
50	40.80	0.31	0.37	**13.82**	**23.36**	75.60	-4.12	0.65	**24.04**	**44.71**
100	43.55	0.22	0.24	**14.67**	**25.01**	83.57	-3.37	0.36	**26.85**	**49.16**
300	43.00	0.33	0.35	**14.56**	**24.63**	73.21	-3.79	-0.33	**23.03**	**43.49**
HepaRG										
	N=1	**N=2**	**N=3**	**mean**	**stDev**	**N=1**	**N=2**	**N=3**	**mean**	**stDev**
0	100.00	100.00	NA	**100.00**	**0.00**	100.00	100.00	NA	**100.00**	**0.00**
3	96.43	134.25	NA	**115.34**	**26.74**	101.89	74.15	NA	**88.02**	**19.62**
5	104.48	142.01	NA	**123.25**	**26.54**	102.13	88.26	NA	**95.19**	**9.81**
10	103.76	144.37	NA	**124.06**	**28.72**	104.33	104.56	NA	**104.45**	**0.16**
30	47.03	83.25	NA	**65.14**	**25.61**	100.66	117.85	NA	**109.25**	**12.15**
50	3.27	2.87	NA	**3.07**	**0.28**	20.92	27.53	NA	**24.23**	**4.67**
100	-0.09	0.06	NA	**-0.02**	**0.10**	1.64	2.06	NA	**1.85**	**0.30**
300	-0.29	-0.22	NA	**-0.26**	**0.05**	-0.27	1.17	NA	**0.45**	**1.02**
Upcyte hepatocytes										
	N=1	**N=2**	**N=3**	**mean**	**stDev**	**N=1**	**N=2**	**N=3**	**mean**	**stDev**
0	100	100	NA	**100.00**	**0.00**	100.00	100.00	NA	**100.00**	**0.00**
3	101.66	82.15	NA	**91.90**	**13.79**	75.37	90.13	NA	**82.75**	**10.44**
5	103.54	58.56	NA	**81.05**	**31.80**	55.26	91.17	NA	**73.22**	**25.39**
10	11.36	1.62	NA	**6.49**	**6.89**	14.98	7.43	NA	**11.21**	**5.34**
30	0.28	0.55	NA	**0.42**	**0.19**	-6.20	1.91	NA	**-2.14**	**5.73**
50	-0.01	0.24	NA	**0.12**	**0.17**	-9.96	2.96	NA	**-3.50**	**9.13**
100	-0.22	-0.05	NA	**-0.14**	**0.12**	-7.86	1.80	NA	**-3.03**	**6.84**
300	-0.44	-0.31	NA	**-0.37**	**0.09**	-7.53	4.08	NA	**-1.73**	**8.21**

Bosentan 24h

BOS [µM]	24h ATP					24h Resazurin				
HepG2										
	N=1	**N=2**	**N=3**	**mean**	**stDev**	**N=1**	**N=2**	**N=3**	**mean**	**stDev**
0	100.00	100.00	100.00	**100.00**	**0.00**	100.00	100.00	100.00	**100.00**	**0.00**
3	109.18	111.14	106.81	**109.04**	**1.77**	100.38	92.12	97.20	**96.57**	**3.40**
5	108.84	109.87	103.37	**107.36**	**2.85**	102.54	98.36	100.20	**100.37**	**1.71**
10	105.07	106.51	100.47	**104.02**	**2.58**	102.02	101.08	100.44	**101.18**	**0.65**
30	101.19	100.78	98.09	**100.02**	**1.37**	101.28	99.88	103.19	**101.45**	**1.35**
50	93.81	96.86	91.83	**94.16**	**2.07**	101.77	102.33	101.66	**101.92**	**0.29**
100	78.14	86.10	81.20	**81.82**	**3.28**	101.26	101.82	102.25	**101.78**	**0.41**
300	70.85	81.53	78.77	**77.05**	**4.53**	90.23	98.50	98.90	**95.88**	**4.00**
HepaRG										
	N=1	**N=2**	**N=3**	**mean**	**stDev**	**N=1**	**N=2**	**N=3**	**mean**	**stDev**
0	100.00	100.00	100.00	**100.00**	**0.00**	100.00	100.00	NA	**100.00**	**0.00**
3	95.89	116.45	105.40	**105.91**	**8.40**	113.74	100.09	NA	**106.91**	**9.65**
5	95.93	117.51	113.17	**108.87**	**9.32**	109.45	103.83	NA	**106.64**	**3.97**
10	93.91	119.91	112.83	**108.88**	**10.97**	114.52	107.77	NA	**111.14**	**4.77**
30	96.31	113.33	112.76	**107.47**	**7.89**	110.68	117.72	NA	**114.20**	**4.97**
50	95.48	110.14	111.52	**105.72**	**7.26**	117.09	112.91	NA	**115.00**	**2.95**
100	94.36	104.87	105.05	**101.42**	**5.00**	121.88	116.81	NA	**119.34**	**3.59**
300	99.67	107.71	59.27	**88.88**	**21.20**	120.03	114.29	NA	**117.16**	**4.06**
Upcyte hepatocytes										
	N=1	**N=2**	**N=3**	**mean**	**stDev**	**N=1**	**N=2**	**N=3**	**mean**	**stDev**
0	100.00	100.00	NA	**100.00**	**0.00**	100.00	100.00	NA	**100.00**	**0.00**
3	107.88	113.42	NA	**110.65**	**3.92**	104.93	94.43	NA	**99.68**	**7.43**
5	111.93	114.75	NA	**113.34**	**1.99**	98.05	98.19	NA	**98.12**	**0.10**
10	114.85	114.93	NA	**114.89**	**0.06**	93.07	105.57	NA	**99.32**	**8.83**
30	111.64	114.68	NA	**113.16**	**2.15**	93.79	105.30	NA	**99.54**	**8.14**
50	105.29	112.25	NA	**108.77**	**4.92**	101.78	107.48	NA	**104.63**	**4.03**
100	96.97	95.69	NA	**96.33**	**0.90**	134.40	108.79	NA	**121.60**	**18.11**
300	68.65	76.84	NA	**72.75**	**5.79**	184.10	103.41	NA	**143.75**	**57.05**

Bosentan 72h

BOS [µM]	72h ATP					72h Resazurin				
HepG2										
	N=1	**N=2**	**N=3**	**mean**	**stDev**	**N=1**	**N=2**	**N=3**	**mean**	**stDev**
0	100.00	100.00	100.00	**100.00**	**0.00**	100.00	100.00	100.00	**100.00**	**0.00**
3	114.23	116.41	114.79	**115.14**	**1.13**	100.50	98.96	105.47	**101.64**	**3.41**
5	136.90	125.60	119.25	**127.25**	**8.94**	105.66	100.78	102.44	**102.96**	**2.48**
10	132.80	112.11	120.08	**121.66**	**10.44**	106.50	99.47	103.78	**103.25**	**3.54**
30	96.06	98.54	97.62	**97.41**	**1.25**	99.23	99.93	105.22	**101.46**	**3.28**
50	110.17	65.52	79.47	**85.05**	**22.84**	101.03	91.84	98.45	**97.10**	**4.74**
100	70.17	39.75	39.30	**49.74**	**17.70**	89.82	94.29	94.34	**92.82**	**2.60**
300	45.36	26.26	22.77	**31.46**	**12.16**	64.85	69.82	67.98	**67.55**	**2.51**
HepaRG										
	N=1	**N=2**	**N=3**	**mean**	**stDev**	**N=1**	**N=2**	**N=3**	**mean**	**stDev**
0	100.00	100.00	NA	**100.00**	**0.00**	100.00	100.00	NA	**100.00**	**0.00**
3	103.75	103.06	NA	**103.40**	**0.48**	100.87	99.71	NA	**100.29**	**0.82**
5	101.71	104.87	NA	**103.29**	**2.24**	102.14	106.57	NA	**104.36**	**3.13**
10	103.74	101.46	NA	**102.60**	**1.61**	101.69	104.24	NA	**102.96**	**1.80**
30	93.54	103.05	NA	**98.29**	**6.72**	103.20	116.19	NA	**109.70**	**9.19**
50	91.89	108.04	NA	**99.97**	**11.42**	102.99	119.43	NA	**111.21**	**11.62**
100	95.24	104.34	NA	**99.79**	**6.43**	103.49	120.86	NA	**112.17**	**12.28**
300	92.62	94.26	NA	**93.44**	**1.16**	106.99	122.02	NA	**114.51**	**10.62**
Upcyte hepatocytes										
	N=1	**N=2**	**N=3**	**mean**	**stDev**	**N=1**	**N=2**	**N=3**	**mean**	**stDev**
0	100.00	100.00	NA	**100.00**	**0.00**	100.00	100.00	NA	**100.00**	**0.00**
3	102.83	100.00	NA	**101.42**	**2.00**	94.88	96.54	NA	**95.71**	**1.18**
5	106.11	110.07	NA	**108.09**	**2.80**	79.72	99.29	NA	**89.50**	**13.84**
10	108.99	115.92	NA	**112.46**	**4.90**	65.67	97.23	NA	**81.45**	**22.31**
30	110.27	118.21	NA	**114.24**	**5.61**	68.46	98.38	NA	**83.42**	**21.16**
50	105.27	107.92	NA	**106.59**	**1.88**	71.06	97.66	NA	**84.36**	**18.81**
100	93.88	72.45	NA	**83.16**	**15.16**	61.62	95.61	NA	**78.61**	**24.04**
300	15.20	13.60	NA	**14.40**	**1.13**	14.72	44.86	NA	**29.79**	**21.31**

Buspirone 24h

BUS [µM]	24h ATP					24h Resazurin				
HepG2										
	N=1	**N=2**	**N=3**	**mean**	**stDev**	**N=1**	**N=2**	**N=3**	**mean**	**stDev**
0	100.00	100.00	100.00	**100.00**	**0.00**	100.00	100.00	100.00	**100.00**	**0.00**
3	106.75	115.19	107.53	**109.82**	**3.81**	99.97	101.71	103.99	**101.89**	**1.65**
5	104.67	118.37	110.41	**111.15**	**5.62**	105.52	102.15	104.29	**103.99**	**1.39**
10	108.12	110.41	110.27	**109.60**	**1.05**	103.93	101.10	100.91	**101.98**	**1.38**
30	97.88	104.13	102.75	**101.59**	**2.68**	106.88	100.83	104.67	**104.13**	**2.50**
50	92.65	94.21	98.53	**95.13**	**2.49**	108.08	100.86	103.47	**104.14**	**2.98**
100	79.96	87.64	87.88	**85.16**	**3.68**	110.16	98.53	104.04	**104.25**	**4.75**
300	72.86	77.96	87.31	**79.38**	**5.98**	98.36	94.10	98.78	**97.08**	**2.12**
HepaRG										
	N=1	**N=2**	**N=3**	**mean**	**stDev**	**N=1**	**N=2**	**N=3**	**mean**	**stDev**
0	100.00	100.00	100.00	**100.00**	**0.00**	100.00	100.00	NA	**100.00**	**0.00**
3	97.38	116.36	112.47	**108.74**	**8.19**	114.37	94.41	NA	**104.39**	**14.12**
5	94.70	108.60	120.32	**107.88**	**10.47**	114.77	105.50	NA	**110.14**	**6.55**
10	98.90	115.15	116.94	**110.33**	**8.11**	109.07	102.70	NA	**105.88**	**4.51**
30	99.16	112.05	122.17	**111.13**	**9.42**	116.92	106.11	NA	**111.51**	**7.64**
50	84.99	111.05	121.47	**105.83**	**15.34**	117.08	102.83	NA	**109.95**	**10.08**
100	104.22	98.46	120.46	**107.71**	**9.32**	122.89	94.26	NA	**108.58**	**20.24**
300	91.28	99.44	97.34	**96.02**	**3.46**	113.56	96.45	NA	**105.01**	**12.10**
Upcyte hepatocytes										
	N=1	**N=2**	**N=3**	**mean**	**stDev**	**N=1**	**N=2**	**N=3**	**mean**	**stDev**
0	100.00	100.00	NA	**100.00**	**0.00**	100.00	100.00	NA	**100.00**	**0.00**
3	94.58	115.73	NA	**105.16**	**14.95**	103.87	96.84	NA	**100.35**	**4.97**
5	97.79	109.98	NA	**103.88**	**8.61**	103.74	99.75	NA	**101.74**	**2.82**
10	93.96	113.00	NA	**103.48**	**13.47**	98.82	98.40	NA	**98.61**	**0.29**
30	99.49	108.32	NA	**103.90**	**6.24**	111.07	100.77	NA	**105.92**	**7.28**
50	94.86	108.73	NA	**101.79**	**9.81**	134.96	98.26	NA	**116.61**	**25.95**
100	95.31	98.42	NA	**96.87**	**2.20**	150.30	101.42	NA	**125.86**	**34.56**
300	79.68	70.82	NA	**75.25**	**6.26**	181.17	95.81	NA	**138.49**	**60.36**

Buspirone 72h

BUS [µM]	72h ATP					72h Resazurin				
HepG2										
	N=1	**N=2**	**N=3**	**mean**	**stDev**	**N=1**	**N=2**	**N=3**	**mean**	**stDev**
0	100.00	100.00	100.00	**100.00**	**0.00**	100.00	100.00	100.00	**100.00**	**0.00**
3	103.41	97.28	101.08	**100.59**	**3.10**	106.55	98.32	82.06	**95.64**	**12.46**
5	119.56	100.77	95.16	**105.16**	**12.78**	112.53	99.34	95.53	**102.47**	**8.92**
10	104.68	81.95	82.97	**89.87**	**12.84**	112.10	92.50	98.56	**101.05**	**10.03**
30	60.67	47.05	39.60	**49.10**	**10.68**	114.15	93.92	99.41	**102.49**	**10.46**
50	57.71	35.99	30.20	**41.30**	**14.50**	114.25	94.73	103.60	**104.19**	**9.77**
100	55.20	24.99	23.02	**34.40**	**18.04**	113.99	97.46	106.98	**106.14**	**8.30**
300	90.13	19.78	21.88	**43.93**	**40.02**	103.14	76.07	103.09	**94.10**	**15.62**
HepaRG										
	N=1	**N=2**	**N=3**	**mean**	**stDev**	**N=1**	**N=2**	**N=3**	**mean**	**stDev**
0	100.00	100.00	NA	**100.00**	**0.00**	100.00	100.00	NA	**100.00**	**0.00**
3	99.38	87.84	NA	**93.61**	**8.16**	101.65	61.08	NA	**81.37**	**28.68**
5	103.18	108.34	NA	**105.76**	**3.65**	102.41	92.21	NA	**97.31**	**7.21**
10	97.18	116.39	NA	**106.79**	**13.58**	102.00	83.22	NA	**92.61**	**13.28**
30	99.94	122.18	NA	**111.06**	**15.73**	103.25	92.06	NA	**97.66**	**7.92**
50	95.10	119.73	NA	**107.42**	**17.42**	103.65	109.66	NA	**106.65**	**4.25**
100	95.47	97.99	NA	**96.73**	**1.78**	105.27	86.44	NA	**95.86**	**13.32**
300	59.73	124.55	NA	**92.14**	**45.84**	86.36	109.34	NA	**97.85**	**16.25**
Upcyte hepatocytes										
	N=1	**N=2**	**N=3**	**mean**	**stDev**	**N=1**	**N=2**	**N=3**	**mean**	**stDev**
0	100.00	100.00	NA	**100.00**	**0.00**	100.00	100.00	NA	**100.00**	**0.00**
3	94.73	109.68	NA	**102.20**	**10.57**	75.95	100.48	NA	**88.22**	**17.35**
5	105.06	113.74	NA	**109.40**	**6.14**	54.05	99.44	NA	**76.75**	**32.10**
10	100.24	118.59	NA	**109.42**	**12.97**	59.73	98.97	NA	**79.35**	**27.74**
30	104.62	118.79	NA	**111.70**	**10.02**	55.37	107.34	NA	**81.36**	**36.75**
50	102.56	119.98	NA	**111.27**	**12.32**	62.22	104.03	NA	**83.12**	**29.57**
100	99.34	125.09	NA	**112.21**	**18.21**	73.25	96.61	NA	**84.93**	**16.52**
30.000	55.33	119.09	NA	**87.21**	**45.09**	55.56	105.41	NA	**80.49**	**35.25**

Diclofenac 24h

DCF [µM]	24h ATP					24h Resazurin				
HepG2										
	N=1	**N=2**	**N=3**	**mean**	**stDev**	**N=1**	**N=2**	**N=3**	**mean**	**stDev**
0	100.00	100.00	100.00	**100.00**	**0.00**	100.00	100.00	100.00	**100.00**	**0.00**
10	116.06	90.21	80.84	**95.70**	**14.89**	94.54	97.04	95.16	**95.58**	**1.06**
30	105.28	92.80	78.92	**92.33**	**10.77**	97.02	96.01	93.91	**95.65**	**1.29**
50	84.56	92.42	79.53	**85.50**	**5.30**	94.65	93.73	92.94	**93.77**	**0.70**
100	84.11	89.52	78.08	**83.90**	**4.67**	87.17	91.20	89.26	**89.21**	**1.65**
300	65.28	82.34	66.53	**71.38**	**7.77**	70.52	83.89	82.42	**78.94**	**5.99**
500	58.19	6.93	2.49	**22.54**	**25.27**	49.13	37.05	34.57	**40.25**	**6.36**
1.000	126.79	103.30	83.77	**104.62**	**17.59**	99.86	99.04	98.77	**99.22**	**0.46**
HepaRG										
	N=1	**N=2**	**N=3**	**mean**	**stDev**	**N=1**	**N=2**	**N=3**	**mean**	**stDev**
0	100.00	100.00	100.00	**100.00**	**0.00**	100.00	100.00	NA	**100.00**	**0.00**
10	91.26	111.07	95.61	**99.31**	**8.50**	105.16	82.38	NA	**93.77**	**16.10**
30	89.18	123.73	100.45	**104.46**	**14.39**	105.44	111.64	NA	**108.54**	**4.38**
50	91.39	114.60	101.18	**102.39**	**9.51**	108.87	126.10	NA	**117.49**	**12.18**
100	100.94	122.48	102.35	**108.59**	**9.84**	106.73	138.79	NA	**122.76**	**22.67**
300	97.57	112.62	99.95	**103.38**	**6.61**	108.05	124.90	NA	**116.48**	**11.91**
500	78.35	69.01	83.94	**77.10**	**6.16**	107.09	106.06	NA	**106.58**	**0.73**
1.000	49.62	64.11	42.12	**51.95**	**9.13**	89.14	67.94	NA	**78.54**	**14.99**
Upcyte hepatocytes										
	N=1	**N=2**	**N=3**	**mean**	**stDev**	**N=1**	**N=2**	**N=3**	**mean**	**stDev**
0	100.00	100.00	NA	**100.00**	**0.00**	100.00	100.00	NA	**100.00**	**0.00**
10	90.93	103.42	NA	**97.18**	**8.83**	100.34	96.61	NA	**98.47**	**2.64**
30	84.07	100.49	NA	**92.28**	**11.61**	104.66	94.76	NA	**99.71**	**7.00**
50	93.77	101.89	NA	**97.83**	**5.74**	103.64	105.93	NA	**104.79**	**1.62**
100	83.73	99.73	NA	**91.73**	**11.31**	97.67	94.92	NA	**96.30**	**1.94**
300	81.26	86.45	NA	**83.85**	**3.67**	99.44	95.20	NA	**97.32**	**3.00**
500	57.08	68.63	NA	**62.85**	**8.16**	100.48	106.97	NA	**103.72**	**4.59**
1.000	87.90	98.47	NA	**93.19**	**7.47**	82.72	101.73	NA	**92.23**	**13.44**

Diclofenac 72h

DCF [µM]	72h ATP					72h Resazurin				
HepG2										
	N=1	**N=2**	**N=3**	**mean**	**stDev**	**N=1**	**N=2**	**N=3**	**mean**	**stDev**
0	100.00	100.00	100.00	**100.00**	**0.00**	100.00	100.00	100.00	**100.00**	**0.00**
10	92.42	124.90	113.48	**110.27**	**16.47**	81.20	97.76	100.77	**93.24**	**10.54**
30	84.75	145.83	116.93	**115.84**	**30.55**	94.83	97.98	97.72	**96.84**	**1.75**
50	51.22	87.70	86.19	**75.04**	**20.64**	76.34	92.80	93.75	**87.63**	**9.79**
100	28.49	29.17	28.83	**28.83**	**0.34**	50.06	67.13	61.98	**59.72**	**8.76**
300	24.36	22.35	21.48	**22.73**	**1.48**	34.28	50.46	43.53	**42.76**	**8.12**
500	13.04	20.59	15.24	**16.29**	**3.89**	15.70	27.66	26.57	**23.31**	**6.62**
1.000	0.25	6.73	6.67	**4.55**	**3.72**	0.09	14.11	10.46	**8.22**	**7.27**
HepaRG										
	N=1	**N=2**	**N=3**	**mean**	**stDev**	**N=1**	**N=2**	**N=3**	**mean**	**stDev**
0	100.00	100.00	100.00	**100.00**	**0.00**	100.00	100.00	NA	**100.00**	**0.00**
10	109.41	95.63	89.36	**98.13**	**10.26**	95.44	95.17	NA	**95.31**	**0.19**
30	115.10	100.00	95.31	**103.47**	**10.34**	95.53	100.00	NA	**97.77**	**3.16**
50	111.16	96.41	91.26	**99.61**	**10.33**	95.14	103.36	NA	**99.25**	**5.81**
100	108.57	94.20	90.48	**97.75**	**9.55**	102.00	102.04	NA	**102.02**	**0.03**
300	106.87	86.60	86.42	**93.30**	**11.76**	98.26	104.56	NA	**101.41**	**4.46**
500	61.86	30.52	46.95	**46.44**	**15.68**	74.93	77.25	NA	**76.09**	**1.64**
1.000	16.52	4.57	8.11	**9.73**	**6.14**	29.04	24.05	NA	**26.55**	**3.53**
Upcyte hepatocytes										
	N=1	**N=2**	**N=3**	**mean**	**stDev**	**N=1**	**N=2**	**N=3**	**mean**	**stDev**
0	100.00	100.00	NA	**100.00**	**0.00**	100.00	100.00	NA	**100.00**	**0.00**
10	102.28	108.80	NA	**105.54**	**4.61**	113.98	100.39	NA	**107.18**	**9.60**
30	113.14	118.13	NA	**115.63**	**3.53**	96.39	101.13	NA	**98.76**	**3.36**
50	108.82	123.47	NA	**116.15**	**10.36**	97.04	103.56	NA	**100.30**	**4.61**
100	116.21	128.94	NA	**122.57**	**9.00**	99.99	93.91	NA	**96.95**	**4.30**
300	123.44	129.94	NA	**126.69**	**4.60**	104.19	97.36	NA	**100.77**	**4.83**
500	80.14	99.91	NA	**90.02**	**13.98**	72.24	68.43	NA	**70.34**	**2.70**
1.000	58.02	44.23	NA	**51.13**	**9.75**	108.85	98.60	NA	**103.73**	**7.25**

Entacapone 24h

ENT [µM]	24h ATP					24h Resazurin				
HepG2										
	N=1	**N=2**	**N=3**	**mean**	**stDev**	**N=1**	**N=2**	**N=3**	**mean**	**stDev**
0	100.00	100.00	100.00	**100.00**	**0.00**	100.00	100.00	100.00	**100.00**	**0.00**
10	84.62	105.22	102.23	**97.35**	**9.09**	97.69	97.77	99.36	**98.27**	**0.77**
30	81.64	97.65	92.54	**90.61**	**6.68**	99.46	98.89	98.89	**99.08**	**0.27**
50	75.45	97.00	92.60	**88.35**	**9.30**	95.76	99.19	98.28	**97.75**	**1.45**
100	71.60	93.36	81.66	**82.21**	**8.89**	98.92	96.80	96.17	**97.30**	**1.18**
300	75.01	80.14	73.07	**76.07**	**2.98**	89.03	94.53	94.21	**92.59**	**2.52**
500	65.70	70.62	61.99	**66.11**	**3.54**	78.17	84.46	88.36	**83.66**	**4.20**
1.000	38.39	44.95	38.75	**40.70**	**3.01**	96.55	96.56	99.91	**97.67**	**1.58**
HepaRG										
	N=1	**N=2**	**N=3**	**mean**	**stDev**	**N=1**	**N=2**	**N=3**	**mean**	**stDev**
0	100.00	100.00	100.00	**100.00**	**0.00**	100.00	100.00	NA	**100.00**	**0.00**
10	99.68	126.17	100.88	**108.91**	**12.21**	99.88	121.55	NA	**110.72**	**15.33**
30	101.65	135.12	107.79	**114.85**	**14.55**	100.56	115.43	NA	**107.99**	**10.51**
50	102.65	137.83	106.34	**115.61**	**15.79**	106.34	117.70	NA	**112.02**	**8.03**
100	103.13	132.54	106.90	**114.19**	**13.07**	109.14	125.42	NA	**117.28**	**11.51**
300	102.45	127.77	100.70	**110.31**	**12.37**	104.85	130.39	NA	**117.62**	**18.06**
500	93.92	100.92	64.32	**86.39**	**15.87**	103.87	125.08	NA	**114.48**	**15.00**
1.000	57.77	14.36	14.55	**28.90**	**20.42**	102.50	86.61	NA	**94.55**	**11.23**
Upcyte hepatocytes										
	N=1	**N=2**	**N=3**	**mean**	**stDev**	**N=1**	**N=2**	**N=3**	**mean**	**stDev**
0	100.00	100.00	NA	**100.00**	**0.00**	100.00	100.00	NA	**100.00**	**0.00**
10	101.73	100.36	NA	**101.04**	**0.97**	103.61	100.58	NA	**102.09**	**2.14**
30	97.15	105.38	NA	**101.27**	**5.82**	92.63	101.61	NA	**97.12**	**6.35**
50	98.62	102.36	NA	**100.49**	**2.64**	114.08	103.71	NA	**108.89**	**7.34**
100	88.73	89.95	NA	**89.34**	**0.86**	106.71	100.14	NA	**103.42**	**4.65**
300	64.72	61.91	NA	**63.32**	**1.98**	154.40	113.94	NA	**134.17**	**28.61**
500	68.29	64.25	NA	**66.27**	**2.86**	164.77	106.58	NA	**135.68**	**41.15**
1.000	54.18	53.82	NA	**54.00**	**0.26**	155.12	106.26	NA	**130.69**	**34.55**

Entacapone 72h

ENT [µM]	72h ATP					72h Resazurin				
HepG2										
	N=1	**N=2**	**N=3**	**mean**	**stDev**	**N=1**	**N=2**	**N=3**	**mean**	**stDev**
0	100.00	100.00	100.00	**100.00**	**0.00**	100.00	100.00	100.00	**100.00**	**0.00**
10	30.58	63.03	59.45	**51.02**	**17.79**	59.63	89.20	93.27	**80.70**	**18.36**
30	25.61	46.55	48.53	**40.23**	**12.70**	52.30	80.99	85.60	**72.96**	**18.04**
50	19.80	10.68	12.54	**14.34**	**4.82**	42.07	41.76	38.46	**40.76**	**2.00**
100	18.60	12.31	13.14	**14.68**	**3.42**	42.83	45.05	43.88	**43.92**	**1.11**
300	19.02	13.10	14.22	**15.45**	**3.14**	41.08	48.34	43.91	**44.44**	**3.66**
500	16.50	11.00	9.77	**12.42**	**3.58**	34.92	30.28	31.20	**32.13**	**2.45**
1.000	4.03	6.32	6.60	**5.65**	**1.41**	9.12	20.70	18.25	**16.02**	**6.10**
HepaRG										
	N=1	**N=2**	**N=3**	**mean**	**stDev**	**N=1**	**N=2**	**N=3**	**mean**	**stDev**
0	100.00	100.00	100.00	**100.00**	**0.00**	100.00	100.00	NA	**100.00**	**0.00**
10	109.88	100.00	103.76	**104.55**	**4.99**	100.53	90.86	NA	**95.70**	**6.83**
30	114.07	101.69	100.07	**105.27**	**7.66**	101.63	94.32	NA	**97.98**	**5.17**
50	114.09	107.91	98.90	**106.97**	**7.64**	101.29	99.47	NA	**100.38**	**1.29**
100	105.60	105.43	97.18	**102.73**	**4.81**	99.55	96.79	NA	**98.17**	**1.95**
300	105.44	97.26	93.18	**98.63**	**6.25**	102.06	103.40	NA	**102.73**	**0.95**
500	6.96	9.24	14.97	**10.39**	**4.13**	93.27	61.32	NA	**77.30**	**22.59**
1.000	1.09	0.07	0.28	**0.48**	**0.54**	6.25	11.74	NA	**8.99**	**3.88**
Upcyte hepatocytes										
	N=1	**N=2**	**N=3**	**mean**	**stDev**	**N=1**	**N=2**	**N=3**	**mean**	**stDev**
0	100.00	100.00	NA	**100.00**	**0.00**	100.00	100.00	NA	**100.00**	**0.00**
10	101.16	116.51	NA	**108.84**	**10.86**	96.27	91.80	NA	**94.04**	**3.16**
30	100.30	121.67	NA	**110.99**	**15.11**	90.49	107.39	NA	**98.94**	**11.95**
50	97.76	114.92	NA	**106.34**	**12.13**	74.06	100.11	NA	**87.09**	**18.42**
100	44.52	71.65	NA	**58.08**	**19.18**	53.74	83.93	NA	**68.84**	**21.35**
300	18.70	40.77	NA	**29.73**	**15.61**	21.67	53.85	NA	**37.76**	**22.75**
500	9.72	8.67	NA	**9.19**	**0.74**	36.30	38.51	NA	**37.40**	**1.57**
1.000	4.19	11.48	NA	**7.83**	**5.15**	24.13	44.64	NA	**34.38**	**14.50**

Metformin 24h

MET [µM]	24h ATP					24h Resazurin				
HepG2										
	N=1	**N=2**	**N=3**	**mean**	**stDev**	**N=1**	**N=2**	**N=3**	**mean**	**stDev**
0	100.00	100.00	100.00	**100.00**	**0.00**	100.00	100.00	100.00	**100.00**	**0.00**
3	110.01	89.37	105.80	**101.73**	**8.91**	99.22	99.72	100.57	**99.84**	**0.56**
5	105.22	92.51	110.83	**102.85**	**7.66**	101.35	100.83	102.45	**101.54**	**0.67**
10	103.41	98.12	107.71	**103.08**	**3.92**	106.68	101.36	94.97	**101.01**	**4.79**
30	111.72	94.11	104.55	**103.46**	**7.23**	103.45	100.73	101.64	**101.94**	**1.13**
50	113.86	95.42	109.00	**106.09**	**7.80**	98.90	99.08	101.76	**99.91**	**1.31**
100	118.51	92.76	109.07	**106.78**	**10.64**	102.76	98.75	100.59	**100.70**	**1.64**
300	109.65	94.90	105.87	**103.47**	**6.25**	102.47	101.18	100.63	**101.43**	**0.77**
HepaRG										
	N=1	**N=2**	**N=3**	**mean**	**stDev**	**N=1**	**N=2**	**N=3**	**mean**	**stDev**
0	100.00	100.00	100.00	**100.00**	**0.00**	100.00	100.00	NA	**100.00**	**0.00**
3	98.64	126.64	105.48	**110.25**	**11.92**	104.99	118.39	NA	**111.69**	**9.47**
5	97.67	146.85	113.14	**119.22**	**20.53**	102.77	125.82	NA	**114.30**	**16.30**
10	100.14	136.93	113.39	**116.82**	**15.21**	109.83	120.56	NA	**115.19**	**7.59**
30	105.36	145.26	116.55	**122.39**	**16.80**	110.84	125.95	NA	**118.39**	**10.69**
50	105.98	145.72	118.31	**123.34**	**16.61**	107.00	123.87	NA	**115.43**	**11.93**
100	105.41	135.68	116.85	**119.31**	**12.48**	108.09	121.76	NA	**114.92**	**9.66**
300	101.78	144.40	103.22	**116.47**	**19.76**	105.10	107.17	NA	**106.14**	**1.46**
Upcyte hepatocytes										
	N=1	**N=2**	**N=3**	**mean**	**stDev**	**N=1**	**N=2**	**N=3**	**mean**	**stDev**
0	100.00	100.00	NA	**100.00**	**0.00**	100.00	100.00	NA	**100.00**	**0.00**
3	86.50	108.88	NA	**97.69**	**15.83**	115.48	97.10	NA	**106.29**	**13.00**
5	88.57	109.66	NA	**99.12**	**14.91**	121.27	94.56	NA	**107.91**	**18.89**
10	90.84	111.74	NA	**101.29**	**14.78**	121.29	95.39	NA	**108.34**	**18.31**
30	93.42	110.59	NA	**102.01**	**12.14**	139.97	96.53	NA	**118.25**	**30.72**
50	97.92	107.64	NA	**102.78**	**6.87**	118.57	97.27	NA	**107.92**	**15.06**
100	92.66	96.70	NA	**94.68**	**2.86**	151.68	94.04	NA	**122.86**	**40.76**
300	92.83	91.67	NA	**92.25**	**0.82**	134.07	101.16	NA	**117.61**	**23.27**

Metformin 72h

MET [µM]	72h ATP					72h Resazurin				
HepG2										
	N=1	**N=2**	**N=3**	**mean**	**stDev**	**N=1**	**N=2**	**N=3**	**mean**	**stDev**
0	100.00	100.00	100.00	**100.00**	**0.00**	100.00	100.00	100.00	**100.00**	**0.00**
3	57.09	82.04	54.62	**64.58**	**15.17**	86.84	96.78	93.17	**92.26**	**5.03**
5	86.52	111.24	44.14	**80.63**	**33.93**	96.74	99.42	92.01	**96.06**	**3.75**
10	81.40	89.87	47.53	**72.93**	**22.41**	96.66	96.09	93.20	**95.31**	**1.86**
30	76.03	83.82	37.42	**65.76**	**24.85**	96.04	96.10	90.57	**94.24**	**3.18**
50	82.25	84.18	53.60	**73.35**	**17.13**	91.58	99.02	94.37	**94.99**	**3.76**
100	92.49	99.40	54.74	**82.21**	**24.04**	94.05	98.56	94.39	**95.67**	**2.51**
300	99.77	93.58	47.68	**80.34**	**28.45**	98.28	97.95	93.78	**96.67**	**2.51**
HepaRG										
	N=1	**N=2**	**N=3**	**mean**	**stDev**	**N=1**	**N=2**	**N=3**	**mean**	**stDev**
0	100.00	100.00	100.00	**100.00**	**0.00**	100.00	100.00	NA	**100.00**	**0.00**
3	116.22	104.61	104.48	**108.44**	**6.74**	101.68	71.04	NA	**86.36**	**21.66**
5	122.25	115.76	105.08	**114.36**	**8.67**	102.99	96.83	NA	**99.91**	**4.36**
10	124.01	106.20	104.30	**111.50**	**10.87**	102.43	98.25	NA	**100.34**	**2.95**
30	124.37	113.32	103.44	**113.71**	**10.47**	103.20	99.09	NA	**101.14**	**2.90**
50	114.01	89.38	105.59	**102.99**	**12.52**	103.59	94.02	NA	**98.80**	**6.76**
100	117.28	100.20	105.45	**107.65**	**8.75**	104.07	98.61	NA	**101.34**	**3.86**
300	97.03	120.70	103.89	**107.21**	**12.18**	103.32	68.24	NA	**85.78**	**24.81**
Upcyte hepatocytes										
	N=1	**N=2**	**N=3**	**mean**	**stDev**	**N=1**	**N=2**	**N=3**	**mean**	**stDev**
0	100.00	100.00	NA	**100.00**	**0.00**	100.00	100.00	NA	**100.00**	**0.00**
3	112.03	111.44	NA	**111.74**	**0.42**	100.06	89.28	NA	**94.67**	**7.62**
5	116.33	128.72	NA	**122.52**	**8.77**	72.85	81.57	NA	**77.21**	**6.17**
10	110.39	127.82	NA	**119.11**	**12.32**	55.08	95.35	NA	**75.21**	**28.47**
30	115.02	125.55	NA	**120.29**	**7.44**	79.67	100.51	NA	**90.09**	**14.74**
50	116.81	131.64	NA	**124.22**	**10.49**	69.90	93.52	NA	**81.71**	**16.70**
100	122.29	137.06	NA	**129.68**	**10.44**	106.18	107.46	NA	**106.82**	**0.90**
300	119.83	124.64	NA	**122.24**	**3.40**	73.50	95.81	NA	**84.66**	**15.77**

Nefazodone 24h

NEF [µM]	24h ATP					24h Resazurin				
HepG2										
	N=1	**N=2**	**N=3**	**mean**	**stDev**	**N=1**	**N=2**	**N=3**	**mean**	**stDev**
0	100.00	100.00	100.00	**100.00**	**0.00**	100.00	100.00	100.00	**100.00**	**0.00**
3	88.09	103.73	99.93	**97.25**	**6.66**	97.11	98.54	100.55	**98.73**	**1.41**
5	80.65	100.04	97.98	**92.89**	**8.70**	101.23	100.28	98.00	**99.84**	**1.36**
10	66.18	94.94	89.72	**83.62**	**12.51**	96.72	98.23	99.18	**98.04**	**1.01**
30	33.74	83.16	80.34	**65.75**	**22.66**	95.49	95.96	96.48	**95.98**	**0.41**
50	7.00	63.77	56.53	**42.43**	**25.23**	93.57	93.91	94.46	**93.98**	**0.37**
100	2.60	10.67	9.30	**7.52**	**3.52**	94.28	67.15	80.47	**80.63**	**11.08**
300	-0.47	2.74	2.39	**1.56**	**1.44**	90.28	33.49	50.29	**58.02**	**23.82**
HepaRG										
	N=1	**N=2**	**N=3**	**mean**	**stDev**	**N=1**	**N=2**	**N=3**	**mean**	**stDev**
0	100.00	100.00	100.00	**100.00**	**0.00**	100.00	100.00	NA	**100.00**	**0.00**
3	94.42	101.46	95.31	**97.06**	**3.13**	99.60	68.86	NA	**84.23**	**21.73**
5	97.05	99.68	97.86	**98.20**	**1.10**	102.80	71.68	NA	**87.24**	**22.01**
10	99.33	102.58	102.50	**101.47**	**1.52**	101.09	95.69	NA	**98.39**	**3.81**
30	100.26	105.46	99.91	**101.88**	**2.54**	105.22	92.61	NA	**98.91**	**8.92**
50	95.22	100.55	99.11	**98.29**	**2.25**	107.80	77.89	NA	**92.85**	**21.15**
100	62.40	74.54	93.38	**76.77**	**12.75**	107.20	61.20	NA	**84.20**	**32.53**
300	-0.21	-0.12	14.12	**4.60**	**6.73**	5.94	6.98	NA	**6.46**	**0.73**
Upcyte hepatocytes										
	N=1	**N=2**	**N=3**	**mean**	**stDev**	**N=1**	**N=2**	**N=3**	**mean**	**stDev**
0	100.00	100.00	NA	**100.00**	**0.00**	100.00	100.00	NA	**100.00**	**0.00**
3	84.24	93.58	NA	**88.91**	**6.60**	132.06	102.23	NA	**117.15**	**21.09**
5	85.49	90.70	NA	**88.09**	**3.68**	127.73	101.21	NA	**114.47**	**18.75**
10	81.07	80.99	NA	**81.03**	**0.06**	144.22	97.69	NA	**120.96**	**32.91**
30	88.98	82.08	NA	**85.53**	**4.88**	121.76	103.31	NA	**112.53**	**13.05**
50	74.33	72.41	NA	**73.37**	**1.36**	176.08	106.92	NA	**141.50**	**48.90**
100	58.51	85.49	NA	**72.00**	**19.08**	163.94	107.73	NA	**135.83**	**39.75**
300	-0.12	64.60	NA	**32.24**	**45.76**	20.41	104.36	NA	**62.39**	**59.36**

Nefazodone 72h

NEF [µM]	72h ATP					72h Resazurin				
HepG2										
	N=1	**N=2**	**N=3**	**mean**	**stDev**	**N=1**	**N=2**	**N=3**	**mean**	**stDev**
0	100.00	100.00	100.00	**100.00**	**0.00**	100.00	100.00	100.00	**100.00**	**0.00**
3	94.95	71.20	95.15	**87.10**	**13.77**	79.01	93.62	95.30	**89.31**	**8.96**
5	87.54	53.93	14.90	**52.12**	**36.35**	97.78	96.67	98.77	**97.74**	**1.05**
10	52.16	14.56	5.13	**23.95**	**24.88**	91.70	87.79	87.70	**89.07**	**2.29**
30	19.46	8.35	0.59	**9.46**	**9.48**	51.88	45.66	32.95	**43.50**	**9.65**
50	10.73	0.91	-0.21	**3.81**	**6.02**	35.17	5.86	-1.05	**13.33**	**19.23**
100	-0.46	-0.24	-0.20	**-0.30**	**0.14**	3.27	3.50	-4.26	**0.83**	**4.41**
300	-0.57	-0.24	-0.16	**-0.32**	**0.22**	-0.31	3.90	-5.10	**-0.50**	**4.51**
HepaRG										
	N=1	**N=2**	**N=3**	**mean**	**stDev**	**N=1**	**N=2**	**N=3**	**mean**	**stDev**
0	100.00	100.00	100.00	**100.00**	**0.00**	100.00	100.00	NA	**100.00**	**0.00**
3	105.47	91.02	99.82	**98.77**	**7.28**	101.40	56.43	NA	**78.92**	**31.80**
5	109.00	102.83	103.70	**105.18**	**3.34**	105.37	83.30	NA	**94.34**	**15.60**
10	113.25	109.11	103.31	**108.56**	**5.00**	105.69	87.65	NA	**96.67**	**12.75**
30	104.98	111.18	103.40	**106.52**	**4.11**	110.06	85.35	NA	**97.71**	**17.47**
50	111.26	107.54	105.69	**108.16**	**2.84**	110.23	84.34	NA	**97.29**	**18.31**
100	83.07	75.13	98.37	**85.52**	**11.81**	96.11	61.52	NA	**78.82**	**24.46**
300	-0.41	-0.37	19.81	**6.34**	**11.66**	0.62	0.79	NA	**0.71**	**0.12**
Upcyte hepatocytes										
	N=1	**N=2**	**N=3**	**mean**	**stDev**	**N=1**	**N=2**	**N=3**	**mean**	**stDev**
0	100.00	100.00	NA	**100.00**	**0.00**	100.00	100.00	NA	**100.00**	**0.00**
3	111.19	100.69	NA	**105.94**	**7.43**	135.99	96.51	NA	**116.25**	**27.92**
5	108.56	107.58	NA	**108.07**	**0.70**	145.91	95.42	NA	**120.66**	**35.70**
10	103.60	99.71	NA	**101.65**	**2.75**	138.22	92.58	NA	**115.40**	**32.27**
30	112.24	102.50	NA	**107.37**	**6.88**	126.38	97.46	NA	**111.92**	**20.45**
50	82.93	109.88	NA	**96.41**	**19.06**	144.74	92.49	NA	**118.61**	**36.94**
100	0.54	104.70	NA	**52.62**	**73.65**	12.22	91.60	NA	**51.91**	**56.13**
300	-0.60	78.56	NA	**38.98**	**55.98**	2.32	117.66	NA	**59.99**	**81.56**

Perhexiline 24h

PER [µM]	24h ATP					24h Resazurin				
HepG2										
	N=1	**N=2**	**N=3**	**mean**	**stDev**	**N=1**	**N=2**	**N=3**	**mean**	**stDev**
0	100.00	100.00	100.00	**100.00**	**0.00**	100.00	100.00	100.00	**100.00**	**0.00**
3	104.58	99.27	96.89	**100.25**	**3.21**	91.99	94.42	97.60	**94.67**	**2.30**
5	95.68	112.03	96.27	**101.32**	**7.57**	95.57	96.72	97.86	**96.72**	**0.94**
10	16.88	101.72	84.07	**67.55**	**36.55**	6.07	91.96	93.72	**63.92**	**40.91**
30	0.24	0.36	0.38	**0.33**	**0.06**	4.89	-1.60	3.18	**2.16**	**2.75**
50	0.08	-0.09	-0.02	**-0.01**	**0.07**	5.49	-2.19	3.37	**2.22**	**3.24**
100	0.12	-0.27	-0.20	**-0.12**	**0.17**	4.89	-3.56	1.87	**1.07**	**3.50**
300	0.34	-0.43	-0.36	**-0.15**	**0.35**	4.28	-4.75	0.87	**0.13**	**3.72**
HepaRG										
	N=1	**N=2**	**N=3**	**mean**	**stDev**	**N=1**	**N=2**	**N=3**	**mean**	**stDev**
0	100.00	100.00	100.00	**100.00**	**0.00**	100.00	100.00	NA	**100.00**	**0.00**
3	103.61	105.08	96.11	**101.60**	**3.93**	106.24	98.10	NA	**102.17**	**5.75**
5	103.65	109.67	96.70	**103.34**	**5.30**	104.47	102.45	NA	**103.46**	**1.43**
10	98.27	103.68	98.59	**100.18**	**2.48**	107.31	109.47	NA	**108.39**	**1.53**
30	83.71	98.68	90.60	**91.00**	**6.12**	103.03	112.77	NA	**107.90**	**6.89**
50	0.39	2.63	0.51	**1.18**	**1.03**	8.75	27.20	NA	**17.98**	**13.05**
100	-0.04	1.09	0.03	**0.36**	**0.52**	5.75	19.18	NA	**12.47**	**9.50**
300	-0.34	-0.10	-0.29	**-0.24**	**0.10**	2.48	2.78	NA	**2.63**	**0.21**
Upcyte hepatocytes										
	N=1	**N=2**	**N=3**	**mean**	**stDev**	**N=1**	**N=2**	**N=3**	**mean**	**stDev**
0	100.00	100.00	NA	**100.00**	**0.00**	100.00	100.00	NA	**100.00**	**0.00**
3	96.00	96.79	NA	**96.40**	**0.56**	80.80	99.27	NA	**90.04**	**13.06**
5	91.97	93.65	NA	**92.81**	**1.18**	145.57	102.87	NA	**124.22**	**30.19**
10	81.94	67.28	NA	**74.61**	**10.36**	125.07	89.45	NA	**107.26**	**25.18**
30	0.48	0.22	NA	**0.35**	**0.19**	25.99	3.81	NA	**14.90**	**15.68**
50	0.06	-0.04	NA	**0.01**	**0.07**	18.43	1.85	NA	**10.14**	**11.73**
100	-0.14	-0.21	NA	**-0.17**	**0.05**	23.67	1.92	NA	**12.80**	**15.38**
300	1.15	-0.39	NA	**0.38**	**1.09**	15.61	-0.32	NA	**7.65**	**11.26**

Perhexiline 72h

PER [µM]	72h ATP					72h Resazurin				
HepG2										
	N=1	**N=2**	**N=3**	**mean**	**stDev**	**N=1**	**N=2**	**N=3**	**mean**	**stDev**
0	100.00	100.00	100.00	**100.00**	**0.00**	100.00	100.00	100.00	**100.00**	**0.00**
3	22.92	54.43	68.77	**48.71**	**23.45**	41.60	98.03	101.05	**80.23**	**33.49**
5	0.17	1.01	14.88	**5.35**	**8.26**	0.15	13.39	79.35	**30.96**	**42.42**
10	0.21	0.26	0.24	**0.24**	**0.03**	0.12	-0.33	0.43	**0.08**	**0.38**
30	0.11	0.03	0.07	**0.07**	**0.04**	0.09	0.88	-0.87	**0.03**	**0.87**
50	-0.20	0.02	0.07	**-0.04**	**0.14**	0.08	1.08	-1.86	**-0.23**	**1.49**
100	-0.31	0.11	0.05	**-0.05**	**0.23**	0.04	0.14	-1.90	**-0.57**	**1.15**
300	-0.38	0.13	0.10	**-0.05**	**0.28**	0.29	-0.46	-3.34	**-1.17**	**1.91**
HepaRG										
	N=1	**N=2**	**N=3**	**mean**	**stDev**	**N=1**	**N=2**	**N=3**	**mean**	**stDev**
0	100.00	100.00	100.00	**100.00**	**0.00**	100.00	100.00	NA	**100.00**	**0.00**
3	114.88	115.97	99.17	**110.01**	**9.40**	102.13	91.08	NA	**96.60**	**7.82**
5	116.83	114.85	101.09	**110.93**	**8.57**	102.36	87.04	NA	**94.70**	**10.83**
10	116.08	110.94	102.05	**109.69**	**7.10**	103.71	90.42	NA	**97.07**	**9.39**
30	0.49	0.60	2.06	**1.05**	**0.88**	5.66	5.13	NA	**5.39**	**0.38**
50	0.02	0.14	0.50	**0.22**	**0.25**	4.05	2.71	NA	**3.38**	**0.95**
100	-0.22	-0.11	0.13	**-0.07**	**0.18**	5.37	1.84	NA	**3.61**	**2.49**
300	-0.47	-0.39	-0.23	**-0.36**	**0.12**	1.27	0.94	NA	**1.10**	**0.24**
Upcyte hepatocytes										
	N=1	**N=2**	**N=3**	**mean**	**stDev**	**N=1**	**N=2**	**N=3**	**mean**	**stDev**
0	100.00	100.00	NA	**100.00**	**0.00**	100.00	100.00	NA	**100.00**	**0.00**
3	110.18	95.48	NA	**102.83**	**10.39**	112.41	99.58	NA	**106.00**	**9.07**
5	109.83	93.80	NA	**101.81**	**11.33**	127.47	99.96	NA	**113.71**	**19.46**
10	88.26	7.54	NA	**47.90**	**57.08**	113.25	15.92	NA	**64.58**	**68.82**
30	0.49	0.11	NA	**0.30**	**0.27**	0.65	1.00	NA	**0.82**	**0.25**
50	0.06	-0.02	NA	**0.02**	**0.06**	-3.03	0.33	NA	**-1.35**	**2.37**
100	-0.19	-0.13	NA	**-0.16**	**0.04**	-0.72	0.55	NA	**-0.08**	**0.89**
300	-0.38	-0.35	NA	**-0.36**	**0.02**	-3.62	2.11	NA	**-0.75**	**4.05**

Pioglitazone 24h

PIO [µM]	24h ATP					24h Resazurin				
HepG2										
	N=1	**N=2**	**N=3**	**mean**	**stDev**	**N=1**	**N=2**	**N=3**	**mean**	**stDev**
0	100.00	100.00	100.00	**100.00**	**0.00**	100.00	100.00	100.00	**100.00**	**0.00**
3	140.37	100.67	103.43	**114.82**	**18.10**	96.84	95.93	99.26	**97.34**	**1.41**
5	128.29	105.58	109.23	**114.37**	**9.96**	102.11	96.48	93.47	**97.35**	**3.58**
10	117.86	104.92	108.05	**110.28**	**5.52**	98.56	96.72	97.72	**97.67**	**0.75**
30	138.92	112.50	107.84	**119.75**	**13.69**	98.64	94.72	95.46	**96.27**	**1.70**
50	130.35	114.45	105.29	**116.70**	**10.35**	97.83	99.04	98.72	**98.53**	**0.51**
100	122.31	110.73	105.33	**112.79**	**7.09**	98.78	100.77	98.18	**99.24**	**1.11**
300	124.02	107.88	104.53	**112.15**	**8.51**	99.65	100.23	98.76	**99.55**	**0.60**
HepaRG										
	N=1	**N=2**	**N=3**	**mean**	**stDev**	**N=1**	**N=2**	**N=3**	**mean**	**stDev**
0	100.00	100.00	100.00	**100.00**	**0.00**	100.00	100.00	NA	**100.00**	**0.00**
3	93.78	97.50	99.34	**96.87**	**2.32**	104.74	133.27	NA	**119.00**	**20.17**
5	95.43	103.30	103.22	**100.65**	**3.69**	104.44	147.30	NA	**125.87**	**30.31**
10	98.80	106.53	102.87	**102.73**	**3.15**	106.03	136.15	NA	**121.09**	**21.30**
30	98.59	104.13	103.39	**102.04**	**2.45**	107.95	145.58	NA	**126.76**	**26.61**
50	100.77	105.80	101.29	**102.62**	**2.26**	109.48	143.51	NA	**126.50**	**24.06**
100	95.40	99.05	103.14	**99.20**	**3.16**	108.69	140.64	NA	**124.66**	**22.59**
300	88.46	78.87	93.77	**87.04**	**6.17**	104.84	109.02	NA	**106.93**	**2.96**
Upcyte hepatocytes										
	N=1	**N=2**	**N=3**	**mean**	**stDev**	**N=1**	**N=2**	**N=3**	**mean**	**stDev**
0	100.00	100.00	NA	**100.00**	**0.00**	100.00	100.00	NA	**100.00**	**0.00**
3	88.43	97.10	NA	**92.77**	**6.13**	82.27	96.67	NA	**89.47**	**10.18**
5	89.70	99.37	NA	**94.53**	**6.84**	85.02	89.46	NA	**87.24**	**3.14**
10	90.57	98.39	NA	**94.48**	**5.53**	105.40	93.97	NA	**99.69**	**8.08**
30	91.79	100.27	NA	**96.03**	**6.00**	154.69	95.01	NA	**124.85**	**42.20**
50	91.64	98.88	NA	**95.26**	**5.12**	114.76	91.61	NA	**103.19**	**16.37**
100	90.37	93.38	NA	**91.88**	**2.13**	138.25	103.96	NA	**121.10**	**24.25**
300	80.09	91.40	NA	**85.74**	**8.00**	145.11	114.58	NA	**129.85**	**21.59**

Pioglitazone 72h

PIO [µM]	72h ATP					72h Resazurin				
HepG2										
	N=1	**N=2**	**N=3**	**mean**	**stDev**	**N=1**	**N=2**	**N=3**	**mean**	**stDev**
0	100.00	100.00	100.00	**100.00**	**0.00**	100.00	100.00	100.00	**100.00**	**0.00**
3	71.97	83.87	71.21	**75.69**	**7.10**	90.68	100.24	97.39	**96.10**	**4.91**
5	87.93	68.70	63.66	**73.43**	**12.81**	93.98	105.40	100.49	**99.95**	**5.73**
10	73.88	77.24	79.95	**77.03**	**3.04**	88.57	103.60	101.29	**97.82**	**8.09**
30	78.79	69.19	70.98	**72.99**	**5.11**	90.78	105.67	100.86	**99.10**	**7.60**
50	72.70	91.19	73.82	**79.24**	**10.36**	89.90	104.97	98.37	**97.74**	**7.55**
100	77.22	107.23	66.34	**83.60**	**21.18**	90.76	104.00	97.28	**97.35**	**6.62**
300	70.68	57.81	58.37	**62.29**	**7.27**	85.35	105.43	98.88	**96.55**	**10.24**
HepaRG										
	N=1	**N=2**	**N=3**	**mean**	**stDev**	**N=1**	**N=2**	**N=3**	**mean**	**stDev**
0	100.00	100.00	100.00	**100.00**	**0.00**	100.00	100.00	NA	**100.00**	**0.00**
3	105.93	115.04	97.88	**106.28**	**8.59**	102.66	92.12	NA	**97.39**	**7.46**
5	108.52	114.40	100.21	**107.71**	**7.13**	104.86	94.13	NA	**99.50**	**7.59**
10	117.17	114.84	101.41	**111.14**	**8.51**	105.29	96.03	NA	**100.66**	**6.55**
30	109.47	119.04	100.06	**109.52**	**9.49**	107.00	96.35	NA	**101.68**	**7.53**
50	108.44	110.40	99.89	**106.24**	**5.59**	109.54	96.34	NA	**102.94**	**9.33**
100	97.72	103.32	97.38	**99.47**	**3.34**	108.39	98.33	NA	**103.36**	**7.11**
300	95.34	39.71	101.38	**78.81**	**34.00**	113.56	86.01	NA	**99.79**	**19.48**
Upcyte hepatocytes										
	N=1	**N=2**	**N=3**	**mean**	**stDev**	**N=1**	**N=2**	**N=3**	**mean**	**stDev**
0	100.00	100.00	NA	**100.00**	**0.00**	100.00	100.00	NA	**100.00**	**0.00**
3	113.34	97.68	NA	**105.51**	**11.08**	88.08	102.67	NA	**95.38**	**10.32**
5	114.65	105.78	NA	**110.21**	**6.27**	114.65	104.14	NA	**109.40**	**7.43**
10	114.88	112.17	NA	**113.52**	**1.92**	109.26	104.23	NA	**106.74**	**3.56**
30	113.18	121.92	NA	**117.55**	**6.18**	108.11	102.27	NA	**105.19**	**4.13**
50	122.97	130.02	NA	**126.50**	**4.99**	113.19	101.68	NA	**107.43**	**8.13**
100	118.61	135.32	NA	**126.97**	**11.82**	72.06	109.70	NA	**90.88**	**26.62**
300	111.94	136.42	NA	**124.18**	**17.31**	78.63	103.91	NA	**91.27**	**17.88**

Tolcapone 24h

TOL [µM]	24h ATP					24h Resazurin				
HepG2										
	N=1	**N=2**	**N=3**	**mean**	**stDev**	**N=1**	**N=2**	**N=3**	**mean**	**stDev**
0	100.00	100.00	100.00	**100.00**	**0.00**	100.00	100.00	100.00	**100.00**	**0.00**
10	89.65	85.80	80.97	**85.47**	**3.55**	94.04	90.62	89.19	**91.29**	**2.03**
30	94.06	71.86	71.88	**79.27**	**10.46**	84.66	81.93	93.30	**86.63**	**4.84**
50	77.91	69.44	71.68	**73.01**	**3.58**	86.26	89.05	92.57	**89.30**	**2.58**
100	47.06	59.34	56.03	**54.15**	**5.19**	75.31	79.32	84.38	**79.67**	**3.71**
300	22.68	36.85	34.16	**31.23**	**6.14**	59.46	80.49	73.94	**71.30**	**8.79**
500	11.63	18.86	17.32	**15.94**	**3.11**	58.73	64.58	64.58	**62.63**	**2.76**
1.000	1.88	1.39	1.07	**1.45**	**0.33**	28.20	14.74	21.39	**21.44**	**5.49**
HepaRG										
	N=1	**N=2**	**N=3**	**mean**	**stDev**	**N=1**	**N=2**	**N=3**	**mean**	**stDev**
0	100.00	100.00	100.00	**100.00**	**0.00**	100.00	100.00	NA	**100.00**	**0.00**
10	93.62	96.17	98.60	**96.13**	**2.03**	106.41	143.02	NA	**124.72**	**25.88**
30	93.21	100.76	99.68	**97.88**	**3.33**	107.25	144.15	NA	**125.70**	**26.10**
50	93.54	89.37	101.57	**94.83**	**5.07**	109.94	142.66	NA	**126.30**	**23.14**
100	95.44	85.65	97.32	**92.80**	**5.12**	107.81	144.37	NA	**126.09**	**25.85**
300	74.86	77.54	100.93	**84.45**	**11.71**	109.10	134.05	NA	**121.58**	**17.64**
500	21.06	18.65	21.19	**20.30**	**1.17**	106.66	124.81	NA	**115.73**	**12.84**
1.000	4.56	0.62	1.10	**2.10**	**1.75**	61.67	28.32	NA	**45.00**	**23.58**
Upcyte hepatocytes										
	N=1	**N=2**	**N=3**	**mean**	**stDev**	**N=1**	**N=2**	**N=3**	**mean**	**stDev**
0	100.00	100.00	NA	**100.00**	**0.00**	100.00	100.00	NA	**100.00**	**0.00**
10	87.32	86.16	NA	**86.74**	**0.82**	73.25	88.67	NA	**80.96**	**10.90**
30	84.45	88.30	NA	**86.37**	**2.72**	84.40	105.82	NA	**95.11**	**15.15**
50	76.79	87.24	NA	**82.02**	**7.39**	84.53	97.12	NA	**90.83**	**8.91**
100	49.13	54.95	NA	**52.04**	**4.11**	107.51	101.71	NA	**104.61**	**4.10**
300	45.94	56.75	NA	**51.34**	**7.64**	114.84	100.22	NA	**107.53**	**10.34**
500	12.57	30.24	NA	**21.41**	**12.50**	168.49	109.53	NA	**139.01**	**41.70**
1.000	85.11	91.64	NA	**88.37**	**4.62**	114.54	103.03	NA	**108.79**	**8.14**

Tolcapone 72h

TOL [µM]	72h ATP					72h Resazurin				
HepG2										
	N=1	**N=2**	**N=3**	**mean**	**stDev**	**N=1**	**N=2**	**N=3**	**mean**	**stDev**
0	100.00	100.00	100.00	**100.00**	**0.00**	100.00	100.00	100.00	**100.00**	**0.00**
10	28.51	28.30	18.19	**25.00**	**5.90**	52.10	71.31	56.62	**60.01**	**10.05**
30	26.17	26.30	18.27	**23.58**	**4.60**	34.26	58.30	50.01	**47.53**	**12.21**
50	25.68	25.56	12.76	**21.33**	**7.43**	35.03	58.82	38.82	**44.22**	**12.78**
100	15.12	11.46	8.72	**11.77**	**3.21**	24.88	31.50	24.84	**27.08**	**3.83**
300	0.53	0.63	0.47	**0.55**	**0.08**	0.56	4.26	-1.03	**1.26**	**2.71**
500	-0.13	0.18	0.22	**0.09**	**0.19**	-1.01	2.64	-0.82	**0.27**	**2.05**
1.000	-0.37	0.33	0.11	**0.02**	**0.36**	-1.61	1.49	-0.57	**-0.23**	**1.58**
HepaRG										
	N=1	**N=2**	**N=3**	**mean**	**stDev**	**N=1**	**N=2**	**N=3**	**mean**	**stDev**
0	100.00	100.00	100.00	**100.00**	**0.00**	100.00	100.00	NA	**100.00**	**0.00**
10	103.44	111.46	101.10	**105.33**	**5.44**	102.04	88.25	NA	**95.14**	**9.75**
30	107.70	115.86	104.55	**109.37**	**5.83**	102.47	86.41	NA	**94.44**	**11.36**
50	110.32	114.46	99.72	**108.17**	**7.60**	102.41	86.04	NA	**94.22**	**11.58**
100	115.14	120.63	96.47	**110.74**	**12.66**	103.03	87.45	NA	**95.24**	**11.01**
300	8.24	2.31	10.89	**7.15**	**4.39**	77.39	36.74	NA	**57.06**	**28.74**
500	0.44	0.30	0.64	**0.46**	**0.17**	7.59	14.88	NA	**11.23**	**5.16**
1.000	-0.43	-0.44	-0.32	**-0.40**	**0.07**	2.39	3.21	NA	**2.80**	**0.58**
Upcyte hepatocytes										
	N=1	**N=2**	**N=3**	**mean**	**stDev**	**N=1**	**N=2**	**N=3**	**mean**	**stDev**
0	100.00	100.00	NA	**100.00**	**0.00**	100.00	100.00	NA	**100.00**	**0.00**
10	107.53	94.42	NA	**100.98**	**9.27**	77.97	91.79	NA	**84.88**	**9.78**
30	105.85	95.13	NA	**100.49**	**7.58**	94.54	108.07	NA	**101.30**	**9.57**
50	99.90	96.75	NA	**98.33**	**2.23**	99.55	98.78	NA	**99.16**	**0.54**
100	71.60	76.53	NA	**74.06**	**3.49**	80.02	100.13	NA	**90.07**	**14.22**
300	11.71	7.16	NA	**9.43**	**3.21**	42.67	35.83	NA	**39.25**	**4.84**
500	11.18	13.39	NA	**12.29**	**1.56**	18.04	60.09	NA	**39.07**	**29.73**
1.000	-0.12	-0.15	NA	**-0.13**	**0.03**	2.24	7.34	NA	**4.79**	**3.61**

Troglitazone 24h

TRO [µM]	24h ATP					24h Resazurin				
HepG2										
	N=1	**N=2**	**N=3**	**mean**	**stDev**	**N=1**	**N=2**	**N=3**	**mean**	**stDev**
0	100.00	100.00	100.00	**100.00**	**0.00**	100.00	100.00	100.00	**100.00**	**0.00**
3	138.76	111.84	102.40	**117.67**	**15.41**	97.42	96.37	96.14	**96.65**	**0.56**
5	137.42	106.69	100.49	**114.87**	**16.15**	105.12	99.47	100.02	**101.54**	**2.54**
10	106.53	101.60	96.77	**101.63**	**3.98**	97.51	96.43	96.22	**96.72**	**0.57**
30	18.88	30.96	27.56	**25.80**	**5.09**	87.56	76.80	70.09	**78.15**	**7.19**
50	7.30	17.38	12.33	**12.34**	**4.11**	76.80	67.38	40.36	**61.51**	**15.44**
100	1.64	0.66	0.43	**0.91**	**0.52**	7.22	15.77	9.53	**10.84**	**3.61**
300	-0.07	-0.42	-0.33	**-0.27**	**0.15**	4.30	-1.65	-0.13	**0.84**	**2.53**
HepaRG										
	N=1	**N=2**	**N=3**	**mean**	**stDev**	**N=1**	**N=2**	**N=3**	**mean**	**stDev**
0	100.00	100.00	100.00	**100.00**	**0.00**	100.00	100.00	NA	**100.00**	**0.00**
3	96.57	102.88	100.45	**99.96**	**2.60**	91.71	122.01	NA	**106.86**	**21.42**
5	93.53	104.74	105.28	**101.18**	**5.42**	107.74	120.47	NA	**114.10**	**9.00**
10	94.54	108.12	104.57	**102.41**	**5.75**	109.29	116.65	NA	**112.97**	**5.21**
30	94.58	102.83	105.82	**101.08**	**4.76**	100.80	126.82	NA	**113.81**	**18.40**
50	94.15	100.04	99.67	**97.95**	**2.69**	105.95	123.64	NA	**114.80**	**12.51**
100	94.55	90.43	101.79	**95.59**	**4.70**	100.27	121.44	NA	**110.85**	**14.96**
300	85.56	15.46	9.91	**36.98**	**34.43**	108.75	92.60	NA	**100.67**	**11.42**
Upcyte hepatocytes										
	N=1	**N=2**	**N=3**	**mean**	**stDev**	**N=1**	**N=2**	**N=3**	**mean**	**stDev**
0	100.00	100.00	NA	**100.00**	**0.00**	100.00	100.00	NA	**100.00**	**0.00**
3	96.40	98.06	NA	**97.23**	**1.17**	121.16	106.43	NA	**113.79**	**10.41**
5	93.07	103.56	NA	**98.32**	**7.42**	128.16	108.11	NA	**118.13**	**14.17**
10	93.39	101.36	NA	**97.37**	**5.64**	155.25	103.98	NA	**129.61**	**36.26**
30	92.38	101.83	NA	**97.10**	**6.68**	153.82	114.83	NA	**134.33**	**27.57**
50	89.57	98.32	NA	**93.95**	**6.18**	147.66	112.82	NA	**130.24**	**24.63**
100	82.98	92.49	NA	**87.73**	**6.72**	162.54	104.28	NA	**133.41**	**41.20**
300	78.62	79.17	NA	**78.89**	**0.38**	194.07	112.51	NA	**153.29**	**57.67**

Troglitazone 72h

TRO [µM]	72h ATP					72h Resazurin				
HepG2										
	N=1	**N=2**	**N=3**	**mean**	**stDev**	**N=1**	**N=2**	**N=3**	**mean**	**stDev**
0	100.00	100.00	100.00	**100.00**	**0.00**	100.00	100.00	100.00	**100.00**	**0.00**
3	66.80	93.21	81.25	**80.42**	**13.22**	79.80	97.00	97.13	**91.31**	**9.97**
5	70.05	70.14	64.28	**68.15**	**3.36**	88.31	100.69	105.05	**98.02**	**8.69**
10	33.44	25.61	25.30	**28.12**	**4.61**	74.25	103.80	104.46	**94.17**	**17.26**
30	9.61	3.32	2.68	**5.20**	**3.83**	18.15	14.77	6.01	**12.98**	**6.27**
50	0.14	0.16	0.00	**0.10**	**0.09**	-0.23	3.59	-2.94	**0.14**	**3.28**
100	-0.31	-0.07	0.09	**-0.10**	**0.20**	-1.11	1.68	-2.75	**-0.73**	**2.24**
300	-0.38	0.03	0.17	**-0.06**	**0.28**	-1.43	0.77	-2.78	**-1.15**	**1.79**
HepaRG										
	N=1	**N=2**	**N=3**	**mean**	**stDev**	**N=1**	**N=2**	**N=3**	**mean**	**stDev**
0	100.00	100.00	100.00	**100.00**	**0.00**	100.00	100.00	NA	**100.00**	**0.00**
3	109.37	91.34	101.59	**100.77**	**9.04**	97.91	96.26	NA	**97.09**	**1.17**
5	111.59	114.29	105.65	**110.51**	**4.42**	96.25	96.76	NA	**96.51**	**0.36**
10	109.39	110.19	101.17	**106.91**	**4.99**	99.38	98.51	NA	**98.94**	**0.61**
30	109.91	107.67	98.52	**105.37**	**6.04**	97.11	101.22	NA	**99.17**	**2.91**
50	92.50	98.97	96.80	**96.09**	**3.29**	101.38	101.89	NA	**101.63**	**0.36**
100	101.71	84.88	91.83	**92.81**	**8.46**	102.99	104.41	NA	**103.70**	**1.01**
300	19.33	5.23	0.07	**8.21**	**9.97**	66.15	2.53	NA	**34.34**	**44.99**
Upcyte hepatocytes										
	N=1	**N=2**	**N=3**	**mean**	**stDev**	**N=1**	**N=2**	**N=3**	**mean**	**stDev**
0	100.00	100.00	NA	**100.00**	**0.00**	100.00	100.00	NA	**100.00**	**0.00**
3	101.70	100.50	NA	**101.10**	**0.85**	102.16	86.20	NA	**94.18**	**11.28**
5	108.77	107.49	NA	**108.13**	**0.91**	116.69	92.44	NA	**104.57**	**17.14**
10	108.38	111.76	NA	**110.07**	**2.39**	76.60	94.39	NA	**85.50**	**12.58**
30	104.88	114.83	NA	**109.86**	**7.04**	96.76	91.88	NA	**94.32**	**3.46**
50	103.10	126.91	NA	**115.00**	**16.83**	95.44	97.27	NA	**96.36**	**1.29**
100	94.80	104.07	NA	**99.44**	**6.56**	104.91	98.98	NA	**101.94**	**4.19**
300	93.75	45.43	NA	**69.59**	**34.17**	89.10	94.40	NA	**91.75**	**3.75**

Ximelagatran 24h

XIM [µM]	24h ATP					24h Resazurin				
HepG2										
	N=1	**N=2**	**N=3**	**mean**	**stDev**	**N=1**	**N=2**	**N=3**	**mean**	**stDev**
0	100.00	100.00	100.00	**100.00**	**0.00**	100.00	100.00	100.00	**100.00**	**0.00**
3	125.40	114.30	108.61	**116.10**	**6.97**	100.75	100.74	98.74	**100.08**	**0.95**
5	132.64	114.83	112.59	**120.02**	**8.97**	92.32	102.45	102.97	**99.25**	**4.90**
10	131.24	116.77	116.26	**121.42**	**6.95**	97.84	101.22	102.28	**100.44**	**1.89**
30	131.83	112.42	108.52	**117.59**	**10.19**	98.47	99.71	101.08	**99.75**	**1.07**
50	127.47	117.74	111.82	**119.01**	**6.45**	99.76	100.39	99.66	**99.93**	**0.32**
100	128.34	108.02	107.94	**114.77**	**9.60**	98.10	101.75	101.47	**100.44**	**1.66**
300	92.55	99.73	105.57	**99.29**	**5.32**	98.56	100.88	97.33	**98.92**	**1.47**
HepaRG										
	N=1	**N=2**	**N=3**	**mean**	**stDev**	**N=1**	**N=2**	**N=3**	**mean**	**stDev**
0	100.00	100.00	100.00	**100.00**	**0.00**	100.00	100.00	NA	**100.00**	**0.00**
3	106.31	109.93	103.74	**106.66**	**2.54**	108.64	119.68	NA	**114.16**	**7.81**
5	108.64	108.67	102.66	**106.66**	**2.83**	112.40	123.63	NA	**118.01**	**7.94**
10	109.47	106.14	105.40	**107.00**	**1.77**	111.81	119.63	NA	**115.72**	**5.53**
30	108.86	105.43	104.80	**106.36**	**1.79**	115.10	119.87	NA	**117.49**	**3.37**
50	108.47	106.64	104.95	**106.68**	**1.44**	115.64	121.91	NA	**118.77**	**4.43**
100	107.66	99.32	105.19	**104.05**	**3.50**	115.59	118.26	NA	**116.93**	**1.88**
300	29.43	87.28	79.66	**65.46**	**25.66**	96.97	110.71	NA	**103.84**	**9.71**
Upcyte hepatocytes										
	N=1	**N=2**	**N=3**	**mean**	**stDev**	**N=1**	**N=2**	**N=3**	**mean**	**stDev**
0	100.00	100.00	NA	**100.00**	**0.00**	100.00	100.00	NA	**100.00**	**0.00**
3	108.96	102.95	NA	**105.96**	**4.25**	84.23	102.95	NA	**93.59**	**13.24**
5	105.42	105.58	NA	**105.50**	**0.11**	80.84	102.13	NA	**91.49**	**15.06**
10	130.99	101.57	NA	**116.28**	**20.80**	84.40	107.25	NA	**95.83**	**16.16**
30	129.98	104.09	NA	**117.03**	**18.31**	82.60	98.28	NA	**90.44**	**11.09**
50	119.67	101.07	NA	**110.37**	**13.15**	83.21	102.48	NA	**92.85**	**13.63**
100	135.88	105.69	NA	**120.78**	**21.35**	80.34	96.07	NA	**88.21**	**11.12**
300	146.25	104.33	NA	**125.29**	**29.64**	78.41	85.74	NA	**82.08**	**5.18**

Ximelagatran 72h

XIM [µM]	72h ATP					72h Resazurin				
HepG2										
	N=1	**N=2**	**N=3**	**mean**	**stDev**	**N=1**	**N=2**	**N=3**	**mean**	**stDev**
0	100.00	100.00	100.00	**100.00**	**0.00**	100.00	100.00	100.00	**100.00**	**0.00**
3	78.55	94.57	97.96	**90.36**	**10.37**	87.50	82.26	93.09	**87.62**	**5.42**
5	92.17	100.58	108.45	**100.40**	**8.15**	90.82	101.67	106.81	**99.77**	**8.16**
10	90.72	93.41	94.38	**92.84**	**1.90**	89.02	101.20	108.44	**99.55**	**9.81**
30	82.96	99.61	90.06	**90.88**	**8.36**	85.64	100.29	108.01	**97.98**	**11.36**
50	85.26	104.11	80.80	**90.06**	**12.37**	82.18	101.39	110.91	**98.16**	**14.63**
100	70.20	93.15	82.52	**81.96**	**11.49**	75.29	100.45	111.73	**95.82**	**18.66**
300	52.45	19.82	20.20	**30.82**	**18.73**	64.32	99.12	111.00	**91.48**	**24.26**
HepaRG										
	N=1	**N=2**	**N=3**	**mean**	**stDev**	**N=1**	**N=2**	**N=3**	**mean**	**stDev**
0	100.00	100.00	100.00	**100.00**	**0.00**	100.00	100.00	NA	**100.00**	**0.00**
3	103.30	100.36	101.60	**101.75**	**1.47**	98.89	92.77	NA	**95.83**	**4.32**
5	111.85	101.69	105.03	**106.19**	**5.18**	97.01	86.57	NA	**91.79**	**7.38**
10	111.56	107.91	102.16	**107.21**	**4.74**	98.54	94.52	NA	**96.53**	**2.84**
30	107.16	105.43	97.84	**103.48**	**4.96**	93.81	93.07	NA	**93.44**	**0.52**
50	100.08	97.26	99.43	**98.92**	**1.48**	93.71	92.37	NA	**93.04**	**0.95**
100	99.01	92.39	96.24	**95.88**	**3.32**	101.32	92.48	NA	**96.90**	**6.25**
300	0.43	0.07	5.10	**1.87**	**2.81**	69.35	82.23	NA	**75.79**	**9.11**
Upcyte hepatocytes										
	N=1	**N=2**	**N=3**	**mean**	**stDev**	**N=1**	**N=2**	**N=3**	**mean**	**stDev**
0	100.00	100.00	NA	**100.00**	**0.00**	100.00	100.00	NA	**100.00**	**0.00**
3	110.89	109.14	NA	**110.02**	**1.24**	75.16	90.58	NA	**82.87**	**10.91**
5	113.76	115.10	NA	**114.43**	**0.95**	98.03	89.03	NA	**93.53**	**6.36**
10	110.86	122.02	NA	**116.44**	**7.89**	91.42	98.41	NA	**94.92**	**4.94**
30	109.29	126.18	NA	**117.73**	**11.94**	66.81	97.27	NA	**82.04**	**21.54**
50	111.92	139.04	NA	**125.48**	**19.18**	84.99	105.75	NA	**95.37**	**14.68**
100	112.68	132.94	NA	**122.81**	**14.32**	37.13	94.93	NA	**66.03**	**40.87**
300	111.55	131.80	NA	**121.67**	**14.32**	48.69	115.87	NA	**82.28**	**47.50**

Appendix 2A: mean flurescence intensities of IF sections per 1,000 pixels.

	HepaRG				PHH			
	Day 3	**Day 7**	**Day 14**	**Day 28**	**Day 3**	**Day 7**	**Day 14**	**Day 28**
Albumin	61,159	41,290	58,739	66,478	61,804	60,372	58,739	NA
	63,100	51,772	53,865	61,059	53,408	63,638	66,478	NA
	64,733	47,228	54,034	63,638	66,478	63,529	61,059	NA
	69,350	47,215	62,294	63,529	52,726	61,744	63,638	NA
	59,025	51,471	49,296	62,175	69,631	66,164	63,529	NA
	66,219	52,880	61,804	51,070	66,219	60,263	61,159	NA
	59,917	44,692	53,408	57,858	62,175	57,858	63,100	NA
	54,444	37,676	51,936	61,741	51,070	61,741	64,733	NA
	65,854	46,109	52,726	52,385	65,854	65,971	69,350	NA
	66,561	58,711	69,631	56,707	66,561	56,707	59,025	NA
Mean	**63,036.2**	**47,904.4**	**56,773.3**	**59,664.0**	**61,592.6**	**61,798.7**	**63,081.0**	NA
StDev	**4,200.1**	**5,762.5**	**5,898.7**	**4,780.9**	**6,398.8**	**2,978.2**	**3,117.2**	NA

	HepaRG				PHH			
	Day 3	**Day 7**	**Day 14**	**Day 28**	**Day 3**	**Day 7**	**Day 14**	**Day 28**
CYP 1A2	50,607	61,182	50,607	66,155	73,347	78,910	77,799	NA
	52,383	63,017	52,383	67,328	86,013	74,442	77,625	NA
	42,418	58,225	42,418	67,124	83,495	76,933	69,485	NA
	55,925	53,824	55,925	71,106	94,451	68,559	71,129	NA
	42,274	57,757	42,274	67,302	81,927	92,290	91,536	NA
	46,579	53,404	46,579	65,730	73,733	66,916	88,910	NA
	49,941	42,748	49,941	57,194	88,910	85,944	65,971	NA
	42,923	61,744	42,923	82,165	92,290	73,344	94,451	NA
	39,452	66,164	39,452	76,179	86,013	86,013	81,927	NA
	39,650	53,413	39,650	62,759	NA	83,495	73,733	NA
Mean	**46,215.2**	**57,147.8**	**46,215.2**	**68,304.2**	**84,464.3**	**78,684.9**	**79,256,6**	NA
StDev	**5,433.8**	**6,332.8**	**5,433.8**	**6,563.3**	**6,925.6**	**7,780.0**	**9,248.3**	NA

	HepaRG				PHH			
	Day 3	**Day 7**	**Day 14**	**Day 28**	**Day 3**	**Day 7**	**Day 14**	**Day 28**
CYP 2B6	35,842	18,164	24,859	37,207	45,971	48,217	43,420	NA
	39,782	31,451	23,788	34,124	62,973	45,827	43,946	NA
	34,737	29,543	23,200	42,537	52,898	64,900	52,189	NA
	47,434	35,492	25,713	33,120	44,856	49,560	51,170	NA
	34,672	22,318	23,080	30,997	53,604	49,079	53,477	NA
	44,783	23,790	23,691	37,617	51,326	45,971	51,326	NA
	36,355	20,794	26,174	37,856	46,583	62,973	46,583	NA
	35,618	26,961	28,072	38,364	47,337	52,898	47,337	NA
	31,795	29,983	26,273	34,979	51,170	44,856	45,633	NA
	37,467	25,639	22,128	36,778	37,467	53,604	46,290	NA
Mean	**37,848,5**	**26,413,5**	**24,697,8**	**36,357,9**	**49,418,5**	**51,788,5**	**48,137,1**	NA
StDev	**4,598,9**	**5,045,0**	**1,743,8**	**3,050,4**	**6,387,2**	**6,663,6**	**3,418,4**	NA

	HepaRG				PHH			
	Day 3	**Day 7**	**Day 14**	**Day 28**	**Day 3**	**Day 7**	**Day 14**	**Day 28**
CYP 3A4	75,641	98,299	72,362	99,476	80,591	110,677	11,0759	NA
	63,247	96,044	91,077	86,998	111,496	96,232	9,4276	NA
	69,702	108,116	82,935	88,498	103,445	105,286	10,8445	NA
	67,478	109,347	77,663	73,575	93,927	101,101	12,3590	NA
	70,681	98,284	83,843	93,793	117,969	108,725	8,8038	NA
	66,899	99,821	75,075	103,502	89,206	80,591	8,3491	NA
	78,560	104,385	90,991	84,254	110,096	111,496	9,3146	NA
	62,338	98,978	79,024	91,744	110,759	103,445	11,7969	NA
	60,598	83,139	83,795	98,105	94,276	93,927	8,9206	NA
	53,413	92,049	87,397	88,874	NA	110,654	11,0096	NA
Mean	**66,855,7**	**98,846,2**	**82,416,2**	**90,881,9**	**101,307.2**	**10,2213,4**	**101,901,6**	NA
StDev	**7,004,2**	**7,274,8**	**6,055,0**	**8,141,1**	**11,700.3**	**9,249,9**	**13,206,5**	NA

	HepaRG				PHH			
	Day 3	**Day 7**	**Day 14**	**Day 28**	**Day 3**	**Day 7**	**Day 14**	**Day 28**
NAT 1/2	51,505	73,084	50,164	64,940	94,976	93,671	102,553	NA
	48,539	56,324	54,599	59,419	84,217	86,598	75,056	NA
	58,383	60,271	57,383	71,325	92,904	95,183	87,961	NA
	48,877	59,197	60,766	68,096	87,961	70,867	85,711	NA
	44,725	60,263	53,962	68,722	85,711	69,528	76,895	NA
	45,481	72,315	47,891	61,513	76,895	94,976	116,756	NA
	46,844	60,372	60,593	64,348	116,756	84,217	96,384	NA
	50,543	71,389	53,959	59,547	96,384	92,904	116,804	NA
	54,648	70,992	54,996	56,931	98,396	73,920	98,396	NA
	44,629	58,392	50,915	65,045	81,026	93,814	81,026	NA
Mean	**49,417,4**	**64,259,9**	**54,522,8**	**63,988,6**	**91,522,6**	**85,567,8**	**93,754,2**	NA
StDev	**4,260,2**	**6,394,8**	**4,010,8**	**4,379,5**	**10,702,4**	**9,901,5**	**14,354,0**	NA

	HepaRG				PHH			
	Day 3	**Day 7**	**Day 14**	**Day 28**	**Day 3**	**Day 7**	**Day 14**	**Day 28**
SULT 1A1	40,379	64,103	80,123	59,448	NA	NA	NA	NA
	40,585	51,991	81,103	66,804	NA	NA	NA	NA
	34,579	53,026	58,388	47,745	NA	NA	NA	NA
	46,136	58,891	74,209	51,445	NA	NA	NA	NA
	37,832	55,207	80,119	57,995	NA	NA	NA	NA
	36,056	54,201	72,387	54,050	NA	NA	NA	NA
	43,652	61,922	60,851	56,169	NA	NA	NA	NA
	36,881	53,191	71,506	52,502	NA	NA	NA	NA
	33,579	46,405	73,569	62,096	NA	NA	NA	NA
	45,491	54,148	62,396	67,759	NA	NA	NA	NA
Mean	**39,517,0**	**55,308,5**	**71,465,1**	**57,601,3**	NA	NA	NA	NA
StDev	**4,241,4**	**4,862,8**	**7,883,3**	**6,223,7**	NA	NA	NA	NA

Appendix 2b) CYP induction in IF stained sections (HepaRG spheroids)

CYP1A2 induction by Omeprazol

	Day 3				Day 7				Day 14			
CYP1A2	**ctrl**	**LD**	**MD**	**HD**	**ctrl**	**LD**	**MD**	**HD**	**ctrl**	**LD**	**MD**	**HD**
	70,905	74,111	111,192	150,583	61,182	66,114	98,965	146,805	50,607	95,627	92,513	145,618
	62,926	119,728	104,477	163,687	63,017	64,052	108,721	159,395	52,383	102,226	154,696	113,723
	66,131	98,433	108,710	142,791	58,225	69,794	129,897	157,526	42,418	88,874	110,666	148,438
	74,110	86,847	107,213	146,823	53,824	59,247	98,197	145,109	55,925	72,223	121,925	136,325
	60,620	88,598	93,813	118,646	57,757	67,801	105,717	150,501	42,274	53,731	124,333	145,122
	72,308	113,408	112,043	155,671	53,404	63,472	98,026	141,634	46,579	51,342	75,397	154,600
	73,925	85,974	99,482	138,273	42,748	78,227	101,431	141,401	49,941	55,504	120,977	132,258
	66,630	119,539	105,277	141,551	61,744	63,393	107,157	138,671	42,923	78,854	123,724	105,238
	75,069	119,827	100,799	NA	66,164	69,511	100,148	137,353	39,452	65,493	101,250	133,104
	71,746	122,016	NA	NA	NA	71,970	108,237	139,370	39,650	62,316	81,693	166,239
Mean	**69,437.0**	**102,848.1**	**104,778.4**	**144,753.1**	**57562,8**	**67358,1**	**105649,6**	**145.777**	**46215,2**	**72619,0**	**110717,4**	**140627,6**
StDev	**4,778.8**	**17,087.6**	**55,75.3**	**12,518.2**	**6545,0**	**5091,7**	**9015,3**	**7390,0649**	**5433,8**	**17229,4**	**22428,8**	**18425,9**

CYP 1A1 induction by Omeprazol

	Day 3				Day 7				Day 14			
CYP1A1	**ctrl**	**LD**	**MD**	**HD**	**ctrl**	**LD**	**MD**	**HD**	**ctrl**	**LD**	**MD**	**HD**
	17,222	30,568	17,344	26,932	17,222	22,027	24,693	26,133	24,508	27,535	36,987	48,748
	17,281	28,195	19,113	31,112	17,281	22,869	29,632	26,340	19,112	30,712	37,435	39,432
	21,550	25,539	16,915	28,295	21,550	24,002	26,383	31,881	18,783	31,226	39,677	48,023
	20,495	30,266	18,531	28,303	20,495	22,372	27,518	29,611	21,874	31,296	34,745	39,911
	23,865	26,893	16,637	27,841	23,865	23,524	28,104	27,747	18,325	29,438	34,936	38,766
	18,382	25,372	19,205	28,998	18,382	19,805	28,460	25,602	23,403	37,167	43,977	43,706
	21,725	25,572	17,633	28,990	21,725	21,982	27,587	32,698	22,006	30,150	38,220	55,793
	22,295	25,156	18,400	27,221	22,295	24,321	23,630	31,809	22,915	28,539	36,153	52,895
	17,170	24,111	18,431	28,831	17,170	19,192	26,591	26,562	22,865	28,597	34,911	51,554
	25,086	26,244	17,268	29,462	25,086	23,129	24,787	30,624	20,231	37,367	34,654	53,218
Mean	20,507,1	26,792	17,948	28,599	20,507	22,322	26,739	28,901	21,402	31,203	37,170	47,205
StDev	2,736,1	2086,7	861,8	1133,9	2736,1	1598,5	1798,1	2591,0	2039,9	3246,2	2777,9	6011,1

	Day 3				Day 7				Day 14			
CYP2B6	**ctrl**	**LD**	**MD**	**HD**	**ctrl**	**LD**	**MD**	**HD**	**ctrl**	**LD**	**MD**	**HD**
	35,842	44,458	60,363	69,669	18,164	38,932	43,582	72,702	24,859	31,473	51,143	65,759
	39,782	40,160	55,131	60,748	31,451	35,425	39,726	59,549	23,788	35,373	46,015	69,946
	34,737	41,167	55,871	68,369	29,543	36,285	44,969	61,946	23,200	24,461	55,872	64,522
	47,434	41,972	52,328	67,614	35,492	44,628	36,249	71,090	25,713	32,176	49,342	60,539
	34,672	40,792	53,879	71,835	22,318	39,096	40,453	69,686	23,080	30,555	50,823	64,442
	44,783	40,996	56,599	67,441	23,790	37,106	40,517	72,172	23,691	38,759	52,606	67,307
	36,355	43,244	51,712	70,766	20,794	42,271	36,978	65,229	26,174	32,158	60,098	66,458
	35,618	42,265	54,919	66,956	26,961	37,839	41,053	60,856	28,072	37,226	48,632	68,747
	31,795	42,056	51,343	68,298	29,983	38,359	38,334	63,037	26,273	30,425	65,064	60,350
	37,467	43,063	57,457	64,131	25,639	43,055	45,480	71,900	22,128	35,911	54,244	59,508
Mean	**37.849**	**42.017**	**54.960**	**67.583**	**26.414**	**39.300**	**40.734**	**66.817**	**24.698**	**32.852**	**53.384**	**64.758**
StDev	**4598,9**	**1238,4**	**2659,0**	**3045,3**	**5.045**	**2.888**	**2.997**	**4.945**	**1.744**	**3.926**	**5.421**	**3.438**

	Day 3				Day 7				Day 14			
CYP3A4	**ctrl**	**LD**	**MD**	**HD**	**ctrl**	**LD**	**MD**	**HD**	**ctrl**	**LD**	**MD**	**HD**
	98,299	132,887	133,569	165,568	75,641	89,342	119,627	150,589	72,362	107,177	119,627	134,674
	96,044	108,743	125,014	165,807	63,247	95,115	121,806	145,601	91,077	100,038	121,806	137,159
	108,116	104,839	146,598	144,037	69,702	99,387	110,379	140,613	82,935	94,174	110,379	146,799
	109,347	94,688	119,492	158,025	67,478	93,516	131,800	164,012	77,663	106,447	131,800	148,580
	98,284	126,277	143,214	161,260	70,681	92,051	129,476	155,137	83,843	94,046	129,476	143,485
	99,821	125,585	149,193	162,549	66,899	89,841	121,533	149,127	75,075	90,941	121,533	137,697
	104,385	86,489	155,632	163,866	78,560	100,423	119,644	162,038	90,991	112,525	119,644	153,287
	98,978	114,402	138,651	163,601	62,338	79,641	103,361	160,899	79,024	105,161	103,361	158,835
	83,139	133,672	134,482	156,263	60,598	111,036	128,955	158,296	83,795	93,354	128,955	157,901
	92,049	97,242	130,016	159,017	NA	102,402	109,619	163,074	87,397	106,447	109,619	164,206
Mean	**98,846**	**112,482**	**137,586**	**159,999**	**68,349**	**95,275**	**119,620**	**154,939**	**82,416**	**101,031**	119,62	**148,262**
StDev	**7,275**	**15,900**	**10,691**	**6,119**	**5674,6**	**8156,5**	**8892,9**	**7686,7**	**6055,0**	**7093,3**	8,892	**9637,2**

Appendix 2 C: CYP Induction HepaRG **monolayer** Day 3
N=1

Flumazenil_3d

	0.003	**0.1**	**0.3**	**1**	**3**	**10**	**30**
CYP1A1	0.6	0.6	0.6	0.5	0.7	0.7	1.2
CYP1A2	0.7	0.6	0.6	0.7	0.6	0.7	0.8
CYP2B6	1.0	1.2	1.0	1.1	1.1	1.2	1.0
CYP2C9	1.0	1.0	1.0	1.2	1.1	1.0	0.9
CYP2C19	1.0	1.0	0.9	1.0	0.9	0.9	0.9
CYP3A4	0.8	0.9	0.8	0.9	0.9	1.1	1.0
ABCB11	1.0	0.9	1.0	0.9	1.2	0.9	0.8

Omeprazol_3d

	1.55	**3.1**	**6.25**	**12.5**	**25**	**50**	**100**
CYP1A1	6.2	10.7	18.8	40.2	55.3	68.2	86.7
CYP1A2	1.5	1.8	3.2	6.4	9.2	17.5	27.3
CYP2B6	0.7	0.9	1.0	1.2	1.4	1.3	1.8
CYP2C9	0.9	0.9	0.8	0.9	0.8	0.6	0.4
CYP2C19	0.8	0.8	0.8	0.8	0.9	0.7	0.8
CYP3A4	0.7	0.8	1.1	1.7	2.2	2.9	4.0
ABCB11	0.9	0.6	0.7	0.8	0.7	0.7	0.7

Rifampicine_3d

	0.1	**0.5**	**1.25**	**2.5**	**5**	**10**	**25**
CYP1A1	0.9	0.5	0.3	0.4	0.3	0.2	0.2
CYP1A2	0.8	0.7	0.6	0.8	0.4	0.5	0.6
CYP2B6	1.3	1.5	2.3	2.7	2.8	3.1	2.8
CYP2C9	1.1	1.3	1.4	1.4	1.3	1.5	1.3
CYP2C19	1.1	1.5	1.5	1.6	1.8	1.9	1.6
CYP3A4	2.1	4.7	7.4	9.0	10.4	11.6	12.7
ABCB11	1.1	1.2	1.0	1.1	0.8	0.9	0.8

Phenobarbital_3d

	31	**62.5**	**125**	**250**	**500**	**750**	**1000**
CYP1A1	0.4	0.4	0.3	0.5	0.5	0.6	1.2
CYP1A2	0.8	0.7	0.7	0.8	0.6	0.6	1.2
CYP2B6	1.0	0.9	1.6	2.3	3.8	3.5	4.8
CYP2C9	1.1	1.0	1.2	1.5	1.5	1.8	1.9
CYP2C19	0.9	0.9	1.0	1.5	1.9	1.9	2.9
CYP3A4	0.9	0.8	2.0	4.0	7.6	7.5	12.6
ABCB11	1.0	1.0	0.9	1.1	1.1	1.1	1.2

N=2

Flumazenil_3d

	0.003	**0.1**	**0.3**	**1**	**3**	**10**	**30**
CYP1A1	0.6	0.7	0.7	0.4	0.7	1.1	*
CYP1A2	0.8	1.4	1.0	1.2	1.5	1.6	*
CYP2B6	1.1	1.4	1.1	1.1	1.1	1.2	*
CYP2C9	1.0	1.2	0.9	1.0	1.0	1.2	*
CYP2C19	0.9	1.1	0.8	0.8	0.8	1.0	*
CYP3A4	1.2	1.3	1.0	1.0	1.0	1.3	*

ABCB11	0.8	1.2	1.1	1.0	1.1	1.1	*
			Omeprazol_3d				
	1.55	**3.1**	**6.25**	**12.5**	**25**	**50**	**100**
CYP1A1	8.3	22.3	54.7	133.6	253.2	340.1	*
CYP1A2	2.4	4.6	12.4	31.1	75.6	139.5	*
CYP2B6	1.4	1.4	2.1	2.3	3.1	3.9	*
CYP2C9	1.2	1.3	1.4	1.4	1.6	1.3	*
CYP2C19	1.1	1.3	1.2	1.6	1.7	2.3	*
CYP3A4	1.6	2.1	2.9	4.5	8.1	11.9	*
ABCB11	1.1	1.1	1.4	1.3	1.5	1.1	*
			Rifampicine_3d				
	0.1	**0.5**	**1.25**	**2.5**	**5**	**10**	**25**
CYP1A1	0.6	0.4	0.1	0.4	0.7	0.6	1.2
CYP1A2	1.0	1.0	0.8	0.9	1.5	1.5	2.6
CYP2B6	1.6	1.8	2.6	3.8	4.1	4.4	3.9
CYP2C9	1.4	1.6	1.9	2.0	2.1	1.7	1.8
CYP2C19	1.2	1.5	1.8	1.9	2.3	2.1	2.1
CYP3A4	5.0	11.4	18.1	20.5	22.0	22.2	26.5
ABCB11	1.0	1.0	0.9	1.0	1.0	1.0	1.0
			Phenobarbital_3d				
	31	**62.5**	**125**	**250**	**500**	**750**	**1000**
CYP1A1	0.2	0.3	0.3	0.6	0.5	0.5	0.8
CYP1A2	0.9	0.8	1.1	1.6	1.6	1.5	1.8
CYP2B6	1.9	3.0	3.7	5.5	6.9	8.5	5.1
CYP2C9	1.2	1.4	1.7	2.0	1.9	2.0	1.7
CYP2C19	1.1	1.3	1.4	1.8	2.3	2.8	2.5
CYP3A4	2.4	4.2	6.9	12.1	18.7	22.2	17.7
ABCB11	1.1	1.2	1.4	1.5	1.3	1.3	1.0

CYP Induction HepaRG **monolayer** Day 7

N=1

			Flumazenil_7d				
	0.003	**0.1**	**0.3**	**1**	**3**	**10**	**30**
CYP1A1	0.7	0.2	1.0	0.3	0.5	0.5	0.8
CYP1A2	0.9	0.6	1.2	0.5	0.9	0.9	1.1
CYP2B6	1.3	1.6	1.8	2.0	2.0	1.7	2.2
CYP2C9	1.0	1.1	1.1	1.1	1.1	0.9	1.1
CYP2C19	1.5	1.6	1.7	1.7	1.6	1.3	1.6
CYP3A4	1.6	2.2	2.7	2.9	3.2	2.7	4.5
ABCB11	1.1	1.0	1.0	0.7	0.8	0.7	0.8
			Omeprazol_7d				
	1.55	**3.1**	**6.25**	**12.5**	**25**	**50**	**100**
CYP1A1	12.5	17.6	39.2	73.4	141.3	246.8	225.4
CYP1A2	2.1	2.5	2.5	4.0	8.0	27.6	23.1
CYP2B6	1.3	1.1	1.3	1.3	1.8	2.8	2.0
CYP2C9	0.8	0.7	0.8	0.8	0.9	0.8	0.6
CYP2C19	1.1	0.9	1.0	1.0	1.0	1.2	0.9
CYP3A4	0.6	0.5	0.6	0.7	1.2	2.2	1.9

ABCB11	1.1	1.1	1.0	0.9	0.9	0.9	0.9
			Rifampicine_7d				
	0.1	**0.5**	**1.25**	**2.5**	**5**	**10**	**25**
CYP1A1	1.3	0.8	1.1	0.6	0.7	0.8	0.5
CYP1A2	1.1	0.8	1.0	0.9	0.9	0.7	0.8
CYP2B6	0.7	1.1	1.0	0.8	0.8	1.0	0.9
CYP2C9	0.9	0.8	0.8	0.7	0.6	0.7	0.7
CYP2C19	0.7	1.0	1.0	0.9	1.0	0.9	0.9
CYP3A4	0.4	0.4	0.3	0.2	0.2	0.2	0.2
ABCB11	1.2	1.1	1.1	0.9	1.1	1.0	0.9
			Phenobarbital_7d				
	31	**62.5**	**125**	**250**	**500**	**750**	**1000**
CYP1A1	0.7	0.6	0.5	1.4	0.6	1.0	0.8
CYP1A2	0.9	0.8	0.8	1.0	0.7	1.3	0.8
CYP2B6	1.0	0.9	1.6	2.3	3.1	3.3	5.0
CYP2C9	0.8	0.7	0.9	1.1	1.2	1.2	1.6
CYP2C19	1.1	1.2	1.4	1.4	1.8	1.8	2.5
CYP3A4	0.3	0.3	0.9	0.9	1.8	2.0	4.5
ABCB11	0.9	0.9	1.1	1.1	1.0	1.2	1.0

N=2

			Flumazenil_7d				
	0.003	**0.1**	**0.3**	**1**	**3**	**10**	**30**
CYP1A1	0.6	0.6	0.8	1.3	0.8	2.0	*
CYP1A2	1.2	0.8	0.9	1.0	1.0	1.4	*
CYP2B6	1.3	1.5	1.5	1.5	1.9	1.7	*
CYP2C9	1.0	1.1	1.0	0.9	1.1	1.1	*
CYP2C19	1.1	1.1	1.1	1.0	1.1	1.2	*
CYP3A4	1.1	1.3	1.5	1.5	1.6	1.3	*
ABCB11	1.1	1.2	1.1	1.1	1.1	1.2	*
			Omeprazol_7d				
	1.55	**3.1**	**6.25**	**12.5**	**25**	**50**	**100**
CYP1A1	6.5	20.0	45.8	109.7	191.3	336.6	*
CYP1A2	1.3	3.1	4.0	8.4	15.0	25.7	*
CYP2B6	1.1	1.5	1.8	2.7	3.9	5.8	*
CYP2C9	0.6	0.8	0.7	0.9	1.1	1.1	*
CYP2C19	0.9	1.1	1.0	1.1	1.2	1.4	*
CYP3A4	0.9	1.4	1.8	4.3	9.8	23.5	*
ABCB11	0.8	0.9	0.9	1.1	1.6	1.8	*
			Rifampicine_7d				
	0.1	**0.5**	**1.25**	**2.5**	**5**	**10**	**25**
CYP1A1	2.9	0.9	0.7	0.9	0.9	1.5	0.8
CYP1A2	0.8	0.8	0.7	1.0	0.7	1.1	1.0
CYP2B6	2.0	2.2	3.3	3.5	4.1	5.7	6.2
CYP2C9	1.0	1.2	1.3	1.6	1.7	1.6	1.8
CYP2C19	0.9	1.0	1.2	1.3	1.4	1.4	1.2
CYP3A4	2.8	8.5	23.4	34.9	50.3	71.0	79.4

ABCB11	0.8	0.9	0.8	0.7	0.8	0.8	0.6
			Phenobarbital_7d				
	31	**62.5**	**125**	**250**	**500**	**750**	**1000**
CYP1A1	0.5	0.8	0.9	1.3	2.0	4.2	3.0
CYP1A2	1.2	0.9	1.0	1.1	1.2	1.4	1.3
CYP2B6	2.1	2.8	4.3	6.9	10.7	14.4	16.2
CYP2C9	1.1	1.0	1.2	1.5	1.7	2.1	2.0
CYP2C19	1.1	1.1	1.2	1.4	1.7	2.0	2.0
CYP3A4	2.0	2.9	6.0	17.1	37.3	55.5	81.9
ABCB11	1.0	1.0	1.0	1.3	1.3	1.5	1.5

CYP Induction HepaRG **monolayer** Day 14

N=1

			Flumazenil_14d				
	0.003	**0.1**	**0.3**	**1**	**3**	**10**	**30**
CYP1A1	0.2	0.2	0.0	0.0	-0.2	-0.2	0.3
CYP1A2	0.4	0.7	0.6	0.7	0.4	0.5	0.5
CYP2B6	0.4	0.5	0.5	0.7	0.5	0.9	3.4
CYP2C9	0.9	0.9	1.1	1.1	0.9	1.3	2.4
CYP2C19	1.2	1.2	1.3	1.2	1.0	1.1	1.7
CYP3A4	1.1	1.2	2.7	4.5	3.8	6.4	20.4
ABCB11	0.9	0.7	0.7	0.7	0.4	0.7	0.9
			Omeprazol_14d				
	1.55	**3.1**	**6.25**	**12.5**	**25**	**50**	**100**
CYP1A1	24.5	24.4	40.7	64.7	124.9	117.8	428.3
CYP1A2	2.4	3.3	3.5	4.7	7.5	5.8	28.1
CYP2B6	1.5	1.9	1.5	2.5	2.8	1.4	5.9
CYP2C9	0.9	1.1	1.0	1.2	1.1	0.8	1.6
CYP2C19	1.2	1.3	1.3	1.3	1.3	1.1	1.0
CYP3A4	1.2	1.5	1.3	1.9	2.3	1.5	12.3
ABCB11	2.1	2.2	2.0	2.0	2.2	1.8	3.0
			Rifampicine_14d				
	0.1	**0.5**	**1.25**	**2.5**	**5**	**10**	**25**
CYP1A1	0.9	1.2	0.4	0.9	0.4	0.6	0.9
CYP1A2	0.8	0.8	0.7	0.7	0.8	0.8	0.7
CYP2B6	1.0	1.7	1.3	0.8	0.8	0.6	1.3
CYP2C9	0.9	1.2	1.0	0.9	0.8	0.8	1.1
CYP2C19	0.7	1.1	1.1	1.1	1.0	1.0	1.1
CYP3A4	0.7	1.0	0.7	0.6	0.7	0.6	0.9
ABCB11	1.1	1.3	1.0	0.9	1.0	0.6	0.9
			Phenobarbital_14d				
	31	**62.5**	**125**	**250**	**500**	**750**	**1000**
CYP1A1	1.5	1.5	1.2	1.4	1.2	1.4	1.8
CYP1A2	1.6	1.9	1.8	2.2	1.4	1.7	1.6
CYP2B6	1.4	1.1	2.0	2.0	3.2	5.7	16.6
CYP2C9	1.2	1.1	1.4	1.4	1.9	2.4	3.3
CYP2C19	1.4	1.4	1.6	1.6	1.9	1.9	3.0
CYP3A4	1.0	0.9	1.4	1.9	5.2	6.9	21.4

ABCB11	2.0	2.1	2.0	2.0	1.8	2.4	2.3

N=2

Flumazenil_14d

	0.003	**0.1**	**0.3**	**1**	**3**	**10**	**30**
CYP1A1	0.3	0.3	0.2	0.4	0.8	0.6	2.1
CYP1A2	0.6	0.5	0.4	0.7	0.7	0.8	0.9
CYP2B6	4.5	5.9	5.6	4.5	5.0	4.4	4.4
CYP2C9	3.1	3.3	3.5	3.1	2.9	3.2	2.4
CYP3A4	3.5	4.0	3.6	3.4	3.5	3.5	2.2
CYP2C19	1.4	1.9	1.8	1.5	1.5	2.0	1.7
ABCB11	1.1	1.2	1.1	1.0	0.9	1.2	1.1

Omeprazol_14d

	1.55	**3.1**	**6.25**	**12.5**	**25**	**50**	**100**
CYP1A1	6.6	16.8	45.6	112.9	176.5	278.5	360.6
CYP1A2	0.9	1.0	2.0	3.8	5.9	11.7	18.9
CYP2B6	3.9	5.1	6.4	9.6	11.5	20.2	19.4
CYP2C9	2.8	3.1	3.1	4.0	4.0	4.8	2.5
CYP3A4	3.7	4.4	4.6	4.3	4.8	4.4	2.6
CYP2C19	1.7	1.9	2.5	5.5	10.2	23.8	14.4
ABCB11	1.0	1.2	1.6	1.7	1.7	3.1	2.3

Rifampicine_14d

	0.1	**0.5**	**1.25**	**2.5**	**5**	**10**	**25**
CYP1A1	0.6	0.7	0.5	0.4	1.1	1.9	0.7
CYP1A2	1.0	0.9	0.8	1.0	1.4	3.2	0.7
CYP2B6	2.1	6.0	8.1	10.9	12.1	17.9	17.3
CYP2C9	1.0	3.2	4.3	5.3	5.6	6.1	6.6
CYP3A4	0.8	2.4	3.0	3.4	3.4	3.9	3.6
CYP2C19	2.3	6.2	11.0	18.1	20.5	29.7	44.5
ABCB11	1.2	1.5	1.0	1.3	1.2	2.0	0.9

Phenobarbital_14d

	31	**62.5**	**125**	**250**	**500**	**750**	**1000**
CYP1A1	0.7	0.7	0.6	0.6	1.0	0.9	3.9
CYP1A2	1.1	1.0	0.9	1.1	1.0	1.0	1.4
CYP2B6	6.9	8.5	9.6	16.4	27.0	39.2	26.8
CYP2C9	4.0	5.0	4.6	6.3	7.3	8.0	6.4
CYP3A4	5.0	4.9	4.8	5.3	6.1	6.6	4.4
CYP2C19	3.1	3.9	6.5	14.1	27.8	42.1	33.3
ABCB11	1.7	1.6	1.2	1.5	1.5	1.9	2.0

CYP induction HepaRG **3D** day 3

N=1

Flumazenil_3d

	0.003	**0.1**	**0.3**	**1**	**3**	**10**	**30**
CYP1A1	0.5	0.5	0.5	0.5	0.5	0.6	1.0
CYP1A2	0.9	0.8	0.8	0.9	0.9	0.8	1.4
CYP2B6	0.7	0.6	0.6	0.6	0.6	0.6	1.2
CYP2C9	1.1	1.1	1.0	1.1	1.1	1.0	1.4

CYP2C19	0.9	0.8	0.9	0.8	0.8	0.7	1.1
CYP3A4	0.7	0.6	0.6	0.6	0.6	0.5	1.1
ABCB11	0.7	0.8	0.8	0.8	0.9	0.7	1.0
			Omeprazol_3d				
	1.55	**3.1**	**6.25**	**12.5**	**25**	**50**	**100**
CYP1A1	7.0	9.8	12.1	16.5	16.0	19.7	18.2
CYP1A2	4.6	8.7	15.4	27.6	39.5	49.8	49.5
CYP2B6	1.0	1.1	0.9	1.0	1.4	1.4	1.1
CYP2C9	1.1	1.0	0.9	0.8	0.9	0.7	0.4
CYP2C19	1.1	1.2	1.2	1.1	1.6	1.0	0.9
CYP3A4	0.9	1.1	1.1	1.1	1.1	1.0	0.8
ABCB11	1.0	0.9	0.8	0.6	0.7	0.4	0.3
			Rifampicine_3d				
	0.1	**0.5**	**1.25**	**2.5**	**5**	**10**	**25**
CYP1A1	0.7	0.5	0.8	0.5	0.5	0.5	0.7
CYP1A2	1.0	1.0	1.0	0.7	0.7	0.7	0.6
CYP2B6	0.7	0.9	0.9	1.0	0.9	0.9	0.8
CYP2C9	0.9	1.2	1.1	1.2	1.3	1.1	1.4
CYP2C19	0.9	1.3	1.5	1.8	1.7	1.7	1.5
CYP3A4	1.1	1.5	1.7	1.9	2.0	1.9	2.0
ABCB11	0.8	0.9	1.0	0.6	0.7	0.6	0.5
			Phenobarbital_3d				
	31	**62.5**	**125**	**250**	**500**	**750**	**1000**
CYP1A1	0.8	0.4	0.6	0.7	0.7	0.9	1.5
CYP1A2	0.8	0.6	0.7	0.6	0.7	0.7	0.9
CYP2B6	0.8	0.8	1.4	1.7	2.1	2.1	2.7
CYP2C9	1.0	1.1	1.2	1.2	1.6	1.5	1.6
CYP2C19	0.7	1.0	1.2	1.5	2.3	1.9	3.1
CYP3A4	0.7	0.6	1.3	1.5	2.0	2.0	2.3
ABCB11	0.8	0.7	1.0	0.9	0.7	0.7	0.7

N=2

			Flumazenil_3d				
	0.003	**0.1**	**0.3**	**1**	**3**	**10**	**30**
CYP1A1	0.5	0.4	0.3	0.3	0.3	0.3	0.8
CYP1A2	1.2	1.0	1.0	0.7	0.6	1.0	1.7
CYP2B6	0.9	0.9	0.9	0.7	0.7	0.8	1.2
CYP2C9	0.9	1.0	1.0	1.0	0.8	0.9	0.9
CYP2C19	0.8	0.8	0.9	0.7	0.8	0.8	1.0
CYP3A4	0.7	0.7	0.7	0.6	0.5	0.7	1.3
ABCB11	1.0	0.8	1.0	0.9	0.9	1.2	1.1
			Omeprazol_3d				
	1.55	**3.1**	**6.25**	**12.5**	**25**	**50**	**100**
CYP1A1	4.9	7.2	9.6	9.4	13.1	12.7	19.7
CYP1A2	6.9	14.2	26.2	56.3	93.5	108.5	123.2
CYP2B6	1.1	1.0	1.1	1.2	2.0	2.3	1.8
CYP2C9	0.9	1.0	0.9	0.9	0.8	0.5	0.2

CYP2C19	0.9	0.9	1.0	1.2	1.2	1.3	0.8
CYP3A4	0.8	0.9	0.9	1.0	1.3	1.2	1.0
ABCB11	1.1	0.9	1.0	0.9	0.6	0.5	0.6
			Rifampicine_3d				
	0.1	**0.5**	**1.25**	**2.5**	**5**	**10**	**25**
CYP1A1	2.4	0.4	0.5	0.4	0.4	0.5	0.5
CYP1A2	1.7	1.1	1.1	1.0	1.4	1.4	1.1
CYP2B6	1.1	1.2	1.7	2.1	2.5	2.3	2.6
CYP2C9	1.0	1.3	1.3	1.4	1.6	1.4	1.3
CYP2C19	1.1	1.6	2.0	2.2	2.8	2.7	2.3
CYP3A4	1.6	2.5	3.2	3.5	4.4	4.0	4.0
ABCB11	0.9	1.0	1.0	0.9	0.9	0.9	0.8
			Phenobarbital_3d				
	31	**62.5**	**125**	**250**	**500**	**750**	**1000**
CYP1A1	0.4	0.4	0.3	0.7	0.4	0.4	4.9
CYP1A2	0.7	0.7	1.1	2.5	1.1	1.5	5.4
CYP2B6	1.4	1.9	1.8	2.7	3.6	4.2	4.1
CYP2C9	1.1	1.3	1.4	1.6	1.8	1.7	1.5
CYP2C19	1.0	1.2	1.4	2.1	2.8	3.7	3.2
CYP3A4	1.0	1.4	2.0	2.6	3.8	3.7	4.2
ABCB11	1.0	1.0	1.2	1.2	1.1	1.1	0.9

CYP induction HepaRG **3D** day 7

N=1

			Flumazenil_7d				
	0.003	**0.1**	**0.3**	**1**	**3**	**10**	**30**
CYP1A1	0.7	0.7	0.7	0.7	0.6	0.7	1.0
CYP1A2	0.8	0.8	1.0	0.8	0.8	0.8	1.1
CYP2B6	1.5	1.4	1.5	1.5	1.3	1.5	2.0
CYP2C9	1.4	1.3	1.4	1.4	1.3	1.4	1.9
CYP2C19	1.5	1.5	1.6	1.6	1.4	1.6	2.1
CYP3A4	1.2	1.2	1.2	1.3	1.1	1.2	1.7
ABCB11	1.3	1.1	1.2	1.3	1.0	1.3	1.1
			Omeprazol_7d				
	1.55	**3.1**	**6.25**	**12.5**	**25**	**50**	**100**
CYP1A1	5.1	7.8	10.6	11.2	13.4	15.1	11.7
CYP1A2	3.1	5.4	9.1	14.3	17.3	23.0	18.4
CYP2B6	1.5	1.6	2.1	2.3	2.5	2.9	1.6
CYP2C9	1.4	1.3	1.5	1.1	1.1	1.1	0.6
CYP2C19	1.5	1.4	1.9	2.1	1.7	1.6	1.0
CYP3A4	1.2	1.0	1.2	1.2	1.3	1.2	0.7
ABCB11	1.1	0.9	1.0	0.7	0.5	0.4	0.4
			Rifampicine_7d				
	0.1	**0.5**	**1.25**	**2.5**	**5**	**10**	**25**
CYP1A1	1.0	0.8	0.8	0.7	0.6	0.7	0.8
CYP1A2	1.1	0.8	0.7	0.7	0.5	0.5	0.6
CYP2B6	1.6	2.0	2.3	2.7	2.8	3.0	2.7
CYP2C9	1.5	1.7	1.9	1.9	2.1	2.0	1.8

CYP2C19	1.9	2.6	2.9	3.6	3.2	3.2	3.2
CYP3A4	1.7	2.1	2.2	2.6	2.5	2.5	2.4
ABCB11	1.5	1.4	1.2	1.3	0.9	0.9	0.9
			Phenobarbital_7d				
	31	**62.5**	**125**	**250**	**500**	**750**	**1000**
CYP1A1	0.8	0.6	0.7	0.7	0.7	0.6	1.3
CYP1A2	0.8	0.8	0.9	0.8	0.7	0.6	1.1
CYP2B6	1.6	1.4	2.5	3.3	3.5	3.5	5.9
CYP2C9	1.4	1.2	1.3	2.0	1.8	1.8	2.8
CYP2C19	1.6	1.5	2.3	2.8	3.2	2.9	5.7
CYP3A4	1.2	1.2	1.6	2.2	2.3	2.2	3.2
ABCB11	1.3	1.2	1.2	1.0	0.8	0.8	1.2
			N=2				
			Flumazenil_7d				
	0.003	**0.1**	**0.3**	**1**	**3**	**10**	**30**
CYP1A1	0.8	0.8	0.6	0.9	0.6	0.8	1.3
CYP1A2	1.2	0.7	1.1	1.9	1.1	0.8	0.8
CYP2B6	1.5	1.5	1.7	1.4	1.6	1.5	1.4
CYP2C9	1.3	1.2	1.3	1.0	1.2	1.2	1.0
CYP2C19	1.4	1.2	1.4	0.8	1.3	1.3	1.0
CYP3A4	1.6	1.6	1.8	1.5	1.7	1.4	1.6
ABCB11	1.2	1.0	1.2	1.5	1.1	1.4	0.9
			Omeprazol_7d				
	1.55	**3.1**	**6.25**	**12.5**	**25**	**50**	**100**
CYP1A1	6.5	11.5	16.7	15.2	27.6	34.1	32.5
CYP1A2	3.0	6.0	12.5	14.5	44.9	71.0	100.0
CYP2B6	1.7	1.7	2.1	1.1	4.2	4.9	3.9
CYP2C9	1.2	1.1	1.2	0.8	0.9	1.0	0.6
CYP2C19	1.2	1.4	1.3	0.8	1.6	1.8	1.1
CYP3A4	1.3	1.5	2.1	1.9	3.3	4.4	3.6
ABCB11	1.0	1.0	0.9	0.5	0.8	0.7	0.5
			Rifampicine_7d				
	0.1	**0.5**	**1.25**	**2.5**	**5**	**10**	**25**
CYP1A1	3.0	1.0	0.9	0.9	0.8	1.0	1.2
CYP1A2	0.5	0.8	0.8	0.6	0.7	0.7	0.6
CYP2B6	1.4	2.9	4.1	5.0	5.9	5.8	6.5
CYP2C9	1.1	1.7	1.9	2.0	1.9	2.0	2.1
CYP2C19	1.1	2.1	2.6	3.0	2.9	3.7	3.7
CYP3A4	2.3	6.1	7.7	10.1	9.9	10.1	12.0
ABCB11	1.0	1.0	0.9	0.9	0.9	0.7	0.9
			Phenobarbital_7d				
	31	**62.5**	**125**	**250**	**500**	**750**	**1000**
CYP1A1	0.9	0.8	1.0	1.3	1.3	1.3	4.9
CYP1A2	1.1	1.0	1.2	1.4	1.3	1.0	2.6
CYP2B6	1.8	2.5	3.6	4.9	5.6	7.1	8.0
CYP2C9	1.3	1.2	1.8	1.7	2.1	1.9	2.1

CYP2C19	1.2	1.4	1.9	2.0	2.8	3.3	3.8
CYP3A4	2.3	3.0	4.5	6.9	9.9	10.6	10.6
ABCB11	0.9	1.0	1.2	1.7	1.1	1.0	1.2

CYP induction HepaRG **3D** day 14

N=1

Flumazenil_14d

	0.003	**0.1**	**0.3**	**1**	**3**	**10**	**30**
CYP1A1	0.7	0.7	0.7	0.7	0.7	0.7	1.1
CYP1A2	0.6	0.7	0.7	0.7	0.6	0.7	1.4
CYP2B6	0.9	0.9	0.8	0.9	0.9	0.8	1.5
CYP2C9	0.8	0.8	0.7	0.9	0.8	0.8	1.4
CYP2C19	0.8	0.7	0.8	0.9	0.8	0.7	1.2
CYP3A4	0.9	0.9	0.9	0.9	0.9	0.8	1.3
ABCB11	0.8	1.0	0.9	1.2	0.9	0.8	1.0

Omeprazol_14d

	1.55	**3.1**	**6.25**	**12.5**	**25**	**50**	**100**
CYP1A1	5.0	4.8	8.9	11.6	16.9	14.0	21.0
CYP1A2	2.7	3.0	6.4	9.2	17.7	13.5	42.9
CYP2B6	1.0	0.9	1.4	1.7	2.0	1.5	2.0
CYP2C9	0.9	0.8	0.8	0.9	0.9	0.8	0.6
CYP2C19	0.9	0.9	1.0	1.0	1.2	1.1	1.2
CYP3A4	1.1	0.9	0.9	1.2	1.2	1.0	0.9
ABCB11	1.0	0.9	0.9	0.8	0.6	0.5	0.4

Rifampicine_14d

	0.1	**0.5**	**1.25**	**2.5**	**5**	**10**	**25**
CYP1A1	1.0	0.8	0.8	0.8	0.8	0.9	0.8
CYP1A2	1.0	0.7	0.7	0.7	0.9	0.6	0.6
CYP2B6	0.9	1.3	1.5	1.8	2.1	2.1	2.7
CYP2C9	1.0	1.2	1.2	1.3	1.4	1.3	1.6
CYP2C19	0.9	1.3	1.2	1.6	1.9	2.0	2.3
CYP3A4	1.2	1.6	1.6	2.0	2.1	2.0	2.3
ABCB11	1.0	1.1	1.0	1.1	1.0	0.8	0.9

Phenobarbital_14d

	31	**62.5**	**125**	**250**	**500**	**750**	**1000**
CYP1A1	1.0	0.7	0.8	0.7	0.8	0.7	1.3
CYP1A2	0.8	0.7	0.8	0.8	0.7	0.7	1.1
CYP2B6	0.9	0.8	1.7	2.0	2.7	2.7	4.3
CYP2C9	0.8	0.7	1.0	1.1	1.2	1.4	1.8
CYP2C19	0.8	0.8	1.2	1.4	1.9	2.0	3.4
CYP3A4	0.9	0.9	1.3	1.4	1.8	1.9	2.3
ABCB11	1.0	1.1	1.1	0.9	1.0	0.9	0.9

N=2

Flumazenil_14d

	0.003	**0.1**	**0.3**	**1**	**3**	**10**	**30**
CYP1A1	0.6	0.7	0.7	0.6	0.8	1.9	1.3
CYP1A2	0.5	0.5	0.4	0.4	0.9	2.3	1.5

CYP2B6	1.0	1.0	0.8	0.8	1.3	1.3	1.1
CYP2C9	1.0	0.9	0.8	0.8	1.1	0.8	0.8
CYP2C19	0.9	0.9	0.8	0.7	1.0	1.1	0.9
CYP3A4	1.1	1.2	1.2	1.5	1.8	1.4	1.5
ABCB11	0.8	0.8	0.7	0.7	0.9	0.9	0.8

Omeprazol_14d

	1.55	**3.1**	**6.25**	**12.5**	**25**	**50**	**100**
CYP1A1	2.8	4.6	8.3	9.0	9.6	10.6	10.0
CYP1A2	2.1	4.6	12.9	16.2	22.4	22.1	16.3
CYP2B6	1.1	0.8	1.8	1.8	1.8	2.4	2.3
CYP2C9	1.0	0.7	0.9	0.7	0.6	0.5	0.5
CYP2C19	1.0	0.7	1.1	1.1	1.0	1.0	1.1
CYP3A4	1.0	0.9	1.4	1.3	1.2	1.3	1.9
ABCB11	0.8	0.4	0.6	0.4	0.5	0.4	0.4

Rifampicine_14d

	0.1	**0.5**	**1.25**	**2.5**	**5**	**10**	**25**
CYP1A1	1.1	0.7	0.6	0.6	0.7	0.6	0.7
CYP1A2	1.2	1.0	0.7	0.5	0.7	0.5	0.7
CYP2B6	1.5	1.3	1.7	1.8	2.4	3.5	3.4
CYP2C9	1.2	1.1	1.4	1.3	1.4	2.1	1.6
CYP2C19	1.2	1.5	1.5	1.7	2.0	2.9	2.9
CYP3A4	1.8	3.1	2.9	2.7	3.6	4.9	3.9
ABCB11	1.0	0.8	1.0	0.8	0.8	0.7	0.8

Phenobarbital_14d

	31	**62.5**	**125**	**250**	**500**	**750**	**1000**
CYP1A1	0.7	0.6	0.7	0.9	0.8	1.0	1.2
CYP1A2	0.7	0.7	0.9	0.9	0.7	1.3	1.5
CYP2B6	1.3	1.6	1.6	2.4	2.9	4.8	3.5
CYP2C9	1.1	1.3	1.3	1.6	1.7	1.9	1.6
CYP2C19	1.2	1.2	1.8	1.8	2.6	4.0	2.0
CYP3A4	2.1	1.8	3.0	3.4	3.7	4.5	4.5
ABCB11	1.0	0.9	0.8	0.8	0.8	0.9	1.4

Appendix 3a: Viability in HepaRG cells 2D vs. 3D at days 3. 7 and 14. Data expressed as % of control

APAP [µM]	DAY 3									
	2D					3D				
	N=1	N=2	N=3	mean	stDev	N=1	N=2	N=3	mean	stDev
0	100.00	100.00	100.00	**100.00**	**0.00**	100.00	100.00	100.00	**100.00**	**0.00**
100	98.35	100.69	105.18	**101.41**	**2.84**	95.73	89.76	102.08	**95.85**	**5.03**
200	99.38	100.27	106.17	**101.94**	**3.02**	95.92	85.87	99.89	**93.89**	**5.90**
500	98.74	95.13	106.24	**100.04**	**4.62**	94.77	83.19	99.32	**92.42**	**6.79**
1.000	91.79	85.41	97.34	**91.51**	**4.87**	76.63	74.22	88.88	**79.91**	**6.42**
2.000	82.45	64.51	72.90	**73.29**	**7.33**	52.26	55.61	77.46	**61.77**	**11.17**
5.000	52.60	20.05	57.34	**43.33**	**16.58**	29.22	32.32	63.26	**41.60**	**15.37**
10.000	19.06	1.51	11.24	**10.60**	**7.18**	3.32	13.46	47.08	**21.28**	**18.70**
	DAY 7									
	N=1	N=2	N=3	mean	stDev	N=1	N=2	N=3	mean	stDev
0	100.00	100.00	100.00	**100.00**	**0.00**	100.00	100.00	100.00	**100.00**	**0.00**
100	100.69	88.72	100.92	**96.78**	**5.70**	95.73	86.92	98.99	**93.88**	**5.10**
200	100.27	91.51	103.83	**98.54**	**5.18**	95.92	94.95	99.34	**96.74**	**1.88**
500	95.12	88.16	96.70	**93.33**	**3.71**	94.77	91.39	81.51	**89.22**	**5.63**
1.000	85.39	79.49	79.96	**81.61**	**2.68**	76.63	74.73	73.62	**74.99**	**1.24**
2.000	64.46	68.29	43.31	**58.69**	**10.99**	52.26	56.85	53.24	**54.12**	**1.97**
5.000	19.93	16.62	1.55	**12.70**	**8.00**	29.22	18.94	21.68	**23.28**	**4.35**
10.000	1.37	2.19	0.16	**1.24**	**0.83**	3.32	6.97	9.59	**6.63**	**2.57**
	DAY 14									
	N=1	N=2	N=3	mean	stDev	N=1	N=2	N=3	mean	stDev
0	100.00	100.00	100.00	**100.00**	**0.00**	100.00	100.00	100.00	**100.00**	**0.00**
100	100.92	86.78	86.47	**91.39**	**6.74**	97.81	76.84	81.79	**85.48**	**8.95**
200	103.83	84.85	85.37	**91.35**	**8.83**	96.90	71.32	76.17	**81.46**	**11.09**
500	96.70	81.68	81.21	**86.53**	**7.19**	84.72	67.33	70.60	**74.22**	**7.54**
1.000	79.96	66.93	69.53	**72.14**	**5.63**	68.85	48.88	53.86	**57.20**	**8.49**
2.000	43.32	33.71	40.37	**39.13**	**4.02**	30.94	27.21	29.20	**29.12**	**1.53**
5.000	1.58	0.71	0.94	**1.08**	**0.37**	3.04	2.29	3.09	**2.81**	**0.37**
10.000	0.19	0.10	0.14	**0.14**	**0.04**	0.40	-0.37	0.33	**0.12**	**0.35**

BOS [µM]	DAY 3									
	2D					3D				
	N=1	N=2	N=3	mean	stDev	N=1	N=2	N=3	mean	stDev
0	100.00	100.00	100.00	**100.00**	**0.00**	100.00	100.00	100.00	**100.00**	**0.00**
4	100.74	105.18	100.69	**102.20**	**2.11**	102.32	95.47	95.77	**97.85**	**3.16**
10	101.80	106.17	94.67	**100.88**	**4.74**	96.03	96.44	100.73	**97.73**	**2.12**
20	102.97	106.24	94.60	**101.27**	**4.90**	83.32	100.82	100.80	**94.98**	**8.24**
40	103.40	97.34	95.84	**98.86**	**3.27**	93.88	96.57	97.86	**96.10**	**1.66**
100	96.74	72.90	92.94	**87.53**	**10.46**	66.07	94.12	82.43	**80.87**	**11.50**
200	79.30	57.34	78.42	**71.69**	**10.15**	37.56	80.48	67.57	**61.87**	**17.98**
400	54.01	11.24	57.54	**40.93**	**21.04**	8.70	38.73	58.79	**35.41**	**20.58**
	DAY 7									
	N=1	N=2	N=3	mean	stDev	N=1	N=2	N=3	mean	stDev
0	100.00	100.00	100.00	**100.00**	**0.00**	100.00	100.00	100.00	**100.00**	**0.00**
4	105.19	97.56	101.12	**101.29**	**3.12**	102.32	94.43	96.38	**97.71**	**3.35**
10	106.18	107.36	102.85	**105.47**	**1.91**	96.03	108.57	95.17	**99.92**	**6.12**
20	106.24	111.76	100.89	**106.30**	**4.44**	83.32	115.65	99.13	**99.37**	**13.20**
40	97.33	99.83	79.94	**92.37**	**8.85**	93.88	110.11	94.63	**99.54**	**7.48**
100	72.86	75.11	36.90	**61.62**	**17.51**	66.07	109.45	89.70	**88.41**	**17.73**
200	57.27	59.99	11.75	**43.00**	**22.12**	37.65	38.727	60.96	**45.75**	**10.77**
400	11.10	13.27	0.25	**8.21**	**5.69**	8.70	14.84	20.37	**14.64**	**4.77**
	DAY 14									
	N=1	N=2	N=3	mean	stDev	N=1	N=2	N=3	mean	stDev
0	100.00	100.00	100.00	**100.00**	**0.00**	100.00	100.00	100.00	**100.00**	**0.00**
4	101.12	103.06	98.13	**100.77**	**2.03**	108.24	87.63	87.21	**94.36**	**9.82**
10	102.85	104.02	96.69	**101.19**	**3.22**	105.61	85.10	85.48	**92.06**	**9.58**
20	100.89	102.20	98.36	**100.48**	**1.59**	98.72	75.71	75.48	**83.30**	**10.90**
40	79.95	95.06	94.83	**89.95**	**7.07**	105.01	82.30	81.95	**89.75**	**10.79**
100	36.92	46.83	48.06	**43.93**	**4.99**	76.94	67.10	66.95	**70.33**	**4.67**
200	11.78	17.96	21.71	**17.15**	**4.09**	24.45	29.08	30.85	**28.13**	**2.70**
400	0.29	0.35	0.42	**0.35**	**0.06**	0.53	-0.10	0.66	**0.36**	**0.33**

DCF [µM]	DAY 3									
	2D					3D				
	N=1	N=2	N=3	mean	stDev	N=1	N=2	N=3	mean	stDev
0	100.00	100.00	100.00	**100.00**	**0.00**	100.00	100.00	100.00	**100.00**	**0.00**
5	106.90	90.55	102.78	**100.08**	**6.94**	87.40	98.45	100.12	**95.32**	**5.64**
10	107.72	96.00	102.83	**102.18**	**4.80**	86.11	102.93	98.92	**95.99**	**7.17**
25	108.93	94.99	101.00	**101.64**	**5.71**	81.06	103.39	97.60	**94.01**	**9.46**
50	109.97	92.10	95.46	**99.18**	**7.75**	79.15	102.34	98.83	**93.44**	**10.21**
100	109.67	89.94	86.38	**95.33**	**10.24**	75.35	89.34	91.04	**85.24**	**7.03**
250	103.26	80.16	82.30	**88.57**	**10.42**	60.94	72.30	84.80	**72.68**	**9.74**
500	57.54	1.70	26.32	**28.52**	**22.85**	17.56	6.03	59.44	**27.68**	**22.95**
	DAY 7									
	N=1	N=2	N=3	mean	stDev	N=1	N=2	N=3	mean	stDev
0	100.00	100.00	100.00	**100.00**	**0.00**	100.00	100.00	100.00	**100.00**	**0.00**
5	90.53	101.15	95.14	**95.61**	**4.35**	98.67	79.12	85.86	**87.88**	**8.11**
10	96.00	110.07	97.35	**101.14**	**6.34**	96.68	72.10	96.68	**88.49**	**11.59**
25	94.98	111.12	95.46	**100.52**	**7.50**	93.50	74.25	93.57	**87.11**	**9.09**
50	92.09	109.35	94.15	**98.53**	**7.70**	86.06	75.00	98.10	**86.39**	**9.43**
100	89.92	101.32	91.45	**94.23**	**5.05**	86.71	68.33	85.33	**80.13**	**8.36**
250	80.13	86.50	68.31	**78.31**	**7.53**	42.73	41.98	61.60	**48.77**	**9.08**
500	1.56	2.19	0.34	**1.36**	**0.77**	0.96	0.85	20.08	**7.30**	**9.04**
	DAY 14									
	N=1	N=2	N=3	mean	stDev	N=1	N=2	N=3	mean	stDev
0	100.00	100.00	100.00	**100.00**	**0.00**	100.00	100.00	100.00	**100.00**	**0.00**
5	95.14	100.39	100.51	**98.68**	**2.50**	72.85	84.05	83.38	**80.09**	**5.13**
10	97.36	101.89	101.78	**100.34**	**2.11**	60.60	81.05	82.58	**74.74**	**10.02**
25	95.46	103.53	102.33	**100.44**	**3.55**	71.68	75.85	77.99	**75.17**	**2.62**
50	94.15	97.83	103.00	**98.33**	**3.63**	60.51	77.75	77.35	**71.87**	**8.04**
100	91.45	93.29	100.21	**94.98**	**3.77**	53.56	74.43	76.54	**68.18**	**10.37**
250	68.32	75.69	88.86	**77.62**	**8.49**	14.83	27.85	29.75	**24.15**	**6.63**
500	0.37	0.42	0.46	**0.42**	**0.04**	0.51	0.58	0.50	**0.53**	**0.04**

FIA [µM]	DAY 3									
	2D					3D				
	N=1	N=2	N=3	mean	stDev	N=1	N=2	N=3	mean	stDev
0	100.00	100.00	100.00	**100.00**	**0.00**	100.00	100.00	100.00	**100.00**	**0.00**
0.3	114.73	103.06	98.72	**105.50**	**6.76**	114.73	129.17	100.38	**114.76**	**11.75**
1	96.69	104.02	96.33	**99.01**	**3.55**	131.03	133.48	94.80	**119.77**	**17.68**
3	98.36	102.20	106.99	**102.52**	**3.53**	141.68	134.00	98.71	**124.79**	**18.71**
10	103.40	95.06	97.75	**98.74**	**3.48**	136.41	116.06	95.54	**116.00**	**16.69**
30	97.56	91.79	106.35	**98.57**	**5.99**	148.05	126.04	98.08	**124.06**	**20.45**
100	95.62	71.59	3.87	**57.03**	**38.85**	95.62	71.59	92.13	**86.45**	**10.60**
300	76.94	68.45	22.41	**55.93**	**23.96**	76.94	67.10	66.07	**70.04**	**4.90**
	DAY 7									
	N=1	N=2	N=3	mean	stDev	N=1	N=2	N=3	mean	stDev
0	100.00	100.00	100.00	**100.00**	**0.00**	100.00	100.00	100.00	**100.00**	**0.00**
0.3	105.70	106.25	105.70	**105.89**	**0.26**	105.70	88.32	98.02	**97.35**	**7.11**
1	104.22	111.14	104.22	**106.53**	**3.26**	104.22	85.74	98.59	**96.18**	**7.73**
3	57.09	60.59	57.09	**58.26**	**1.65**	57.09	75.95	97.86	**76.96**	**16.66**
10	86.22	108.14	86.22	**93.53**	**10.33**	86.22	82.65	88.02	**85.63**	**2.23**
30	0.67	77.05	0.67	**26.13**	**36.00**	0.67	10.35	8.70	**6.57**	**4.23**
100	0.11	0.43	0.11	**0.22**	**0.15**	0.11	0.32	1.58	**0.67**	**0.65**
300	0.00	0.06	0.00	**0.02**	**0.03**	0.00	0.00	1.51	**0.50**	**0.71**
	DAY 14									
	N=1	N=2	N=3	mean	stDev	N=1	N=2	N=3	mean	stDev
0	100.00	100.00	100.00	**100.00**	**0.00**	100.00	100.00	100.00	**100.00**	**0.00**
0.3	93.19	104.34	101.02	**99.52**	**4.68**	93.19	81.16	81.14	**85.16**	**5.67**
1	94.17	108.36	101.30	**101.28**	**5.79**	94.17	74.79	75.17	**81.38**	**9.05**
3	78.66	106.21	104.32	**96.40**	**12.57**	78.66	37.56	53.61	**56.61**	**16.91**
10	1.11	0.82	40.37	**14.10**	**18.58**	1.11	1.63	2.63	**1.79**	**0.63**
30	0.37	0.29	0.59	**0.42**	**0.13**	0.37	5.63	22.35	**9.45**	**9.37**
100	0.16	0.09	0.16	**0.14**	**0.03**	0.16	0.32	1.02	**0.50**	**0.37**
300	0.00	0.00	0.00	**0.00**	**0.00**	0.00	0.00	0.70	**0.23**	**0.33**

PIO [µM]	DAY 3									
	2D					3D				
	N=1	N=2	N=3	mean	stDev	N=1	N=2	N=3	mean	stDev
0	100.00	100.00	NA	**100.00**	**0.00**	100.00	100.00	100.00	**100.00**	**0.00**
4	103.47	94.68	NA	**99.07**	**4.40**	94.76	103.19	97.27	**98.41**	**3.54**
10	103.68	94.61	NA	**99.14**	**4.54**	97.57	109.08	91.68	**99.44**	**7.23**
20	103.14	95.85	NA	**99.49**	**3.65**	95.95	96.71	89.90	**94.19**	**3.05**
40	102.22	92.95	NA	**97.59**	**4.64**	87.05	90.80	93.64	**90.50**	**2.70**
100	103.55	90.93	NA	**97.24**	**6.31**	81.30	86.78	101.49	**89.86**	**8.52**
200	99.41	91.16	NA	**95.28**	**4.13**	79.35	79.73	87.92	**82.33**	**3.95**
400	97.92	89.58	NA	**93.75**	**4.17**	77.54	61.81	92.61	**77.32**	**12.58**
	DAY 7									
	N=1	N=2	N=3	mean	stDev	N=1	N=2	N=3	mean	stDev
0	100.00	100.00	100.00	**100.00**	**0.00**	100.00	100.00	100.00	**100.00**	**0.00**
4	88.79	115.57	94.67	**99.68**	**11.49**	74.77	78.05	87.57	**80.13**	**5.43**
10	90.60	112.16	94.60	**99.12**	**9.36**	66.42	84.47	86.43	**79.11**	**9.01**
20	89.20	112.55	95.84	**99.20**	**9.82**	65.68	82.06	81.60	**76.45**	**7.61**
40	88.38	110.17	92.94	**97.17**	**9.38**	65.89	81.84	62.39	**70.04**	**8.47**
100	86.30	105.80	90.92	**94.34**	**8.32**	61.72	77.50	65.62	**68.28**	**6.71**
200	81.70	110.25	91.14	**94.36**	**11.88**	53.71	63.57	62.13	**59.80**	**4.35**
400	77.47	100.37	89.57	**89.14**	**9.36**	61.63	66.86	58.89	**62.46**	**3.31**
	DAY 14									
	N=1	N=2	N=3	mean	stDev	N=1	N=2	N=3	mean	stDev
0	100.00	100.00	100.00	**100.00**	**0.00**	100.00	100.00	100.00	**100.00**	**0.00**
4	88.79	101.17	97.24	**95.73**	**5.16**	62.98	75.54	82.48	**73.66**	**8.07**
10	90.60	101.33	95.46	**95.80**	**4.39**	63.07	76.91	83.96	**74.65**	**8.68**
20	89.21	97.85	95.34	**94.13**	**3.63**	59.15	67.46	73.73	**66.78**	**5.97**
40	88.39	101.03	93.69	**94.37**	**5.19**	53.60	62.73	68.61	**61.65**	**6.17**
100	86.30	93.26	91.26	**90.28**	**2.93**	52.39	54.96	59.76	**55.70**	**3.05**
200	81.70	87.41	87.98	**85.70**	**2.84**	47.78	47.14	49.53	**48.15**	**1.01**
400	77.47	81.15	81.99	**80.20**	**1.96**	58.70	38.87	42.78	**46.78**	**8.57**

TRO [µM]	DAY 3									
	2D					3D				
	N=1	N=2	N=3	mean	stDev	N=1	N=2	N=3	mean	stDev
0	100.00	100.00	NA	**100.00**	**0.00**	100.00	100.00	100.00	**100.00**	**0.00**
4	103.31	94.60	NA	**98.96**	**4.36**	93.65	98.51	103.19	**98.45**	**3.90**
10	102.83	98.48	NA	**100.65**	**2.18**	92.38	95.27	109.08	**98.91**	**7.29**
20	99.77	101.31	NA	**100.54**	**0.77**	93.87	90.86	96.71	**93.81**	**2.39**
40	98.01	98.30	NA	**98.16**	**0.15**	88.11	94.28	81.84	**88.08**	**5.08**
100	103.86	96.54	NA	**100.20**	**3.66**	81.23	91.61	77.50	**83.45**	**5.97**
200	93.00	95.57	NA	**94.28**	**1.29**	77.60	88.58	63.57	**76.58**	**10.24**
400	93.54	89.56	NA	**91.55**	**1.99**	76.77	71.88	66.86	**71.84**	**4.05**
	DAY 7									
	N=1	N=2	N=3	mean	stDev	N=1	N=2	N=3	mean	stDev
0	100.00	100.00	100.00	**100.00**	**0.00**	100.00	100.00	100.00	**100.00**	**0.00**
4	85.44	111.04	94.59	**97.02**	**10.59**	76.34	82.48	86.99	**81.94**	**4.36**
10	90.16	114.19	98.47	**100.94**	**9.96**	76.45	83.96	80.39	**80.27**	**3.07**
20	94.80	121.79	101.32	**105.97**	**11.50**	75.36	75.85	77.53	**76.24**	**0.93**
40	85.87	113.34	98.30	**99.17**	**11.23**	70.66	77.75	75.38	**74.60**	**2.95**
100	92.92	115.72	96.53	**101.72**	**10.01**	62.02	74.43	61.87	**66.11**	**5.88**
200	82.64	105.22	95.56	**94.47**	**9.25**	60.26	62.73	48.47	**57.15**	**6.22**
400	76.75	92.33	89.54	**86.21**	**6.78**	64.37	54.96	36.14	**51.82**	**11.74**
	DAY 14									
	N=1	N=2	N=3	mean	stDev	N=1	N=2	N=3	mean	stDev
0	100.00	100.00	100.00	**100.00**	**0.00**	100.00	100.00	100.00	**100.00**	**0.00**
4	85.45	105.04	103.67	**98.05**	**8.93**	64.81	72.52	72.61	**69.98**	**3.65**
10	90.16	101.93	99.40	**97.16**	**5.06**	66.98	69.14	68.62	**68.25**	**0.92**
20	94.80	103.02	103.34	**100.39**	**3.95**	63.06	61.48	61.38	**61.97**	**0.77**
40	85.87	95.85	100.62	**94.12**	**6.15**	53.66	48.99	49.53	**50.73**	**2.09**
100	90.07	88.37	93.69	**90.71**	**2.22**	51.63	32.15	32.43	**38.73**	**9.12**
200	84.60	102.76	6.93	**64.76**	**41.56**	51.32	15.76	16.88	**27.99**	**16.50**
400	78.42	102.23	18.16	**66.27**	**35.38**	53.23	7.37	8.22	**22.94**	**21.42**

Appendix 3b: Viability in PHH 3D from two donors at day 3, 7 and 14. Data expressed as % of control.

Acetaminophen

	Donor 1						Donor 2					
cAPAP [µM]	Day 3		Day 7		Day 14		Day 3		Day 7		Day 14	
	% viability	% StDev	% viability	% StDev	% viability	% StDev	% viability	% StDev	% viability	% StDev	% viability	% StDev
0	100.00	24.63	100.00	17.74	100.00	13.18	100.00	21.32	100.00	25.99	100.00	25.00
100	95.19	12.97	79.46	16.26	71.44	19.52	89.99	15.09	130.89	31.96	94.19	12.17
200	115.40	17.68	89.74	15.06	76.90	22.08	78.28	18.35	103.94	13.46	85.08	15.97
500	77.83	19.46	105.88	19.19	70.76	39.13	36.19	7.10	100.36	19.92	93.12	9.56
1,000	91.71	14.34	94.68	11.46	93.38	34.55	71.25	8.30	92.13	13.25	91.42	27.06
2,000	74.95	15.97	76.84	2.79	46.32	23.70	74.90	10.31	81.19	11.68	44.22	13.75
5,000	61.43	22.49	38.58	4.29	8.26	2.03	59.03	13.44	45.22	7.69	8.90	0.54
10,000	53.83	9.07	22.71	1.14	2.76	2.09	38.51	8.43	36.62	16.91	0.30	0.46

Bosentane

	Donor 1						Donor 2					
cBOS [µM]	Day 3		Day 7		Day 14		Day 3		Day 7		Day 14	
	% viability	% StDev	% viability	% StDev	% viability	% StDev	% viability	% StDev	% viability	% StDev	% viability	% StDev
0	100.00	42.33	100.00	9.98	100.00	20.64	100.26	17.88	100.00	5.96	100.00	18. 03
4	66.33	39.44	90.74	14.08	83.82	7.98	82.79	11.52	131.25	24.20	102.27	10.21
10	58.36	41.18	89.42	11.29	75.42	9.14	98.87	15.34	109.79	25.40	88.30	15.09
20	40.22	9.12	94.34	18.15	63.77	15.44	79.21	12.55	100.81	11.74	88.44	30.10
40	36.76	12.67	63.03	37.93	50.69	16.80	78.85	20.35	87.46	3.64	59.88	12.87
100	40.40	9.41	55.38	6.13	9.09	4.62	90.29	9.86	69.95	17.54	10.52	2.26
200	65.96	39.08	58.94	13.42	0.45	0.01	76.41	8.85	51.78	8.63	1.18	0.35
400	40.36	25.23	19.33	10.07	-0.34	0.41	51.40	14.00	1.34	1.51	-0.05	0.03

Diclofenac

cDCF [µM]	Donor 1						Donor 2					
	Day 3		Day 7		Day 14		Day 3		Day 7		Day 14	
	% viability	% StDev	% viability	% StDev	% viability	% StDev	% viability	% StDev	% viability	% StDev	% viability	% StDev
0	100.00	16.79	100.00	0.12	100.00	7.50	106.10	27.49	100.00	15.69	100.00	11.00
5	112.57	27.38	107.83	6.71	111.27	14.05	89.30	28.51	174.48	46.03	91.55	23.52
10	116.93	18.04	103.59	10.00	128.26	20.85	70.27	13.16	139.30	10.90	104.81	19.06
25	123.26	47.25	78.09	18.75	108.24	10.88	67.36	16.82	132.53	38.36	66.26	12.21
50	83.53	38.14	67.08	16.86	58.52	13.50	60.52	13.41	99.81	16.39	24.06	4.18
100	73.55	14.07	41.00	6.26	27.76	1.46	61.13	20.74	52.13	2.40	4.38	0.25
250	38.67	19.97	0.63	0.35	-0.29	0.11	43.03	6.74	1.14	0.79	-0.12	0.01
500	9.38	3.39	-0.13	0.12	-0.28	0.02	4.41	1.02	-0.15	0.02	-0.13	0.01

Fialuridine

cFIA [µM]	Donor 1						Donor 2					
	Day 3		Day 7		Day 14		Day 3		Day 7		Day 14	
	% viability	% StDev	% viability	% StDev	% viability	% StDev	% viability	% StDev	% viability	% StDev	% viability	% StDev
0	100.00	11.10	100.00	12.32	100.00	13.48	100.00	14.29	100.00	41.79	100.00	36.00
0.3	93.42	28.56	72.16	11.76	63.19	7.08	69.05	20.49	85.73	19.69	52.77	32.01
1	90.59	18.18	65.15	9.29	44.68	4.25	90.32	6.99	81.09	18.33	47.11	9.84
3	63.29	24.05	50.59	10.97	43.20	19.46	64.42	22.70	69.10	13.69	24.93	11.31
10	78.52	39.49	74.57	11.93	14.17	4.07	72.80	21.30	51.24	17.42	13.18	4.28
30	83.25	29.53	57.80	9.60	9.79	5.99	66.50	10.96	47.85	10.40	7.24	4.51
100	84.86	22.44	42.07	7.80	3.41	0.16	71.55	14.75	29.93	9.39	0.20	0.32
300	83.84	14.12	6.27	1.23	-0.22	0.75	72.41	23.69	2.01	1.28	-0.12	0.00

Pioglitazone

cPIO [µM]	Donor 1						Donor 2					
	Day 3		Day 7		Day 14		Day 3		Day 7		Day 14	
	% viability	% StDev	% viability	% StDev	% viability	% StDev	% viability	% StDev	% viability	% StDev	% viability	% StDev
0	100.00	34.62	100.00	17.48	100.00	14.11	100.00	22.70	100.00	13.49	100.00	23.91
0.4	98.29	26.07	99.29	21.41	111.76	7.20	70.97	21.23	100.00	15.08	79.31	18.86
1	91.69	21.37	118.71	19.37	112.50	8.30	84.34	14.65	83.91	11.05	85.05	19.83
2	84.58	20.67	83.25	23.18	85.70	14.84	83.95	11.86	86.93	20.74	81.37	25.46
4	91.21	21.61	88.01	16.33	79.18	15.13	61.64	18.38	62.50	14.75	53.17	12.40
10	104.05	11.12	62.83	8.10	51.41	14.30	38.94	15.98	60.89	3.96	49.62	13.39
20	105.08	10.69	69.38	16.13	61.76	13.46	61.37	8.17	80.11	11.76	64.75	6.45
40	-0.28	0.02	78.93	6.24	59.93	6.85	92.50	43.53	71.33	9.15	57.92	17.30

Troglitazone

cTRO [µM]	Donor 1						Donor 2					
	Day 3		Day 7		Day 14		Day 3		Day 7		Day 14	
	% viability	% StDev	% viability	% StDev	% viability	% StDev	% viability	% StDev	% viability	% StDev	% viability	% StDev
0	100.00	8.47	100.00	12.14	100.00	3.12	100.00	43.19	100.00	13.10	100.00	7.00
0.4	80.10	34.11	84.12	17.06	76.93	25.48	163.28	49.68	99.12	21.83	72.60	15.68
1	82.02	25.56	62.22	17.11	76.72	8.13	119.67	23.91	109.33	16.35	43.70	4.47
2	59.92	16.17	67.79	21.32	2.38	0.00	119.61	22.37	93.64	32.22	-0.05	0.02
4	70.74	17.90	72.66	27.11	-0.34	0.01	94.62	18.27	79.68	36.47	-0.09	0.01
10	80.30	12.64	4.57	4.22	-0.33	0.01	74.34	19.19	0.80	0.99	-0.09	0.00
20	-0.14	0.10	-0.07	0.15	-0.33	0.00	0.38	0.54	-0.14	0.01	-0.07	0.03
40	-0.36	0.02	-0.19	0.10	-0.33	0.07	-0.21	0.05	-0.15	0.02	-0.04	0.07

Esther Johann

CURRICULUM VITAE

EXPERTISE

Exposure Limits (PDEs/OELs)

Leachables & Extractables

Toxicological risk assessment

Alternative test methods

GLP

Mammalian cell culture

Molecular Biology/ Toxicology

Three-dimensional cell culture

Microfluidic cell culture

PROFESSIONAL EXPERTISE

Since May 2018: Toxicologist
Merck KGaA Darmstadt, Non-Clinical Safety, Chemistry Toxicology

- Toxicological risk assessment and derivation of health-based exposure limits (PDEs/OELs) for chemicals and APIs
- Toxicological risk assessment for leachables and extractables from filter systems and container closure systems

Apr 2017 – Apr 2018: Safety assessment consultant
Merck KGaA Darmstadt, Non-Clinical Safety, Chemistry Toxicology

- Toxicological risk assessment and derivation of health-based exposure limits (PDEs/OELs) for chemicals and APIs
- Toxicological risk assessment for leachables and extractables from filter systems and container closure systems

Jan 2013 – Mar 2017: Promotion
Merck KGaA Darmstadt, Non-Clinical Safety
Title: Improved early *in vitro* prediction of drug induced Liver Injury (DILI) in man: Assessment of novel 3D hepatic cell models.

- Characterization of physiologic and pharmacologic profiles for improved early *in vitro* risk assessment of drug candidates
- Project is part of the IMI MIP-DILI project (Mechanism-based Integrated systems for the Prediction of Drug-Induced Liver Injury)
- Initiation and organization of collaborations
- Organization of MIP-DILI/ CRO meetings in Darmstadt

Sept 2014: Guest scientist
Karolinska Institutet Stockholm, Department of Pharmacology and Toxicology

- Expertise exchange and workshop in hepatic 3D cell culture methods within MIP-DILI partners
- Planning and setup of ring trials

Sept 2013: Guest scientist
CellASIC (part of Merck Millipore), Hayward (San Francisco)

- Workshop in hepatic microfluidic systems *in vitro*
- Initiation and planning of beta-testing different microfluidic approaches

Mar 2012 – May 2012: Internship
Merck KGaA Darmstadt, Institute of Toxicology/ Non-Clinical Safety
- Evaluation of renal drug targeting approaches

Aug 2011 – Oct 2011: Internship
Merck KGaA Darmstadt, Institute of Toxicology/ Non-Clinical Safety
- Immunohistochemistry as a sensitive method for the detection of Kim-1
- Proof of principle of Kim-1 as a novel biomarker for kidney injury

Feb 2011 – Mar 2011: Internship
Boehringer-Ingelheim Pharma GmbH & Co. KG, Biberach, Institute of Toxicology
- General introduction to pre-clinical safety assessment in early drug development
- Introduction to standard test batteries *in vitro* and *in vivo*

Mar 2007 – July 2007: Internship
Across Barriers GmbH, Saarbrücken
- Introduction to standard and special cell culture methods
- Introduction to *in vitro/ ex vivo* skin models
- Introduction to analytics (HPLC, LC-MS)

SKILLS

LANGUAGES

German (native speaker)

English (fluent)

French (basic)

COMPUTER LITERACY

Nexus/ Toxtree

MS office

GraphPad Prism/ OriginLab

SOFT SKILLS

Communicative

Collaborative

Personal responsibility

Problem-solving

Self-disciplined

OTHER

Microscopy

Immunofluorescence

EDUCATION

Oct 2010 – Dec 2012: Master of Science in Toxicology (2,0)
Technical University Kaiserslautern, Department of Chemistry and Merck KGaA, Darmstadt
- Title: Cytotoxicity screening in multiple hepatic derived cells in a multi-site ring trial (1,7)

Oct 2007 – June 2010: Bachelor of Science in Biosciences (2,3)
Technical University Kaiserslautern, Department of Biology/ Phytopathology
- Title: Regulation of expression of cutinase genes during early development In *Botrytis cinerea* (1,3)

Mar 2005 – Mar 2007: Studies on teaching post (Biology, Chemistry and Arts)
University Koblenz-Landau, Department of Education

Aug 1994 – July 2004: University entrance Diploma
Gymnasium am Stefansberg, Merzig

PUBLICATIONS

Hewitt P, Fuchs TC, Johann E and Zheng W, White Paper: **Detection of vancomycin-induced subacute nephrotoxicity using MILLIPLEX MAP rat kidney toxicity multiplex panels.** Available on www.merckmillipore.com

Sison-Young R, Mitsa D, Jenkins RE, Mottram D, Alexandre E, Richert L, Aerts H, Weaver R, Jones RP, Johann E, Hewitt PG, Ingelman-Sundberg M, Goldring CEP, Kitteringham NR and Park BK (2015): **Comparative proteomic characterization of four human liver-derived single cell culture models reveals significant variation in the capacity for drug disposition, bioactivation and detoxification.** Arch Toxicol. 2015, 147(2): 412-24.

Pfannkuch F and Suter-Dick L: **Predictive Toxicology: From vision to reality (1st edition), Chapter 5: Genomic applications for assessing toxicities of liver and kidney injury** (Esther Johann and Philip Hewitt). ISBN: 3527336087

Rowena Sison-Young[1*], Volker M. Lauschke[2*], Esther Johann[3], Eliane Alexandre[4], Sebastien Anthérieu[5], Hélène Aerts[5], Helga Gerets[6], Gilles Labbe[7], Christopher Schofield[8], Simone Stahl[9], Cerys Lovatt[8], Julie Holder[8], Lysiane Richert[4], Neil Kitteringham[1], Robert Jones[10], Mohamed Elmasry[10], Richard Weaver[5], Phil Hewitt[3], Magnus Ingelman-Sundberg[2], Chris Goldring[1a] and Kevin Park[1]
A multicenter assessment of single cell models aligned to standard measures of cell health for prediction of acute hepatotoxicity. Arch Toxicol. 2017, 91: 1385-1400.

Numerous oral presentations and poster presentations